

Functionalized Dinuclear Clathrochelates as Supramolecular Building Blocks

THÈSE N° 7310 (2016)

PRÉSENTÉE LE 14 OCTOBRE 2016

À LA FACULTÉ DES SCIENCES DE BASE

LABORATOIRE DE CHIMIE SUPRAMOLÉCULAIRE

PROGRAMME DOCTORAL EN CHIMIE ET GÉNIE CHIMIQUE

ÉCOLE POLYTECHNIQUE FÉDÉRALE DE LAUSANNE

POUR L'OBTENTION DU GRADE DE DOCTEUR ÈS SCIENCES

PAR

Mathieu Jérémie MARMIER

acceptée sur proposition du jury:

Prof. G. Laurenczy, président du jury

Prof. K. Severin, directeur de thèse

Prof. A. F. Williams, rapporteur

Dr G. Timco, rapporteur

Prof. W. L. Queen, rapporteuse



ÉCOLE POLYTECHNIQUE
FÉDÉRALE DE LAUSANNE

Suisse
2016

Acknowledgements

A PhD thesis, despite being nominative, cannot be achieved without a lot of external help. This help has been found from various environments and people, and I would like to express here my gratitude to them.

Foremost, I want to thank my thesis director, Prof. Kay Severin, for his unfailing support all along these last four years. Since the first day as a LCS member, I always found solution to impossible problems by simply knocking at his office's door. His input and knowledge, as well as some key tips and advices, were without any doubts determinant for my career as a researcher.

I would like also to thank Prof. Wendy L. Queen, Prof. Alan F. Williams and Dr. Grigore Timco, the examiners of my thesis examination jury, for devoting their time to the arduous and long task of reading, correcting and evaluating this thesis. I would like also to thank Prof. Gabor Laurenczy for fulfilling the role of the jury President during the private defense.

People working in the BCH building have the chance to be surrounded by people that will take care of your daily problems: Anne-Lene Odegaard for all issues related with the doctoral school; Gladys, Anne-Lise and Benjamin for the help provided for anything related with delivery of chemicals (such as rhum or wine bottles, bikes or other goods of indisputable necessity in a chemistry lab); Dr. Pascal Mieville, for his support in many occasions, firstly related to NMR, but that quickly gave way to other physical questionings (do a headstand after three days in Piedmont, test the limit of the human body to Haggis, ...).

Thanks also to Dr. HDR Christophe Roussel for his mentoring during my PhD, with all the coffees breaks that are implied in this task, and for the fruitful discussions that followed.

I would like also express my gratitude to some people of paramount importance for supramolecular chemists, who are nothing without proper crystal structures. Usually this list is not that long, highlighting the difficulty encountered by these people working with my crystals (all of fantastic quality): Dr. Rosario Scopelliti, Dr. Julian J. Holstein, Dr. Kurt Schenk, Dr. Philip Pattison and Dr. Anna V. Vologzhanina for the tremendous work achieved all along my thesis. I want also to thank Euro Solari for the daily input in the lab, from the maintenance of all secret instruments to the extreme care with which he was mounting the numerous crystals I was handling.

Thank you also to the ISIC mass service, Dr. Laure Menin, Fransisco Sepulveda, Daniel Baumman and Daniel Ortiz for their help with my mass requests. A special thank to Dr. Konstantine O. Zhurov, who did a fantastic job with the "chemical soup", and whose tingling ideas were of great help in key aspects of this thesis.

I owe a lot to Dr. Mirela Pascu, who handed on her magic tricks for crystal growing, and the special care you have to offer to your crystals, and for her patience and her dedication at the early stage of my thesis.

The last four years being a LCS member took place very quickly, and this is also thanks to the nice atmosphere created by the people working here. I would like to thank the people I met in the third floor, fourth sector of the BCH building during the last four years: Alba, Albert, Alex, Basile, Bo, Clément, Florian, Gregor, Jonathan, José, Julie, Justus, Léonard, Marcus (the master of slaves), Matt, Mirela, Ophélie, Suzanne, Yizhu, Ziya. A special big up for the dream team of the coffee break, the masters of the jest, I named Giacomo, Loïc and Nicolas. I don't think the working atmosphere would have been so nice without their unceasing proposals for coffees, rum or wine tastings, aperos, skiing, hiking and other working-related activities.

I would like also to thank Dr. Basile Curchod, for his invaluable support during the last stages of this thesis, and for being one of the most passionate scientific I met so far. He could almost convince me that computational chemistry is a non-that-opaque field. Thanks also for the "rich" weekends spent with some of the teammates present in the last paragraphs.

Thank you also to all friends met during my studies at EPFL, who constitute a more than solid basis for the mental health: Adrien, Chloé, Joëlle, Pierre, Nadine, Jean-Phi, Laurent, Stéphanie, Matthias, Yulia, Zoubida, Nicolas, Nicolas and Nicolas.

My parents and sister, for their unswerving support during all my studies and beyond. It is thanks to them that I am where and who I am today.

Abstract

This thesis details the synthesis and characterization of dinuclear clathrochelates functionalized with groups suitable for supramolecular applications. Their successful incorporation into self-assembled discrete and polymeric structures is related. These novel dinuclear clathrochelate complexes possess several features that make them highly interesting metalloligands for applications in supramolecular chemistry: they are large, rigid, modular and easy-to-access building blocks, and they display additional properties (charge, luminescence) depending on the metals they are constituted of.

Syntheses and characterization of pyridyl-functionalized clathrochelates, and their subsequent incorporation into supramolecular architectures, are described in Chapter 2. Two distinct approaches have been employed: a direct synthesis or the postsynthetic functionalization of brominated clathrochelates *via* Pd-catalyzed cross-coupling reactions, resulting in metalloligands with up to seven pyridyl groups. Reaction of linear, ditopic clathrochelates with Zn(II) resulted in the formation of polymeric two-dimensional coordination polymer, and pentatopic clathrochelates were shown to form networks of novel topologies. Furthermore, pentameric $M_{10}L_5$ barrel structures were obtained from tetratopic clathrochelates.

Incorporation of carboxylic acid-appended clathrochelates into several metal-organic frameworks is described in the third chapter. Studies revealed that the gas sorption properties of Zr-based metal-organic frameworks constituted of ditopic clathrochelates were influenced by the lateral substituents of the dioximato ligands. Furthermore, some of these metal-organic frameworks showed high CO₂ uptake.

Chapter 4 entails the synthesis of clathrochelates functionalized with cyano groups and their subsequent incorporation into one-, two-, and three-dimensional silver(I)-based coordination polymers. One network, obtained from a pentatopic clathrochelate, displayed an unprecedented network topology and a very high topological density.

The syntheses of clathrochelates with different functional groups are described in the last chapter. The modular nature of these clathrochelate ligands was demonstrated through the analysis of a complex mixture obtained from different metal ions and dioximato ligands. This study also revealed that heterometallic clathrochelates can be obtained.

Keywords

Clathrochelate complexes • metalloligands • supramolecular chemistry • self-assembly
metal-organic framework • coordination polymer

Résumé

Cette thèse détaille la synthèse et la caractérisation de clathrochélates dinucléaires fonctionnalisés avec des groupes utilisables pour des applications en chimie supramoléculaire. Leur incorporation ultérieure dans des structures discrètes et polymériques par auto-assemblage y est décrite. Ces nouveaux clathrochélates dinucléaires possèdent plusieurs caractéristiques qui rendent ces métalloligands très intéressants pour des applications en chimie supramoléculaire: ils sont grands, rigides, modulaires et facilement accessibles, et ils présentent des propriétés supplémentaires (charge, luminescence) en fonction des métaux dont ils sont constitués.

Les synthèses et caractérisation de clathrochélates fonctionnalisés avec des groupes pyridyl, ainsi que leur incorporation ultérieure dans des architectures supramoléculaires, sont décrites dans le Chapitre 2. Deux approches distinctes ont été utilisées: une synthèse directe ou la fonctionnalisation post-synthétique de clathrochélates possédant des atomes de brome grâce à des réactions de couplage croisé catalysées par du palladium. Des métalloligands avec jusqu'à sept groupements pyridyl sont reportés. La réaction entre des clathrochélates ditopiques linéaires et Zn (II) conduit à la formation d'un polymère de coordination bidimensionnel, et des clathrochélates pentatopiques ont montré la formation de réseaux possédant de nouvelles topologies. En outre, des structures en forme de baril pentamérique $M_{10}L_5$ ont été obtenues à partir de clathrochélates tétratopiques.

L'incorporation de clathrochélates fonctionnalisés par des acides carboxylique dans plusieurs réseaux métallo-organiques est décrite dans le troisième chapitre. Les études ont révélé que des réseaux constitués de zirconium et de clathrochélates ditopiques sont influencés par les substituants latéraux des ligands dioximato. En outre, certains de ces réseaux métallo-organiques ont montré une forte absorption de CO_2 .

Le Chapitre 4 relate la synthèse de clathrochélates fonctionnalisés avec des groupes cyano et leur incorporation dans des polymères de coordination mono-, bi- et tridimensionnels à base d'argent(I). Un des polymères, obtenu à partir d'un clathrochélate pentatopique, possède une nouvelle topologie ainsi qu'une densité topologique très élevée.

Les synthèses de clathrochélates avec différents groupes fonctionnels sont décrites dans le dernier chapitre. La nature modulaire de ces ligands a été démontrée par l'analyse d'un mélange complexe obtenu à partir de différents ions métalliques et de plusieurs ligands dioximato. Cette étude a également révélé que des clathrochélates hétérométalliques peuvent être obtenus.

Mots-clés

Complexes de clathrochélates • métalloligands • chimie supramoléculaire • auto-assemblage
réseau métallo-organique • polymère de coordination

Abbreviations and Symbols

°	degree
1D	one-dimensional
2D	two-dimensional
3D	three-dimensional
Å	Ångström
Ar	aryl
β	beta
BET	Brunauer-Emmet-Teller
bpda	4,4'-biphenyldicarboxylic acid
bpy	4,4'-bipyridyl
^t Bu	<i>tert</i> -butyl
°C	degree Celsius
calcd	calculated
CMOF	chiral metal-organic framework
CP	coordination polymer
Cp*	η^5 -1,2,3,4,5- pentamethylcyclopentadienyl
d	doublet
dd	doublet of doublet
DCC	dynamic covalent chemistry
DEF	N,N'-diethylformamide
DMA	N,N'-dimethylacetamide
DMF	N,N'-dimethylformamide
DMSO	dimethylsulfoxide
DOSY	diffusion-ordered NMR spectroscopy
dt	doublet of triplet
δ	chemical shift
ee	enantiomeric excess
e.g.	exempla gratia
ESI-MS	electrospray ionisation mass spectrometry
Et	ethyl
Et ₂ O	diethyl ether
EtOAc	ethyl acetate

EtOH	ethanol
<i>et al.</i>	<i>et alia</i> , and others
g	gram
h	hour
HRMS	high-resolution mass spectrometry
Hz	Hertz (s^{-1})
<i>J</i>	coupling constant
K	Kelvin
m	multiplet, or minute
<i>m</i>	meta
M	molar ($\text{mol}\cdot\text{l}^{-1}$)
m/z	mass:charge ratio
Me	methyl
mg	milligram
MHz	megahertz
ml	millilitre
mM	millimolar ($\text{mmol}\cdot\text{l}^{-1}$)
mmol	millimole
MOF	metal–organic framework
mol	mole
μmol	micromole
nm	nanometer
NMR	nuclear magnetic resonance
<i>o</i>	ortho
OTf	triflate, trifluoromethanesulfonate
<i>p</i>	para
Ph	phenyl
ppm	parts per million
<i>ⁱPr</i>	<i>iso</i> -propyl
<i>p</i> -TsO [−]	<i>para</i> -toluenesulfonate
q	quartet
RT	room temperature
s	singlet
SBU	secondary building unit
T	temperature

TFA	trifluoroacetic acid
TGA	thermogravimetric analysis
TOF	time of flight
UiO	University of Oslo
UV	ultraviolet
UV-VIS	ultraviolet-visible
WOC	water oxidation catalyst
wt	weight

Table of Contents

Acknowledgements	iii
Abstract	v
Résumé	vii
Abbreviations and Symbols.....	ix
Chapter 1 Introduction	1
1.1 Coordination-driven self-assembly	3
1.2 Metalloligands.....	6
1.2.1 Metalloligands versus organic ligands	7
1.2.2 Selected applications of metalloligands in supramolecular assemblies.....	7
1.2.3 Conclusion.....	18
1.3 Boronate ester-capped clathrochelates complexes	19
1.3.1 Mononuclear boronate ester-capped clathrochelate complexes	19
1.3.2 Mononuclear clathrochelate complexes as supramolecular building blocks.....	21
1.4 Dinuclear boronate ester-capped clathrochelate complexes.....	26
1.5 Aims of the project.....	28
Chapter 2 Dinuclear clathrochelates functionalized with pyridyl groups	31
2.1 Introduction	33
2.2 Direct synthesis of polypyridyl-decorated clathrochelates	34
2.3 Synthesis of polypyridyl clathrochelates <i>via</i> Pd catalyzed cross-coupling reactions.....	38
2.4 Use of pyridyl-decorated clathrochelates as supramolecular building blocks	46
2.4.1 Synthesis of a two-dimensional network based on a 4-pyridyl-capped clathrochelate	46
2.4.2 Synthesis of a $M_{10}L_5$ molecular cage	48
2.4.3 MOFs based on pentatopic clathrochelates	57
2.5 Conclusion.....	62
Chapter 3 Dinuclear clathrochelates functionalized with carboxylic acid groups	63
3.1 Introduction	65
3.2 Synthesis of polytopic clathrochelates sharing carboxylic acid groups	67

3.3	Use of carboxylic acid-decorated clathrochelates as supramolecular building blocks..	71
3.3.1	Synthesis of MOF-5 derivatives using 4,4'-dicarboxylic acid clathrochelates.....	71
3.4	Conclusion	83
Chapter 4	Dinuclear clathrochelates functionalized with pendant cyano groups.....	85
4.1	Introduction.....	87
4.2	Direct synthesis of cyano-functionalized clathrochelates.....	89
4.3	Synthesis of cyano-functionalized clathrochelates by postsynthetic cross-coupling reactions	91
4.4	Coordination polymers with silver(I).....	93
4.5	Conclusion	100
Chapter 5	Miscellaneous structural variations of dinuclear clathrochelates.....	101
5.1	Introduction.....	103
5.2	Synthesis of formyl- and amine-functionalized dinuclear clathrochelates.....	106
5.3	Formyl- and amine-functionalized dinuclear clathrochelates as building blocks	108
5.4	Synthesis of clathrochelates decorated with terminal acetylene groups, and their use in “click” chemistry.....	112
5.5	Synthesis of clathrochelates appended with different functional groups	114
5.6	MS analysis of clathrochelate mixtures.....	116
5.7	Studies on the relative stability of clathrochelate complexes	120
5.8	Deliberate synthesis of heterometallic, dinuclear clathrochelates	123
5.9	Conclusion	125
Chapter 6	Conclusions and Outlook.....	127
Chapter 7	Experimental Part	131
7.1	General	133
7.2	Experimental Procedures	135
Chapter 8	Appendix.....	179
8.1	Crystallographic Tables.....	181
Chapter 9	References	195
	Curriculum vitae	211

Chapter 1 Introduction

In this chapter, some general aspects of supramolecular chemistry will be discussed. Since the pioneering work of Lehn in 1978,¹ this field of chemistry has exploded into an unbounded, multi-disciplinary topic that includes nowadays research from organic and inorganic chemistry to biology or material sciences. Owing to this fantastic expansion of supramolecular chemistry in the course of the past years, it is not possible to deal with all its aspects. Therefore, only the most relevant concepts of supramolecular chemistry will be discussed. The work presented in this thesis being mostly related to metalloligands, whose ins and outs will be detailed, some selected examples of incorporation of metalloligands in supramolecular architectures will be discussed. Secondly, an update on the state-of-the-art research on clathrochelates, members of the metalloligands developed in our group among others, will be exposed.

1.1 Coordination-driven self-assembly

Among all aspects of supramolecular chemistry, coordination-driven self-assembly is without any doubt one of the most powerful implement for a supramolecular chemist. This tool has allowed the preparation and characterization of discrete² or polymeric³ two- or three-dimensional structures. The coordination-driven self-assembly approach is based on the reversible interaction between a donor unit (ligand) and an acceptor unit (metal complex). In metallasupramolecular architectures, the donor unit is composed of a ligand sharing Lewis-basic moieties and the acceptor is tailored with a metal center having vacant coordination sites. The process of binding a ligand to the vacant coordination site of the metal being reversible, errors are not conclusive. Indeed, the system can correct these errors, by moving the equilibrium towards the most thermodynamically stable species. Nevertheless, ligand-metal interactions are highly directional, which allows the supramolecular chemist to predict in a relatively confident way the possible products that will be formed given the donor and acceptor units used. This approach has allowed constructing macrocyclic or three-dimensional architectures by designing in a rational way metal centers and ligands that will occupy either the edges or the vertices of the desired complex. This approach has been formulated as “edge-directed self-assembly”⁴ By using building blocks with defined geometry (length, angles), one can construct assemblies of increased complexity (Figure 1.1).

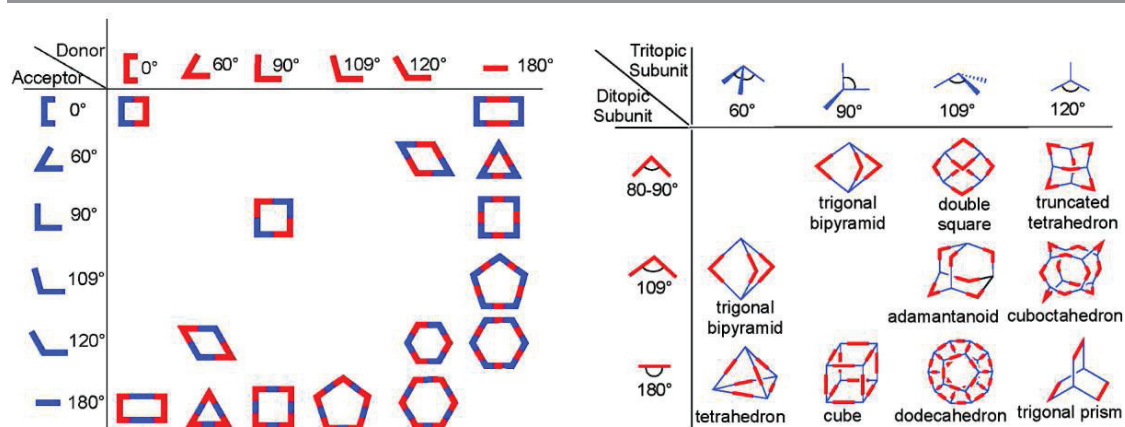


Figure 1.1 – Edge-directed self-assembly of two ditopic building blocks (left) and a combination of di- and tritopic subunits to generate two- and three-dimensional polygons of defined geometry. Reprinted with permission from reference [4b]. Copyright 2011 American Chemical Society.

By having a closer look to the acceptor units, one can see that some of the angles that are found in Figure 1.1 can be easily reached using simple inorganic buildings blocks, whose selected examples are shown in Figure 1.2.

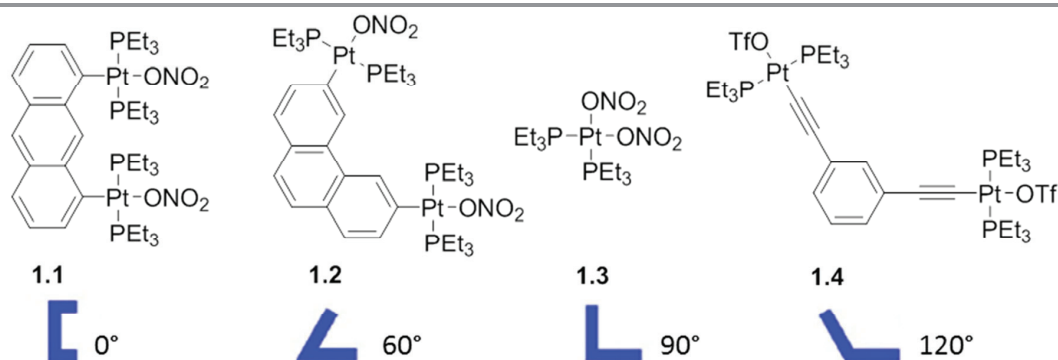


Figure 1.2 – Metal-based acceptor units **1.1–1.4** with a defined angle given below the chemical structure. Adapted with permission from reference [4]. Copyright 2011 American Chemical Society.

The group of Stang⁵ and Fujita⁶ reported in the 1990's the formation of two molecular squares based on the same donor unit, 4,4'-bipyridyl (bpy), and with square planar Pt(II) or Pd(II) centers. Their judicious use of *cis*-protected metal centers, with the help of chelating ligands (ethylenediamine or bis(diphenylphosphino)ethane), allowed the preparation of the structures **1.5** and **1.6** depicted in Figure 1.3. Interestingly, while Pd(II)-based **1.6** could be obtained under ambient conditions, its Pt(II) analogue required heating at 100°C for several days. This indicates that the Pt–N bond is way less labile than the Pd–N bond. Similarly, reaction of **1.1** with bpy resulted in the formation of the molecular rectangle **1.7** as described by Stang in 2001 (Figure 1.4).⁷

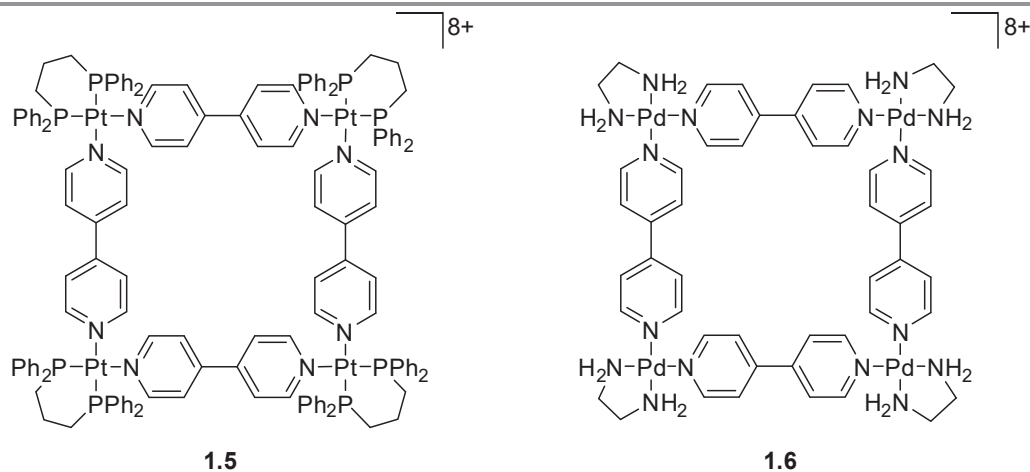


Figure 1.3 – Molecular squares reported by Stang⁸ (**1.5**) and Fujita⁹ (**1.6**).

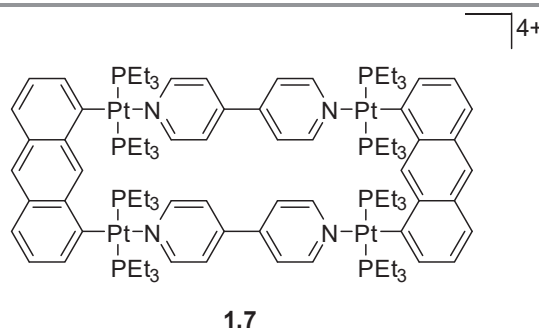


Figure 1.4 – Molecular rectangle obtained from the [2+2] self-assembly of Pt(II) acceptor **1.1** and bpy donor.⁷

Only discrete architectures were presented in Figure 1.1. Naturally, coordination polymers (CPs) can be obtained by intelligently selecting appropriate acceptor and donor units. In the representative examples described so far, the two units had convergent angles. By choosing acceptor units with divergent coordination vectors, and keeping using the simple bpy ligand, CP **1.8** was discovered by Fujita *et al.* four years after their hallmark discovery of molecular square **1.6**. CP **1.8** is composed of naked Cd(II) ions coordinated to four pyridyl moieties in a square-planar fashion.⁸ Two nitrate (NO_3^-) ions are coordinated to the Cd(II) centers in *trans* for charge balance considerations, giving an infinite network of stoichiometry $[\text{Cd}(\text{bpy})_2(\text{NO}_3)_2]$ (Figure 1.5).

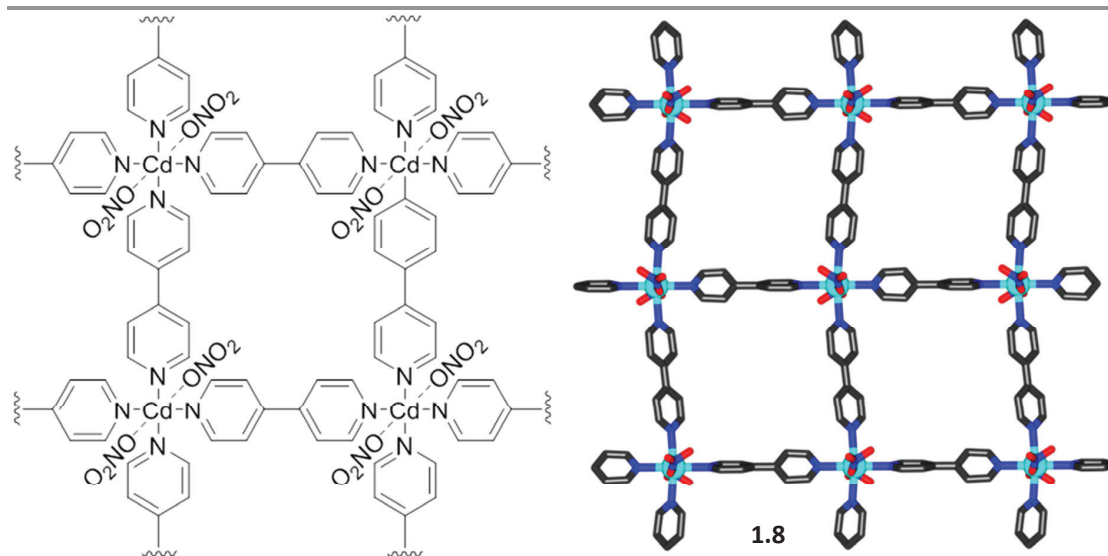


Figure 1.5 – Molecular structure of $[\text{Cd}(\text{bpy})_2(\text{NO}_3)_2]$ network **1.8**, and part of the network in the crystal. Color coding: C: gray; Cd: cyan; N: blue; O: red. Hydrogen atoms and unbound solvent molecules have been omitted for clarity.

Given the oversized amount of donor and acceptor units developed since the stammering of supramolecular chemistry, a complete overview of the structures and their properties would be a task far beyond this thesis. Therefore, a non-exhaustive overview of one particular class of building blocks – metalloligands – will be discussed in the following section 1.2.

1.2 Metalloligands

“A ligand system that incorporates a primary coordinated metal that directs a secondary donor site [...] to be suitably oriented for coordination to a further metal center” is the definition that has been given to metalloligands by Lindoy in 2015.^{2b} A metal-containing coordination complex used as a supramolecular building block has the advantage of providing structural rigidity, and one can tailor it by anchoring functional groups on its periphery.⁹ Naturally, since all metal-containing complexes can not be defined as metalloligands, the separation between a metalloligand and a “simple” metal-containing complex has to be drawn. A metal center surrounded by ligands can be placed in the metalloligand catalog as soon as at least one of the ligands from which it is formed possesses appended functional groups. These functional groups can be of various kinds, from Lewis basic sites for further coordination to metal acceptor units as defined in section 1.1, to H-bond sensitive groups, as pictured in Figure 1.6. There is no required number of functional groups mandatory for a complex to be classified as metalloligand. However, following the strategy described in section 1.1, one can see that a higher number of functional groups will tend to form polymeric structures.

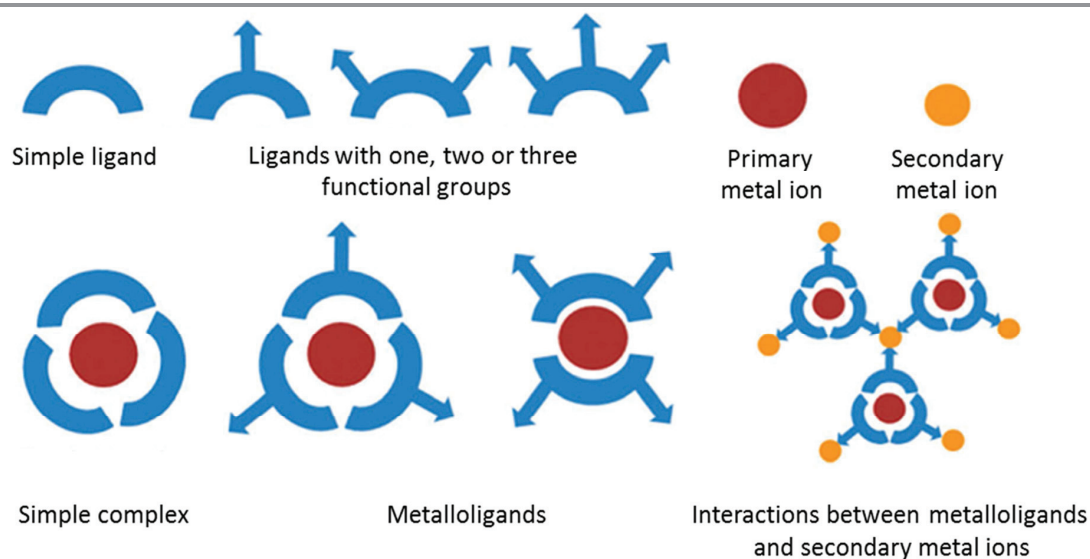


Figure 1.6 – Schematic representation of the difference between simple complexes and metalloligands, and one example of metalloligand propagation upon complexation to secondary metal ions. Adapted from reference [9] with permission from The Royal Society of Chemistry.

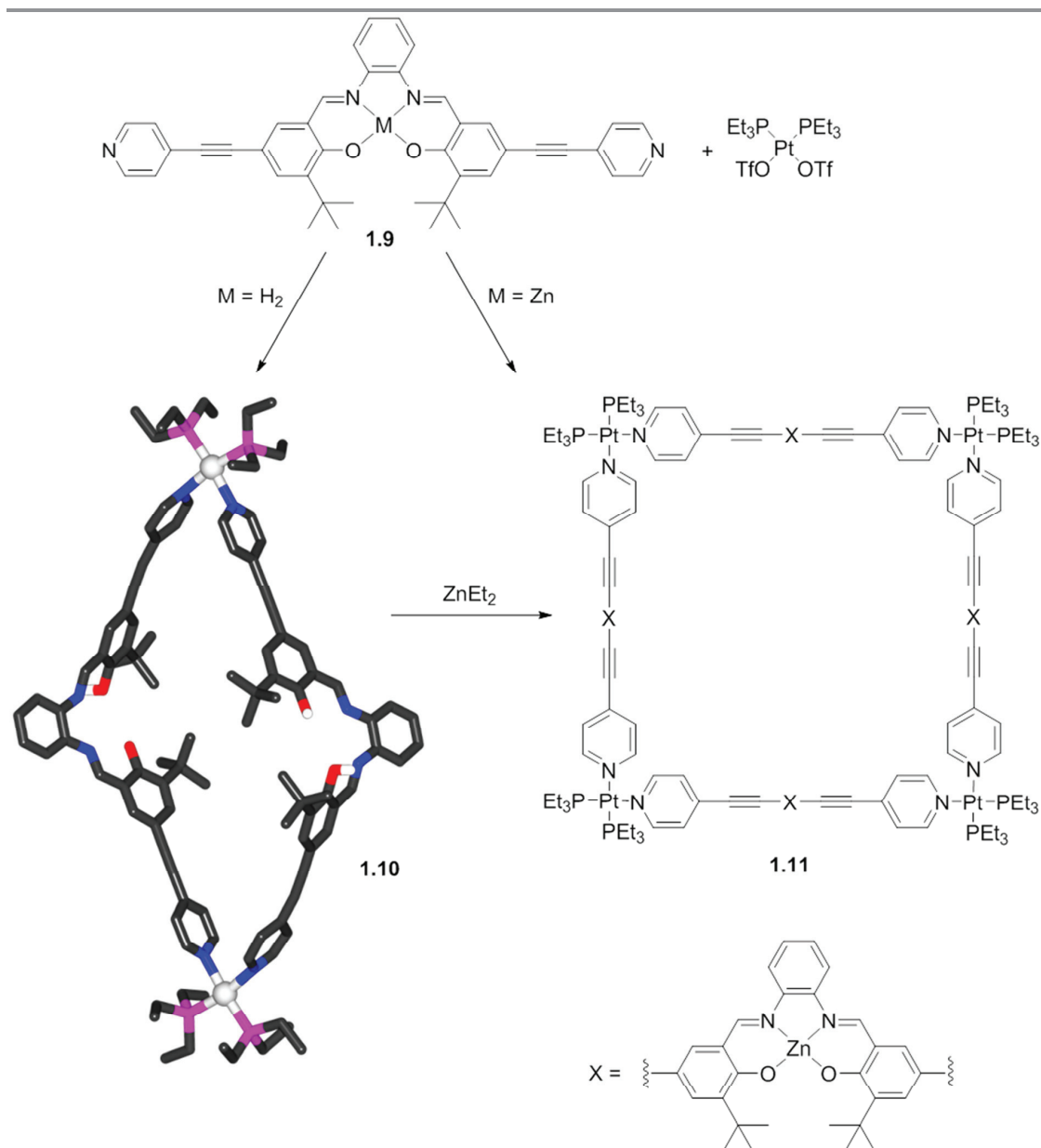
1.2.1 Metalloligands versus organic ligands

One might wonder what are the profits of using a metal-containing ligand in a system often already composed of metal ions, whilst organic synthesis provides tools allowing chemists to create organic molecules of increasing complexity. This section does not claim to fully cover all aspects of the comparison between purely organic ligands and metalloligands, however, key points will be discussed. Thereafter, selected examples that are most relevant to the advantages of metalloligands over organic ligands discussed in this section will be covered. With regards to a purely organic scaffold, the metalloligand approach allows to precisely control the orientation of the functional ligands decorating the metal complex. This property allows the metalloligands to be used as substrates for highly ordered and rigid supramolecular architectures. Indeed, for molecules of similar sizes, an organic linker is often way more flexible than a metal-containing analogue. Rigidity does not only lead to more rigid structures, but also allows a much better predictability of the geometry of the complexes obtained. Owing to this precise assessment of geometry, the supramolecular chemist can then tailor and design the size of the cavity of a discrete structure, or the shape and size of the pores within a polymeric network by selecting the appropriate combination of metalloligands and its secondary anchoring unit. The metal-metalloligand interaction is thereby synthetically interesting, since it allows the close proximity of two metals centers that can be different, leading to an easy method to construct heterometallic coordination polymers. The approach of using a metalloligand as building block for the construction of a network can be also seen as a way to immobilize one or several metal sites in an ordered, controlled manner. These metal sites can be of great interest: open-metal sites or catalytically active sites,¹⁰ redox properties,¹¹ etc.

1.2.2 Selected applications of metalloligands in supramolecular assemblies

The molecular squares **1.5** and **1.6** were obtained by combination of linear donor ligands in combination with acceptor metal complexes with a coordination vector of 90°. Similarly, metalloligands can successfully replace the 4,4'-bipyridyl ligand to lead to larger structures. An example of such a replacement is shown in Scheme 1.1. Hupp and coworkers demonstrated that combining a *cis*-protected Pt(II) corner together with a bis(4-ethynylpyridyl) functionalized salen linker **1.9** led to the formation of the [2+2] molecular loop **1.10**.¹² While using the metallated form of salen **1.9**, the selective formation of the [4+4] molecular square **1.11** was observed. Transition from **1.10** to **1.11** could also be performed upon postmetallation of **1.10** with ZnEt₂. Reduction of the intrinsic flexibility of the organic bis(4-ethynylpyridyl) salen linker while coordinated to Zn(II) led to linear, rigid ditopic metalloligands that reassemble to the molecular square **1.11**. This further

exemplifies the reversible interactions between the N-donor ligand, in its metallated or its free base form, and the Pt(II) acceptor.



Scheme 1.1 – Molecular loop (**1.10**) compared to molecular square (**1.11**) obtained by using either a flexible organic salen ligand or its rigid metallated analog. Color coding: C: gray; H: white; N: blue; O: red; P: pink; Pt: light grey. Most hydrogen atoms and solvent molecules have been omitted for clarity.

Metalloligands do not always act as donor building blocks; they can also act simultaneously as a donor and an acceptor unit. For the latter, the unsaturated metal center within the metalloligand is capable of coordinating its own Lewis basic ligands, allowing the system to form homomolecular supramolecular architectures. Reek's group demonstrated in 2007 that the insertion of a pyridyl motif on a salen architecture, leading to a Zn(II)-salpyr [salpyr = N,N'-3-pyridylenebis

(salicylideneimine)] building block capable of self-assembling into the discrete assembly **1.12** (Figure 1.7).¹³ The Lewis basic 3-pyridyl group on the salpyr being self-complementary with the Lewis acidic unsaturated Zn(II) center, the authors observed the formation of a homomolecular tetrameric open vase structure, with a wide and a narrow rim. Interestingly, the metalloligand itself is achiral but its tetrameric assembly becomes chiral by breaking the symmetry induced by the mirror plane present in the monomer.

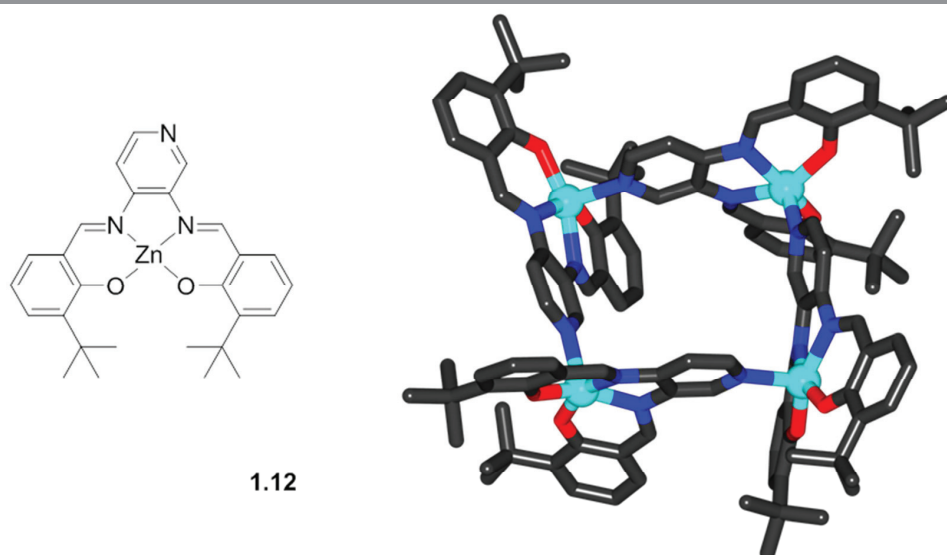


Figure 1.7 – Representation of the Zn(II)-salpyr metalloligand **1.12** developed by Reek. The metalloligand aggregates into a tetrameric open-vase structure upon coordination of the pyridyl to the vacant site of Zn(II) center. Color coding: C: grey; N: blue; O: red; Zn: cyan. Hydrogen atoms and unbound solvent molecules have been omitted for clarity.

Another striking example of a metalloligand belonging to this dual donor-acceptor family is the Zn-TPyP (TPyP = tetra(4-pyridyl)porphyrin). Similarly to **1.12**, the central Zn(II) is unsaturated and can coordinate to one pyridyl group. Goldberg described in 2010 the tetrameric assembly **1.13** of stoichiometry $(\text{Zn-TPyP})_4$ as shown in Figure 1.8a.¹⁴ Within the tetramer, the porphyrin units are oriented perpendicular to one another, leading to a square motif. The non-coordinated pyridyl moieties were solvated by the *o*-chlorophenol used during the synthetic procedure. Nevertheless, one can easily imagine that a minor change in the connectivity pattern would lead to polymeric structure **1.14**. Indeed, a two-dimensional grid was observed by the authors (Figure 1.8b). The central Zn(II) is six-fold coordinated *trans*-axially to two pyridyl group from different Zn-TPyP subunits. Two *trans*-related pyridyl moieties on the Zn-TPyP are further coordinated to two extra porphyrins *via* pyridyl-Zn(II) interactions. On each porphyrin subunit, two unbound pyridyl groups are pointing in the upper and lower part of the two-dimensional network. Despite the presence of void channels in **1.14**, the network collapses upon removal of unbound solvent. Self-aggregation of Zn-TPyP is not limited to the tetrameric **1.13** or the two-dimensional CP **1.14**. One-dimensional¹⁵ or

three-dimensional^{14,16} polymeric assemblies were obtained in a similar fashion by finely-tuning the crystallization parameters.

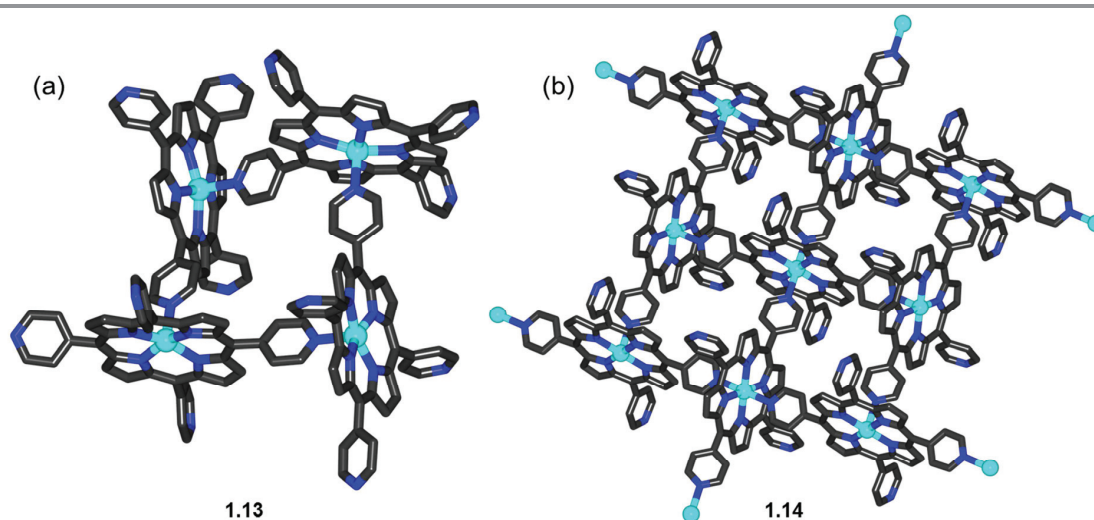


Figure 1.8 – Molecular structure of (a) tetrameric (b) polymeric assemblies of Zn-TPyP upon self-aggregation. Color coding: C: grey; N: blue; O: red; Zn: cyan. Hydrogen atoms and unbound solvent molecules have been omitted for clarity.

Fujita *et al.* used a slightly different porphyrin metalloligand, Zn-T3PyP (T3PyP = tetra(3-pyridyl) porphyrin) in combination with *cis*-protected Pd(II) corner to synthesize a molecular trigonal prism **1.15** (Figure 1.9) following a coordination-driven face-directed self-assembly approach.¹⁷ The Zn-T3PyP subunits are spanning the lateral faces of the prism, and the *cis*-protected Pd(II) corners are located on the its vertices. The authors observed a change of the symmetry of the supramolecular prism upon coordination of a pyrene molecule within the central pocket.

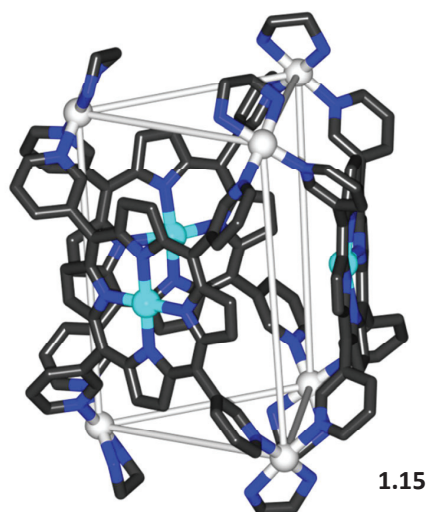


Figure 1.9 – Molecular structure of the trigonal prism **1.15** obtained from Zn-T3PyP and *cis*-protected Pd(II) corners. Color coding: C: grey; N: blue; O: red; N: blue; Pt: light grey; Zn: cyan. Hydrogen atoms and solvent molecules have been omitted for clarity. Light grey lines are guidelines for the eyes.

In 2006, Hupp and co-workers reported the synthesis of a microporous metal-organic framework (MOF) constituted from a chiral Mn(salphen) building block.¹⁸ In combination with biphenyl-4,4'-dicarboxylic acid (bpdc) and $[\text{Zn}(\text{H}_2\text{O})_6](\text{NO}_3)_2$, a pillared paddlewheel-based MOF **1.16** was obtained (Figure 1.10). The metallosalen used in this study was catalytically active for the enantioselective epoxidation of olefins. While the free metalloligand is highly active at the beginning of the catalytic process, it loses most of its activity after a few minutes, mainly due to oxidation of the salphen ligand. By immobilizing the catalyst in a robust framework, the authors managed to observe an almost constant reactivity, increasing the turnover number to about four times the one of the free Mn(salphen). The enantiomeric excess (ee) was almost as high (82%) for the framework-immobilized catalyst compared to its free analogue (88%), however, the stability cannot be compared. The robustness of the network further allowed the catalyst separation and reuse.

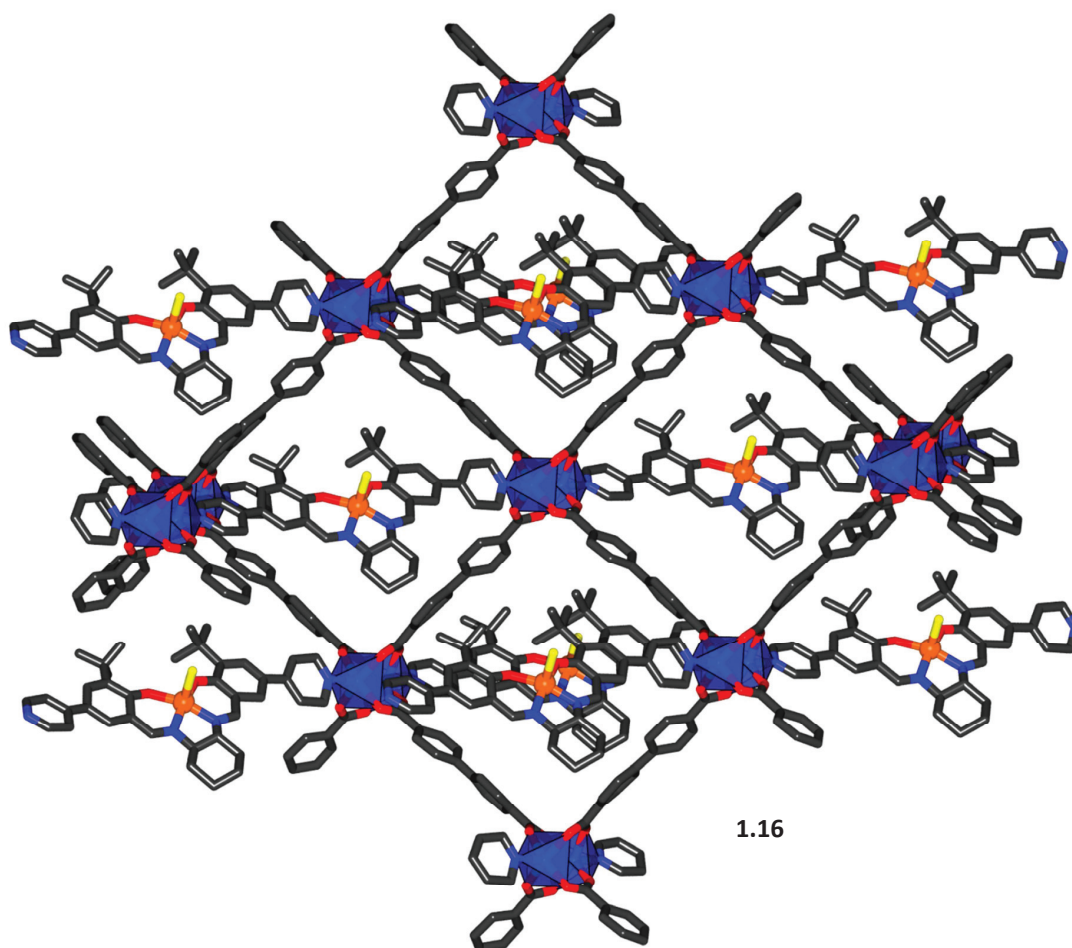


Figure 1.10 – Molecular structure of catalytically-active MOF **1.16**. The blue polyhedra correspond to Zn(II) paddlewheels. Color coding: C: grey; Cl: yellow; Mn: orange; N: blue; O: red; Zn: cyan. Hydrogen atoms and solvent molecules have been omitted for clarity.

Pyridines are naturally not the only coordinating units that have been attached to metalloligands. Lin *et al.* described the synthesis of a series of isorecticular chiral MOFs (CMOFs) with tunable open channel sizes based on a chiral salen ligand.¹⁹ They used a core composed of (*R,R*)-1,2-cyclohexandiamino-*N,N'*-bis(3-*tert*-butyl-salicylidene) functionalized in their *para* position with carboxylic acid moieties in combination with octahedral $[\text{Zn}_4(\mu_4\text{-O})(\text{O}_2\text{CR})_6]$ secondary building unit (SBU) to obtain MOFs containing catalytically active metal sites, comparably to **1.16**. CMOF-5, an example of such MOF, is shown in Figure 1.11. Asymmetric epoxidation of alkenes could be controlled *via* the fine-tuning of the metalloligand length leading to interpenetration of the network. Indeed, they proved that larger open channel dimensions observed for networks with low or no interpenetration can increase the reaction rate by dint of an increased diffusion of reactant and product molecules. Other examples of materials based on metallosalen ligands can be found in the literature, most of them being studied for catalytic reactions.²⁰

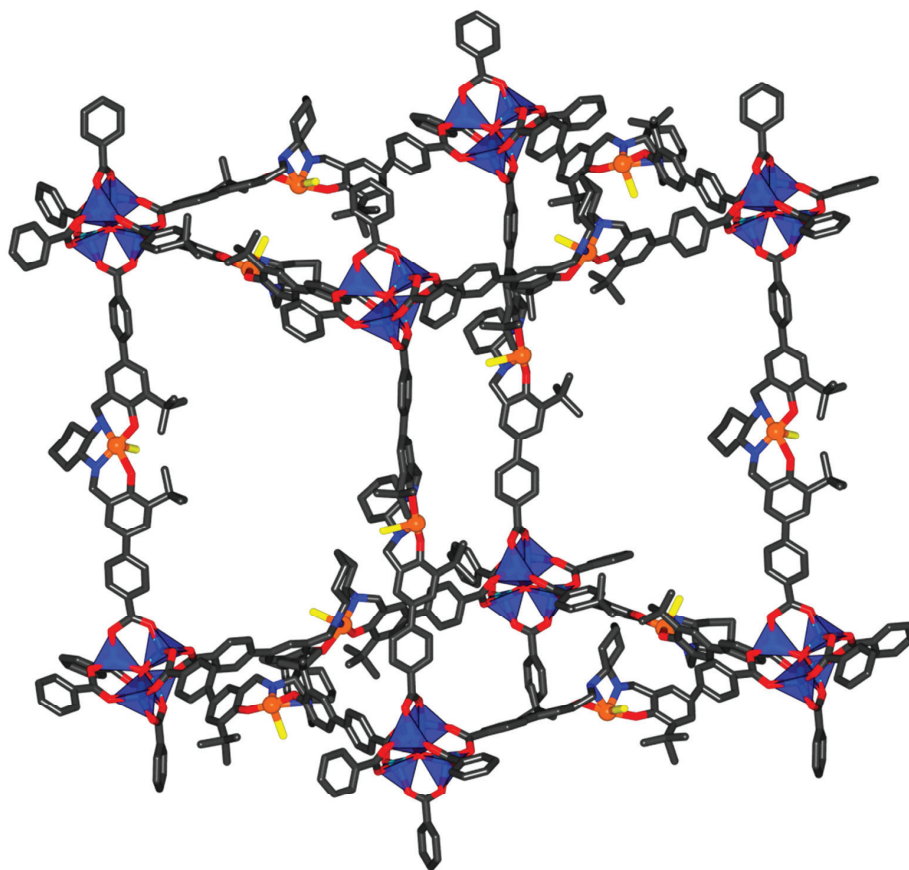


Figure 1.11 – Part of the molecular structure of CMOF-5. A single network (from the three-fold interpenetration) is represented. The blue polyhedra correspond to Zn(II) centers. Color coding: C: grey; Cl: yellow; Mn: orange; N: blue; O: red; N: blue; Zn: cyan. Hydrogen atoms and solvent molecules have been omitted for clarity.

MOFs based on zinc clusters and linear ditopic metalloligands often display low chemical stability.²¹ When Lillerud and coworkers reported in 2008 the synthesis of UiO-66,²² a MOF based on

a new 12-connected $[\text{Zr}_6(\mu_3\text{-O})_4(\mu_3\text{-OH})_4(\text{O}_2\text{CR})_{12}]$ cluster, attention has been attracted towards this category of MOF. Since the pioneering discovery of UiO-66 and its reticular analogues, many efforts have been put into the discovery of new materials, by incorporating polytopic²³ or flexible²⁴ carboxylate ligands. Compared to MOFs based on other types of oxoclusters, Zr-based MOFs have the advantages of offering a fascinating stability, both chemically and thermally.²⁵ One of their drawbacks is the difficulty of growing single-crystals suitable for X-ray crystallography which leads to difficulties in assessing the structure of the materials. One of the many metalloligands that are known for their ease of crystallizing are metalloporphyrins. They are also of broad interest for their photochemical properties, being present naturally as biocatalysts or light harvesting antennas. Incorporation of a rigid porphyrinic core into a ultra-stable network provided by Zr-based MOFs was studied recently.²⁶ A representative example of such a structure is given by the CPM-99X (X = H₂, Zn, Co, Fe) frameworks developed by Feng *et al.*^{26a} Using a tetratopic porphyrin ligand together with a Zr(IV) source, cubic zirconium-porphyrin frameworks were obtained and characterized by single crystal X-ray spectroscopy. Figure 1.12 shows the representation of CPM-99Zn constructed from the Zn(II)-metallated tetratopic porphyrin. A cubic network is observed, in which faces are occupied by the planar porphyrin units and the vertices by the Zr₆ clusters. The edges possess a length of about 2.5nm. The rational use of biphenylcarboxylic acid groups allowed restoring the coplanarity between all four ligands. Indeed, studies showed that using TCPP (TCPP = tetrakis(4-carboxyphenyl)-porphyrin) networks with Zr₆ cluster of lower connectivity were obtained.²⁷ Despite the considerable voids within the networks, they were stable up to 450°C. Interestingly, upon pyrolysis of CPM-99X into their carbonized analogues CPM-99X/C, the networks retained their cubic geometry and were found to be efficient catalyst for the oxygen reduction reaction. The carbonized sample obtained from the Fe(II) derivative showed catalytic activity, comparable to the well-known 20% Pd/C used daily in the lab, but with a much higher chemical stability. This fascinating work highlights that combining Zr₆ cluster and porphyrin ligands allows synthesizing materials possessing both chemical and thermal stability, and high catalytic activities.

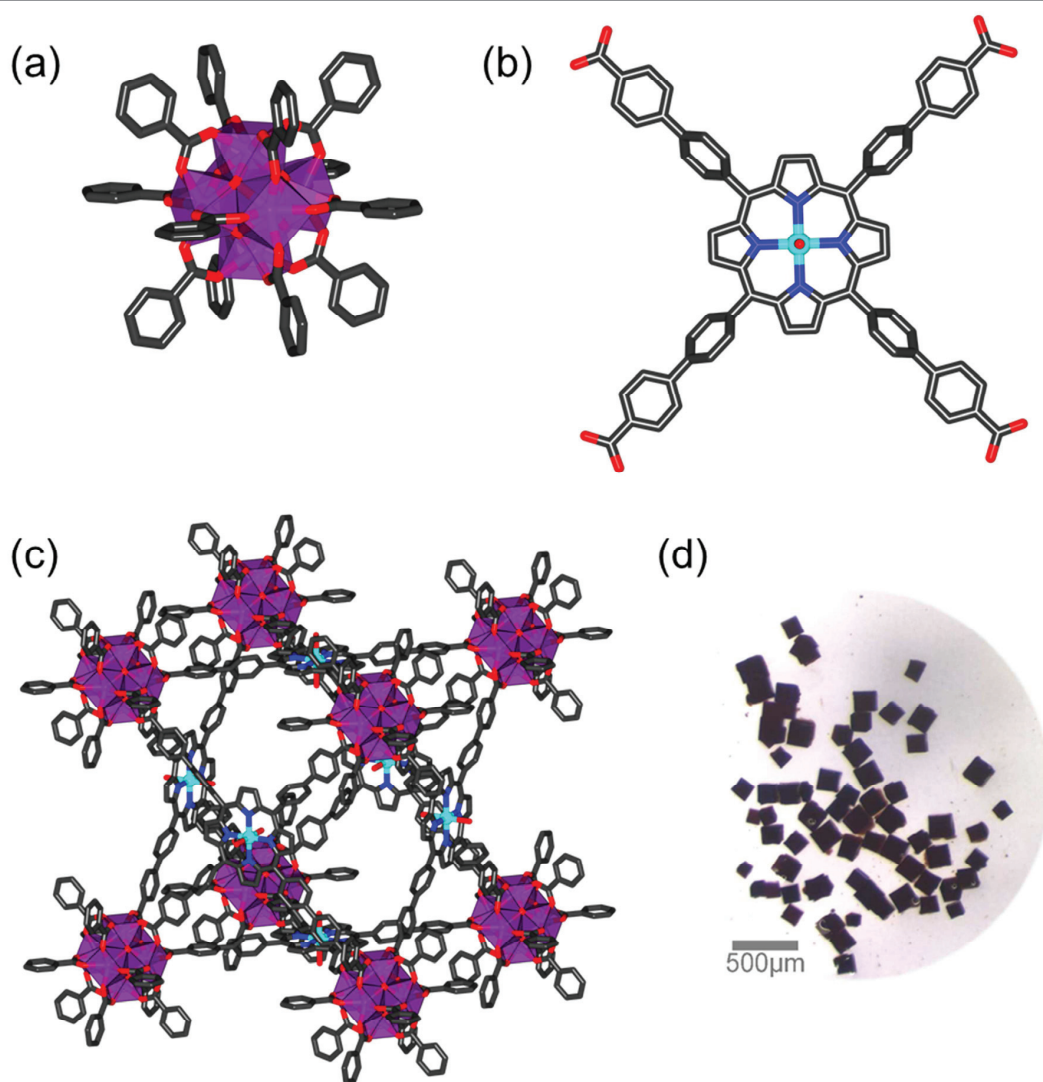


Figure 1.12 – (a) Molecular representation of Zr₆ cluster within CPM-99Zn; (b) Tetratopic carboxylate ligand used in this study, showing the coplanarity between each carboxylate moiety; (c) Part of the molecular structure of CPM-99Zn in the crystal. Color coding: C: grey; N: blue; O: red; Zn: cyan; Zr: purple. Hydrogen atoms and solvent molecules have been omitted for clarity; (d) Photography of crystals of CPM-99Zn. Reprinted with permission from reference [26a]. Copyright 2015 American Chemical Society.

The incorporation of metalloligands into network structure can also be pursued for other applications. One representative example was provided by Lin *et al.* who reported in 2008 the construction of a nanoscale coordination polymer (NCP) out of Pt(IV) metalloligands appended with carboxylic acids (dscp, disuccinatocisplatin) and Tb³⁺ ions (Figure 1.13a,b).²⁸ Recently, much attention has been given to applications of nanoscale materials for clinical purposes, mainly for particle-mediated drug delivery for cancer therapies.²⁹ Lin *et al.* showed that this analogon of cisplatin, a blockbuster anticancer drug, could be incorporated in a NCP, leading to a material that could release specifically the Pt-based drug in a controlled manner *via* encapsulation in amorphous silica shells (Figure 1.13b,c). The authors demonstrated the anticancer activity of the released

Pt-based drug in *in vitro* experiments, opening a new route for delivery cargoes such as anticancer, imaging or other medically important agents.

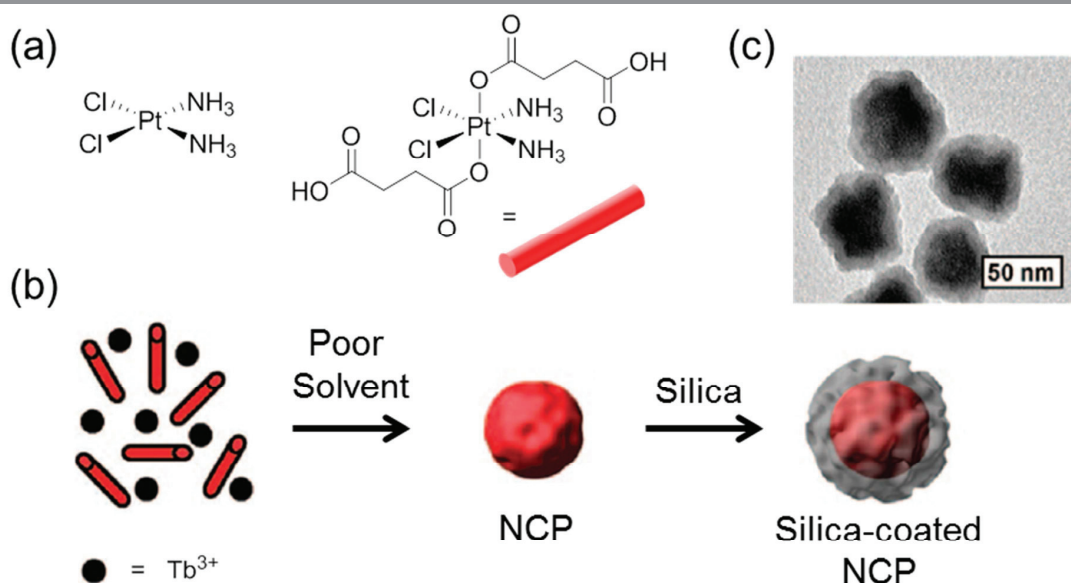


Figure 1.13 – (a) Molecular structure of cisplatin (left) and disuccinatocisplatin (right) used in this study; (b) Synthesis of NCP upon coordination of dicarboxylate ligand to Tb^{3+} ions and subsequent coating with amorphous silica; (c) Scanning-electron microscopy photograph of Silica-coated NCP. Adapted with permission from reference [28]. Copyright 2008 American Chemical Society.

In the cases of the previously described CMOF-5 (Figure 1.11) and CPM-99X (Figure 1.12), the metalloligands were always sitting on the faces or the edges of the networks, with metal clusters located on the vertices. Carlucci *et al.*³⁰ and Burrows *et al.*³¹ used a different approach, in which the role of the donor and acceptor were exchanged compared to CMOF-5, CPM-99X and most of other MOFs. They used a β -diketonate ligand functionalized with two pyridyl moieties to coordinate $\text{Ga}(\text{III})$, $\text{Al}(\text{III})$ or $\text{Fe}(\text{III})$ octahedral ions. Upon coordination of three of these β -diketonate ligands, the resulting metal complexes were sharing 6 pyridyl rings oriented in a divergent fashion, as shown in Figure 1.14. Further coordination of the pyridyl groups of to $\text{Ag}(\text{I})$ ions led to the formation of a coordination polymer sharing MOF-5 topology, thus being constituted of metal ions on the edges and metalloligands as the vertices. Interestingly, the $\text{Fe}(\text{III})$ analog formed a range of two- and three-dimensional polymers whose topology and stoichiometry was found to be dependent on the counterion from the $\text{Ag}(\text{I})$ salt.

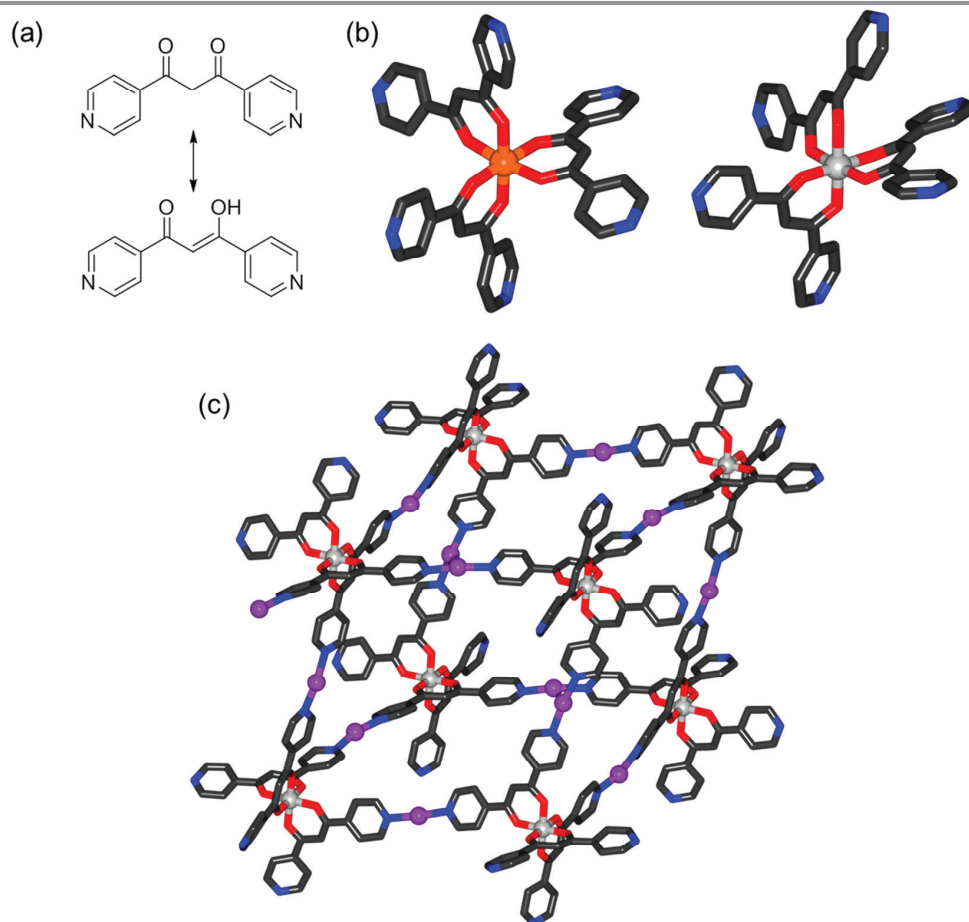


Figure 1.14 – (a) Structure of the β -diketone functionalized with pyridyl groups, showing the keto-enol tautomerism; (b) Molecular structure of the Fe(III) complex (left) and Al(III) complex; (c) Part of the network structure of the Al(III) complex coordinated to Ag(I) ions. Color coding: C: grey; Ag: purple; Al: light grey; Fe: orange; N: blue; O: red. Hydrogen atoms and solvent molecules have been omitted for clarity.

Capitalizing on the chemical stability and the high directionality offered by the Zr_6 cluster, Lin *et al.* incorporated photocatalysts in Zr-based MOFs.³² They modified several linear, ditopic carboxylate ligands bearing a 2,2'-bipyridyl motif by attaching monomeric Ir(III), Re(I) or Ru(II)-based catalysts (Figure 1.15a). These metal complexes are known to act as water oxidation catalysts (WOCs) (**1.17–1.19**), as photochemical CO_2 reduction catalysts (**1.20**), or as catalysts for other photocatalytic organic transformations (**1.21–1.22**). The water oxidation reaction is of particular interest since it is one of the half-reactions in artificial photosynthesis,³³ and photocatalytic reduction of CO_2 into fuels or other value-added products is of paramount importance nowadays.³⁴ Owing to the equivalent size of the M(III)-functionalized short ditopic ligands shown in Figure 1.15a and 4,4'-biphenylcarboxylic acid, the authors synthesized an isostructural UiO-67 analogue containing a small amount of the catalyst (2-8 wt %). Zr-MOFs containing **1.17–1.20** showed expected WOCs or photocatalytic CO_2 reduction properties, and Zr-MOFs composed of **1.21–1.22** were used for the photocatalytic aerobic amine coupling, for the aerobic thioanisole oxidation, and for aza-Henzy

reactions. All of these Zr-MOFs-based catalysts could be recycled thanks to the robustness of the material, and the modular nature of this approach (doping catalytically inactive UiO-67 by incorporating small amount of catalyst-containing ligands) allows incorporating other relevant catalysts. Using the elongated metalloligand **1.23**, they synthesized another UiO-67 analog constituted exclusively of this ligand and Zr_6 clusters. Using this Zr-MOF, Lin *et al.* studied the mechanistic details of water oxidation reactions. This would not have been possible without the well-defined catalytic sites, immobilized in the three-dimensional architecture.

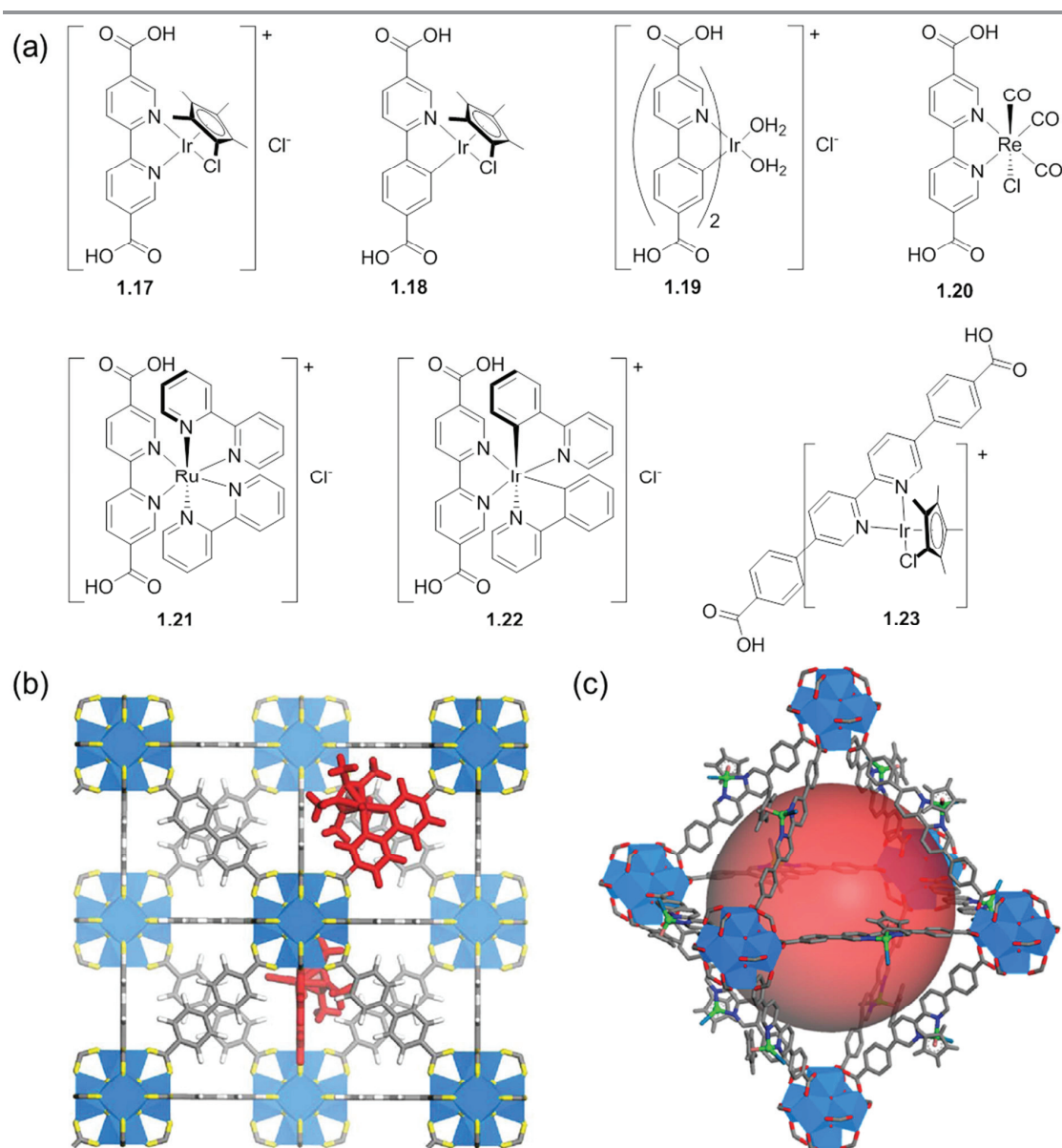


Figure 1.15 – (a) Structure of the different metalloligands **1.17–1.23**; (b) Structure model of UiO-67 analog doped with ligand **1.17**; (c) Structure model of UiO-67 analog built from **1.23**. Reprinted with permission from references [32]. Copyright 2011-2012 American Chemical Society.

1.2.3 Conclusion

The metalloligands presented in the last section are only the tip of an iceberg containing many other classes. These examples were chosen to illustrate some selected applications that would have been difficult, if not impossible, to achieve with purely organic ligands. Amongst the other classes of metalloligands that have not been described, one can cite acetylacetonate-based metalloligands (**1.24**),³⁵ dipyrin-based metalloligands (**1.25**),³⁶ complexes bearing mixed-ligands moieties (**1.26**),³⁷ oxamide- and oxamate-based³⁸ metalloligands (**1.27**), pyridine-amide complexes,³⁹ metal-alkynyl complexes,⁴⁰ terpyridyl-based organometallic complexes,⁴¹ and counting. Figure 1.16 summarizes the structures of some metalloligands present on this list. Metalloligands do possess intrinsic characteristics that can be found in their subsequent supramolecular assemblies. These characteristics, whose non-exhaustive list is composed of rigidity, structure-oriented predictability, chirality, photochemical activity, catalytic activity or even ease of synthesis as shown before, can derive either from the metal ion incorporated in the metalloligand or from the metalloligand itself. Despite the tremendous amount of metalloligands described in the literature, and their incontestable interesting properties, they only represent a small fraction of the supramolecular assemblies described so far. Still, they then represent a rising class of ligands that will tend to increase in the next years, and this thesis contributes humbly to this rise. In the next section, a very specific class of metalloligands, boronate-ester-capped clathrochelates, will be discussed.

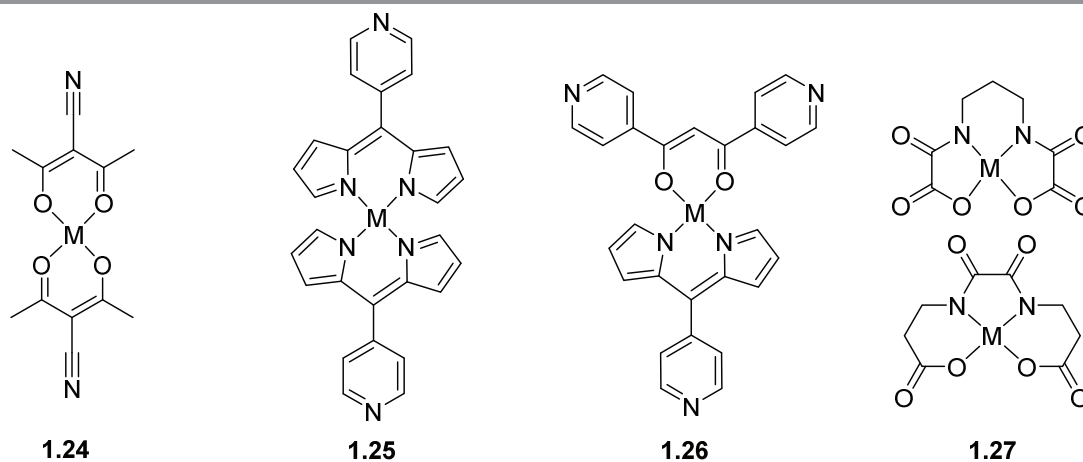
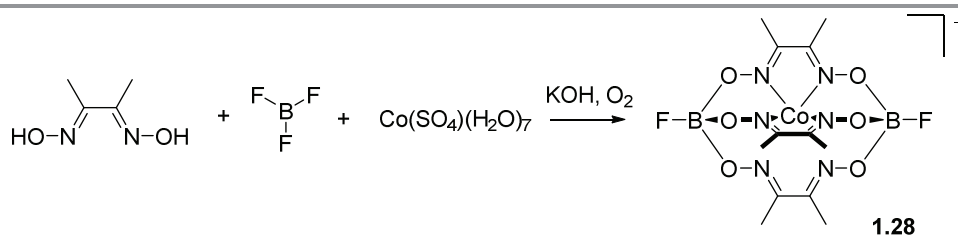


Figure 1.16 – Structure of some metalloligands composed of acetylacetonate (**1.24**), dipyrin (**1.25**), mixed dipyrin-β-diketonate (**1.26**) or oxamate/oxamide (**1.27**) ligands.

1.3 Boronate ester-capped clathrochelates complexes

1.3.1 Mononuclear boronate ester-capped clathrochelate complexes

The first definition of clathrochelates was given by Busch in 1964.⁴² He described clathrochelates as complexes composed of cage-type ligands encapsulating a central, coordinatively saturated metal ion. This broad definition of clathrochelates has evolved with time. Now, a clathrochelate is defined as a complex composed of one macrobicyclic ligand containing donor atoms that coordinatively saturate the central metal ion, isolating it from the exterior. Based on the definition of a macrobicyclic ligand, two atoms (or atom groups) are part of all three macrocycles. These are called capping moieties. This section will focus on one particular class of clathrochelates, those which are capped with boronate esters units. Rose described in 1968 the synthesis of the Co(III) complex **1.28** whose central atom is coordinated to three dimethylglyoximate ligands, and having BF moieties as capping units, forming boronate esters with the oxygen of the dimethylglyoximate chelating ligands (Scheme 1.2).⁴³



Scheme 1.2 – Synthesis of tris(dimethylglyoximate)-based clathrochelate **1.28** sharing boronate esters as capping groups.

This landmark discovery has not been limited to dimethylglyoxime ligands. Other groups can be introduced on the dioximes, allowing structural variations and incorporation of functional groups in the periphery of the clathrochelates. Two distinct approaches can be used in order to reach this goal: the first one requires synthesizing the clathrochelate from its sub components, with an isolated dioxime ligand. The second one is based on the post-synthetic modification of a preformed clathrochelate core, entailing reactive functional groups on the initial complex (mostly using dichloroglyoxime).⁴⁴ The first approach can also be used to obtain clathrochelates bearing different dioxime ligands. Indeed, pioneering studies of clathrochelates formations by Rose⁴⁶ revealed that the formation of the macrobicyclic complex occurred in two distinct steps. The rate-determining step is the formation of a complex in which the central metal atom is coordinated by three dioximes. This step is then followed by the reaction of the Lewis-acidic boron source, mainly boronic acids, with the oxygens of the dioximes, closing the macrobicyclic clathrochelate. By choosing appropriate stoichiometry and metal sources, it is possible to isolate a $M(\text{dioxime})_2(\text{capping})_2$, which can further react with another dioxime ligand to yield assymetric complexes. A tremendous work has been done

on the synthesis of numerous dioxime ligands, some of which are represented in Figure 1.17. Nowadays, due to the development of cross-coupling reactions, many boronic acids are commercially available, and synthetic routes towards the synthesis of new boronic are well-established. One can see that by combining the two approaches and given the library of dioximes available, it is possible to synthesize an almost infinite number of different complexes. The following section will highlight some representative examples.

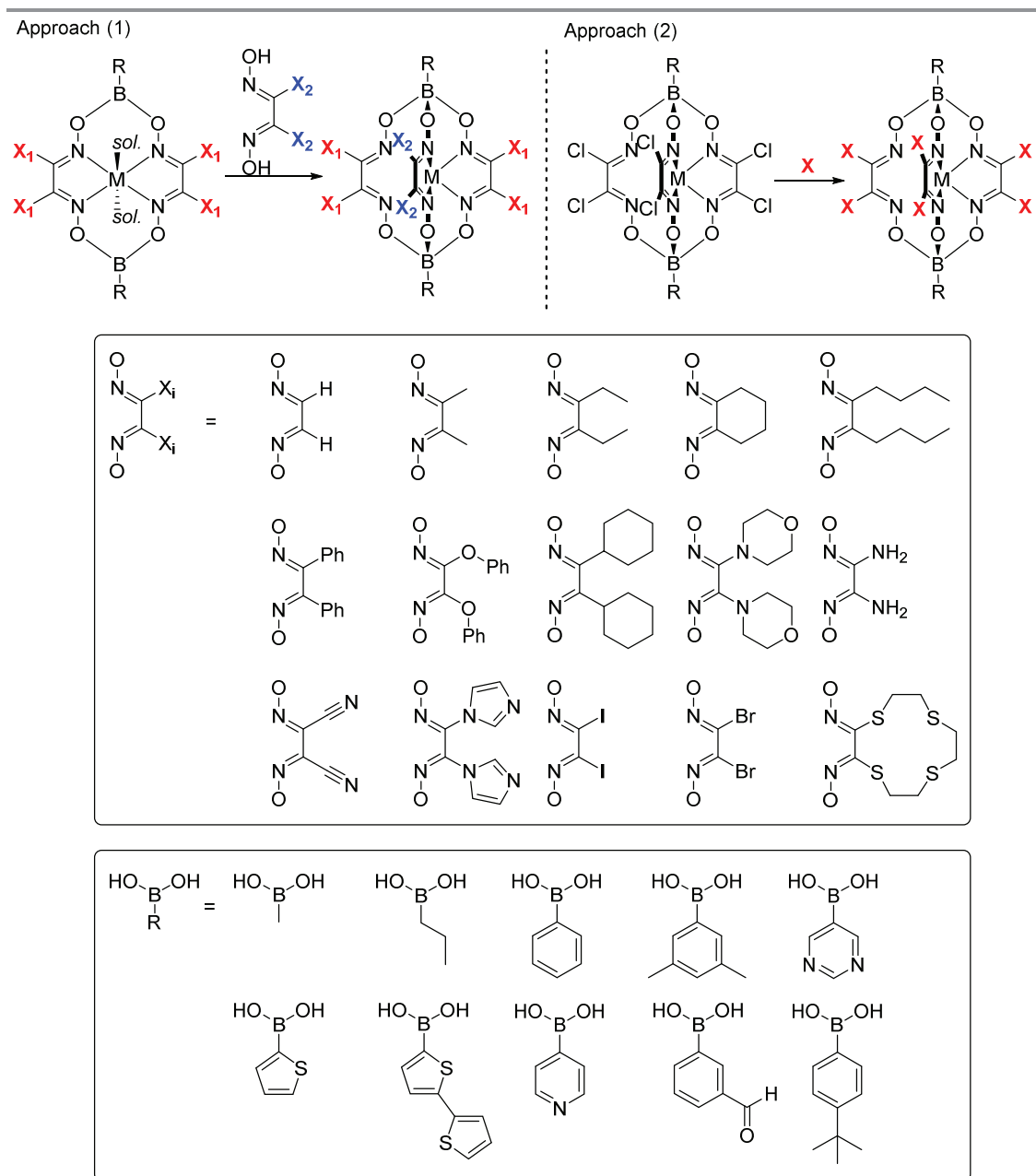


Figure 1.17 – Structure of some selected example of dioximes and boronic acids. The top part represent the two approaches followed to synthesize clathrochelates (1) Sequential synthesis using one or two dioximes ligands and (2) post-synthetic modification of clathrochelates constructed from dichloroglyoxime.

1.3.2 Mononuclear clathrochelate complexes as supramolecular building blocks

This section does not claim to cover all application of mononuclear boronate esters-capped clathrochelates, since this is way beyond the scope of this thesis. Some of the mononuclear clathrochelates have been studied for their electrocatalytic⁴⁵ or photocatalytic⁴⁶ properties, or for structural or analytical studies.⁴⁷ For sake of clarity, this section will exclusively focus on the use of mononuclear, boronate esters-capped clathrochelates as building blocks for supramolecular chemistry. To avoid redundancy, this section will now refer to mononuclear boronate esters-capped clathrochelates as simply clathrochelates. The first example of incorporation of clathrochelates into a supramolecular assembly was published in 2000 by Grzybowski *et al.* They synthesized a tris(oximehydrazone) Fe(II) clathrochelate complex bearing one pyridyl moiety as one of the capping groups. Its subsequent coordination to a Co(III) cobaloxime, yielding complex **1.29** was elucidated by X-Ray crystallography (Figure 1.18).

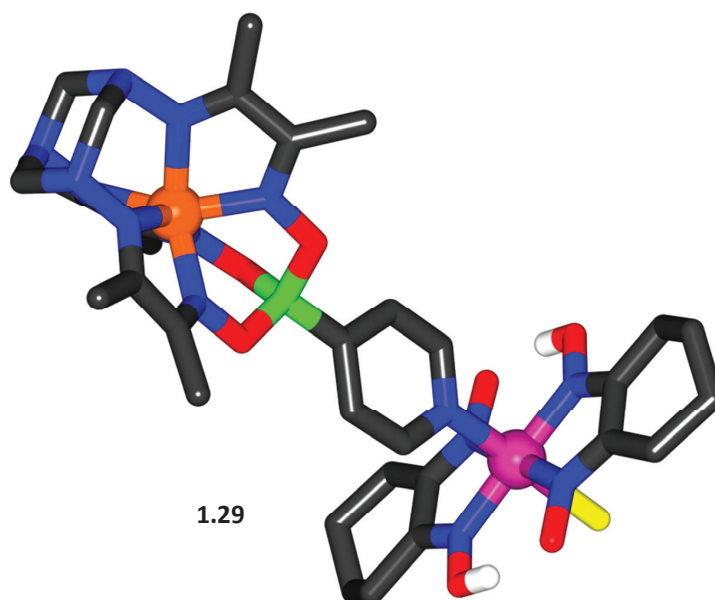


Figure 1.18 – Coordination of the complex **1.29**. Color coding: C: grey; H: white; B: green; Br: yellow; Co: purple; Fe: orange; N: blue; O: red. Most hydrogen atoms, unbound anions (PF_6^-) and solvent molecules have been omitted for clarity.

This first example proved that clathrochelates complexes were suited for applications as metalloligands in supramolecular chemistry. In 2013, Severin *et al.* reported the synthesis of a 4,4'-bipyridyl Fe(II) clathrochelate (**1.30**) of 1.5 nm length by reaction between nioxime (1,2-cyclohexanedione dioxime), FeCl_2 and 4-pyridylboronic acid.⁴⁸ Clathrochelate **1.30** was subsequently incorporated into the discrete molecular square **1.31** upon reaction with *fac*- $\text{ReCl}(\text{CO})_3(\text{CH}_3\text{CN})_2$ (Figure 1.19a). The authors selected this 90° orientation complex to prove that the steric bulk brought by the lateral cyclohexyl substituents was not a pitfall for its successful use.

Furthermore, the CO ligands were used as a spectroscopic (IR) probe to prove that the electron-donating properties of the pyridyl groups on the clathrochelates were similar to 4,4'-bipyridine ligand. The same clathrochelate was successfully incorporated in a three-dimensional coordination polymer. This CP was by solvothermal reaction between Zn(II), 4,4'-biphenyldicarboxylic acid (bpda) and **1.30**. X-ray structural analysis revealed that **1.30** subunits were pillaring layers of $\text{Zn}(\text{bpda})_2$, composed of Zn-based paddlewheels clusters (Figure 1.21b). Conversely to many other pillared systems based on bipyridyl ligands of similar size, which are often three-fold interpenetrated,⁴⁹ they observed a reduced, two-fold interpenetration. This was attributed to the steric bulk induced by the lateral cyclohexyl substituents, preventing further interpenetration.

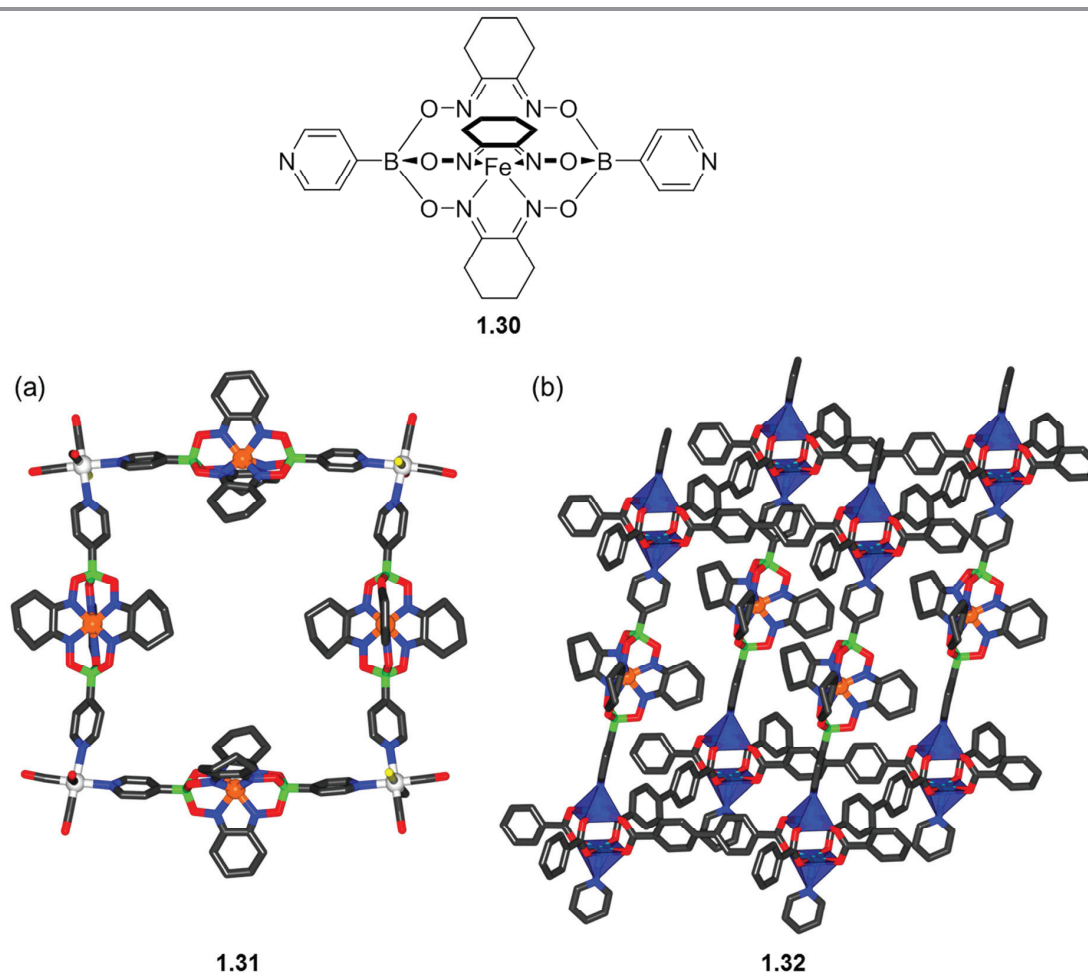


Figure 1.19 – (a) Molecular structure of square **1.31** constructed from 4,4'-bipyridyl decorated clathrochelate **1.30**; (b) Part of the molecular structure of three-dimensional CP **1.32**. Color coding: C: grey; H: white; B: green; Cl: yellow; Fe: orange; N: blue; O: red; Re: pale grey; Zn: cyan. Most hydrogen atoms, unbound anions (PF_6^-) and solvent molecules have been omitted for clarity.

Jin *et al.* followed a similar strategy to synthesize two heterometallic molecular rectangles based on **1.30** (Figure 1.20).⁵⁰ They first realized a bimetallic Cp^*Ir complex (**1.33**), which was subsequently

coordinated by clathrochelate **1.30**. Using Cp*Ir complexes of different lengths, they were able to isolate molecular rectangles **1.34** and **1.35**, with a nano-scaled cavity of 19 x 11 Å (**1.34**) or 19 x 15 Å (**1.35**). Together with the work of Severin *et al.*, these examples showed that 4-pyridyl-capped clathrochelates can be incorporated into discrete structures, as well as three-dimensional CPs.

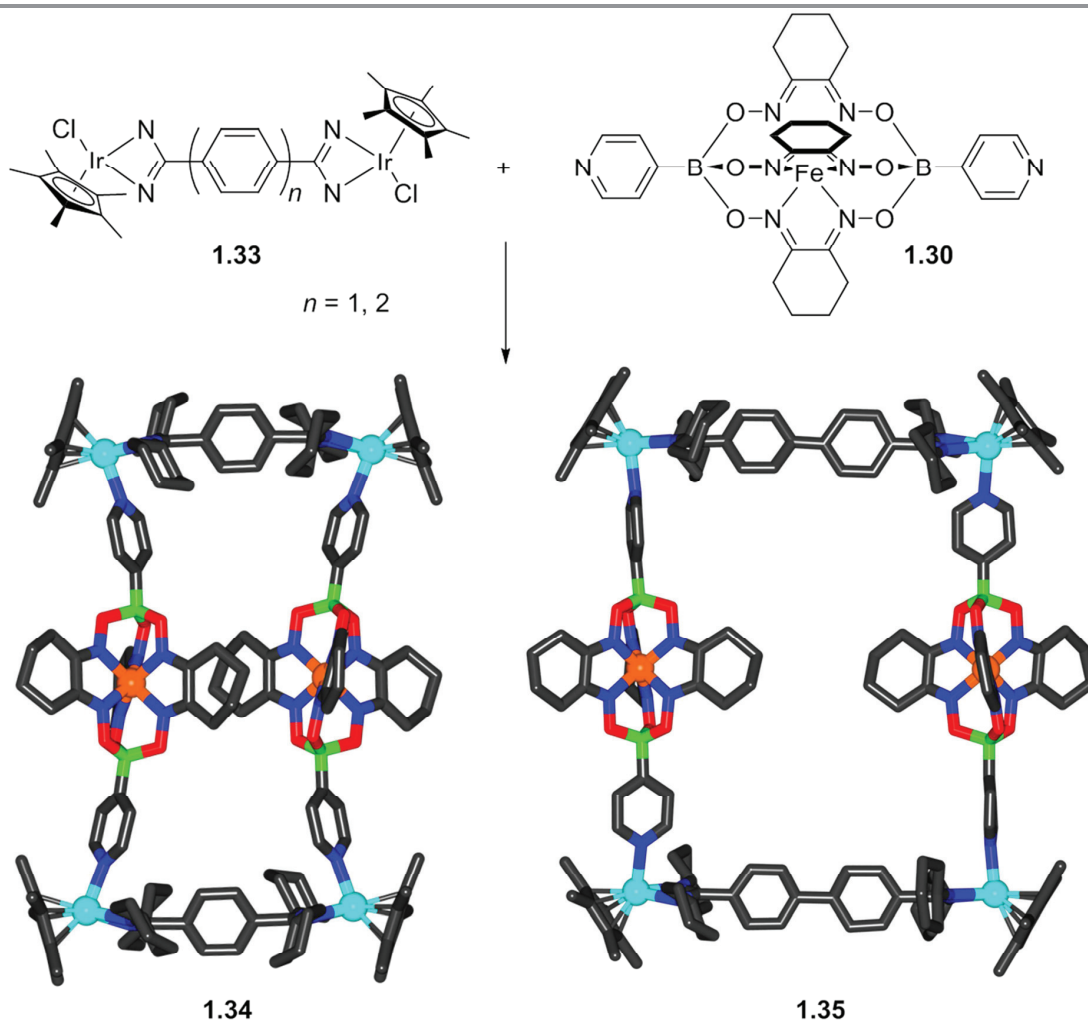


Figure 1.20 – Molecular structure of heterometallic rectangles **1.34** and **1.35** obtained from the subcomponent self-assembly between Cp*Ir complexes and clathrochelate **1.30**. Color coding: C: grey; B: green; Fe: orange; Ir: cyan; N: blue; O: red. Hydrogen atoms, anions (OTf) and solvent molecules have been omitted for clarity.

Ditopic 3-pyridyl terminated ligands are far less common than their 4-pyridyl terminated analogues. Indeed, 3-pyridyl ligands possess an intrinsic conformational flexibility that entropically favors the formation of aggregates containing a smaller amount of building blocks while coordinating to metal ions.⁵¹ Severin *et al.* hypothesized that the steric bulk induced by the lateral dioxime substituents could overcome this entropic contribution, and that supramolecular architectures of larger size could be achieved using 3-pyridyl-decorated clathrochelates. They synthesized clathrochelates **1.36** and **1.37** following a well-established synthetic procedure (Figure 1.21a,b).⁵²

Clathrochelates **1.36** and **1.37** only differ by their lateral substituents: while **1.36** is constructed from dimethylglyoxime, **1.37** is more bulky with its cyclohexyl substituents. Subsequent reaction with naked Pd(II) ions led to the formation of discrete structures of stoichiometry $[\text{Pd}_6(\mathbf{1.36})_{12}]^{12+}$ and $[\text{Pd}_6(\mathbf{1.37})_{12}]^{12+}$. X-ray structural analysis revealed the formation of octahedral cages, with Pd(II) ions located on the vertices (Figure 1.21c). The interior of these cages is hydrophobic, whereas the cages themselves are positively charged. The authors successfully encapsulated a BPh_4^- anion within the cage constructed from **1.36** (Figure 1.21d). Encapsulation of this large anion further proved the intrinsic cavity present within these architectures, and kinetic studies revealed that BF_4^- encapsulation was strongly dependent on the nature of the dioxime substituents.

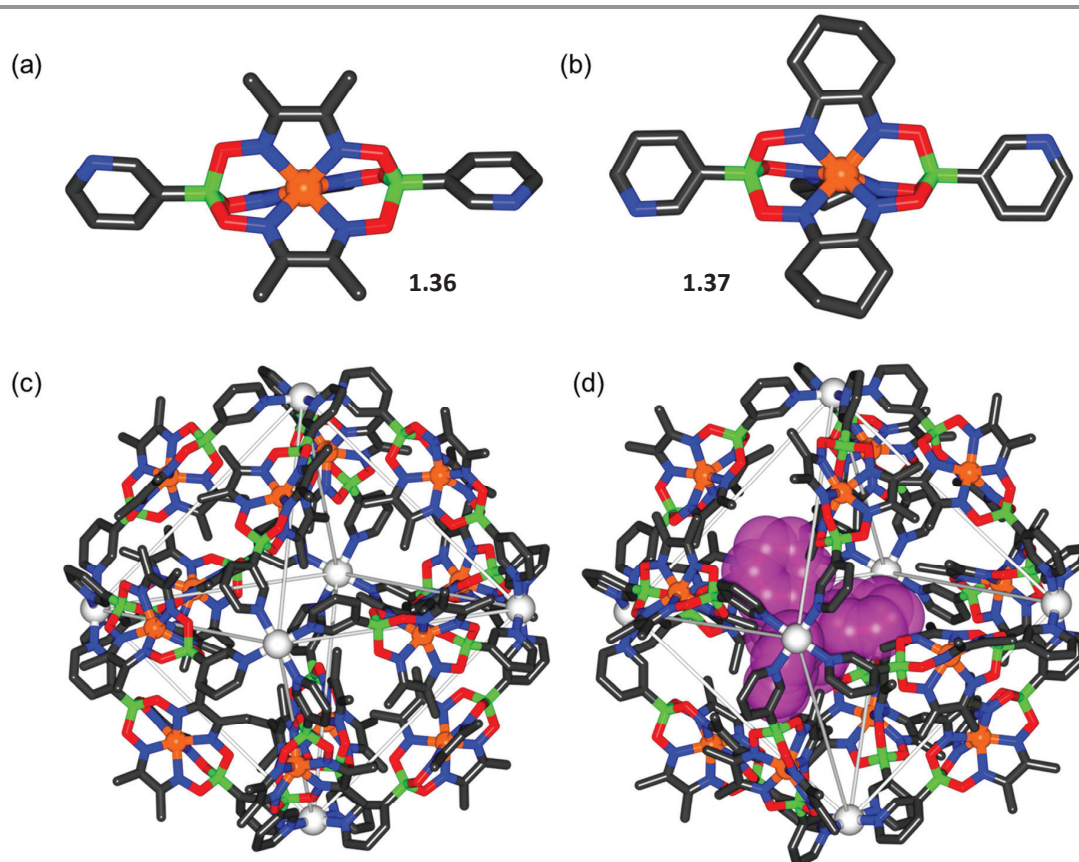


Figure 1.21 – Molecular structures of 3-pyridyl decorated clathrochelates **1.36** (a) and **1.37** (b). Octahedral cages constructed from **1.36** (c) and its subsequent BPh_4^- encapsulation (d). Color coding: C: grey; B: green; Fe: orange; N: blue; O: red; Pd: light grey. Hydrogen atoms, anions and solvent molecules have been omitted for clarity. The purple spacefilling model represents the encapsulated BPh_4^- anion.

Obtaining such large cages from linear 3,3'-bipyridyl ligands was unprecedented, and the authors speculated that the lateral size of the clathrochelates prevented the formation of smaller aggregates. The balance between entropic and enthalpic contributions can be finely tuned using appropriate dioxime ligands. Indeed, Severin *et al.* showed in 2016 that the aspect-ratio (length-to-width ratio) of

clathrochelates was of paramount importance for the construction of supramolecular cages.⁵³ By utilizing a 3,3'-bipyridyl clathrochelate having only hydrogen atoms on the dioximes (**1.38**), they observed the unique formation of a tetrahedron with two doubly bridged edges (Figure 1.22a), having a geometry similar to cages described by Fujita.⁵⁴ On the other hand, by selecting clathrochelate **1.39** having more equatorial steric bulk, i.e. having a smaller aspect-ratio, they observed the formation of an octahedral cage. The concept was extended to other clathrochelates sharing apical formylpyridine substituents. Upon reaction with *para*-toluidine and Fe(II) salts, a clathrochelate composed of methyl substituents on the dioxime led to the formation of a tetrahedron, whereas the more bulky cyclohexyl-decorated showed the formation of a molecular cube.

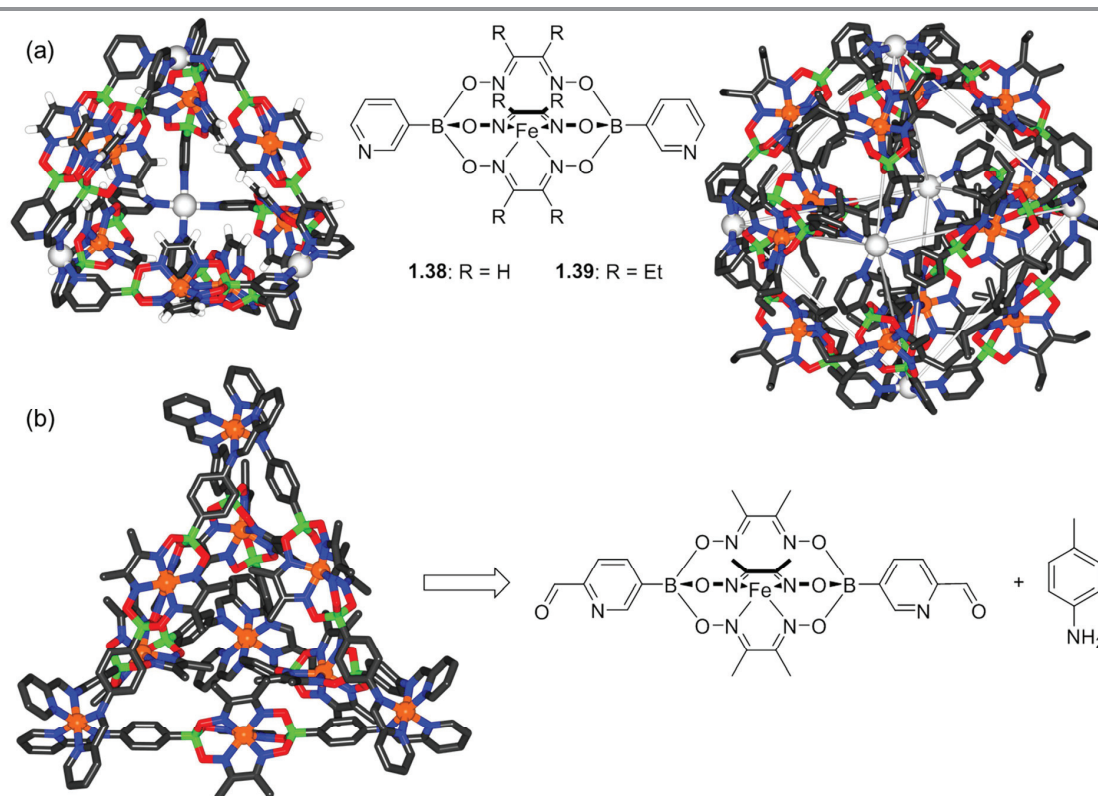


Figure 1.22 – (a) Synthesis of a tetrahedron (left) or octahedron (right) using clathrochelates with different dioxime substituents, (b) Synthesis of a tetrahedron by subcomponent self-assembly between formylpyridine-appended clathrochelate, Fe(II) and *p*-toluidine. Color coding: C: grey; H: white; B: green; Fe: orange; N: blue; O: red; Pd: light grey. Most hydrogen atoms, anions and solvent molecules have been omitted for clarity.

In this work, the authors showed that the length and the lateral size of a clathrochelate could have a dramatic effect on the type of architectures that can be reached. Starting from easily-available starting material, tetrahedral, octahedral, or cubic cages were obtained. Figure 1.23 summarizes the effect of the aspect-ratio on the self-assembly to molecularly defines architectures.

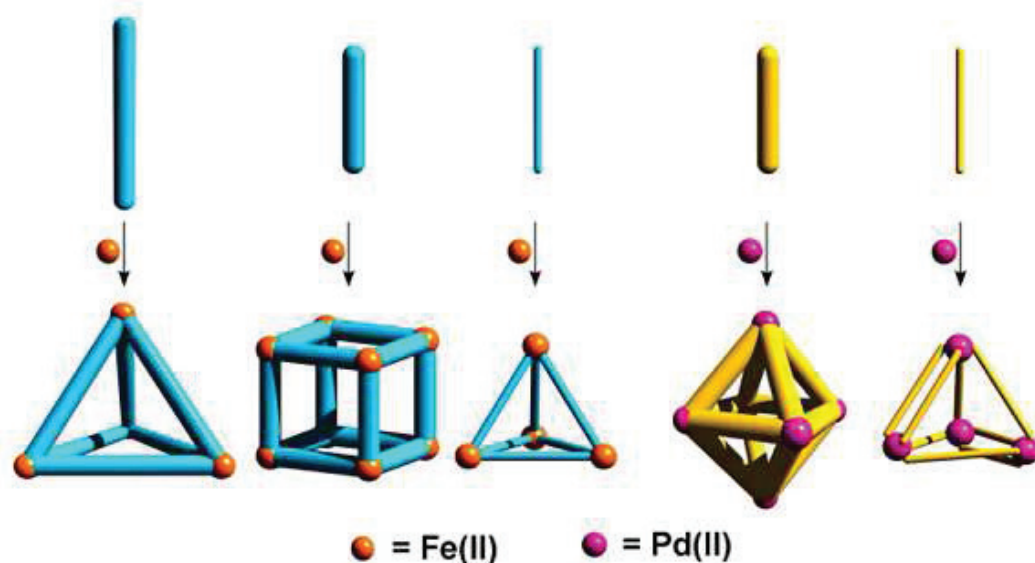


Figure 1.23 – Summary of the molecularly defined architectures reachable with clathrochelates, by closely selecting dioxime substituents and metal sources. Reprinted with permission from reference [53]. Copyright 2016 American Chemical Society.

1.4 Dinuclear boronate ester-capped clathrochelate complexes

In 1990, Chaudhuri *et al.* reported the synthesis of a metallamacrobicycle composed of three dimethylglyoxime ligands chelating a central $M(II)$ ion ($M = Cu, Zn, Ni, Co, Fe, Mn$).⁵⁵ Conversely to the work described in section 1.3, they used a terminal *fac*-protected $Fe(III)$ complex as the capping groups. The $Fe(III)$ capping units are composed of a tridentate cyclic amine (1,4,7-trimethyl-1,4,7-triazacyclononane) as shown in Figure 1.24a. The resulting clathrochelates can be seen as linear, heterotrimetallic complexes that were investigated for their magnetic properties. Further studies explored the formation of other trimetallic species using the same strategy, by varying the external metal complexes ($M = Cr, Mn, \dots$) or the central chelated metal center, whose magnetic properties were of major concerns (Figure 1.24b).⁵⁶ Few year later, the same group explored the magnetic exchange coupling in a nearly linear $Fe(III)Ni(II)Ni(II)Fe(III)$ complex.⁵⁷ As for their previous work, they used a *fac*-protected $Fe(III)$ complex, however the dioxime used in this study was of a different nature. By using 2,6-diformyl-4-methylphenol dioxime, they were able to coordinate two $Ni(II)$ centers upon coordination *via* the N-donor and O-donor atoms on the dioximes. This complex was not classified as a clathrochelate complex, since only two dioximes were chelating the central $Ni(II)$, the remaining coordination sites being occupied by solvent (MeOH) molecules. Complete isolation of the central metal ions was achieved in 2006,⁵⁸ where Chaudhuri *et al.* reported the synthesis of tetranuclear complexes based on 2,6-diformyl-4-methylphenol dioxime encapsulating $Mn(II)$ ions. Conversely to complexes based on $Ni(II)$, these complexes are composed of trisphenoxo-bridged dimanganese(II) cores, and are capped with $M(III)$ ($M = Fe, Cr$) or $M(IV)$

(M = Mn) *fac*-protected complexes (Figure 1.24c). Since they were interested in studying the magnetic properties of these complexes, they synthesized a diamagnetic B(III)-capped complex as a dinuclear Mn(II) complex (Figure 1.24d). The idea was to explore the effect of the terminal paramagnetic metal complexes in these tetranuclear chelated complexes. The B(III)-capped complexes was obtained by the reaction between methylboronic acid, the dioxime and a Mn(II) salt. Interestingly, this boronate esters-capped clathrochelate is negatively charged and was isolated as its triethylammonium salt.

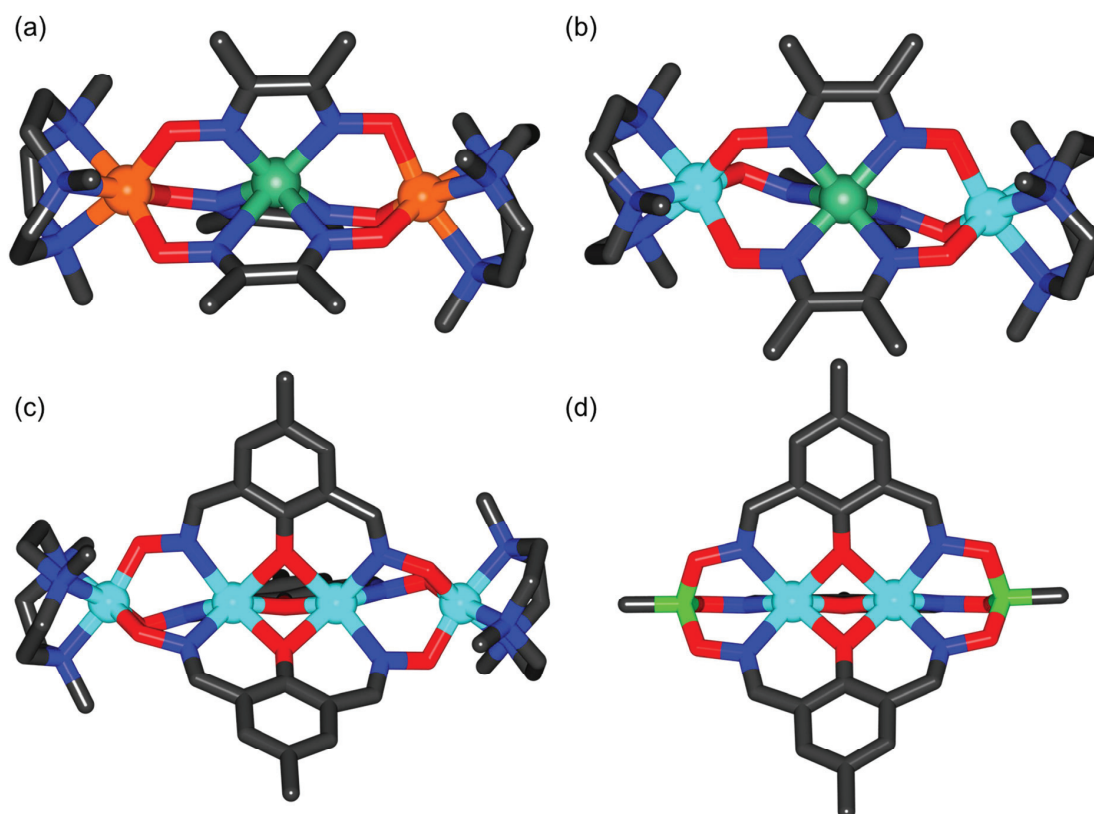


Figure 1.24 – (top): Molecular structures of (a) Fe(III)Cu(II)Fe(III) and (b) Mn(III)Cu(II)Mn(III) clathrochelates based on tris(dimethylglyoxime) ligands. (bottom): Molecular structures of (c) Mn(III)Mn(II)Mn(II)Mn(III) and (d) B(III)Mn(II)Mn(II)B(III) tetranuclear clathrochelates developed by Chaudhuri *et al.* Color coding: C: grey; B: green; Cu: dark green; Fe: orange; Mn: cyan; N: blue; O: red. Hydrogen atoms, solvent molecules, anions for (a) and (b) and cations for (c) and (d) have been omitted for clarity.

1.5 Aims of the project

The work of Chaudhuri on dinuclear clathrochelates described in section 1.4 showed that it was possible to encapsulate two metal ions using dinucleating phenol-dioximes. Moreover, many similarities can be found between the synthetic routes towards tris(dioxime) clathrochelates described by Voloshin and Severin and the B(III)-capped clathrochelate developed by Chaudhuri. Indeed, they are obtained by reaction of dioxime ligands, metal salts and boronic acids. This prompted us to explore the chemistry of dinuclear clathrochelates in the context of supramolecular chemistry. The versatility of tris(dioxime)-based clathrochelates, their rigidity as well as their modular nature, combined with the anionic nature of the dinuclear M(II) core would represent a vast, new playground for supramolecular chemists. We hypothesized that the anionic character of these clathrochelates would have a strong influence on the stability of supramolecular architectures.⁵⁹ Preliminary work in this direction was performed in our lab by Dr. Mirela Pascu who realized pyridyl-functionalized M(II) (M = Zn, Mn, Co) clathrochelates from 2,6-diformyl-4-methylphenol dioxime ligands. This work showed that the synthesis of dinuclear clathrochelates was feasible with other boronic acids than methylboronic acid used by Chaudhuri (Figure 1.25).⁶⁰

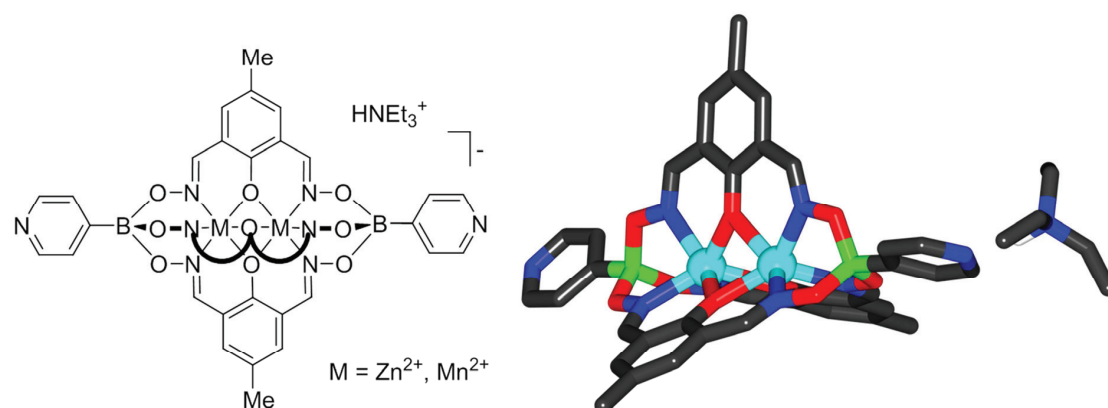


Figure 1.25 – Molecular structure of a 4-pyridyl functionalized dinuclear, anionic Zn(II) clathrochelate. Color coding: C: grey; H: white; B: green; Mn: cyan; N: blue; O: red. Most of hydrogen atoms and solvent molecules have been omitted for clarity.

While performing joint work together with Dr. Clément Schouwey, the influence of these anionic clathrochelates on the stability of a molecular square (**1.40**) was studied. The synthesis of the clathrochelate used in this study will be described in section 2.2, but the synthesis of the molecular square **1.40** (Figure 1.26) as well as the stability assessments are to the credit of Dr. Clément Schouwey. Molecular square **1.40** was obtained upon reaction of a *cis*-protected Pt(II) corner and the clathrochelate. The stability of this complex was then compared with that of square **1.5** (Figure 1.3). By adding competing *d*₅-pyridine to the solution of **1.5**, rupture of the assembly was observed. The

Chapter 2 Dinuclear clathrochelates functionalized with pyridyl groups

The results presented in this chapter detail the synthesis of homometallic dinuclear Co^{2+} , Mn^{2+} and Zn^{2+} clathrochelates decorated with pyridyl groups, following either a direct synthesis approach or the surface functionalization via Pd-catalyzed cross-coupling reactions. Subsequent incorporation of the clathrochelates into two- or three-dimensional CPs as well as discrete structures are presented. Part of the results presented in this chapter were published in “Anionic Bipyridyl Ligands for Applications in Metallasupramolecular Chemistry”, Mirela Pascu, Mathieu Marmier, Clément Schouwey, Rosario Scopelliti, Julian J. Holstein, Gérard Bricogne and Kay Severin, *Chem.-Eur. J.*, 2014, **20**, 5592,⁶⁰ and in “Surface functionalization of dinuclear clathrochelates via Pd-catalyzed cross-coupling reactions: facile synthesis of polypyridyl metalloligands”, Mathieu Marmier, Giacomo Cecot, Basile F. E. Curchod, Philip Pattison, Euro Solari, Rosario Scopelliti and Kay Severin, *Dalton Trans.*, 2016, **45**, 8422.⁶¹

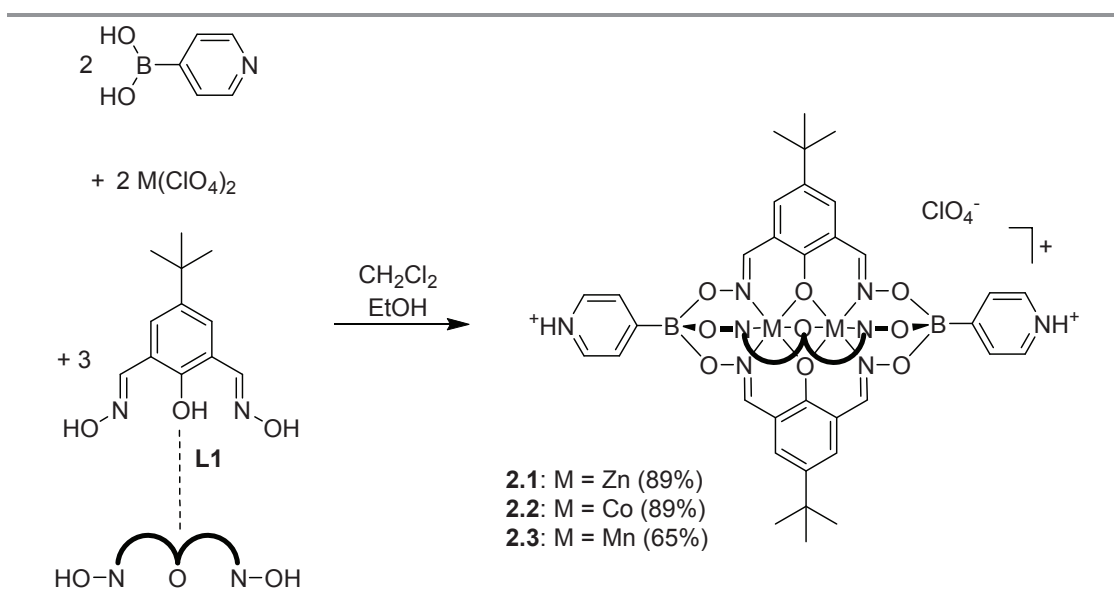
2.1 Introduction

The work described in this chapter represents a continuation of the work performed by Dr. Mirela Pascu, who designed and synthesized pyridyl-functionalized M(II) (M = Zn, Mn, Co) clathrochelates from 2,6-diformyl-4-methylphenol dioxime ligand, as discussed in section 1.5. Polypyridyl ligands are of paramount importance in structural supramolecular chemistry. The simplest bipyridyl ligand, 4,4'-bipyridine, is the most common ditopic N-donor molecule incorporated in supramolecular architectures. Naturally, many variants of bipyridyl ligands have been used, for example by changing the length, rigidity, steric hindrance of the ligands. Moreover, the use of metalloligands, some examples of which having been detailed in Chapter 1, allowed the synthesis of materials possessing new properties (catalytic activities, redox properties, ...) in a relatively simple way. Extension of the ditopic nature to higher numbers of coordinating units led to the synthesis of more complex systems, from discrete complexes to infinite two- or three-dimensional assemblies. The work of Severin *et al.* showed that tris(dioxime) clathrochelates based on Fe(II) core can be successfully incorporated into supramolecular complexes, and the experiments performed by Dr. Clément Schouwey (section 1.5) showed that anionic Zn(II) clathrochelates tended to form supramolecular assemblies of higher stability. This chapter describes the synthesis of various pyridyl-based anionic clathrochelates, and then lists the different assemblies that were obtained using these complexes.

Part of section 2.2 is adapted with permission from reference [60]. Copyright 2014 WILEY-VCH Verlag GmbH & Co. KGaA, Weinheim.

2.2 Direct synthesis of polypyridyl-decorated clathrochelates

The initial goal of this project was the synthesis of 4-pyridyl-capped dinuclear clathrochelates, and their incorporation into supramolecular architectures. Indeed, macrobicyclic M(II) tris(dioximato) complexes ($M^{2+} = \text{Zn, Co, Mn}$) with terminal pyridyl groups were obtained by reaction of $M(\text{ClO}_4)_2(\text{H}_2\text{O})_6$, 4-pyridylboronic acid and 2,6-diformyl-4-tert-butylphenol oxime (**L1**) in a mixture of MeOH and EtOH (1:1) (Scheme 2.1). The products **2.1–2.3** precipitated from the reaction mixture in the form of a microcrystalline material. All complexes were obtained in good to high yields (**2.1**: 88%; **2.2**: 89%; **2.3**: 65%). Since the reactions were performed without addition of a base, the clathrochelates were obtained in the diprotonated form with perchlorate as counter anion. The cationic complexes are only soluble in polar organic solvents such as DMF or DMSO.



Scheme 2.1 – Synthesis of the clathrochelates **2.1–2.3**.

The clathrochelates **2.1–2.3** were analyzed by FT-IR and high-resolution mass spectrometry. The diamagnetic Zn complex **2.1** was also characterized by NMR spectroscopy. As expected, only one set of signals was observed for the three phenolatodioximato ligands, revealing the *pseudo*- C_3 symmetry of the complex. The 'free' ligand **L1** shows luminescence with an emission maxima at 387 nm (DMF, $\lambda_{\text{ex}} = 340$ nm). Solutions of the Co(II) and Mn(II) complexes did not show significant luminescence, presumably due to quenching by the paramagnetic metal ions. Clathrochelate **2.1**, however, was highly emissive, with maxima at 445 nm (DMF, $\lambda_{\text{ex}} = 340$ nm). Due to the inert character of the Zn^{2+} ions, the photoluminescence can be assigned to intraligand (IL) and/or ligand-to-ligand charge transfer (LLCT) emissions. The magnetic properties of the Co and Mn complexes were not investigated. However, it is expected that the Mn complex **2.3** shows a very

similar behavior as the previously reported clathrochelate with methylboronate ester capping groups.⁵⁸ For the latter, a magnetic moment of $7.13 \mu_B$ (290 K) and antiferromagnetic exchange coupling between the two paramagnetic Mn(II) centers was observed. Single crystal X-ray structural analysis of **2.1** and **2.2** confirmed the presence of dinuclear clathrochelate cores with terminal pyridyl groups. A graphical representation of the structure of complex **2.1** is given in Figure 2.1, and selected bonds lengths and angles of **2.1** and **2.2** are summarized in Table 2.1. The two M(II) ions in **2.1** and **2.2** are coordinated in a trigonal prismatic fashion by three nitrogen and three oxygen atoms. The latter bridge the two metal ions resulting in M...M distances of 2.9400(17) Å (**2.1**) and 2.9591(10) Å (**2.2**). With 1.490 Å, the average B–O bond distance of the tetragonal boronate esters is similar to what is found for mononuclear clathrochelates with boronate ester caps.^{44,47,48,52,53} The N-atoms of the pyridyl groups in **2.1** and **2.2** are 17.91 Å and 17.87 Å apart from each other. The clathrochelate ligands are thus substantially longer than mononuclear clathrochelates previously described (14.95 Å).⁴⁸ The NH groups of the protonated pyridyl groups are involved in hydrogen bonding to the perchlorate anion (**2.1**: NH...O = 2.729 Å; **2.2**: NH...O = 2.817 Å).

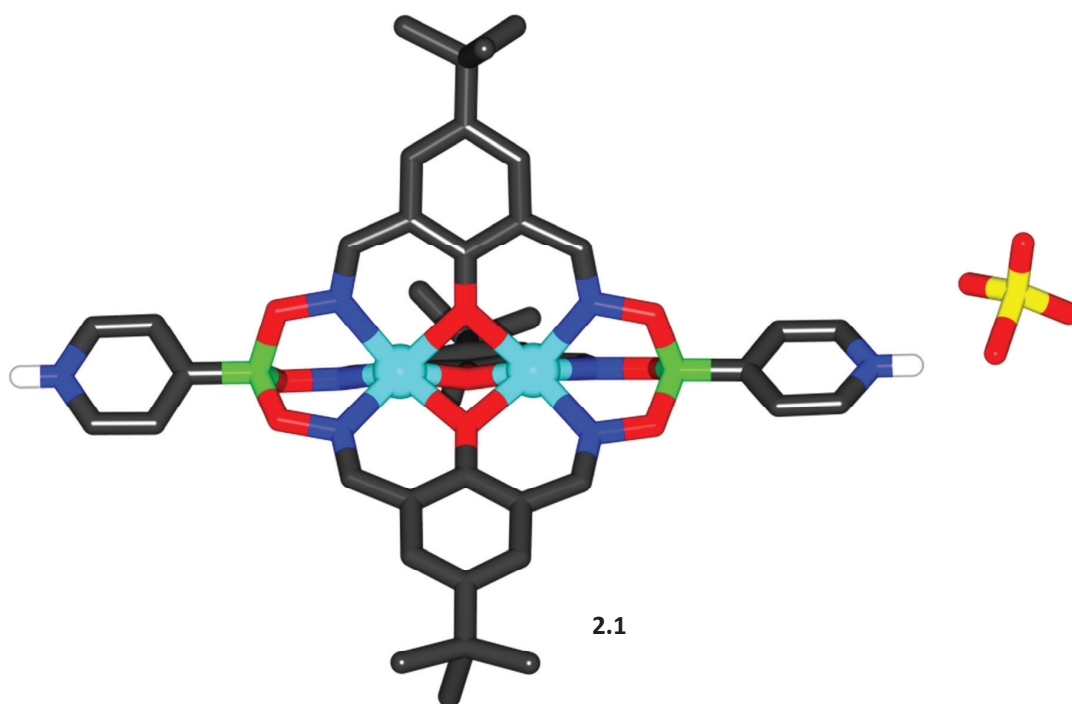
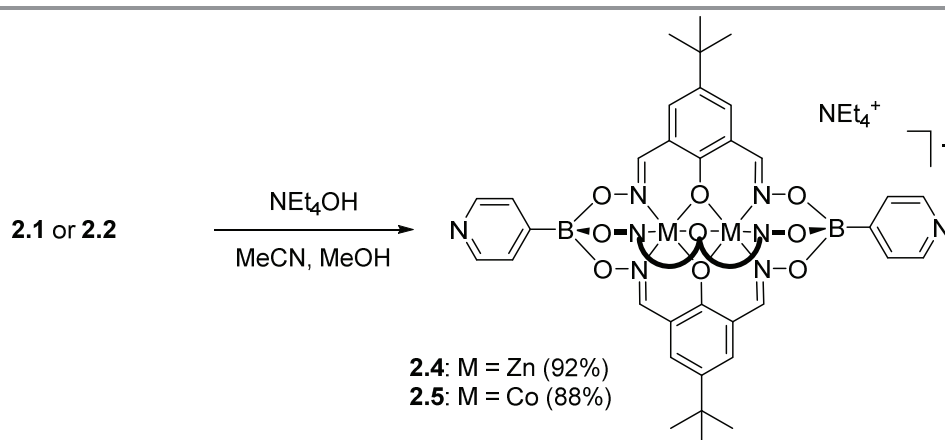


Figure 2.1 – Molecular structure of complex **2.1** in the crystal. Most hydrogen atoms and unbound solvent molecules have been omitted for clarity. Color coding: C: gray; H: white; B: green; Cl: yellow; N: blue; O: red; Zn: cyan.

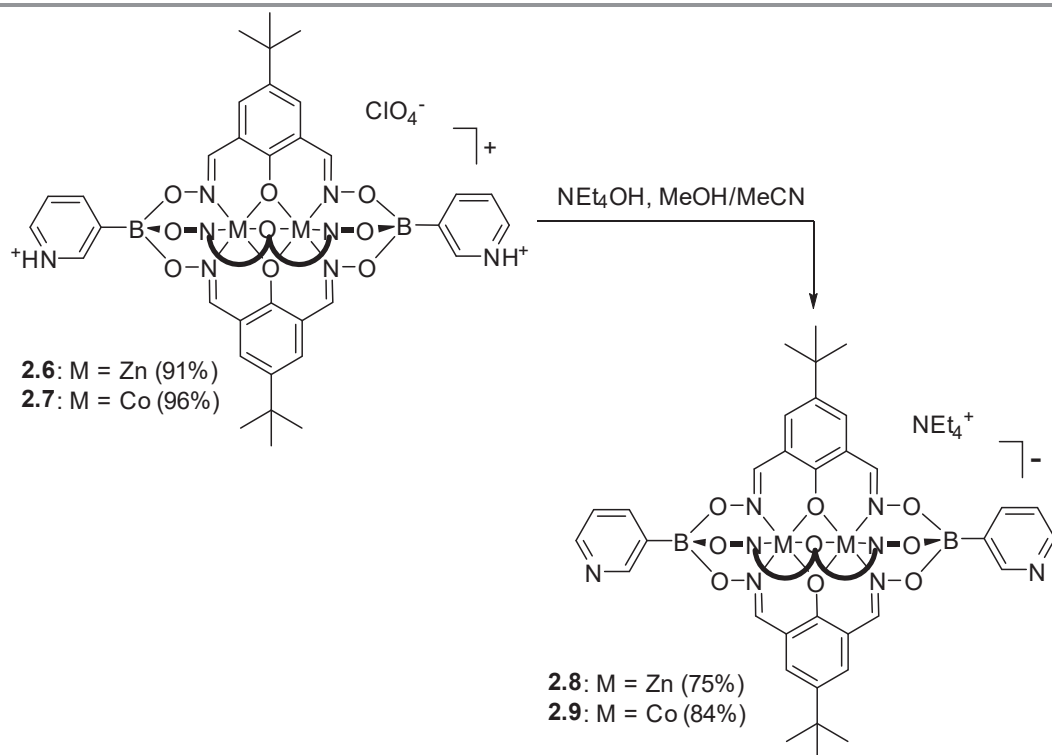
Table 2.1 – Selected bond lengths (Å) and angles (°) for the complexes **2.1** and **2.2**.

	M·····M	M–N _{av}	M–O _{av}	M–O–M _{av}	N–M–O _{av}
2.1	2.9401(17)	2.12	2.10	88.9	82.4
2.2	2.9591(10)	2.10	2.10	89.6	83.0

The cationic clathrochelates can be deprotonated by addition of base: when tetraethylammonium hydroxide was added to a solution of **2.1** or **2.2** in MeCN/MeOH, the anionic complexes **2.4** and **2.5** were obtained in high yield (Scheme 2.2). The solubility of the anionic complexes is higher than that of the cationic perchlorates: the complexes display a good solubility (> 10 mg/ml) in methanol/acetonitrile (1:1), acetone, CH₂Cl₂ or CHCl₃.

**Scheme 2.2** – Synthesis of the anionic bipyriddy clathrochelates **2.4** and **2.5**.

A similar strategy was followed in order to obtain 3,3'-bipyridyl clathrochelates, by using 3-pyridylboronic acid in the synthetic procedure. Similarly to complexes **2.1** and **2.2**, the protonated 3,3'-bipyridyl clathrochelates **2.6–2.8** precipitated from the reaction mixture in the form of microcrystalline powders. Subsequent deprotonation in the presence of tetraethylammonium hydroxide led to the anionic metalloligands **2.8** and **2.9** (Scheme 2.3). Single crystal X-ray structural analysis of **2.6** and **2.7** confirmed the presence of the terminal protonated 3-pyridyl groups. A graphical representation of the structure of complex **2.7** is given in Figure 2.2. The two Co(II) centers adopt a trigonal prismatic geometry similar to what was observed for **2.1** and **2.2**. The M···M distances of 2.9442(6) Å (**2.6**) and 2.9456(6) Å (**2.7**) are comparable to the one observed for the 4,4'-bipyridyl derivatives, indicating that the boronate ester capping group does not significantly affects the geometry of the complexes. The N-atoms of the pyridyl groups in **2.6** and **2.7** are 16.34 Å and 16.33 Å apart from each other. However, in solution, this distance is expected to vary because of the rotational freedom of the 3-pyridyl group.^{52,53,62}



Scheme 2.3 – Synthesis of the clathrochelates **2.6–2.9**.

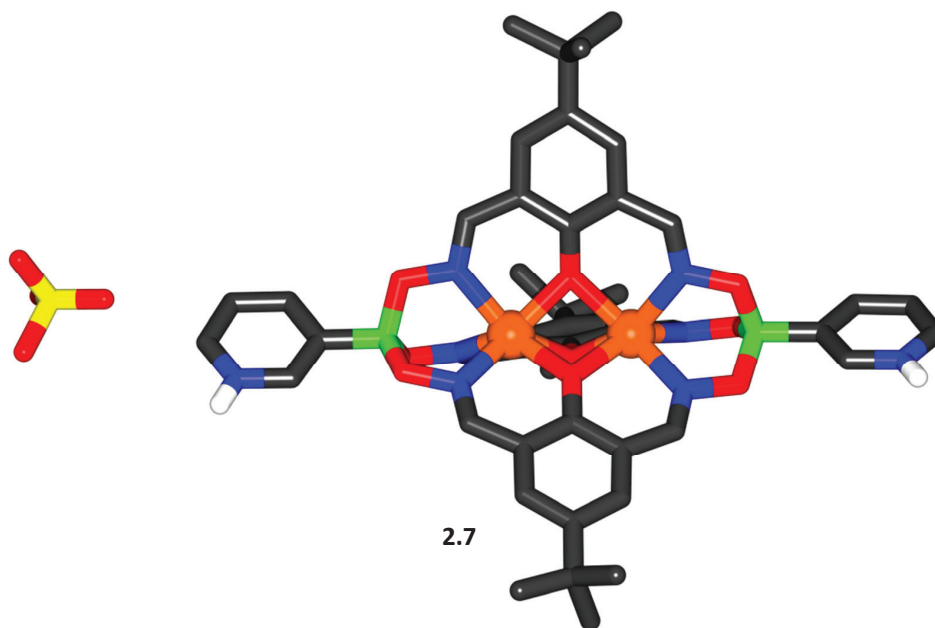
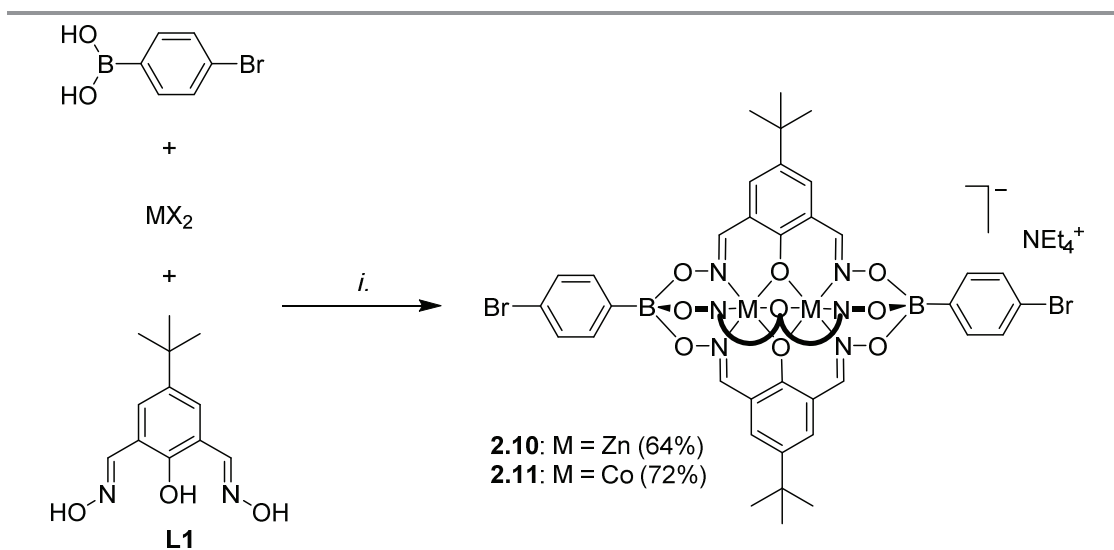


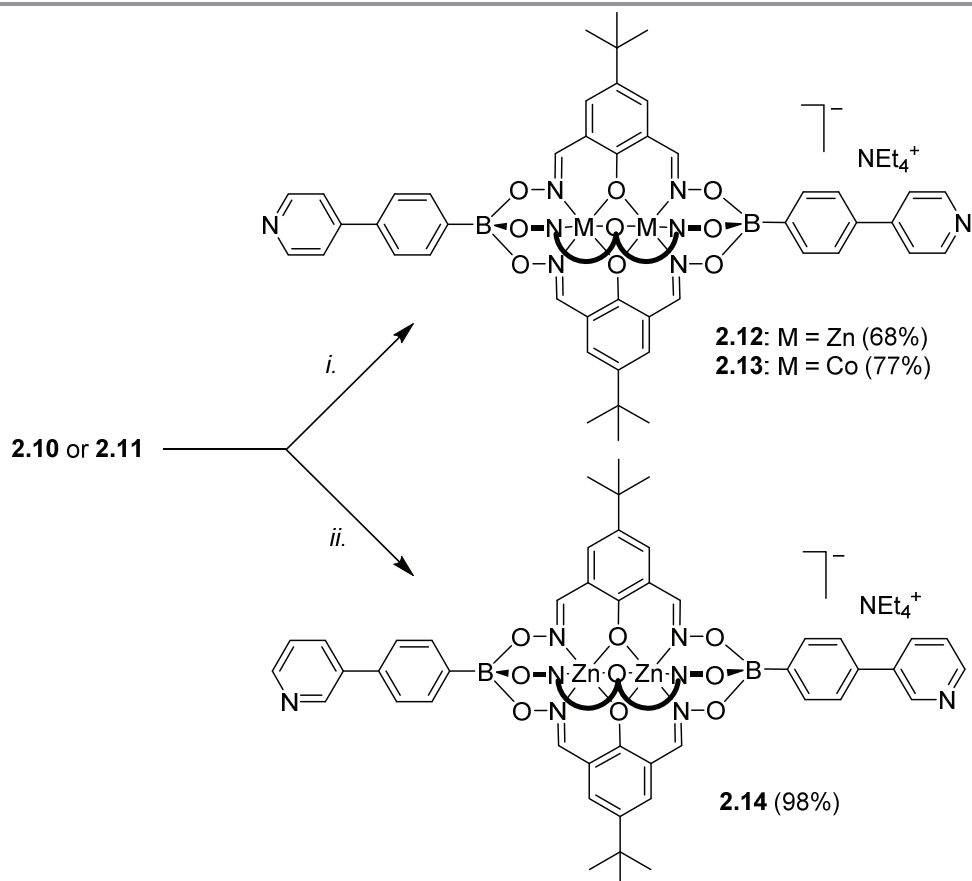
Figure 2.2 – Molecular structure of complex **2.7** in the crystal. Most hydrogen atoms and unbound solvent molecules have been omitted for clarity. Color coding: C: gray; H: white; B: green; Cl: yellow, Co: orange; N: blue; O: red.

2.3 Synthesis of polypyridyl clathrochelates *via* Pd catalyzed cross-coupling reactions

The 3,3'- and 4,4'-bipyridyl ligands depicted in section 2.2 were obtained by reaction of a Zn- or Co-salt with 4-pyridylboronic acid and a phenoldioxime. For mononuclear clathrochelates based on glyoximato ligands and Fe(II) centers, it had been reported that metal-catalyzed reactions can be used for the post-functionalization of the clathrochelate skeleton.^{48,63} We were wondering if a similar strategy could be employed for the post-modification of dinuclear clathrochelates. To investigate this question, we have prepared the Zn(II) complex **2.10** and the Co(II) complex **2.11** having two bromine atoms in apical position following the protocol described previously, using 4-bromophenylboronic acid for the boronate ester capping groups (Scheme 2.4). Notably, the use of more easily handable Zn(OTf)₂ and [Co(H₂O)₆](NO₃)₂ as the M(II) salts, conversely to the perchlorate salts used previously, led to the desired clathrochelates sharing bromine atoms in their apical position in good yields. The complexes **2.10** and **2.11** were then used as substrates for a Pd-catalyzed Suzuki-Miyaura cross-coupling reactions with 3- or 4-pyridylboronic acid using Buchwald's ligand SPhos.^{41b,64} The reactions were found to give the desired coupling products **2.12**, **2.13** and **2.14** in good to excellent yields (Scheme 2.5).

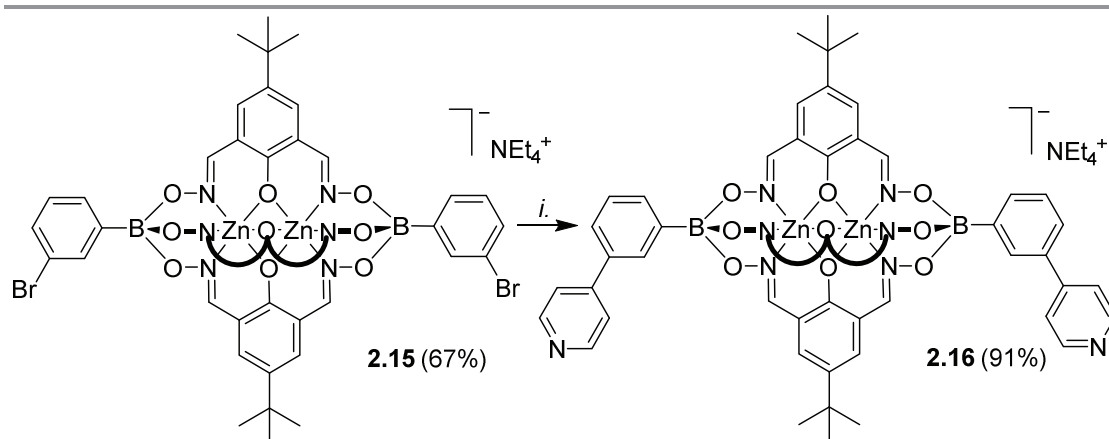


Scheme 2.4 – Synthesis of the clathrochelates **2.10** and **2.11**. Reagents and conditions: (i.): 4 bromophenylboronic acid, **L1**, Zn(OTf)₂ or [Co(H₂O)₆](NO₃)₂, MeOH, 70 °C, then NEt₄OH.



Scheme 2.5 – Synthesis of the clathrochelates **2.12–2.14**. Reagents and conditions: (*i.*): **2.10** or **2.11** (1 eq.), 4-pyridylboronic acid (6 eq.), K₃PO₄ (3 eq.), Pd₂(dba)₃ (5 mol%), SPhos (10 mol%), n-BuOH/toluene (1:1), 120 °C, 12 h, then NEt₄OH; (*ii.*): **2.10** (1 eq.), 3-pyridylboronic acid (6 eq.), K₃PO₄ (3 eq.), Pd₂(dba)₃ (5 mol%), SPhos (10 mol%), n-BuOH/toluene (1:1), 120 °C, 12 h, then NEt₄OH.

Subsequently, we have examined whether coupling reactions in *meta* position with respect to the boronate ester function are possible. We have therefore prepared clathrochelate **2.15** (Scheme 2.6) using 3-bromophenylboronic acid (yield: 67%). This complex was then subjected to the Buchwald-type coupling conditions used before. The desired dipyridyl ligand **2.16** could be isolated in 91% yield (Scheme 2.6). The metalloligands **2.12–2.14** and **2.16** are well soluble in polar organic solvents such as DMSO, MeOH, MeCN or CH₂Cl₂. In line with the depicted structure, the NMR spectra of the diamagnetic Zn complexes **2.12**, **2.14** and **2.16** show one set of signals for the three lateral oximate ligands and one set of signals for the two terminal phenylpyridyl groups. The successful coupling of two pyridyl groups to the clathrochelates was also confirmed by high-resolution mass spectrometry.



Scheme 2.6 – Synthesis of the bent metalloligand **2.16**. Reagents and conditions: (i.): **2.15** (1 eq.), 4-pyridylboronic acid (6 eq.), K_3PO_4 (3 eq.), $Pd_2(dba)_3$ (5 mol%), SPhos (10 mol%), n-BuOH/toluene (1:1), 120 °C, 12 h, then NEt_4OH .

As observed for the Zn-based clathrochelates **2.4** and **2.8**, solutions of **2.12**, **2.14** or **2.16** are luminescent, with an emission maximum of 445 nm (DMF, λ_{ex} = 330 nm). Figure 2.4 shows characteristic excitation and emission spectra for complex **2.14**.

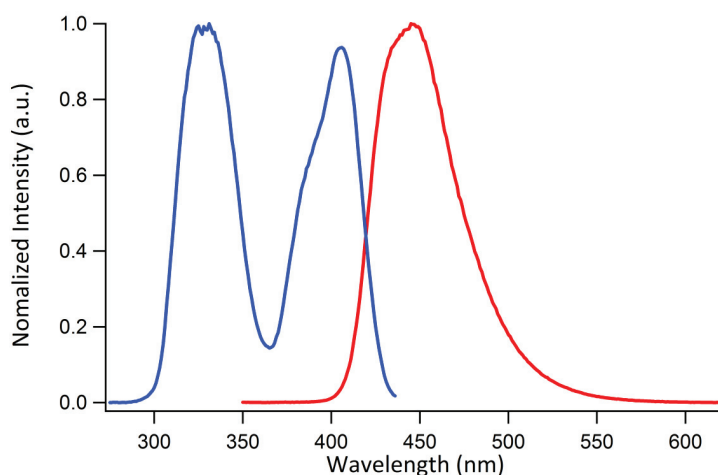


Figure 2.4 – Excitation (blue) and emission (red, λ_{ex} = 330 nm) spectra of **2.14** in DMF.

The molecular structure of complex **2.12** in the crystal was determined by single crystal X-ray crystallography (Figure 2.5). The two Zn^{2+} ions are coordinated in a trigonal prismatic fashion by three nitrogen ($Zn-N_{av}$ = 2.13 Å) and three oxygen atoms ($Zn-O_{av}$ = 2.12 Å). The oxygen atoms bridge the two metal ions resulting in a $M \cdots M$ distance of 2.971(1) Å. The terminal nitrogen atoms of the two pyridyl groups are 26.7 Å apart from each other. This metalloligand is thus substantially longer than the previously reported clathrochelate based on 4-pyridylboronic acid (1.8 nm; Figure 2.1), and it is comparable in size to pyridyl-capped double clathrochelates introduced by our group (2.7 nm)⁴⁸ and to bis-(4'-ethynylpyridyl)-functionalized salen ligands (2.4 nm).^{12,65}

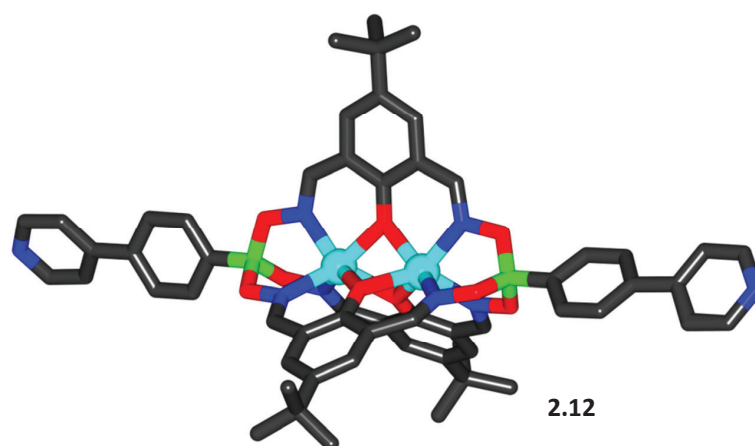
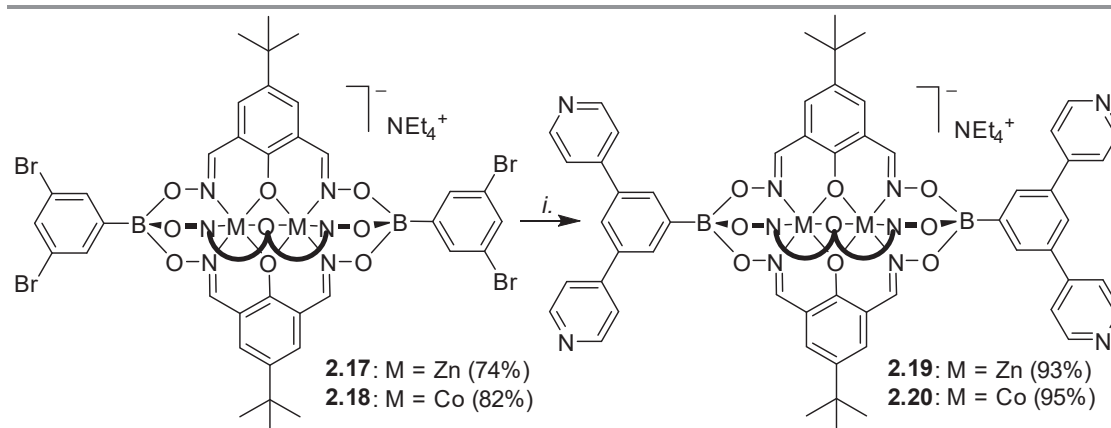


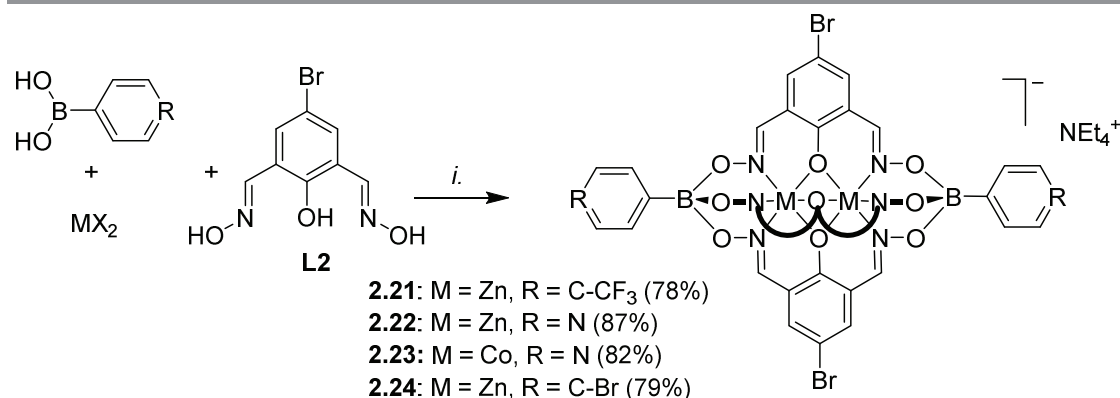
Figure 2.5 – Molecular structure of **2.12** in the crystal. Hydrogen atoms, the counterion (NEt_4^+), and solvent molecules have been omitted for clarity. Color coding: C: grey; B: green; N: blue; O: red; Zn: cyan.

Having shown that coupling in *meta* position was feasible, we further exploited those findings and synthesized the tetrabromo-decorated Zn(II) and Co(II) clathrochelates **2.17** and **2.18** using 3,5-dibromophenylboronic acid as the boronate ester capping moiety in 74% and 82% yield, respectively. Their subsequent Pd-catalyzed cross-coupling reaction with 4-pyridylboronic acid led to the desired tetrapyridyl derivatives **2.19** and **2.20** in excellent yields (Scheme 2.7).

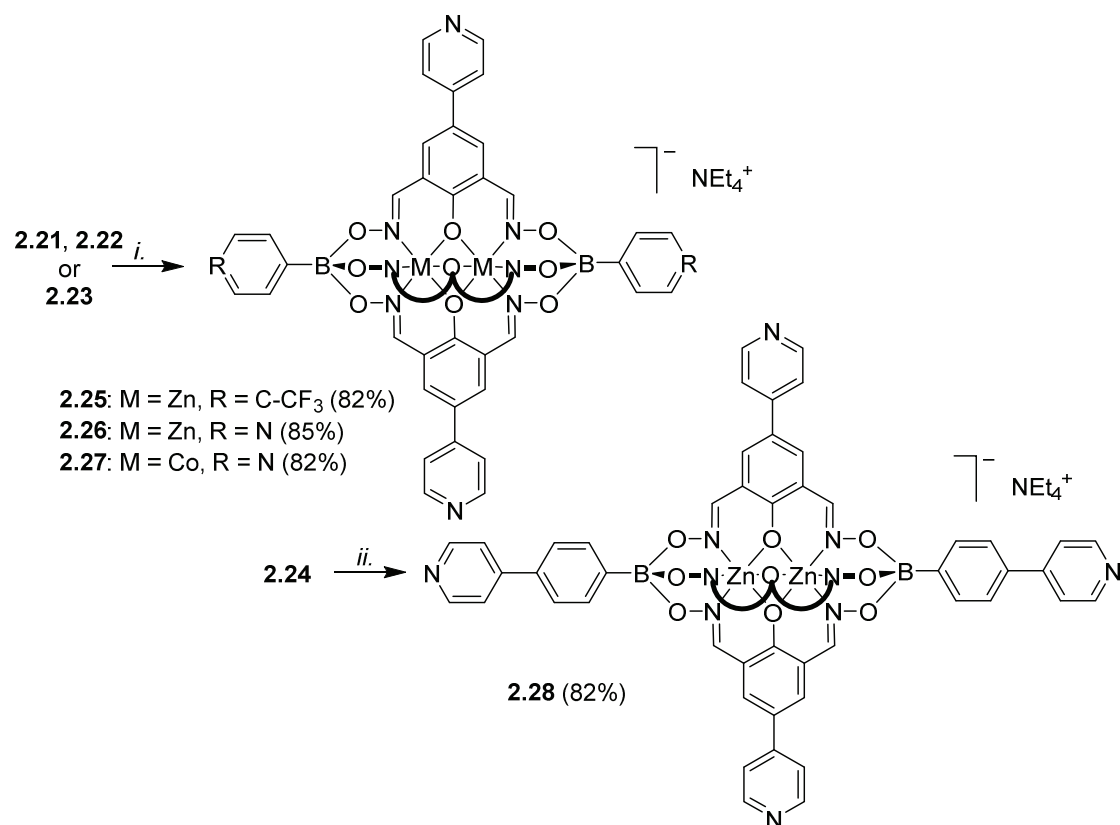


Scheme 2.7 – Synthesis of the tetrapyridyl metalloligands **2.19** and **2.20**. Reagents and conditions: (*i.*): **2.17** or **2.18** (1 eq.), 4-pyridylboronic acid (20 eq.), K_3PO_4 (10 eq.), $\text{Pd}_2(\text{dba})_3$ (5 mol%), SPhos (10 mol%), $n\text{-BuOH/toluene}$ (1:1), 120 °C, 12 h, then NEt_4OH .

Next, we explored the reactivity of clathrochelates having bromo-substituents on the lateral oximate ligands. Reaction of 2,6-diformyl-4-bromophenol dioxime (**L2**) with zinc triflate or cobalt nitrate and the respective boronic acid afforded the complexes **2.21–2.24** in good yields (Scheme 2.8). The clathrochelates **2.21–2.23** have three lateral bromo atoms, whereas complex **2.24** features a total of five arylbromide groups.



Scheme 2.8 – Synthesis of the polybrominated clathrochelates **2.21–2.24**. Reagents and conditions: (i.): Selected boronic acid, Zn(OTf)₂ or [Co^{II}(H₂O)₆](NO₃)₂, MeOH, 70 °C, then NEt₄OH.



Scheme 2.9 – Synthesis of the tri- and pentatopic metalloligands **2.25–2.28**. Reagents and conditions: (i.): **2.21**, **2.22** or **2.23** (1 eq.), 4-pyridylboronic acid (15 eq.), K₃PO₄ (7.5 eq.), Pd₂(dba)₃ (5 mol%), SPhos (10 mol%), n-BuOH/toluene (1:1), 120 °C, 12 h, then NEt₄OH; (ii.): **2.24** (1 eq.), 4-pyridylboronic acid (20 eq.), K₃PO₄ (10 eq.), Pd₂(dba)₃ (7.5 mol%), SPhos (15 mol%), n BuOH/toluene (1:1), 120 °C, 12 h, then NEt₄OH.

Subsequent Pd-catalyzed cross-coupling with 4-pyridylboronic acid afforded the tripyridyl ligand **2.25** as well as the pentatopic metalloligands **2.26–2.28** (Scheme 2.9). The polypyridyl ligands **2.25–2.28** are well soluble in DMSO and moderately soluble in CH₂Cl₂ and acetonitrile.

The solution-based analysis by NMR spectroscopy and high resolution mass spectrometry confirmed the exhaustive replacement of the bromo atoms with 4-pyridyl groups. The luminescent properties of the Zn complexes **2.25**, **2.26**, and **2.28** were in line with what was observed previously, with emission maxima at 445 nm (DMF, $\lambda_{\text{ex}} = 330$ nm). Single crystal X-ray structural analyses of **2.26** and **2.28** confirmed the presence of five 4-pyridyl groups with divergent coordinate vectors (Figure 2.6). The five peripheral nitrogen atoms are arranged in a distorted trigonal bipyramidal fashion. The distances between the two axial nitrogen atoms are 18.0 (**2.26**) and 26.6 Å (**2.28**), and thus similar to what was found for the ditopic metalloligands described above. The average N...N distances for pairs of lateral pyridyl substituents are 17.2 Å (**2.26**) and 17.1 Å (**2.28**) and the angles between the oximate ligands are 117.22°, 117.22°, and 125.57° for **2.26**, and 100.15°, 126.60° and 138.25° for **2.28**. The deviation of up to 18.25° from the ideal 120° angle is likely due to packing effects in the crystal. The bond lengths and angles observed for the bimetallic core of the clathrochelates are within the expected range.

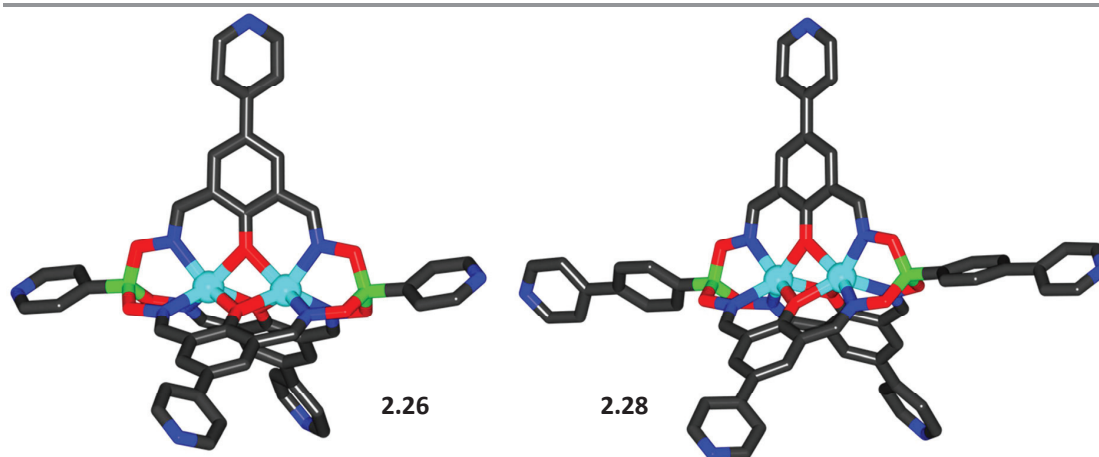
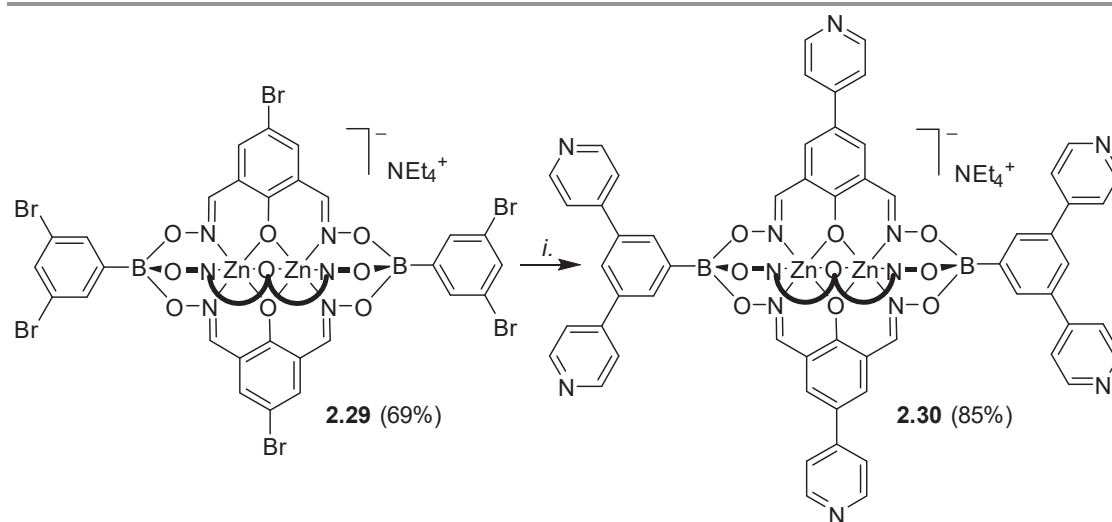


Figure 2.6 – Molecular structures of the pentatopic metalloligands **2.26** (left) and **2.28** (right) in the crystal. Hydrogen atoms, counterions (NEt_4^+), and solvent molecules have been omitted for clarity. Color coding: C: gray; B: green; N: blue; O: red; Zn: cyan.

The good success of the five-fold coupling reactions with precursor **2.24** prompted us to push the synthetic concept even further. We thus synthesized clathrochelate **2.29** having seven bromine atoms. The complete surface functionalization of this complex was achieved under slightly more forcing coupling conditions (10 mol% Pd; Scheme 2.10). The resulting heptapyridyl ligand **2.30** was characterized by NMR spectroscopy and high resolution mass spectrometry. Attempts to obtain single crystals of **2.30** were unfortunately not successful. In order to obtain an estimate of the dimensions of this metalloligand, we have performed an exploratory computational study of its geometry using Density Functional Theory (DFT)⁶⁶ with the PBE0 exchange-correlation functional.⁶⁷ The robustness of the method was first evaluated by comparing the XRD structure of clathrochelates

2.1 and **2.12** with their computed geometries, which resulted in a good match. We then calculated the minimum-energy structure of **2.30**, and the result is shown in Figure 2.7. For clathrochelate **2.30**, the computed average N...N distance for pairs of lateral pyridyl substituents is 17.3 Å, a value which is in line with the measured values for **2.26** and **2.28**. The maximum N...N distance between opposite pyridyl groups of the terminal 3,5-(dipyridin-4-yl)phenyl moieties is 22.7 Å. These values give an idea about the size of this unusual heptatopic metalloligand.



Scheme 2.10 – Synthesis of the heptatopic metalloligand **2.30**. Reagents and conditions: (i.): **2.29** (1 eq.), 4-pyridylboronic acid (28 eq.), K_3PO_4 (14 eq.), $Pd_2(dba)_3$ (10 mol%), SPhos (20 mol%), n-BuOH/toluene (1:1), 120 °C, 12 h, then NEt_4OH

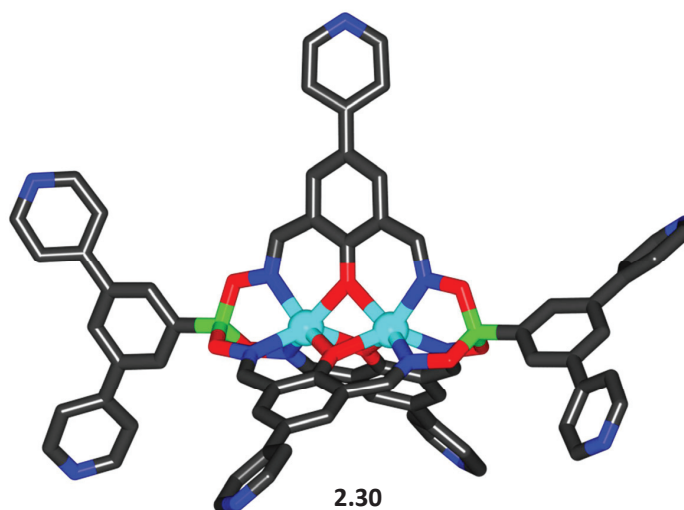
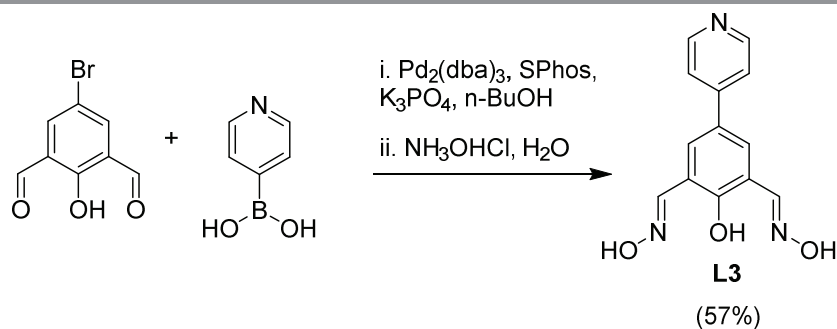


Figure 2.7 – Minimum-energy structure of the heptatopic metalloligand **2.30** obtained by DFT/PBE0. Only the anionic clathrochelate was calculated. Hydrogen atoms have been omitted for clarity. Color coding: C: gray; B: green; N: blue; O: red; Zn: cyan.

The results described above showed that cross-coupling reactions can be extremely efficient to obtain metalloligands featuring up to seven pyridyl groups. Nevertheless, one drawback of this methodology, conversely to the one-pot approach detailed in section 2.2, is that it would not be possible to obtain a metalloligand sharing both pyridyl groups on the phenolatodioximato part and bromine atoms on the boronate ester part. Indeed, it is not possible to perform Pd-catalyzed cross-coupling reactions selectively on the lateral or apical positions. We envisioned that it should also be possible to use the oximato ligands for introducing additional pyridyl groups, thereby broadening the variety and hence potential applications of clathrochelate-based metalloligands. This goal was accomplished through synthesis of the pyridyl-functionalized dioximato ligand **L3**. Suzuki-Miyaura coupling of 4-pyridylboronic acid and 2,6-diformyl-4-bromophenol in the presence of $\text{Pd}_2(\text{dba})_3$ and Buchwald's SPhos ligand⁶⁴ in *n*-BuOH afforded the crude diformylphenol intermediate, which was converted to the corresponding dioxime **L3** by treatment with hydroxylamine hydrochloride (Scheme 2.11).



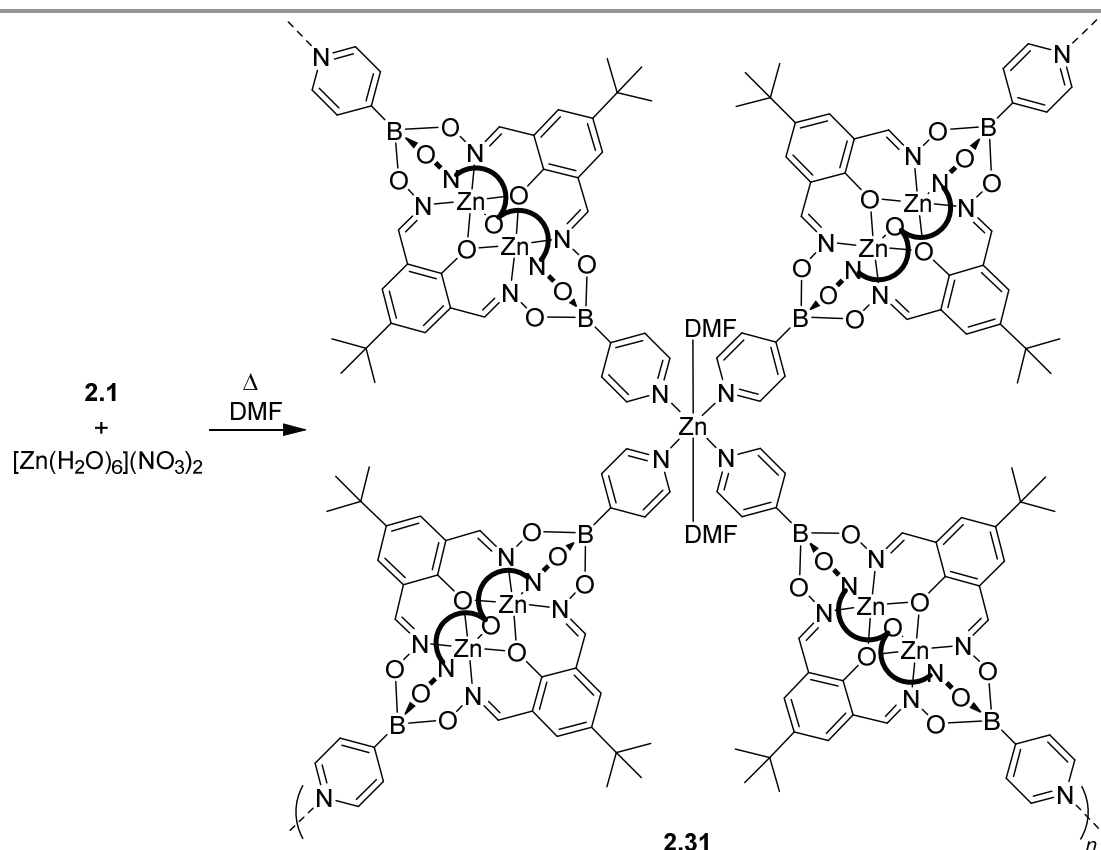
Scheme 2.11 – Synthesis of the pyridyl-decorated dioxime ligand **L3**.

The use of **L3** dioxime ligand for the synthesis of clathrochelates was evidenced by synthesizing **2.26** using a one-pot approach, followed by deprotonation of the pyridyl groups. However, the one-pot approach using **L3**, though, was lower-yielding compared to the postfunctionalization. Therefore, we recommend to use the cross-coupling approach if the desired metalloligand allows it.

2.4 Use of pyridyl-decorated clathrochelates as supramolecular building blocks

2.4.1 Synthesis of a two-dimensional network based on a 4-pyridyl-capped clathrochelate

Bipyridyl ligands have been used extensively for the construction of metal-organic frameworks (MOFs), some of which have been described in Chapter 1. To demonstrate that our clathrochelate-based bipyridyl ligands can also be used in this area, we have investigated reaction of **2.1** with Zn^{2+} ions. Heating a mixture of $[\text{Zn}(\text{H}_2\text{O})_6](\text{NO}_3)_2$ and the protonated metalloligands **2.1** in *N,N*-dimethylformamide (DMF) in a sealed vial resulted in the formation of the crystalline coordination polymer **2.31** (yield: 89%) (Scheme 2.12). It is known that DMF decomposes slowly upon heating to generate a basic medium.⁶⁸ The base can deprotonate the pyridyl groups of **2.1**. In this way, the network is formed slowly and crystallizes directly from the reaction mixture. Attempts to perform the same reaction with the deprotonated metalloligands **2.4** resulted in the immediate formation of amorphous powders.



Scheme 2.12 – Synthesis of the two-dimensional coordination polymer **2.31**.

Crystallographic analyses of the coordination polymer **2.31** revealed a 2D square grid-type layer structure with square dimensions of 22.3 x 22.3 Å (Figure 2.6), with the stoichiometry $[\text{Zn}(\mathbf{2.1})_2(\text{C}_3\text{H}_7\text{NO})_2]$. Four metalloligands are connected through Zn^{II} ions. The latter have an octahedral coordination geometry with two additional DMF molecules in *trans* position. Overall, the network is neutral since the anionic clathrochelate ligands compensate the charge of the Zn^{II} ions. It is worth mentioning that M^{II} -based MOFs with square grid-type layer structures have been reported in the literature.⁶⁹ In contrast to **2.31**, the square sub-structures are typically smaller and anions are coordinated to the bridging M^{2+} ions. The 2D network **2.31** shows an ABAB-type packing arrangement (Figure 2.8). Due to the presence of the bulky *tert*-butyl groups, the inter-layer distance of the planes defined by the bridging Zn^{2+} ions is relatively large (23.7 Å). The solvent-accessible volume, as calculated by the PLATON software,⁷⁰ corresponds to 21% of the unit cell.

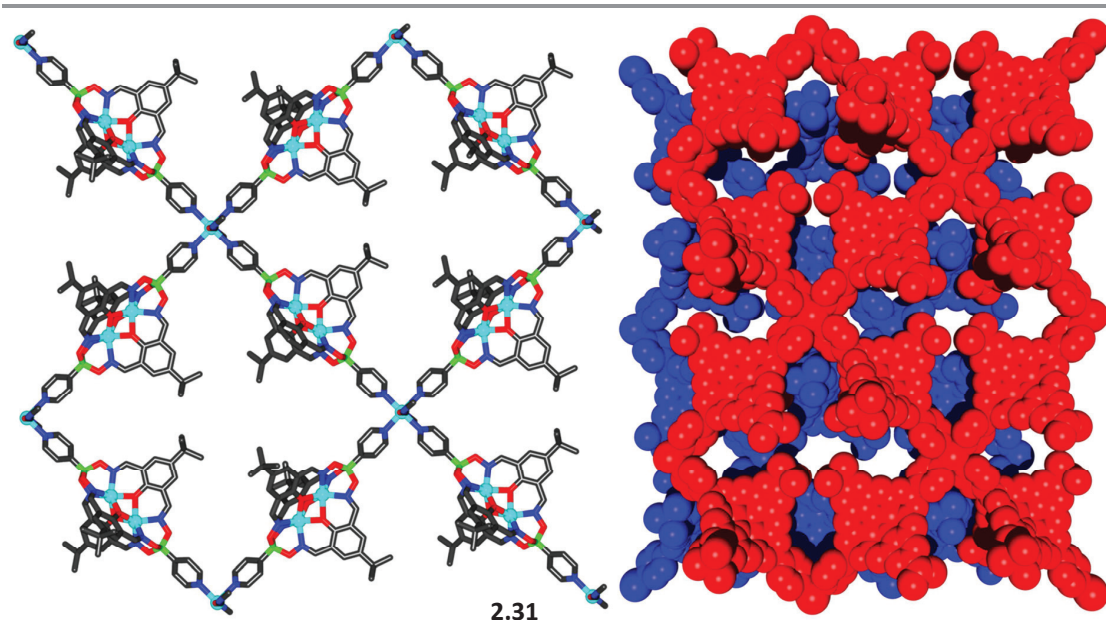


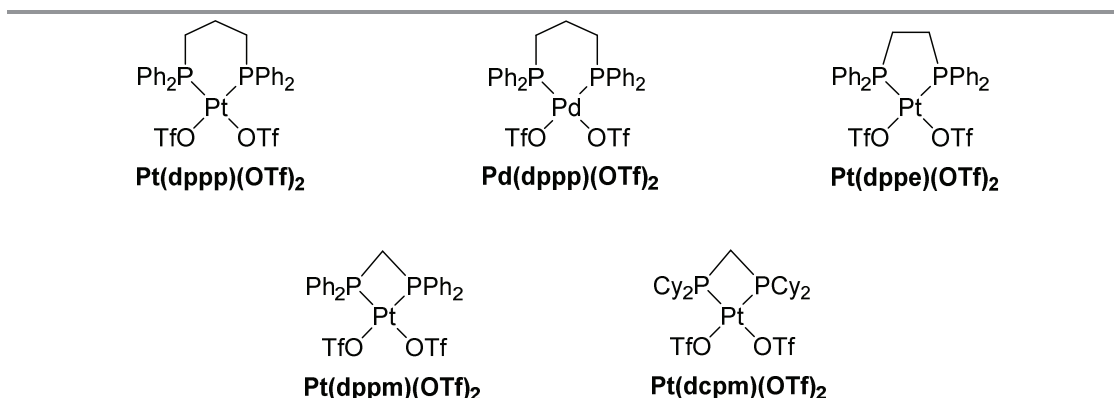
Figure 2.8 – (left) Part of the layer structure of coordination polymer **2.31** with view along the crystallographic *c* axis. Hydrogen atoms and unbound solvent molecules have been omitted for clarity. Color coding: C: grey; B: green; N: blue; O: red; Zn: cyan; (right) Superimposition of two independent adjacent layers, showing the ABAB-type packing arrangement.

Thermogravimetric analysis (TGA) of **2.31** shows that the network is thermally stable up to ~ 300 °C. This value is relatively high, showing that our dinuclear clathrochelates are interesting candidates for metallasupramolecular applications. BET surface measurements (N_2 , 77 K) after drying in vacuum gave a moderate value of $556 \text{ m}^2\cdot\text{g}^{-1}$. Dr. Pascu, who worked in parallel on that research project, synthesized similar two-dimensional networks based on dinuclear clathrochelates sharing methyl substituents on the lateral oximes. Surprisingly, the values for the coordination polymers based on these less bulky clathrochelates gave low BET values between $10 \text{ m}^2\cdot\text{g}^{-1}$ and $54 \text{ m}^2\cdot\text{g}^{-1}$. A significantly higher value is observed for the *tert*-butyl-group containing **2.31**: these differences

show that the lateral size of the clathrochelates can have a pronounced influence on the physical properties of the resulting assemblies.

2.4.2 Synthesis of a $M_{10}L_5$ molecular cage

We saw in previous sections 1.5 and 2.4.1 that 4-pyridyl-decorated clathrochelates are able to act as ligands in discrete or polymeric supramolecular assemblies. The anionic nature of the ligands added an extra stability to the M_4L_4 molecular square, as found by Dr. Schouwey, and played an important role in the charge balance of the two-dimensional CP **2.31**, preventing the incorporation of counter ions in the crystal structure. We therefore decided to explore the reactivity of our pyridyl-decorated clathrochelates with *cis*-protected platinum or palladium corners. Scheme 2.13 highlights the different corners used in this study.



Scheme 2.13 – Palladium(II) or Platinum(II) corners used in this study. List of abbreviations: dppe = bis(diphenylphosphino)ethane; dppp = bis(diphenylphosphino)propane; dppm = bis(diphenylphosphino)methane; dcpm = bis(dicyclohexylphosphino)methane

Typically, the reactions were performed in NMR tubes, using deuterated solvents as the reaction media. Most attempts led to the immediate formation of amorphous precipitates upon addition of the corner to the solutions of the clathrochelate. Monitoring of the reaction by NMR spectroscopy showed that regardless of the conditions followed (heating or RT) or the solvents used (acetonitrile, DMSO, nitromethane, chloroform or dichloromethane), the formation of the precipitate was irreversible and acted as a kinetic trap. These observations suggested that the electrostatic interactions between the positively charged Pt(II) or Pd(II) centers and the negatively charged clathrochelates promote the formation of insoluble oligomers/polymers under kinetic control. We thus tried to slow down the reaction by layering techniques. Typically, solutions of the Pt(II) or Pd(II) complexes in nitromethane, methanol or ethanol were layered onto solutions of the clathrochelates in chlorinated solvents. This technique has the drawback of being controlled by the diffusion of reactants, therefore leading to a non-controlled stoichiometry of the building blocks. We were able to obtain a crystal upon reaction of the tritopic clathrochelate **2.32** in 1,2,4-trichlorobenzene / DMF

with Pt(dppp)(OTf)_2 in MeOH (Scheme 2.14). The initial purpose of such a combination was to obtain a M_6L_4 truncated tetrahedron, similarly to what has been described by Fujita (Figure 2.9).⁷¹

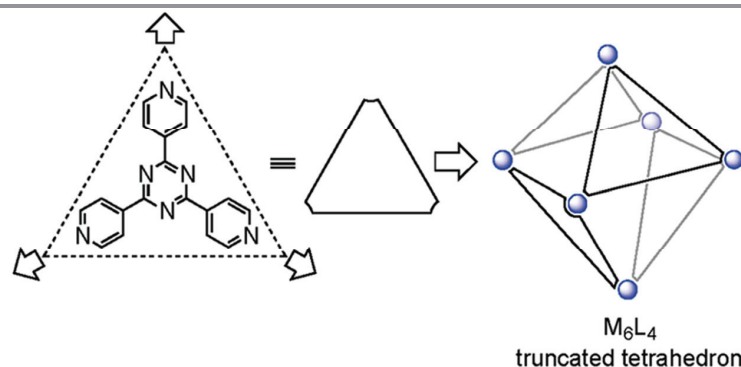
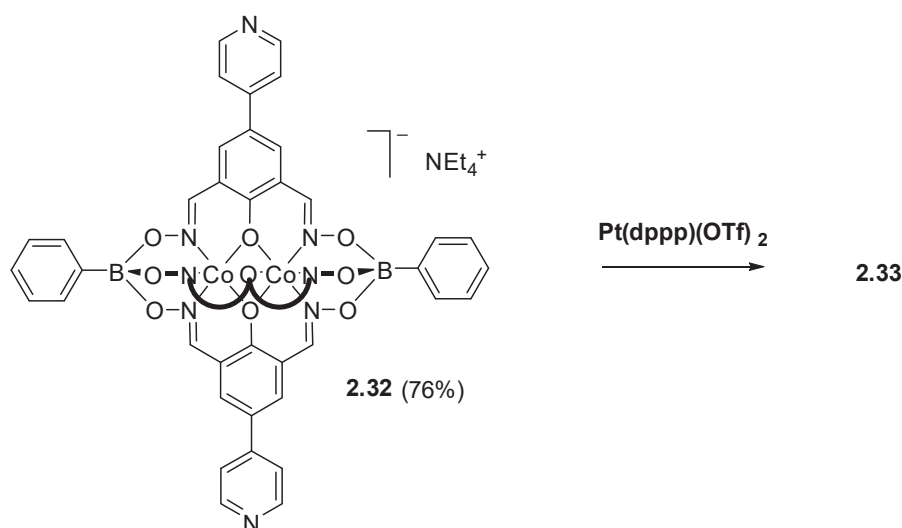


Figure 2.8 – Representation of Fujita's M_6L_4 truncated tetrahedron. Blue spheres represent Pd(en) corners (en = ethylenediamine). Reprinted with permission from reference [7b]. Copyright 2011 American Chemical Society.



Scheme 2.14 – Synthesis of discrete architecture **2.33** from **2.32** and Pt(dppp)(OTf)_2 .

Crystallographic analyses of the crystal of **2.33** revealed that instead of forming a M_6L_4 truncated tetrahedron, reaction of **2.32** with Pt(dppp)(OTf)_2 led to the formation of a M_2L_2 macrocyclic dimer (Figure 2.9). Due to the poor quality of the crystallographic data, it is not possible to discuss in detail the molecular structure of **2.33**. Yet, one can observe that the complex possesses C_2 -symmetry (Figure 2.9, bottom), with only two pyridyl groups of the clathrochelate coordinated to the Pt(II) corner. For each metalloligand **2.32**, one of the dioximato pyridyl group remains free, the two unbound moieties pointing in opposite directions. Despite numerous efforts to reproduce this dimeric complex on purpose, we never managed to obtain **2.33** again. This may highlight the caution one has to take while performing reactions by layering of two reactants.

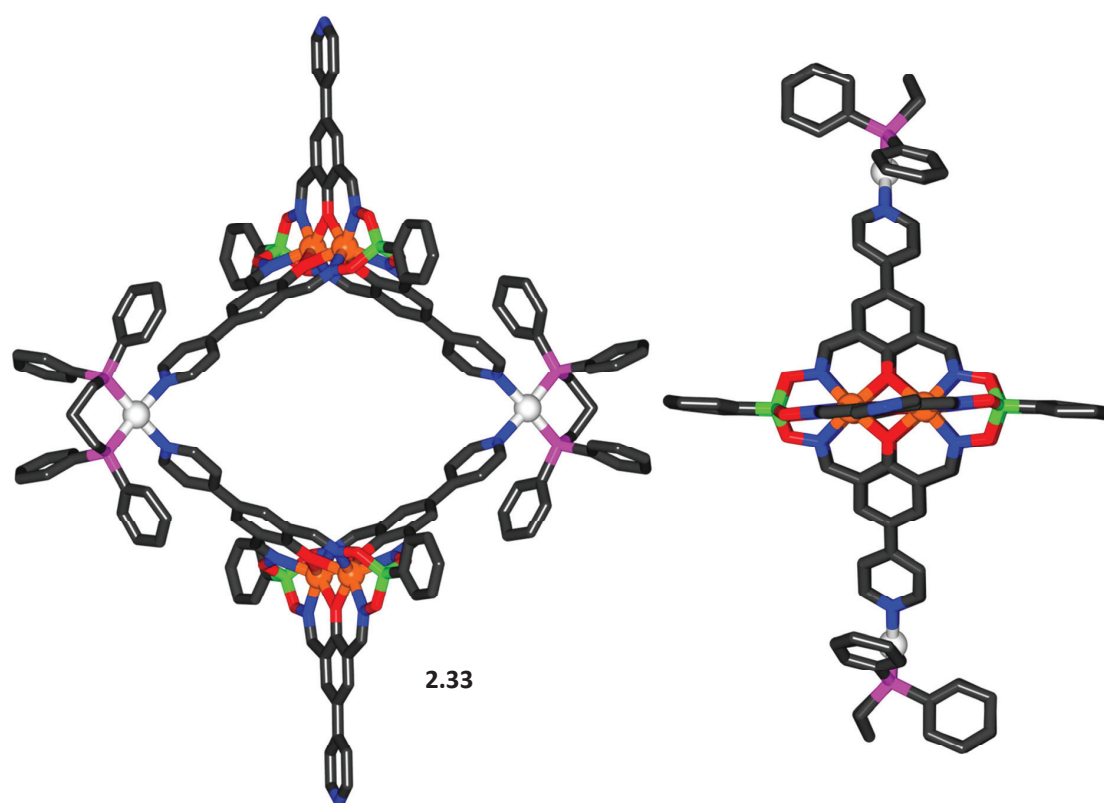
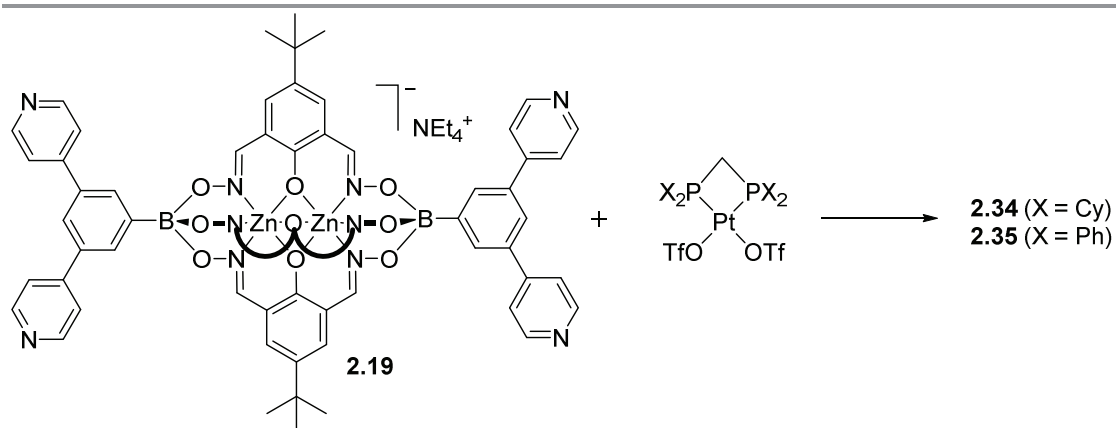


Figure 2.9 – Molecular structure of the dimer **2.33** in the crystal. Hydrogen atoms, counterions (OTf), and solvent molecules have been omitted for clarity. Color coding: C: gray; O: red; N: blue; B: green; Co: orange; P: pink; Pt: light grey.

The formation of the dimer **2.33** instead of the truncated tetrahedron depicted in Figure 2.8 can be partially explained by the relative orientation of the pyridyl groups on the clathrochelate **2.32**. Indeed, the tritopic ligand shown in Figure 2.8 is composed of a central triazine core that forces the coplanarity between the three divergent pyridyl groups. In the case of clathrochelate **2.32**, the three pyridyl groups can only be coplanar if each pyridyl group is oriented perpendicular to its phenolate ring. Figure 2.9 shows that the three pyridyl groups of **2.33** are not coplanar, however, X-ray analysis of **2.26** and **2.28** showed that pyridyl groups were slightly tilted with respect to the phenolate ring, confirming that rotation was feasible. Nevertheless, a significant driving force is necessary in order to overcome the energy barrier of a 90° rotation, precluding the formation of the expected truncated tetrahedron.

Among the many trials to synthesize discrete architectures, one particular clathrochelate metalloligand showed promising results. Indeed, reaction between tetratopic **2.19** and $\text{Pt}(\text{dcpm})(\text{OTf})_2$ or $\text{Pt}(\text{dppm})(\text{OTf})_2$ in $\text{DMSO-}d_6$ resulted in the fast formation of two discrete new species (Scheme 2.14).



Scheme 2.14 – Reaction between tetratopic **2.19** and $\text{Pt}(\text{dcpm})(\text{OTf})_2$ or $\text{Pt}(\text{dppm})(\text{OTf})_2$ in $\text{DMSO-}d_6$.

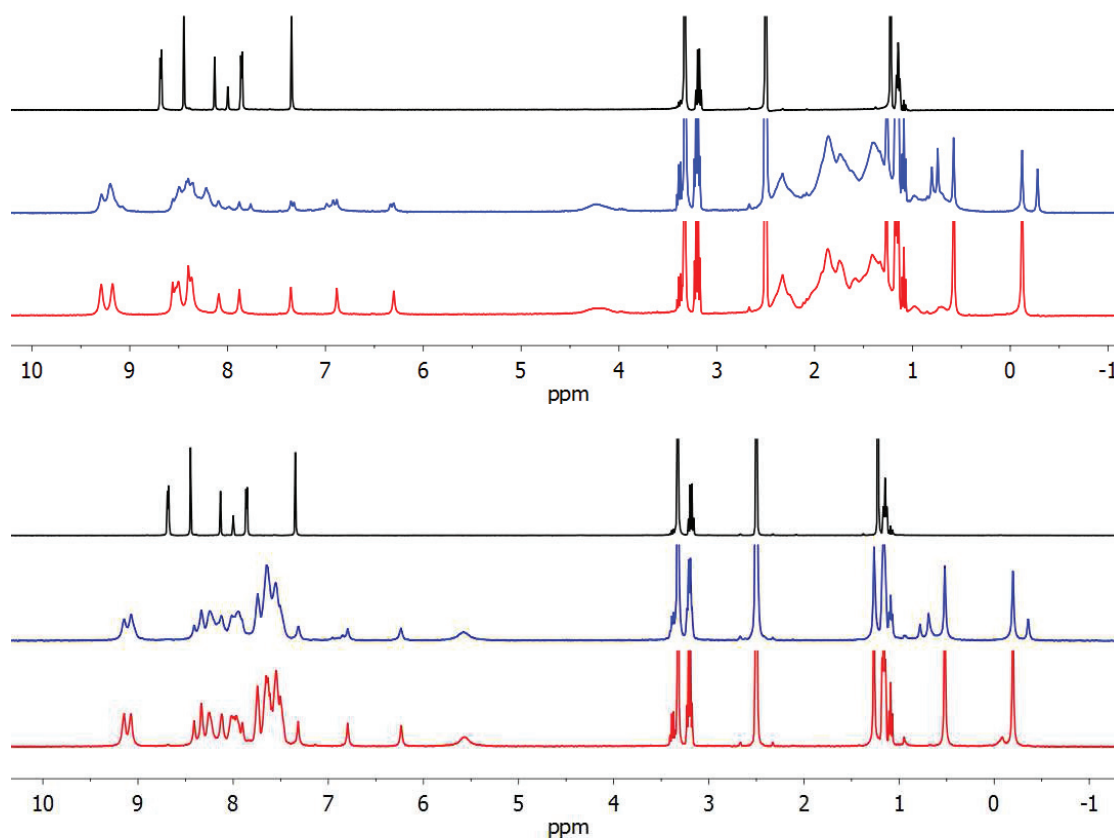


Figure 2.10 – (top): $^1\text{H-NMR}$ monitoring of the reaction between tetratopic **2.19** and $\text{Pt}(\text{dcpm})(\text{OTf})_2$ leading to **2.34**; (bottom): $^1\text{H-NMR}$ monitoring of the reaction between tetratopic **2.19** and $\text{Pt}(\text{dppm})(\text{OTf})_2$ leading to **2.35**. (black curves): **2.19** in $\text{DMSO-}d_6$; (blue curves): reaction mixture in $\text{DMSO-}d_6$ after heating 1h at 50 °C; (red curves): reaction mixture in $\text{DMSO-}d_6$ after heating 3h at 50 °C.

Attribution of the peaks was performed using several 2D-NMR experiments: HMBC, HSQC, COSY and ROESY. These analyses revealed that all three phenolatodioximato ligands were magnetically non-equivalent, as shown for **2.34** by the splitting of the *tert*-butyl protons at $\delta = 1.27$, 0.58 and -0.12 ppm with an integral of 9H and of the *Ar*-H protons on the dioxime ligand at $\delta = 7.35$, 6.88 and 6.30 with an integral of 2H (Figure 2.11). **2.35** shows similar behavior, but the peak attribution was more complex due to the presence of the aromatic phosphine protons.

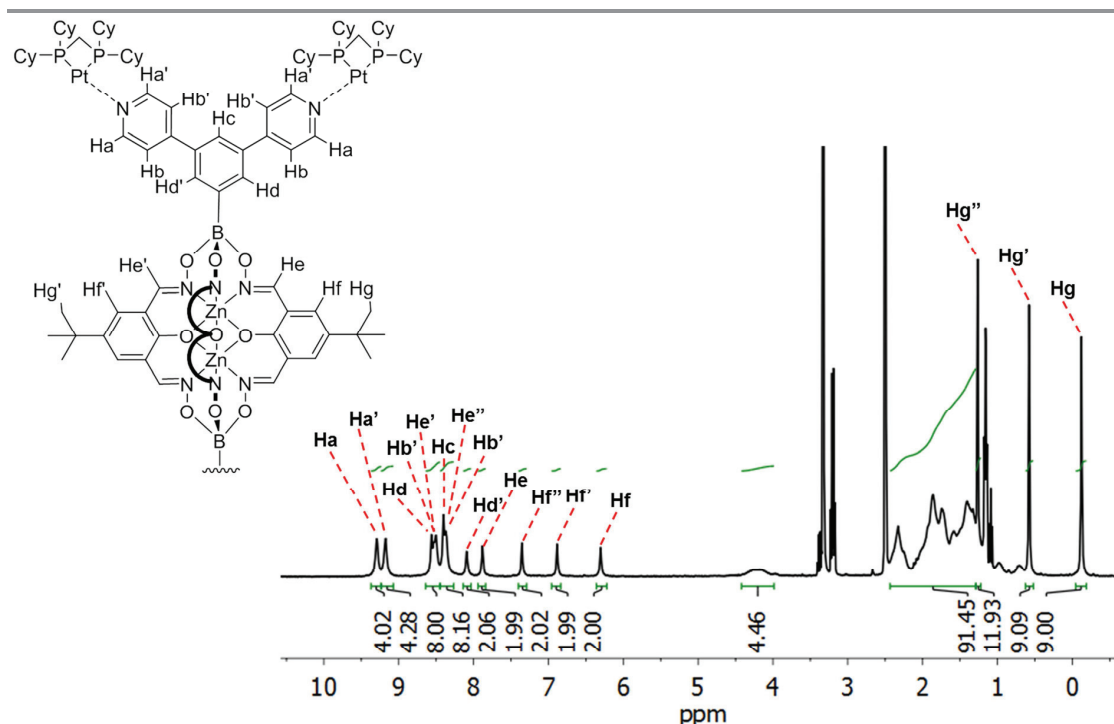


Figure 2.11 – Peaks assignments for **2.34** based on ROESY, HMBC and HSQC experiments.

The strong shielding of one of the dioxime ligand indicates that one arm of the clathrochelate could be pointing inside a cavity, such shielding being generally characteristic of the formation of a cage structure. Diffusion-Ordered Spectroscopy (DOSY, Figure 2.12) experiments further showed that in both cases, one single product was obtained, with a hydrodynamic radius close to 1.9 nm as calculated by the Stokes-Einstein equation. As expected, the tetraethylammonium counterion does not possess the same diffusion coefficient than **2.34** subunit (NEt_4^+ : $3.72 \cdot 10^{-6} \text{ cm}^2 \cdot \text{s}^{-1}$; **2.34**: $4.94 \cdot 10^{-7} \text{ cm}^2 \cdot \text{s}^{-1}$; **2.35**: $5.04 \cdot 10^{-7} \text{ cm}^2 \cdot \text{s}^{-1}$). The ^{31}P -NMR spectra of **2.34** and **2.35** show a single peak at $\delta = -49.5$ ppm, respectively -57.4 ppm, indicating that the *cis*-protected Pt corner are in magnetically equivalent environments. Based on these observations, we expect **2.34** and **2.35** to adopt cage structures, with a hindered rotation of the clathrochelate metalloligands, explaining the non-equivalent dioxime ligands as well as the non-equivalent protons on the 3,5-bis(4-pyridyl)phenyl boronate ester capping groups.

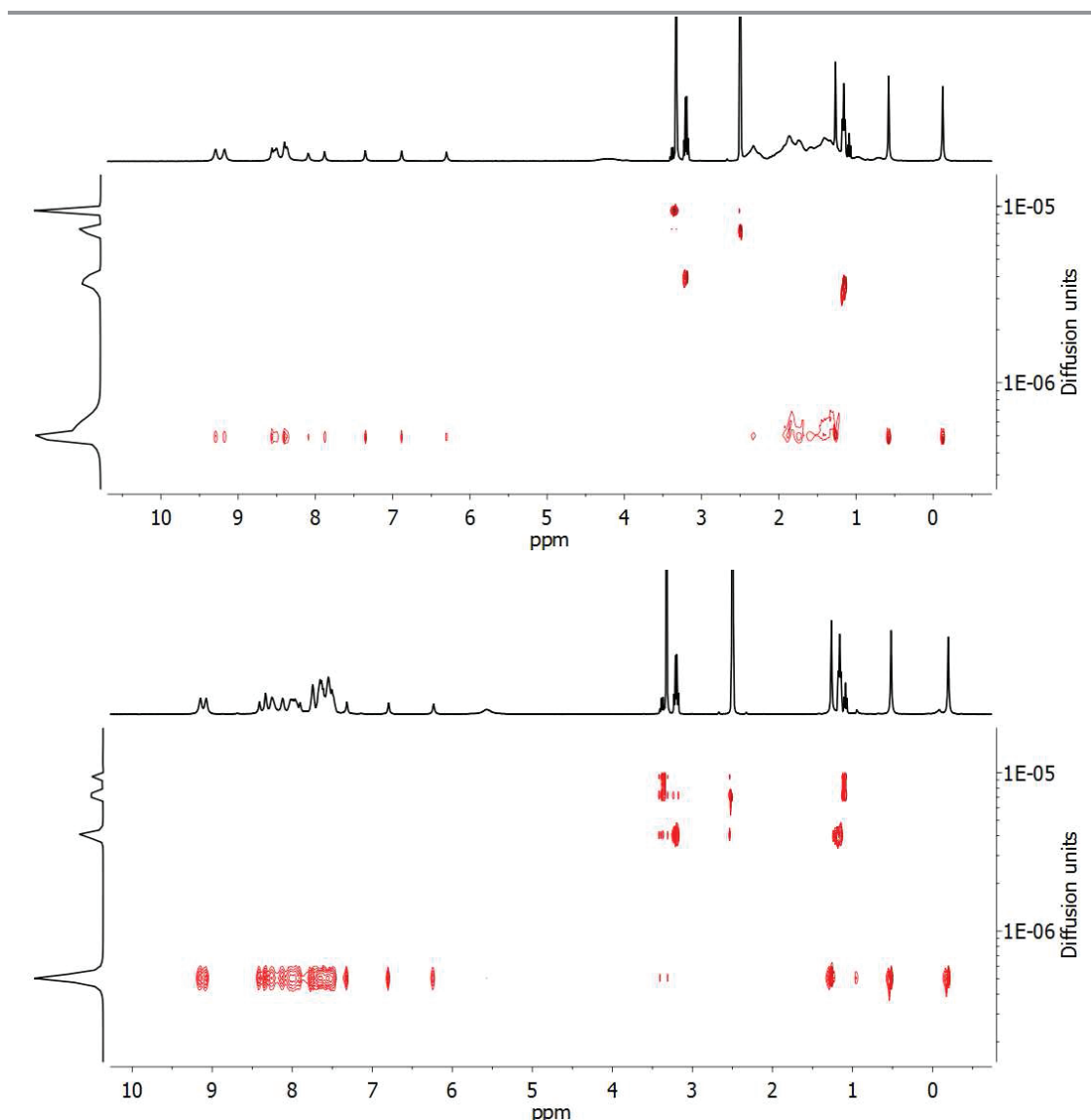


Figure 2.12 – (top) DOSY experiment for **2.34**. The diffusion coefficient for **2.34** is $4.94 \cdot 10^{-7} \text{ cm}^2 \cdot \text{s}^{-1}$; (bottom) DOSY experiment for **2.35**. The diffusion coefficient for **2.35** is $5.04 \cdot 10^{-7} \text{ cm}^2 \cdot \text{s}^{-1}$; One can clearly see the NEt_4^+ cation with a lower diffusion coefficient.

Taken together, the 1D- and 2D-NMR data suggested that a defined large product had formed in nearly quantitative yield. Analyses of **2.34** and **2.35** were performed using high-resolution mass spectrometry, and after optimization of the parameters we manage to obtain nice mass spectra for the complexes **2.34** and **2.35**. Figure 2.13 shows the mass spectrum of complex **2.35**. We observe several isotopic clusters, all belonging to the parent $[\text{Pt}_{10}(\text{dcpm})_{10}(\mathbf{2.19})_5]^{15+}$ cation, with a varying number of triflate (OTf) bound to the cage. Typically, one can see the cage with a number of counteranion between seven (8^+ cluster) and 10 (5^+ cluster). The theoretical isotopic distribution of the clusters match well with the experimental one, as shown by the right insert on Figure 2.13.

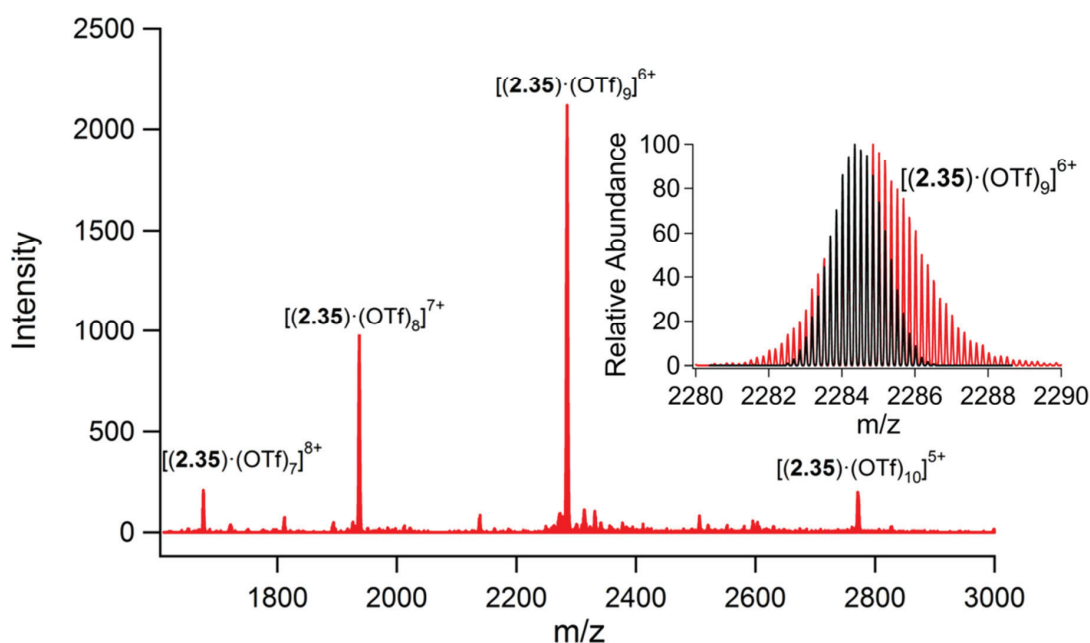


Figure 2.13 – Mass spectrum of **2.35** and its key fragments annotated between brackets. The right insert shows an overlay of the theoretical (black) and experimental (red) isotopic distribution of the cluster $[(\mathbf{2.35})\cdot(\text{OTf})_9]^{6+}$.

By combining HRMS results together with the NMR analyses, we have two $M_{10}L_5$ ($M = \text{cis-protected platinum corner}$; $L = \mathbf{2.19}$) molecular cages with a high symmetry with respect to the bridging corners, but whose clathrochelates have a forbidden rotation, leading to non-equivalent side groups. A proposed representation of such a cage is given in Figure 2.14. We hypothesize to be in presence of an open pentameric barrel, with platinum corners schematized as black spheres and **2.19** subunits as blue tetratopic rods. Due to the *pseudo*- C_3 symmetry of **2.19**, we can expect one of the three phenolatodioximate arm to point inside the cavity, leading to a strong shielding of the protons as observed for one *tert*-butyl group with $\delta = -0.12$ ppm (**2.34**) and $\delta = -0.20$ ppm (**2.35**). A total of five lateral dioxime pointing inside the cavity further leads to an extreme steric hindrance, preventing the rotation of the clathrochelate core around the B-C bond. The splitting of the pyridyl protons could be explained by a tilted coordination angle to the Pt(II) center, with half of the protons pointing towards the cavity. The formation of a barrel structure is in line with literature reports. In fact, the combination of *cis*-blocked Pd(II) or Pt(II) complexes having two available coordination sites with tetratopic N-donor ligands is a well explored synthetic strategy for the formation of coordination barrels. For ligands which can adopt a concave geometry (the coordinate vectors all point towards one side), the formation of small $M(II)_4L_2$ complexes is possible.⁷² However, the utilization of ligands with a ‘flat’ backbone is more common. For such ligands, the resulting barrels have mostly trigonal prismatic $M(II)_6L_3$ structures⁷³ or tetragonal prismatic $M(II)_8L_4$ structures.⁷⁴ So far, only one example of an $M(II)_{2n}L_n$ -type barrel with more than eight metal centers has been described, and that is a

hexagonal $\text{Pt(II)}_{12}\text{L}_6$ complex which was reported the group of Mukherjee in 2008.⁷⁵ This complex was obtained by combination of a tetrapyrrolyl-porphyrin ligand and $(\text{dppf})\text{Pt}(\text{OTf})_2$ (dppf = bis(diphenylphosphino)ferrocene). To the best of our knowledge, the complexes **2.34** and **2.35** are the first examples of pentameric barrels of type $\text{M(II)}_{10}\text{L}_5$.

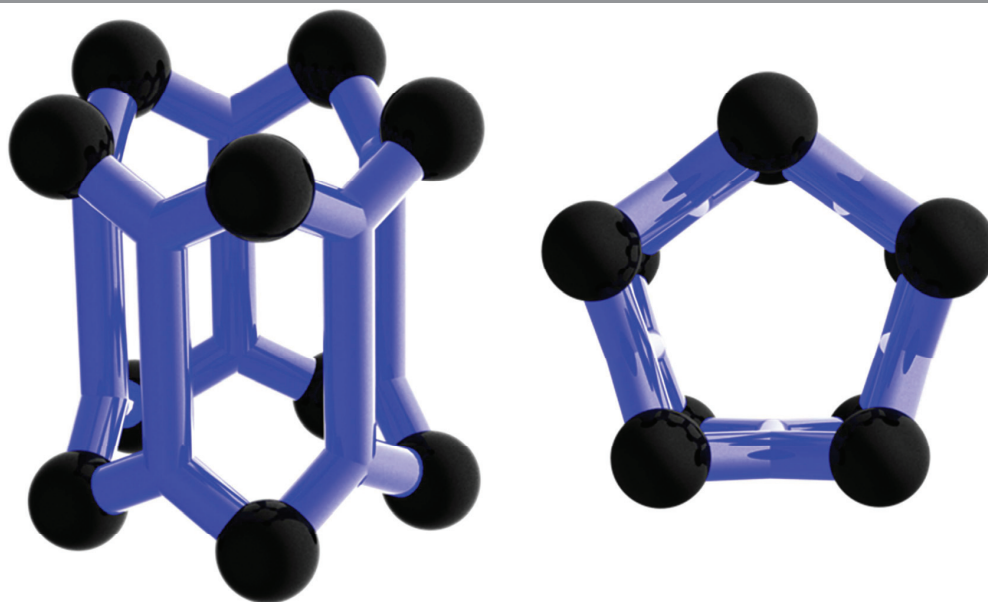


Figure 2.14 – Graphical representation of the proposed structure of **2.34** and **2.35**. The black spheres correspond to the *cis*-protected platinum corners and the tetra-topic blue rods to **2.19** subunits.

Among the many attempts to crystallize the cages, vapor diffusion of CH_2Cl_2 in solutions of **2.34** or **2.35** in $\text{DMSO}-d_6$ led to crystals that unfortunately did not diffract. Crystals were also obtained from the slow evaporation of the reaction mixture of **2.34** over several months. Crystallographic analysis of the crystal obtained following this strategy revealed the disruption of the molecular cage, since a dimer was obtained (Figure 2.15). Nevertheless, no peaks corresponding to this dimeric structure were found in the respective mass spectra.

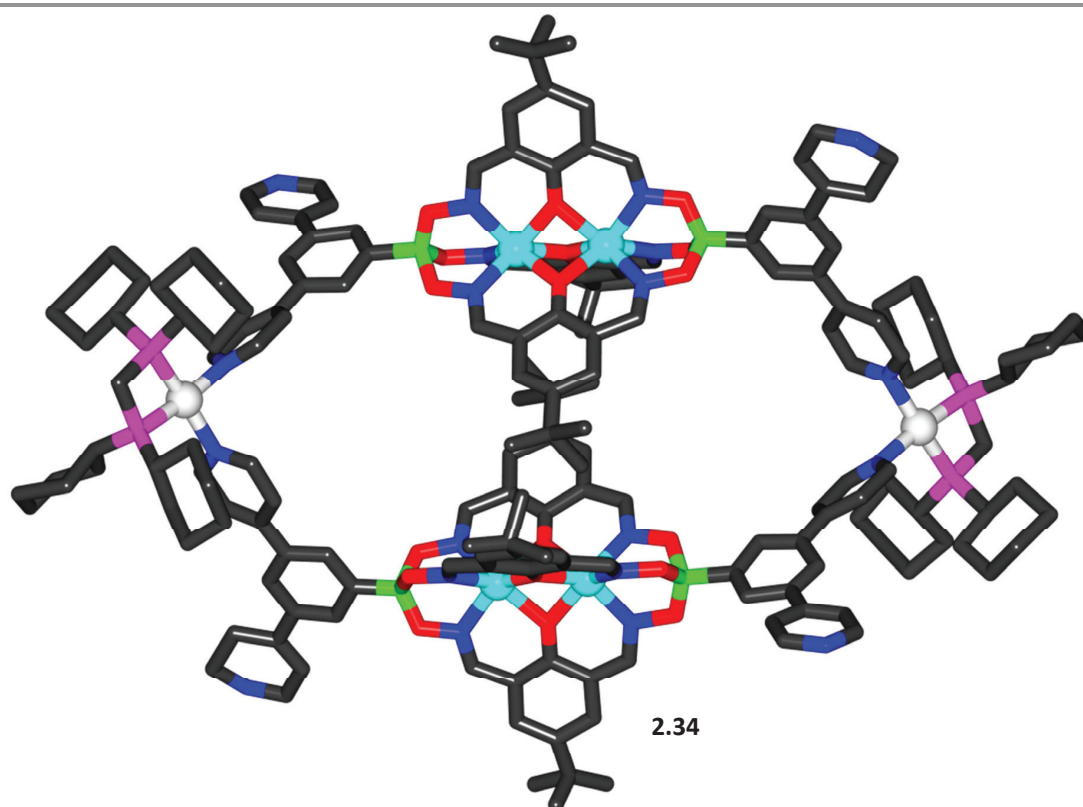
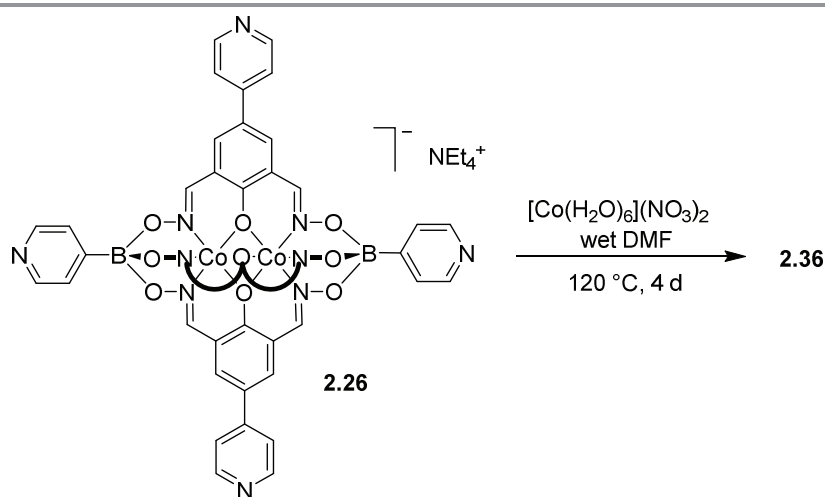


Figure 2.15 – Molecular structure of the dimer obtained by slow evaporation of a solution of **2.34**. Hydrogen atoms, counterions (OTf), and solvent molecules have been omitted for clarity. Color coding: C: gray; O: red; N: blue; B: green; Zn: cyan; P: pink; Pt: light grey.

2.4.3 MOFs based on pentatopic clathrochelates

In section 2.3, we described the syntheses of several polytopic clathrochelates. All these metalloligands have pyridyl groups with divergent coordinate vectors. The N-donor atoms of the pentatopic ligands **2.26**–**2.28** are arranged in a trigonal bipyramidal fashion. So far, there are few examples of MOFs based on pentafunctional ligands.⁷⁶ The utilization of a pentapyridyl ligand is, to the best of our knowledge, unprecedented. To demonstrate that coordination networks can indeed be obtained with pentatopic pyridyl ligands, we have synthesized a MOF by solvothermal reaction of **2.27** and $[\text{Co}(\text{H}_2\text{O})_6](\text{NO}_3)_2$ in wet DMF (Scheme 2.15). From the reaction mixture, we were able to isolate red crystals of **2.36** in moderate yield (due to an uncertainty with regard to its composition, a precise yield is not given).



Scheme 2.15 – Synthesis of MOF **2.36** using the pentapyridyl ligand **2.26**.

Crystallographic analysis of **2.36** revealed that all five pyridyl groups of the anionic metalloligand are coordinated to octahedral Co ions (Figure 2.15). One can observe two kinds of Co nodes with a different connectivity. The first one (Co1, green polyhedra) is connected to three pyridyl groups, two of which come from the boronate ester capping group, and one from the lateral oximato group. The second one (Co2, blue polyhedra) is connected to four pyridyl units, all of which come from lateral oximato ligands of the clathrochelate, resulting in an overall (3,4,5)-connected network structure.⁷⁷ The remaining coordination sites of Co1 and Co2 are occupied by oxygen atoms, coming from DMF (Co1), water or hydroxide (Co1 and Co2). A crystallographic distinction between water and hydroxide was not possible. The presence of hydroxide ligands is a necessity for balancing the charge of the network, since tetraethylammonium cations were not observed. It is noteworthy that the bridging clathrochelate ligands display a strong distortion from an ideal trigonal bipyramidal geometry. The planes defined by the three oximato ligands form angles of approximately 90° and 2 x 135°. This

distortion is further evidence for the intrinsic flexibility of these metalloligands. Interestingly, the network is two-fold interpenetrated. Attempts to desolvate MOF **2.36** by heating under vacuum resulted in a degradation of the material, as evidenced by visual inspection. Accordingly, we were not able to detect any permanent porosity by BET surface measurements (N_2 , 77 K) after activation of the crystals by heating at 120 °C under dynamic vacuum for 12 hours.

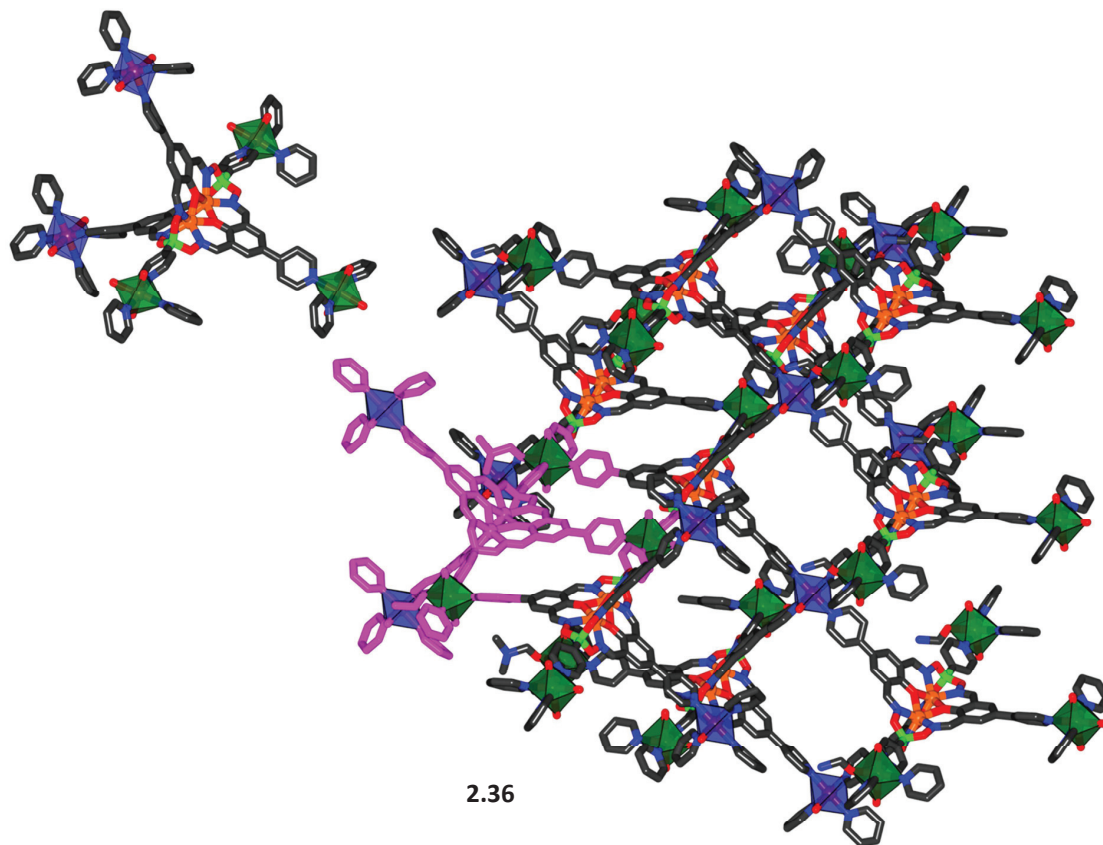


Figure 2.15 – (a) Graphic representation of the connectivity in MOF **2.36** with focus on one metalloligand. Blue polyhedral correspond to octahedral Co nodes connected to four pyridyl groups, green ones to octahedral Co nodes coordinated to three pyridyl groups. (b) Part of the crystal packing of MOF **2.36**. The structure represented in (a) is highlighted in pink. Hydrogen atoms and unbound solvent molecules have been omitted for clarity. Color coding: C: grey; O: red; N: blue; B: green; Co: orange.

Unfortunately, the quality of the crystals of **2.36** was not good enough to allow us assigning all atoms (notably, the amount of hydroxyl groups as well as their precise locations). While reproducing the reaction in order to get crystals of better quality, we obtained crystals similar in shape to the ones of **2.36** (orange shiny prisms). While solving the structure, we realized that we had obtained a new MOF structure, **2.37** (Figure 2.16), with the stoichiometry $[Co(2.26)(C_2O_4)_{0.5}]$. While **2.36** crystallizes in the P_{121}/n space group, **2.37** crystallizes in the C_2/c space group. The asymmetric unit of the crystal contains one clathrochelate subunit of **2.26**, one Co(II) ion as well as half an oxalate (C_2O_4)

ligand. The presence of this oxalate group was surprising, since oxalic acid was not used during the synthesis. We think that it results from the slow degradation of the DMF, known to form dimethylamine and formate (or formic acid) upon heating in presence of water.⁶⁸ Oxalate would then be formed by the oxidative coupling of two formate moieties. As a result, **2.37** contains clathrochelates having only four pyridyl coordinated to Co(II) nodes, one of the boronate ester capping group remaining free. The Co(II) nodes have an octahedral geometry, with four N-donors and two *cis* O-donors from the oxalate. The latter bridges another Co(II) node, resulting in Co-Co distances of 5.2958(12) Å. This distance being relatively short, packing is achieved by a major distortion of the clathrochelates arms, with angles between the planes defined by the three oximate ligands of 103.30°, 108.12° and 148.51°. Repeating the reaction by either following the same procedure or applying small variations (concentration of the reagents, temperature, and stoichiometry of the reagents) never allowed us to obtain crystals of **2.36** again. However, several crystals analyzed by X-ray crystallography revealed a structure identical to **2.37**.

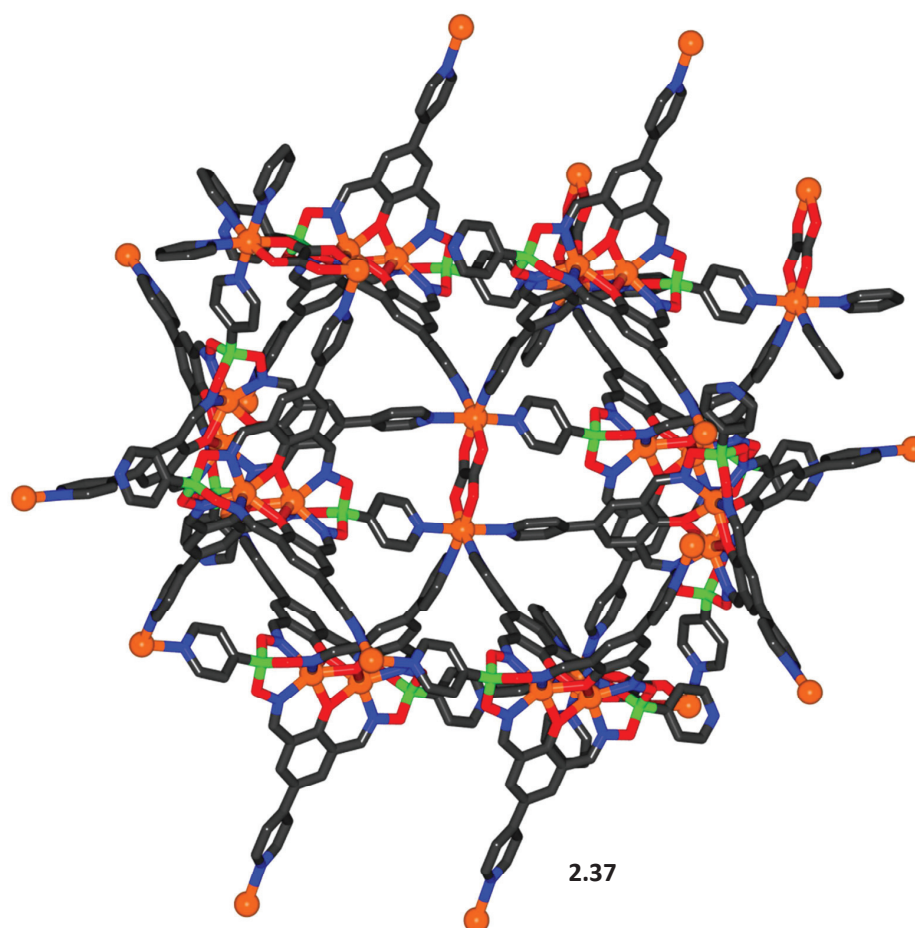
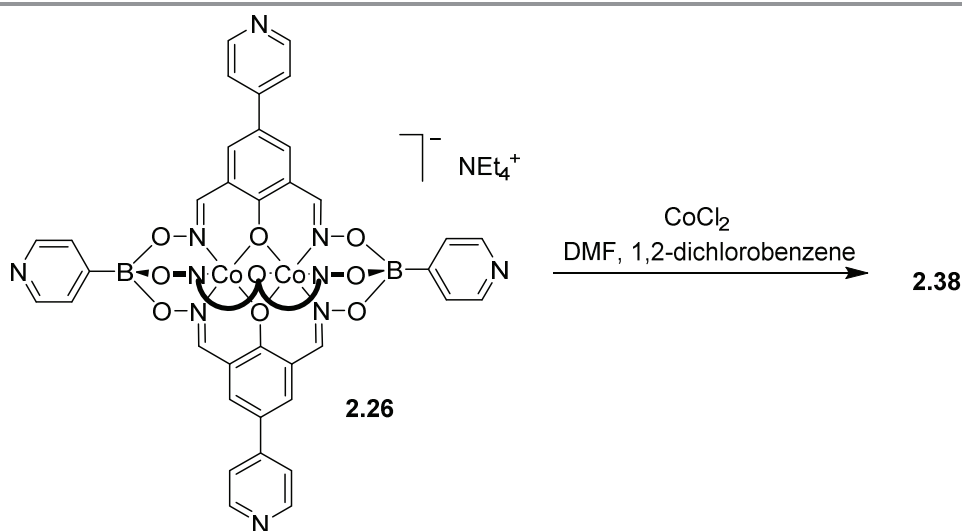


Figure 2.16 – Graphic representation of **2.37** in the crystal. Hydrogen atoms and unbound solvent molecules have been omitted for clarity. Color coding: C: grey; O: red; N: blue; B: green; Co: orange.

Being curious whether pentatopic clathrochelate **2.26** could be incorporated in other three-dimensional networks or MOFs, we explored the reaction of **2.26** with various metal ions. We chose the reagents diffusion technique, since in most of the cases an immediate precipitate formed upon mixing of the two reagents. We were able to obtain crystals of coordination polymer **2.38** (Scheme 2.16) by diffusion of a solution of CoCl_2 in MeOH into a solution of **2.26** in a mixture of DMF and 1,2-dichlorobenzene (1:1).



Scheme 2.16 – Synthesis of MOF **2.38** using the pentapyridyl ligand **2.26**.

Crystallographic analysis of **2.38** revealed the formation of two-dimensional layers, with CoCl_2 as the connection node between the clathrochelates (Figure 2.17). The octahedral Co(II) node is connected to two *cis* N-donor from the boronate ester capping groups, to two *cis* N-donor from the lateral dioximato ligands and to two *trans* chloride atoms. This results in a negatively charged network with the stoichiometry $[\text{CoCl}_2(\mathbf{2.26})](\text{sol.})_n$, however due to the poor crystal quality we were not able to observe either tetraethylammonium counterions or protonated pyridyl groups that would validate the charge balance considerations. As for MOF **2.37**, one of the pyridyl is not coordinated to the Co(II) node, and remains free (or protonated, as discussed above). This four-fold coordination of the clathrochelate results in the formation of zig-zag shaped two-dimensional layers (Figure 2.17a), with the free pyridyl group pointing alternately up or down (Figure 2.17b). Close packing of adjacent two-dimensional layers leads to the formation of one-dimensional channels that are filled with disordered solvent molecules (Figure 2.17c). Due to the very few amount of crystals collected for **2.38**, we were not able to determine its gas sorption properties. All attempts to obtain **2.38** on a larger scale were unfortunately unsuccessful.

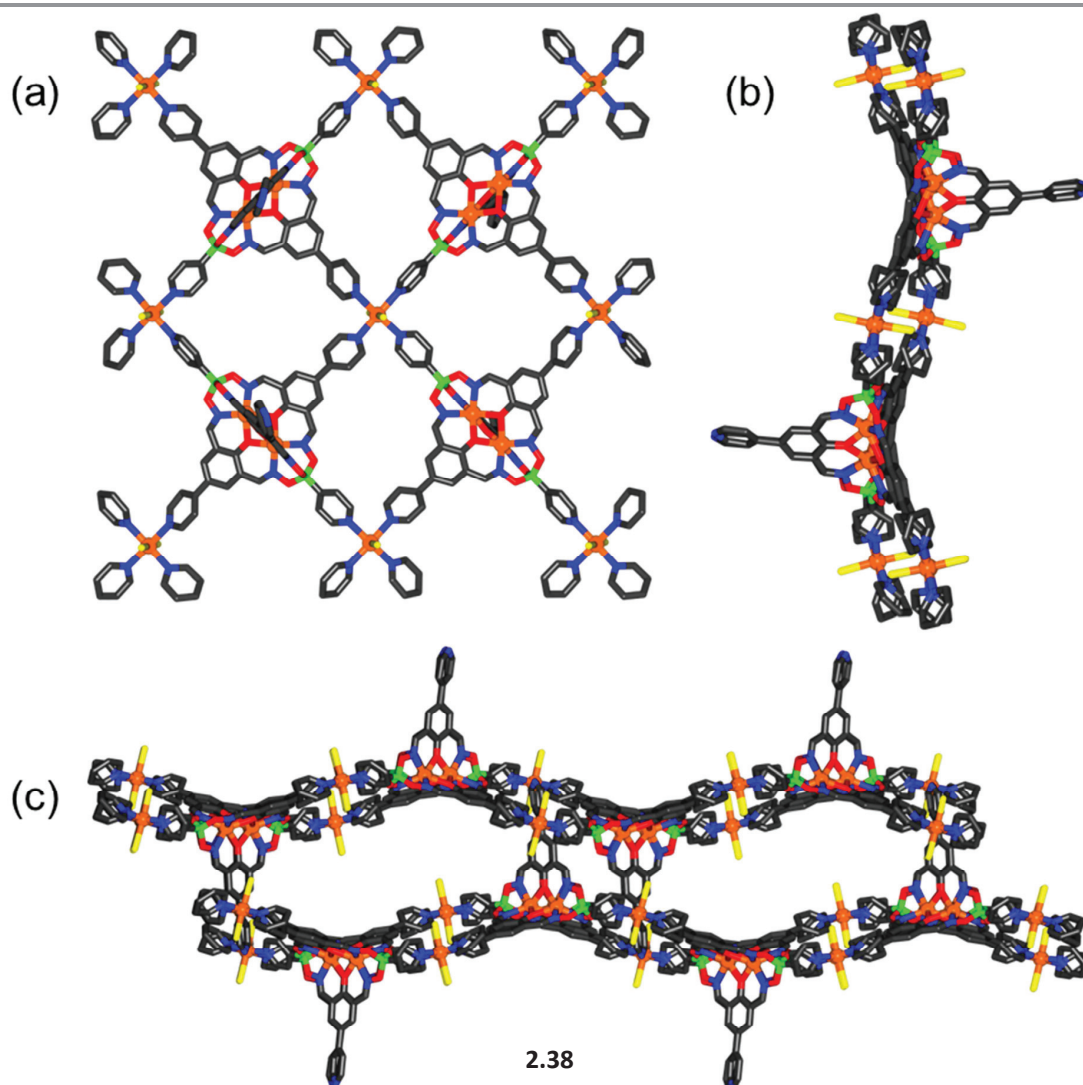


Figure 2.17 – Graphic representation of **2.38** in the crystal. Hydrogen atoms and unbound solvent molecules have been omitted for clarity. Color coding: C: grey; O: red; N: blue; B: green; Co: orange.

2.5 Conclusion

In this chapter, the synthesis of Zn(II), Co(II) or Mn(II) dinuclear clathrochelates functionalized with pyridyl groups are reported. They can be obtained either *via* direct synthesis from easily available starting materials, or *via* Pd-catalyzed cross-coupling reactions of brominated clathrochelates and pyridyl boronic acid. The poly-cross-coupling reactions are remarkably efficient and give the desired functionalized clathrochelates in high yield. In view of the characteristics of the new polypyridyl ligands (large, relatively rigid, anionic, and luminescent in case of $M = \text{Zn}$), we expected that they will be of interest as building blocks for supramolecular chemistry and materials science. Indeed, we successfully incorporated a ditopic clathrochelate in the two-dimensional network **2.31**. This network has a well-established connectivity, however the charge balance of our ligand **2.1** prevented the incorporation of an additional anion, leading to a material with intrinsic porosity. The incorporation of clathrochelates with a higher number of attached pyridyls in supramolecular assemblies was also successful. We were able to obtain two pentameric barrels of formula $M_{10}L_5$, by using the tetratopic clathrochelate **2.19**. Furthermore, we synthesized new MOFs with the pentatopic clathrochelate **2.36** having a trigonal bipyramidal geometry.

Chapter 3 Dinuclear clathrochelates functionalized with carboxylic acid groups

The results presented in this chapter detail the synthesis of homometallic dinuclear Co^{2+} and Zn^{2+} clathrochelates decorated with carboxylic acid groups. Furthermore, the successful incorporation of these clathrochelates into MOF structures is reported. The results presented in this chapter were published in “Carboxylic acid-functionalized clathrochelate complexes: large, robust and easy-to-access metalloligands”, Mathieu Marmier, Matthew D. Wise, Julian J. Holstein, Philip Pattison, Kurt Schenk, Euro Solari and Kay Severin, *Inorg. Chem.*, **2016**, 55, 4006-4015.

3.1 Introduction

Carboxylic acid-functionalized ligands are of paramount importance in supramolecular chemistry, most notably in the preparation of metal–organic frameworks (MOFs). Since the pioneering discovery of compounds such as MOF-5 by Yaghi and coworkers (Figure 3.1a),⁷⁸ and HKUST-1 by the group of Williams (Figure 3.1b),⁷⁹ the number of reported MOF structures continues to grow exponentially.⁸⁰

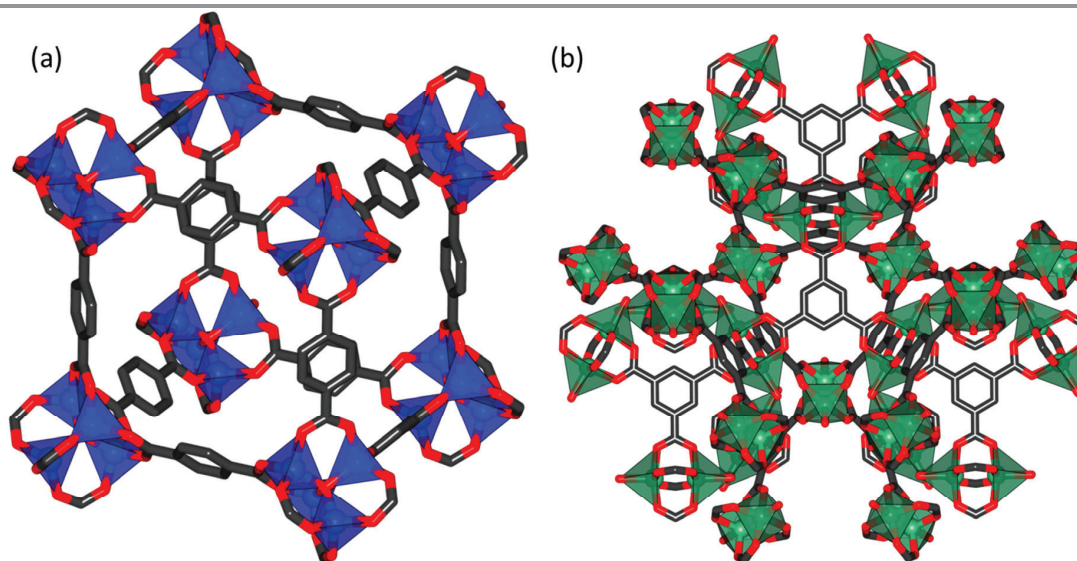


Figure 3.1 – Graphical representation of (a) MOF-5 and (b) HKUST-1. Zn(II) and Cu(II) atoms in the MOFs clusters are represented in blue, respectively green polyhedral.

The development of MOF chemistry has in part been driven by the variety of ligands employed in the preparation of these materials. The concept of reticular chemistry,^{3c,81} along with a range of well-established synthetic techniques for MOF preparation, has enabled the strategic incorporation of increasingly elaborate ligands into MOFs, the properties and structural characteristics of which are determined by those of the ligands themselves. This powerful, modular means to prepare bespoke materials in a targeted manner is exemplified by MOF-5 and its isorecticular analogues, which have been constructed from a wide range of ditopic carboxylic acid ligands such as those based on extended oligo(phenylenes) and terephthalic acid derivatives,^{3b,4a,82} and even metal complexes (metalloligands), some of which having been described in section 1.2.2. The incorporation of functional moieties, including photoactive groups,^{32b,83} catalytically active metal centers,^{20b,84} or simple organic functional groups,⁸⁵ into carboxylic acid-based MOF building blocks has facilitated the preparation of materials with new and interesting properties.

Another ligand property that has received a significant amount of attention in recent times is size. The preparation of longer or expanded building blocks has enabled MOFs with greater internal void

volumes, cavity dimensions and surface areas to be made. Consequently, these materials are, for example, capable of the uptake of larger guest species⁸⁶ or greater volumes of adsorbed gas.⁸⁷ Again, reticular synthesis has encouraged the design of numerous expanded MOF structures based upon well-known network topologies,⁸⁸ but common setbacks encountered during research into these materials include the observation of extensive network interpenetration.⁸⁹ Other obstacles are the synthetic efforts and the costs associated with the preparation of large ligands. This point is exemplified by work of the groups of Yaghi and Stoddart,⁹⁰ who developed a series of ditopic linear α -hydroxycarboxylic acid ligands up to 5 nm in length (Figure 3.2). These building blocks were subsequently incorporated into a range of isostructural MOFs (the IRMOF-74 series), which possessed interior channel apertures of up to 98 Å. The synthesis of the longest ligand employed in this study required eight steps and gave an overall yield of 14%.

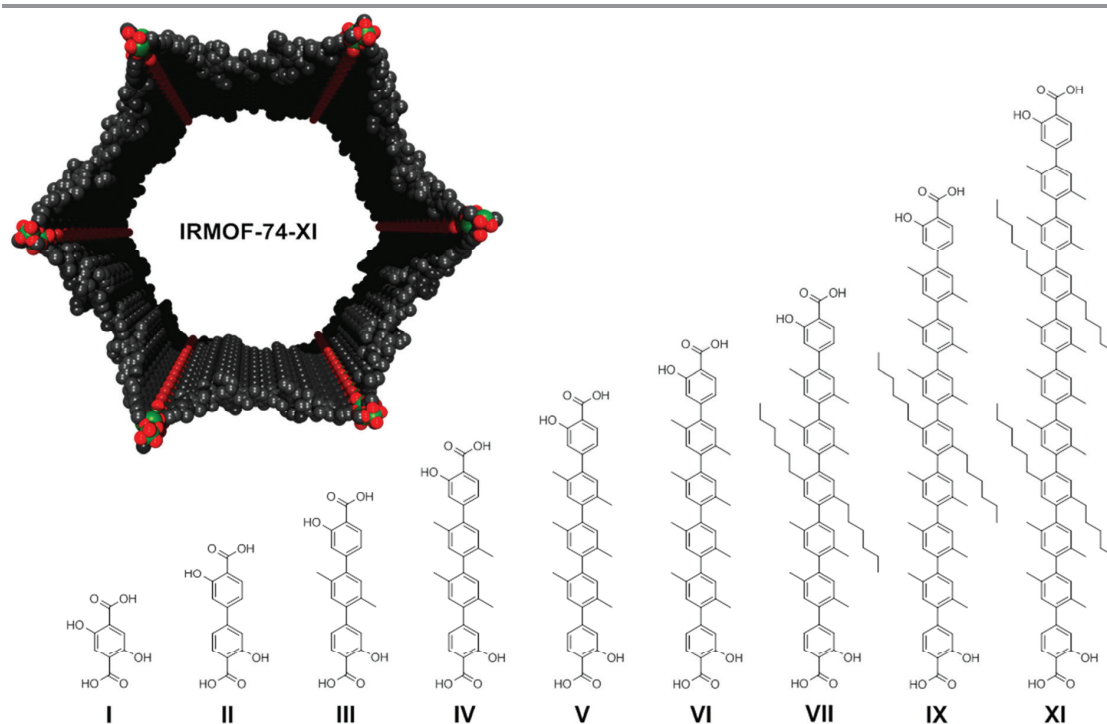
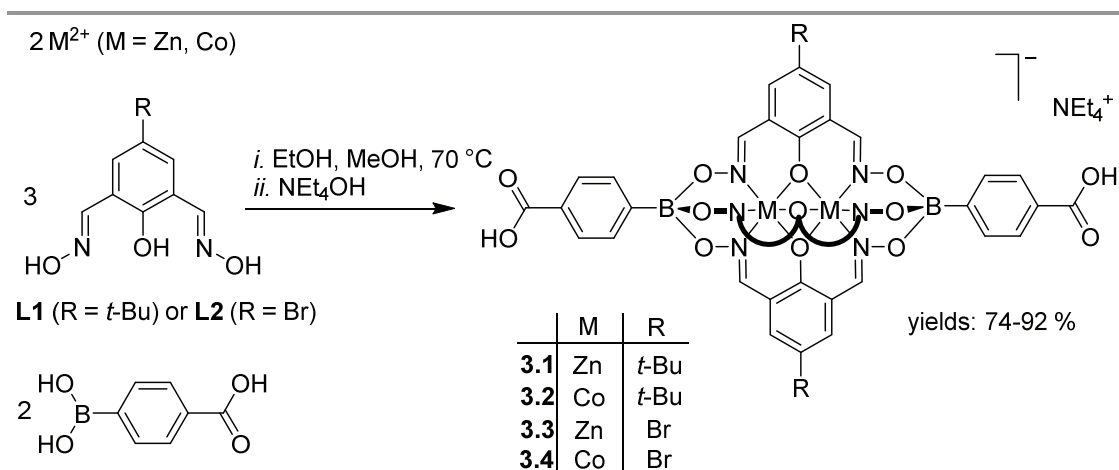


Figure 3.2 – Graphical representation the ligands used for the synthesis of the IRMOF-74 series. The roman numbering corresponds to the number of oligophenylene spacers between the α -hydroxycarboxylic acid moieties. The left insert shows the 98 Å aperture of IRMOF-74-XI.

3.2 Synthesis of polytopic clathrochelates sharing carboxylic acid groups

We discussed in Chapter 2 the construction of 4,4'-bipyridyl metalloligands based on M(II) dinuclear complexes. A unique feature of these pyridyl-capped metalloligands is their negative charge, which may bestow supramolecular assemblies with extra stability, as exemplified by the studies on the molecular square described by Dr. Schouwey. We hypothesized that dinuclear clathrochelates could also be used as scaffolds for the preparation of new polycarboxylate ligands, which should represent highly interesting building blocks for MOF chemistry. Indeed, anionic M(II) tris(dioximato) complexes ($M^{2+} = \text{Co}, \text{Zn}$) with two appended carboxylic acid groups were obtained by reaction of 4-carboxyphenylboronic acid, 2,6-diformyl-4-*tert*-butylphenol dioxime (**L1**) or 2,6-diformyl-4-bromophenol dioxime (**L2**) and the appropriate metal salt ($\text{Zn}(\text{OTf})_2$ or $[\text{Co}(\text{H}_2\text{O})_6](\text{NO}_3)_2$) in a mixture of MeOH and EtOH (Scheme 3.1). It should be noted that the boronic acid is commercially available, and the dioximes can be prepared easily from the corresponding dialdehydes, as discussed previously. Conversely to the synthesis of the pyridyl-capped clathrochelates, presence of a base was required for the insertion of the third phenolatodioximato ligand. Tetraethylammonium hydroxide was chosen for this purpose since the NEt_4^+ cation enhances the solubility of the final complexes. The products **3.1–3.4** precipitated from solution upon concentration of the mother liquor as amorphous solids. The high yields of 74–92% indicate that the CO_2H functions on the boronic acid do not interfere with the formation of the dinuclear clathrochelate core, even though Zn^{2+} and Co^{2+} ions are known to bind carboxylate ligands. The anionic clathrochelates **3.1–3.4** are well soluble in polar aprotic solvents such as DMF, DMA and DMSO.



Scheme 3.1 – Synthesis of the ditopic clathrochelate complexes **3.1–3.4**.

Clathrochelates **3.1–3.4** were analyzed by high-resolution mass spectrometry, Fourier-transform infrared spectroscopy and, for the diamagnetic complexes **3.1** and **3.3**, NMR spectroscopy. As expected, only one set of signals was observed for the phenolatodioximato ligands, revealing the *pseudo*- C_3 symmetry of the complexes. Single crystal X-ray structural analysis of **3.2** revealed the presence of the expected dinuclear clathrochelate core with terminal carboxylic acid groups (Figure 3.3a). The two Co^{2+} ions in complex **3.2** are coordinated in a trigonal prismatic fashion by three nitrogen and three oxygen atoms. The two carbon atoms of the terminal CO_2H groups are 21 Å apart from each other. This length is notably far from the 50 Å of IRMOF-74-XI ligand,⁹⁰ but the synthetic efforts cannot be confronted. Clathrochelate **3.2** is however comparable to ditopic linkers having up to five phenylene spacers, such as ligand V (about 22 Å) in the IRMOF-74-V,⁹⁰ or slightly larger than *trans*-biscarboxylate tetraarylporphyrins such as $\text{H}_4\text{DCPMes}_2\text{P}$ in PIZA-4,⁹¹ or ditopic ligands with four aryl rings spacers.⁹² In solution, the Zn complexes **3.1** and **3.3** display *pseudo*- C_3 symmetry as revealed by a single set of NMR signals for the three oximato ligands. In the solid state, one can observe a small deviation from this ‘ideal’ geometry, with angles between the planes of the three lateral oximato ligands between 116.90° and 123.13° (Figure 3.3b).

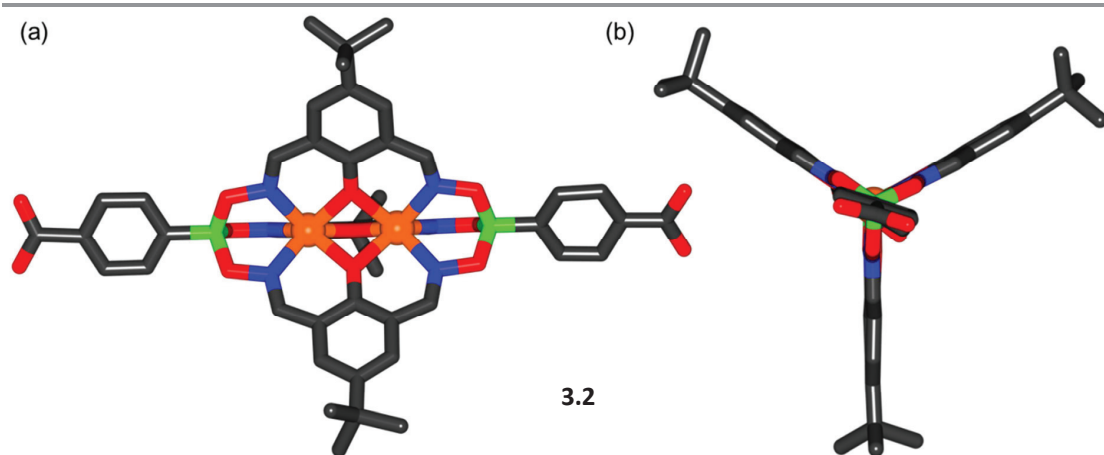
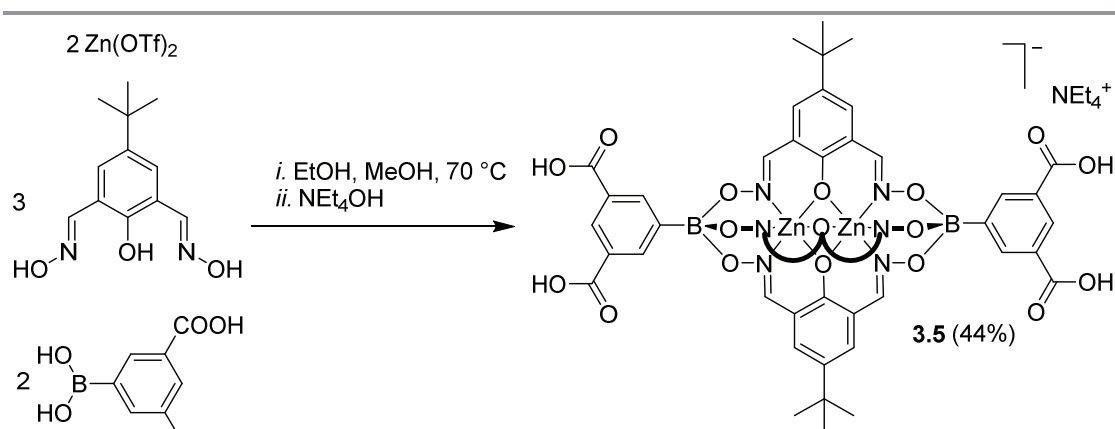


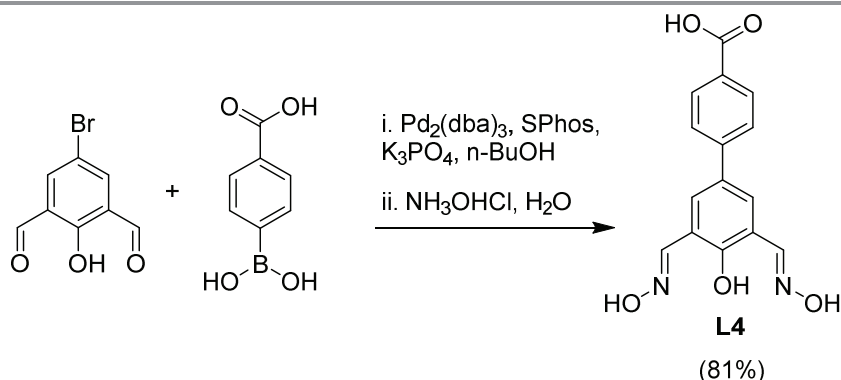
Figure 3.3 – Molecular structure of metalloligand **3.2** in the crystal with view from the side (top) and along the *pseudo*- C_3 symmetry axis (bottom). Hydrogen atoms, the counter ion (NEt_4^+), and solvent molecules have been omitted for clarity. Color coding: C: gray; O: red; N: blue; B: green; Co: orange.

A similar synthetic strategy as employed for **3.1–3.4** was used to prepare the clathrochelate complex **3.5** featuring four carboxylic acid functions attached to the terminal arylboronate ester groups (Scheme 3.2). Clathrochelate **3.5** was obtained as a fully protonated tetraethylammonium salt in 44% yield, and characterized by high-resolution mass spectrometry, Fourier-transform infrared spectroscopy and NMR.



Scheme 3.2 – Synthesis of the tetratopic clathrochelate complex **3.5**.

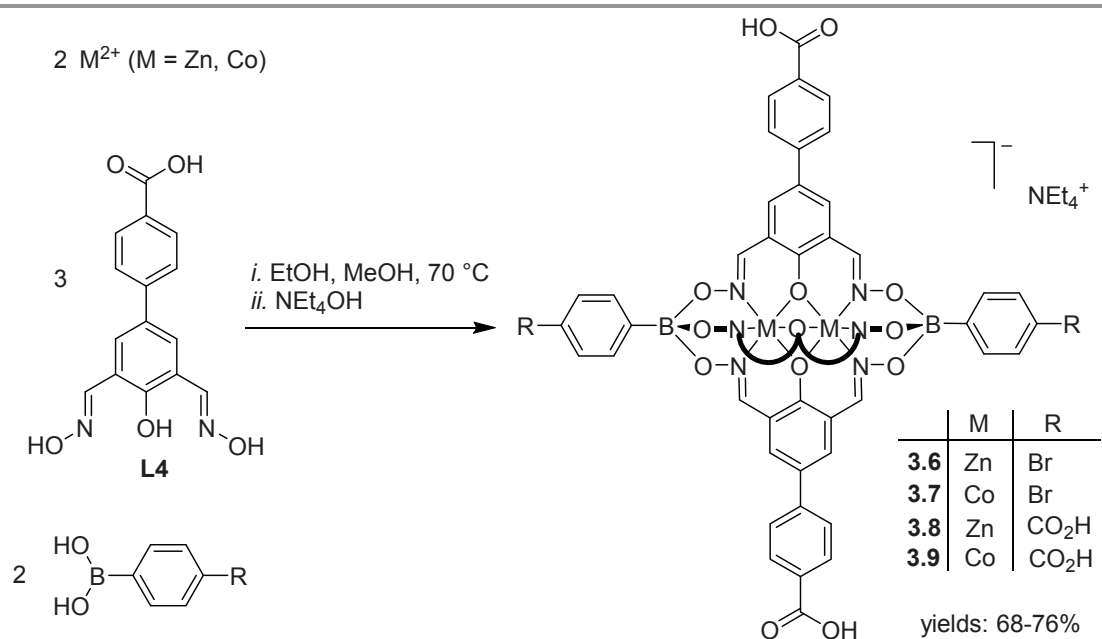
We envisioned that it should also be possible to use the dioximate ligands for introducing additional CO₂H groups, thereby broadening the variety and hence potential applications of clathrochelate-based metalloligands. This goal was accomplished through synthesis of the CO₂H-functionalized dioximate ligand **L4**. Similarly to the synthesis of **L3** (section 2.3), Suzuki-Miyaura coupling of 4-carboxyphenylboronic acid and 2,6-diformyl-4-bromophenol in the presence of Pd₂(dba)₃ and Buchwald's SPhos ligand⁶⁴ in *n*-BuOH afforded the crude diformylphenol intermediate, which was converted to its corresponding dioxime **L4** by treatment with hydroxylamine hydrochloride (Scheme 3.3).



Scheme 3.3 – Synthesis of the carboxylic acid-decorated dioxime ligand **L4**.

The new ligand **L4** was subsequently used for the synthesis of the clathrochelates **3.6** and **3.7** (Scheme 3.4). These complexes feature three CO₂H groups in equatorial position and two bromo atoms in axial position. Based on simple molecular modelling considerations, we expect a distance of approximately 18.6 Å between the carbon atoms of the carboxylic acid groups. Consequently, these trigonal metalloligands are significantly larger than the commonly employed 1,3,5-tris(4-carboxyphenyl)benzene ligand (C...C = 12.55 Å). The bromo atoms were introduced

because they were found to slightly improve the solubility of the clathrochelates. By using ligand **L4** in combination with the capping agent 4-carboxyphenylboronic acid, we obtained the pentatopic clathrochelate ligands **3.8** and **3.9** (Scheme 3.4). To date, very few examples of 5-fold coordinating ligands have been studied,^{76a,c-e,93} and our clathrochelates are, to the best of our knowledge, the largest such ligands ever reported.



Scheme 3.4 – Synthesis of the tri- and pentatopic clathrochelate complexes **3.6–3.9**.

In the discussion so far, we have mainly focused on the size and the geometry of the new metalloligands. However, there are also other properties which are worth noting. The Zn-based clathrochelates **3.1**, **3.3**, **3.5**, **3.6**, and **3.8** are all luminescent, with emission maxima at around 450 nm (**3.1**: 445nm, λ_{ex} = 325nm; **3.3**: 452nm, λ_{ex} = 335nm; **3.5**: 445nm, λ_{ex} = 335nm; **3.6**: 457nm, λ_{ex} = 335nm; **3.8**: 445nm, λ_{ex} = 335nm, in DMF/DMSO, Figure 3.4). Due to the inert character of the Zn²⁺ ions, the luminescence can be assigned to intraligand and/or ligand-to-ligand charge transfer emissions as observed for pyridyl-appended clathrochelates. The dinuclear Co complexes are not emissive, presumably due to quenching by the paramagnetic metal ions. The magnetic properties of the Co clathrochelates were not studied in detail, however for complexes **3.2** and **3.4** we have determined effective magnetic moments (μ_{eff}) of 5.37 μ_{B} and 5.81 μ_{B} , respectively, by using the Evans method. We would also like to stress the intrinsic charge displayed by the dinuclear Zn- and Co-containing clathrochelates. This additional negative charge represents a fundamental difference compared to standard carboxylic acid ligands, which only become charged after deprotonation of the CO₂H groups.

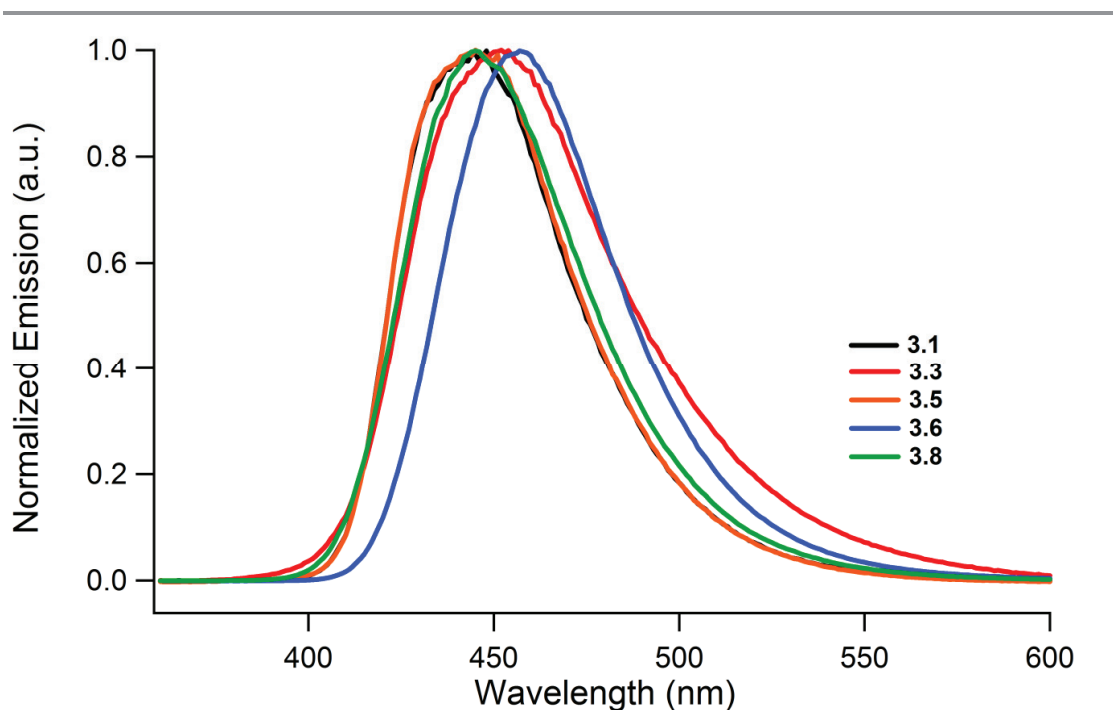


Figure 3.4 – Emission spectra in DMF/DMSO (1:1) solution of **3.1** (λ_{ex} = 325 nm), **3.3** (λ_{ex} = 335 nm), **3.5** (λ_{ex} = 325 nm), **3.6** (λ_{ex} = 335 nm) and **3.8** (λ_{ex} = 335 nm).

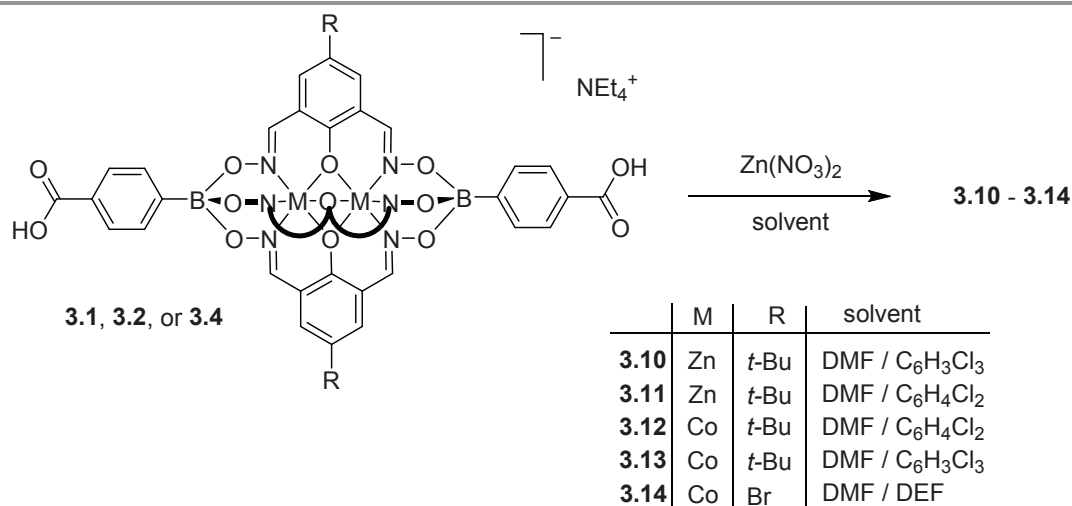
Having shown that carboxylic acid-functionalized clathrochelate complexes can be synthesized in one pot from simple and readily available starting materials, we examined applications as supramolecular building blocks. The lateral side groups of the oximes were a challenging part, since it was difficult to estimate if the steric bulk from adjacent clathrochelates was not a pitfall for the formation of rectangular coordination pattern found in many MOFs. On the other hand, the lateral groups could be found as a virtue, preventing interpenetration of the networks. The effect of the intrinsic negative charge shared by the bimetallic clathrochelates was also an unknown parameter to take into account.

3.3 Use of carboxylic acid-decorated clathrochelates as supramolecular building blocks

3.3.1 Synthesis of MOF-5 derivatives using 4,4'-dicarboxylic acid clathrochelates

In order to demonstrate that our clathrochelate-based polycarboxylic acids are suitable for incorporation into MOFs, we targeted the synthesis of a representative coordination polymer class, sharing MOF-5 topology. MOF-5 is amongst the most extensively studied porous materials since its discovery in 1999,⁷⁸ and given the vast range of isostructural MOF-5 analogues that have been reported, along with the interesting functional properties possessed by many of these materials,⁹⁴

this framework structure was considered to be an ideal initial candidate for the incorporation of carboxylic acid-functionalized clathrochelate complexes into MOFs. Solvothermal reaction of ditopic ligands **3.1**, **3.2** and **3.4** and $[\text{Zn}(\text{H}_2\text{O})_6](\text{NO}_3)_2$ in a mixture of DMF and a chlorinated aromatic solvent (chlorobenzene, 1,2-dichlorobenzene or 1,2,4-trichlorobenzene) or N,N-diethylformamide (DEF) at 120°C resulted in the formation of single crystals upon heating (Scheme 3.5).



Scheme 3.5 – Synthesis of the MOFs **3.10–3.14** following a solvothermal strategy.

Single crystals suitable for X-ray structural analysis were obtained for all the different solvent systems. Due to the high disorder observed in the crystals, the key to a successful refinement was the utilization of stereochemical restraints for the clathrochelate ligands within MOFs **3.10–3.11**, which were generated by the GRADE program.^{95,96} This macromolecular refinement technique has been adapted to be used in the program SHELXL.⁹⁷ We have already used this methodology for other clathrochelate-based structures,¹⁶ and it was found to drastically increase the robustness of the refinement, especially when being combined with the new rigid bond restraint in SHELXL 2013 (RIGU).⁹⁸ The program ShelXle,⁹⁹ which supports the macromolecular residue grouping, was used as a GUI. Crystallographic analysis of MOF **3.10** revealed a topology identical to MOF-5 and the IRMOF-n series.¹⁰⁰ The framework is composed of clathrochelate complexes ligated to Zn_4O clusters by their carboxylate groups (Figure 3.5), with the stoichiometry $[\text{Zn}_4\text{O}(\mathbf{3.1})_3](\text{C}_8\text{H}_{20}\text{N})_3(\text{sol.})_n$. These clusters are composed of four tetrahedral Zn^{2+} cations and a central $\mu_4\text{-O}$ atom. Unlike MOF-5, where each Zn_4O node adopts an octahedral geometry with respect to the organic linkers, **3.10** showed a slightly distorted geometry. Indeed, the zinc SBUs are linked together by the deprotonated dicarboxylic acid ligands in a trigonal antiprismatic fashion. The central oxygen atoms from adjacent zinc SBUs are separated by a distance of 27.750(5) Å, the angles between the axis of the clathrochelate ligands (as defined by the central $\mu_4\text{-O}$ atoms of the Zn_4O nodes) are 71° and 109° for *cis*- pairs of

clathrochelates, respectively, to be compared to the average 90° angle in the IRMOF-n series. Somewhat surprisingly, the network is two-fold interpenetrated (Figure 3.5b). Such interpenetration has frequently been observed for MOF-5 assemblies constructed from long carboxylate ligands,^{89a,101} but we had anticipated that the steric bulk of the equatorial *tert*-butyl groups of the phenolatodioximate ligands within **3.1** might prevent such interpenetration. A unique feature of **3.10** compared to standard MOF-5-type structures is the fact that the network is negatively charged (the bridging carboxylate ligands display a charge of -3). The charge is compensated by NEt_4^+ cations, which are found in the voids of the structure.

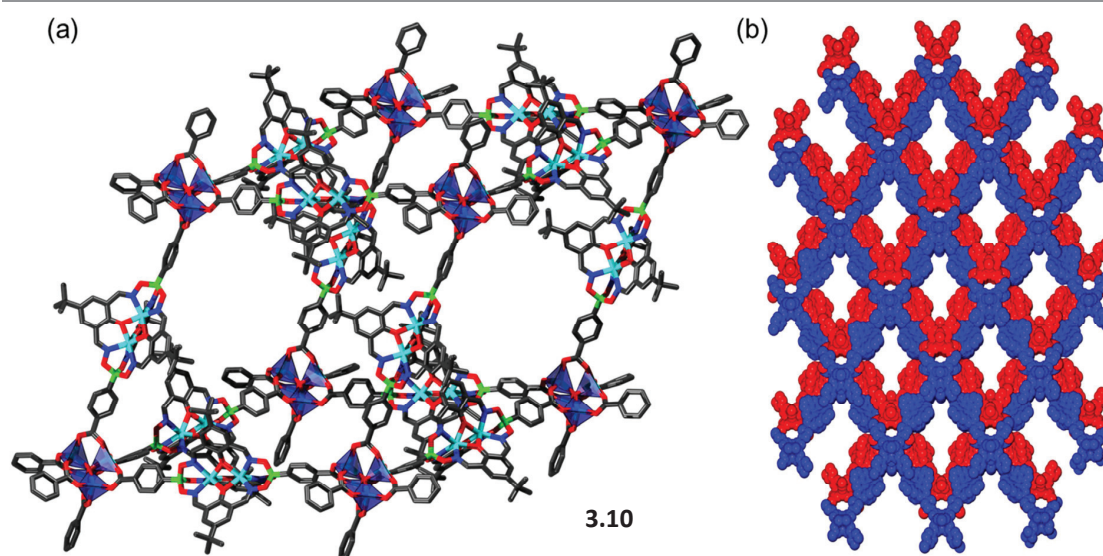


Figure 3.5 – (a) Part of the structure of MOF **3.10**. Hydrogen atoms, NEt_4^+ cations, and solvent molecules have been omitted for clarity. Color coding: C: gray; O: red; N: blue; B: green; Zn: cyan. Blue polyhedral represent the tetrahedral Zn atoms in the tetranuclear SBU; (b) The red and blue parts represent two independent, interpenetrated networks of **3.10**. Solvent and tetraethylammonium ions have been omitted for clarity.

Whereas structural analyses of MOFs **3.12** and **3.13** exhibited only minor structural differences compared to **3.10** (Figures 3.6a,b), presumably due to the different solvents employed during their synthesis, MOF **3.11** revealed different behaviour. The three-dimensional framework is likewise composed of clathrochelate metalloligands connected to Zn_4O clusters (Figure 3.6c). However, three of the Zn^{2+} cations adopt a classical tetrahedral geometry, whilst the fourth is six-coordinate and octahedral (Figure 3.6d).

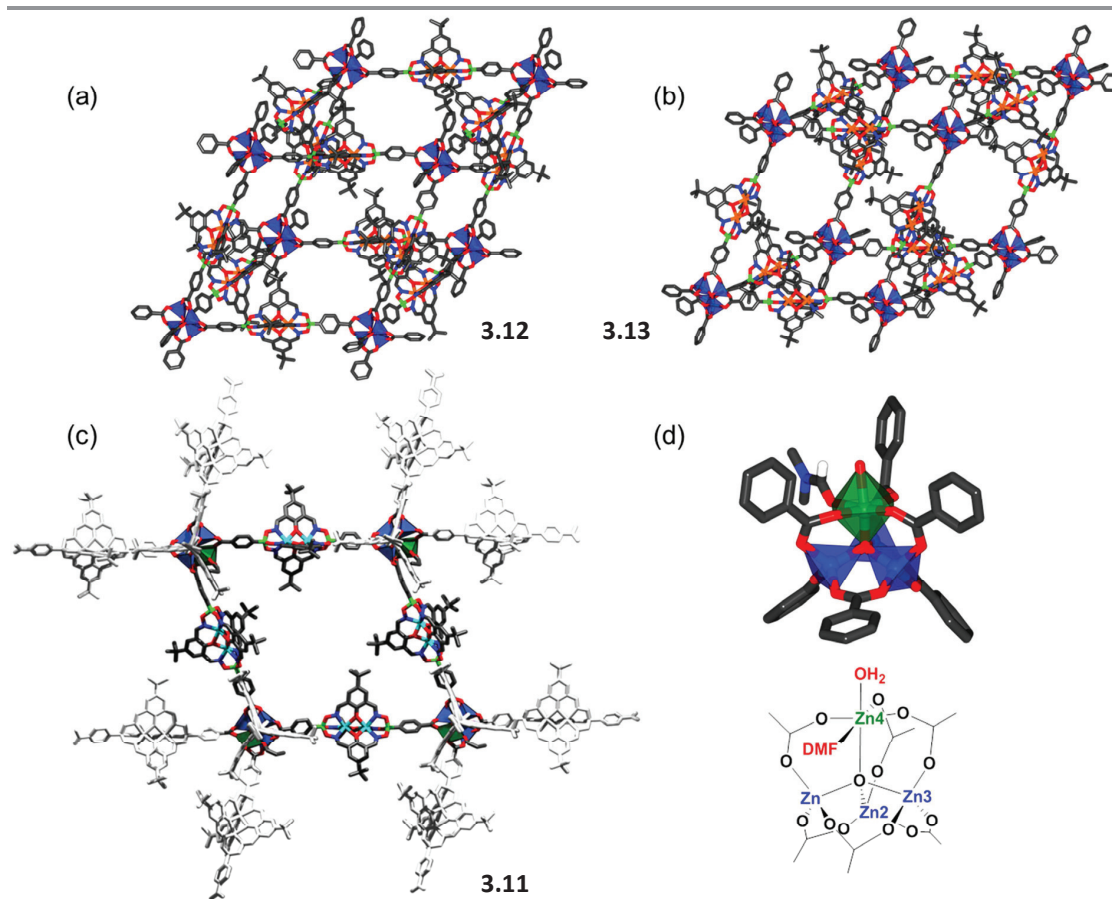


Figure 3.6 – (a) Part of the structure of MOF **3.12**; (b) Part of the structure of MOF **3.13**; (c) Part of the structure of MOF **3.11** with view along the crystallographic *c* axis and (d) Molecular structure of the tetranuclear SBU of MOF **3.11**. Most hydrogen atoms, NEt_4^+ cations, and unbound solvent molecules have been omitted for clarity. Color coding: C: gray; H: white; O: red; N: blue; B: green; Co: orange; Zn: cyan. Blue and green polyhedra represent the tetrahedral, respectively octahedral Zn atoms in the tetranuclear SBUs.

Several groups have studied the exchange of one tetrahedral Zn^{2+} ion within a Zn_4O SBU with another, octahedral metal ion,¹⁰² but reports of the formation of unusual geometries for one of the Zn^{2+} ions are scarce. Notably, the group of Gao reported in 2010 the synthesis of a rare Kagomé topology with a five-coordinate trigonal bipyramidal geometry for one of the Zn^{2+} ions and an octahedral geometry for another after binding of two DMSO molecules.¹⁰³ Within the Zn_4O clusters of **3.11**, three Zn^{2+} ions (Zn1, Zn2 and Zn3) are located in tetrahedral environments, each metal ion being coordinated by three carboxylate oxygen atoms from different clathrochelate ligands and the $\mu_4\text{-O}$ atom in the center of the cluster (Figure 3.6d). The remaining zinc atom (Zn4) adopts an unusual octahedral geometry, coordinated by the $\mu_4\text{-O}$ central atom, three carboxylate oxygen atoms and two extra oxygen atoms that were attributed to one DMF molecule and one water molecule, the latter coming most likely from the hydrated zinc salt used in the synthesis of the MOFs, leading to a network with the stoichiometry $[\text{Zn}_4\text{O}(\mathbf{3.1})_3(\text{H}_2\text{O})(\text{C}_3\text{H}_7\text{NO})](\text{C}_8\text{H}_{20}\text{N})_3(\text{sol.})_n$. It should be noted that the unusual SBU can be found in the bulk material of **3.11** as evidenced by powder XRD, but due to

the poor quality of the diffraction data, we cannot exclude the presence of small amounts of a different phase (Figure 3.7).

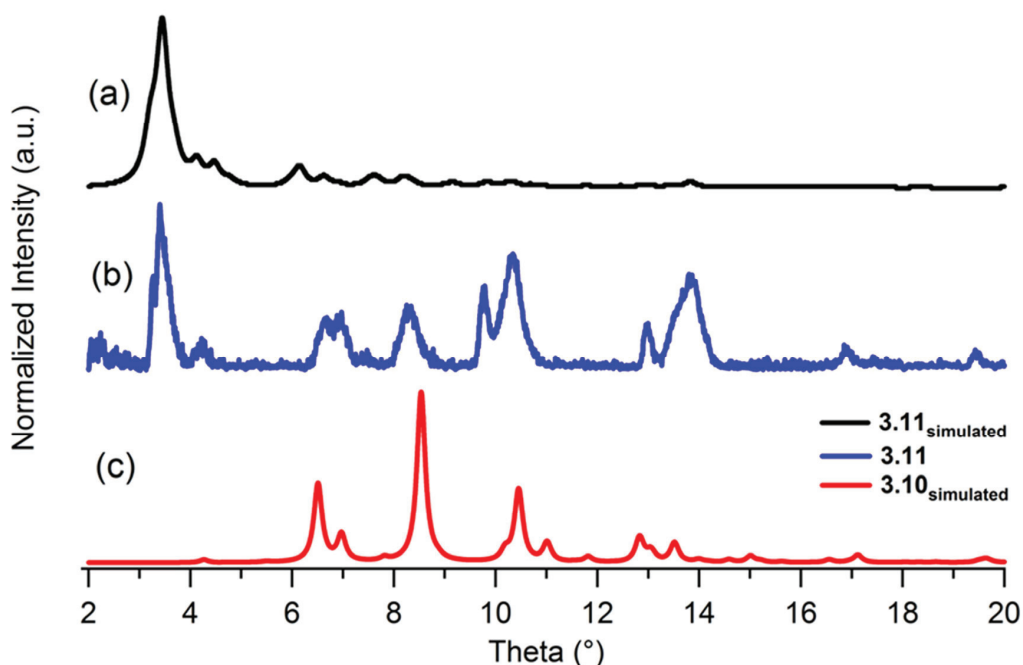


Figure 3.7 – (a) Simulated PXRD diagram of **17** calculated from its single-crystal structure, (b) Experimental PXRD diagram of **17**, (c) Simulated PXRD diagram of **16** calculated from its single-crystal structure.

The presence of one octahedral Zn^{2+} ion within the Zn_4O cluster significantly affects the structure of MOF **3.11**. In contrast to the IRMOF-n series or MOF **3.10**, where the tetranuclear cluster connects three collinear pairs of bis(carboxylate) ligands, MOF **3.11** contains one pair of clathrocholate ligands, the axis of which are tilted with respect to each other. The angles between opposite pairs of clathrocholate ligands are 180° , 180° and 135° . The latter results in a distortion of the framework structure, which displays a zigzag shape along the crystallographic c axis (Figure 3.6c). The central $\mu_4\text{-O}$ atoms of adjacent Zn_4O SBUs are separated by a distance of $27.471(2)$ Å and $27.894(1)$ Å, the latter being only slightly longer than for **3.10**. The coordination of one DMF molecule to one of the Zn^{2+} ions in the tetranuclear cluster was only observed for MOF **3.11**, whereas **3.10**, **3.12**, and **3.13** did not feature this asymmetric SBU. A convincing rationale for the formation of this octahedral Zn^{2+} ion has not yet been formulated.

We also investigated the formation of network structures using metalloligand **3.4** having less sterically demanding phenolatodioximate ligands (Br instead of *tert*-butyl). Solvothermal treatment of **3.4** with $[\text{Zn}(\text{H}_2\text{O})_6](\text{NO}_3)_2$ in a DMF/DEF mixture at 120°C resulted in the formation of orange cubic single crystals of MOF **3.14** (Scheme 3.4). Structural analysis of **3.14** revealed minor differences compared to previously described MOFs (Figure 3.8). Reducing considerably the steric bulk by

exchanging the *tert*-butyl side chains by a bromo substituent did not influence the network interpenetration (2-fold). The channels found in **3.14** are occupied by the NEt_4^+ cations, however the global disorder of the crystal did not allow us to locate precisely its alkyl chains.

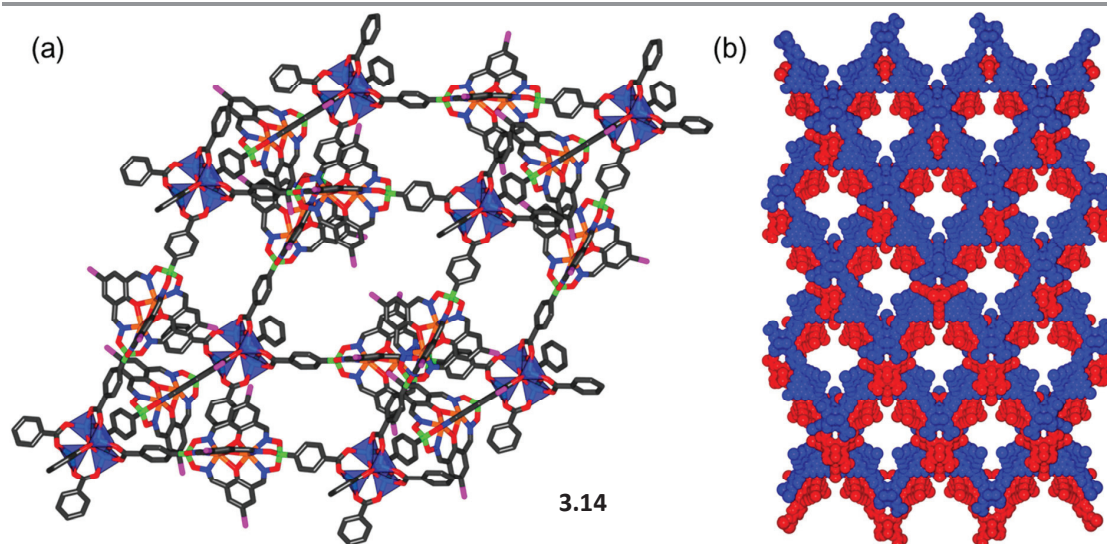


Figure 3.8 – (a) Part of the structure of MOF **3.14**. Hydrogen atoms and solvent molecules have been omitted for clarity. Color coding: C: grey; O: red; N: blue; B: green; Br: purple; Co: orange; Zn: cyan. Blue polyhedral represent the tetrahedral Zn atoms in the tetranuclear SBU; (b) The red and blue parts represent two independent, interpenetrated networks of **3.14**. Solvent and tetraethylammonium ions have been omitted for clarity.

In order to assess the gas sorption properties of the Zn-based MOFs **3.10–3.14**, nitrogen physisorption experiments were performed. BET surface measurements (N_2 , 77K) after activation of the crystals by heating at 150°C under dynamic vacuum gave only low values (**3.10**: 98 m^2/g ; **3.11**: 125 m^2/g ; **3.12**: 58 m^2/g ; **3.13**: 26 m^2/g ; **3.14**: 32 m^2/g). The low N_2 adsorption is likely due to the two-fold interpenetration of the networks and due to the presence of the NEt_4^+ cations, resulting in a drastically reduced accessible void volume. Digestion ^1H -NMR of **3.10–3.14** after the gas sorption measurement revealed the presence of residual DMF despite the activation process. Digestion ^1H -NMR experiments also unambiguously confirmed the presence of the NEt_4^+ cations within the network pores. Figure 3.9 shows a representative example of a NMR spectrum of a digested sample of MOF **3.10** in $\text{DMSO}-d_6$ after addition of a small amount of DCl in D_2O . Attempts to activate the crystals by solvent exchange with methanol or acetone gave even lower values for the BET measurements due to the collapse of networks during the exchange process. Powder XRD analyses of **3.10** and **3.12–3.14** revealed a complete loss of crystallinity upon network collapsing during the isolation procedure.

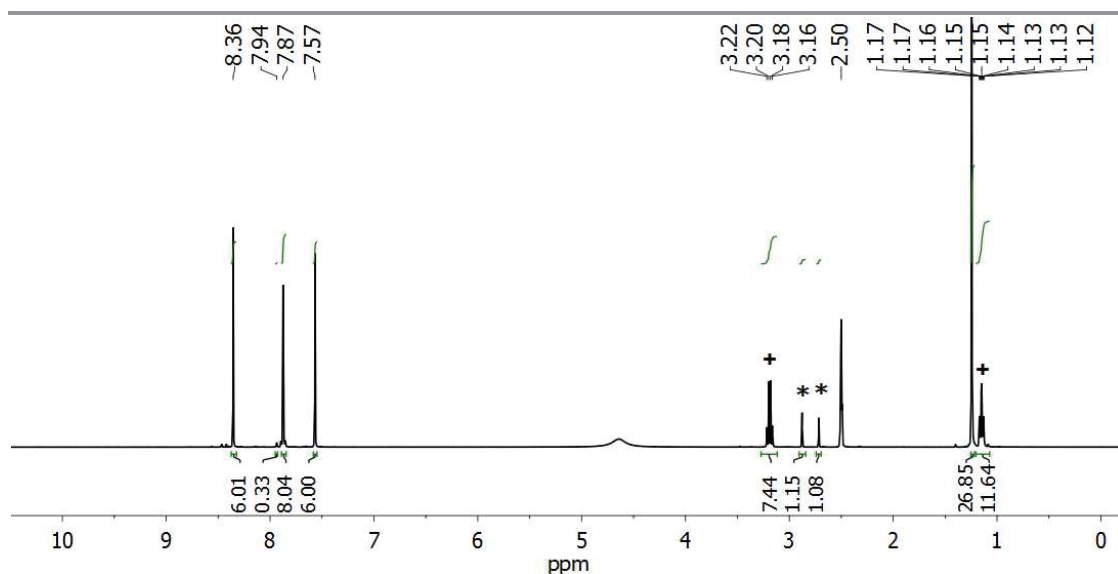
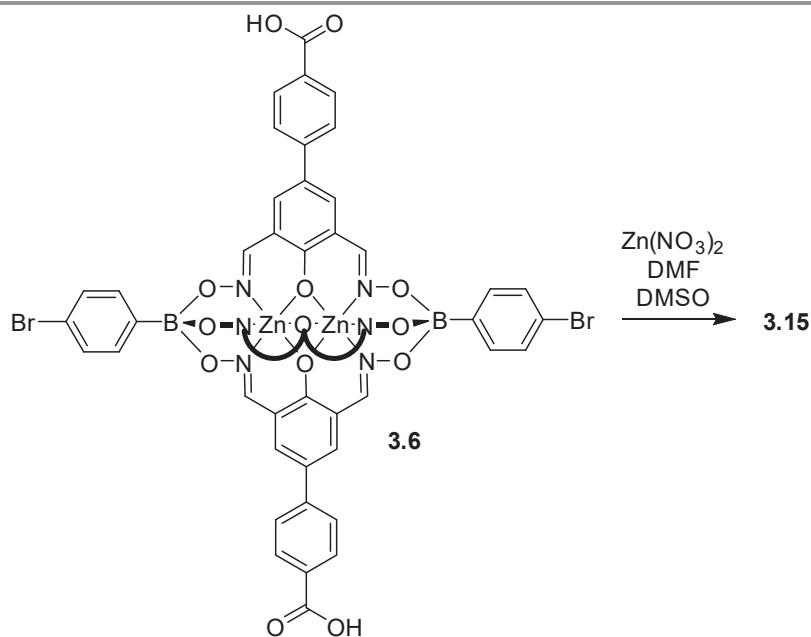


Figure 3.9 – ^1H -NMR spectrum of **3.10** after digestion upon addition of DCl in D_2O . Presence of DMF (*) and tetraethylammonium cation (+) is unambiguously confirmed.

We also studied the formation of networks using our tritopic clathrochelate **3.6**. Reaction of **3.6** with $[\text{Zn}(\text{H}_2\text{O})_6](\text{NO}_3)_2$ in a mixture of DMF and DMSO resulted in the formation of transparent block-shaped crystals of **3.15** (Scheme 3.6). Crystallographic analysis of **3.15** showed a three-dimensional network with the stoichiometry $[\text{Zn}_4\text{O}(\text{3.6})_2(\text{C}_2\text{H}_6\text{OS})_2](\text{C}_8\text{H}_{20}\text{N})_2(\text{sol.})_n$ in which all carboxylic acid units of **3.6** are coordinated to a Zn_4O cluster (Figure 3.10). As it was observed for **3.11**, the zinc cluster is composed of three tetrahedral and one octahedral Zn^{2+} ion (shown as blue and green polyhedra respectively). The octahedral ion is coordinated by the central $\mu_4\text{-O}$ atom, three oxygen atoms from the deprotonated carboxylate groups, and two DMSO molecules. Several examples of tritopic carboxylate ligands connected by Zn_4O clusters have been reported so far, but to the best of our knowledge the presence of one octahedral zinc within the Zn_4O cluster is unprecedented.¹⁰⁴ Consequently, **3.15** displays a connectivity slightly different from what has been observed for MOFs constructed from tritopic carboxylates ligands. The network of **3.15** is two-fold interpenetrated and anionic, hence contains NEt_4^+ cations as verified by digestion NMR, leading to a material with very low porosity (BET surface area of $21 \text{ m}^2/\text{g}$).



Scheme 3.6 – Synthesis of MOF **3.15** following a solvothermal strategy.

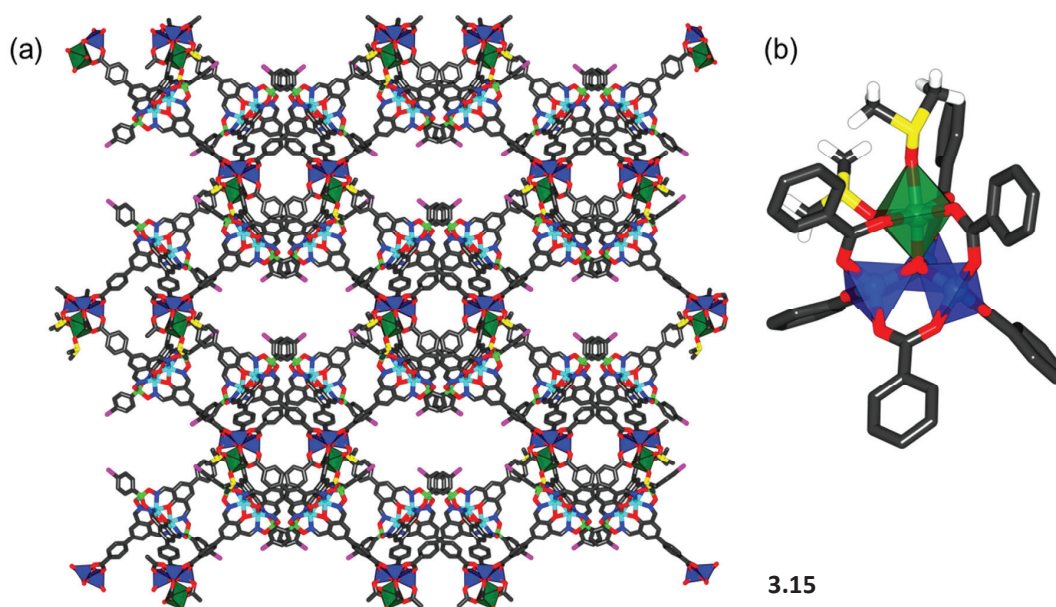
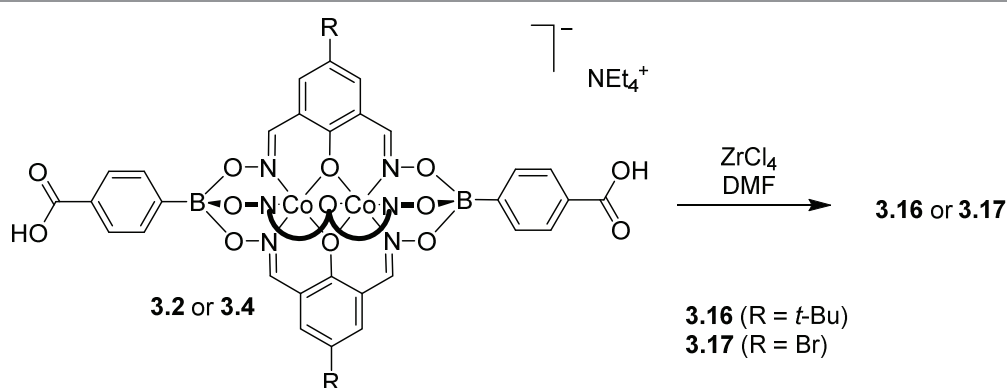


Figure 3.10 – (a) Part of the structure of MOF **3.15**; (b) Molecular structure of the tetranuclear SBU of MOF **3.11**. Hydrogen atoms, NEt_4^+ cations, and solvent molecules have been omitted for clarity. Color coding: C: gray; O: red; N: blue; B: green; Br: pink; S: yellow; Zn: cyan. Blue and green polyhedra represent the tetrahedral and respectively octahedral zinc atoms in the tetranuclear SBU.

In order to assess the versatility of our clathrochelates in the synthesis of other types of MOF, we turned to zirconium-based MOFs. In 2008, Lillerud and co-workers reported the synthesis of a new inorganic building unit, namely $\text{Zr}_6\text{O}_4(\text{OH})_4(\text{CO}_2)_{12}$.²² The solvothermal reaction between ZrCl_4 and terephthalic acid or terphenyldicarboxylic acid resulted in the formation of porous materials with

specific surface areas of $1187 \text{ m}^2\text{g}^{-1}$ and $4170 \text{ m}^2\text{g}^{-1}$, which were designated UiO-66 and UiO-68, respectively. Subsequent work has shown that the 12-fold coordinated cluster $\text{Zr}_6\text{O}_4(\text{OH})_4(\text{CO}_2)_{12}$ can be reduced to 8-fold^{23b,105} and even 6-fold SBUs^{23c,106} by using appropriate polycarboxylate ligands. MOFs based on Zr clusters have attracted a lot of attention because these materials can display very high chemical stability.^{26a,107} Capitalizing on this characteristic, numerous applications have emerged over the last years, including the utilization of transition metal-functionalized Zr-MOFs as catalysts for organic syntheses,^{26c,84c,108} or the utilization of Zr-MOFs for the hydrolytic decontamination of chemical warfare agents.^{84b,109} In order to examine if our clathrochelate-based metalloligands could be used to synthesize Zr-MOFs, we have investigated the reaction of the ditopic complexes **3.2** and **3.4** with ZrCl_4 in DMF. Initial worries that the clathrochelates would not withstand the rather harsh reaction conditions (120°C , presence of the strong Lewis acid ZrCl_4) were not justified: after 3 days, we were able to obtain the Zr-MOFs **3.16** and **3.17** in the form of orange powders in good yields (Scheme 3.7).



Scheme 3.7 – Synthesis of the Zr-MOFs **3.16** and **3.17**

Powder XRD analyses of **3.16** and **3.17** showed that the materials were poorly (**3.17**, Figure 3.11) or non-crystalline (**3.16**). Attempts to increase the crystallinity by using modulators such as benzoic or acetic acid¹¹⁰ were unfortunately, not successful. In view of the poorly resolved PXRD spectra, we can only speculate about the type of Zr cluster which is present in **3.16** and **3.17**. In order to have an idea whether our clathrochelate could be incorporated in a network composed of the sterically demanding 12-fold coordinated Zr_6 cluster, we created a simple geometric model of the system. We used *SolidWorks 2013* to create a hypothesized structure of **3.16**, by preassembling the two distinct part *via* their coordinates obtained from the X-ray single-crystal data of **3.2** and of UiO-66 SBU. The final assembly was obtained by restraining the system *via* coordination of the Zr_6 cluster to the clathrochelate core. Based on these simple steric considerations, even the 12-fold coordinated Zr_6 cluster seems possible despite the substantial lateral size of metalloligand **3.2** (Figure 3.12). Interestingly, **3.16** and **3.17** appear to be neutral network structures because the NMR spectra of

digested samples do not show signals corresponding to the NEt_4^+ cations (Figure 3.13). The necessary charge compensation could be accomplished by exchange of a hydroxide for a water ligand on the Zr cluster.

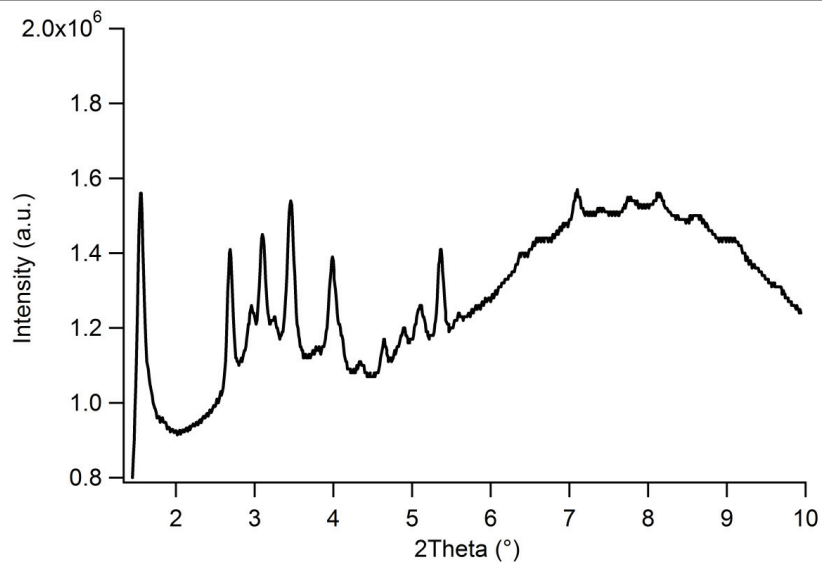


Figure 3.11 – Experimental PXRD spectrum of **3.17**.

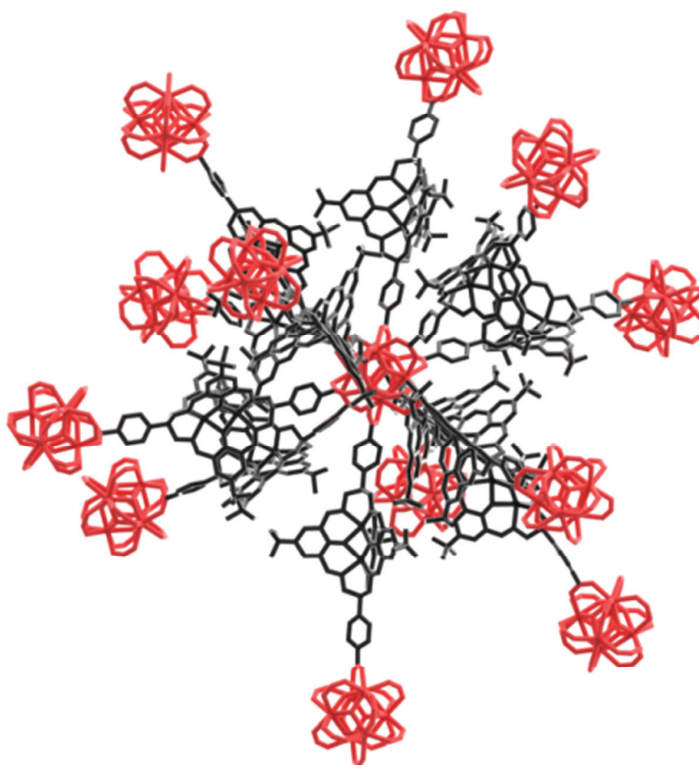


Figure 3.12 – Graphical representation of part of the hypothetical structure of **3.16**. The red part corresponds to the $\text{Zr}_6\text{O}_4(\text{OH})_4(\text{CO}_2)_{12}$ cluster and the black one to the clathrochelate core of **3.2**. The structure was obtained using *SolidWorks 2013*.

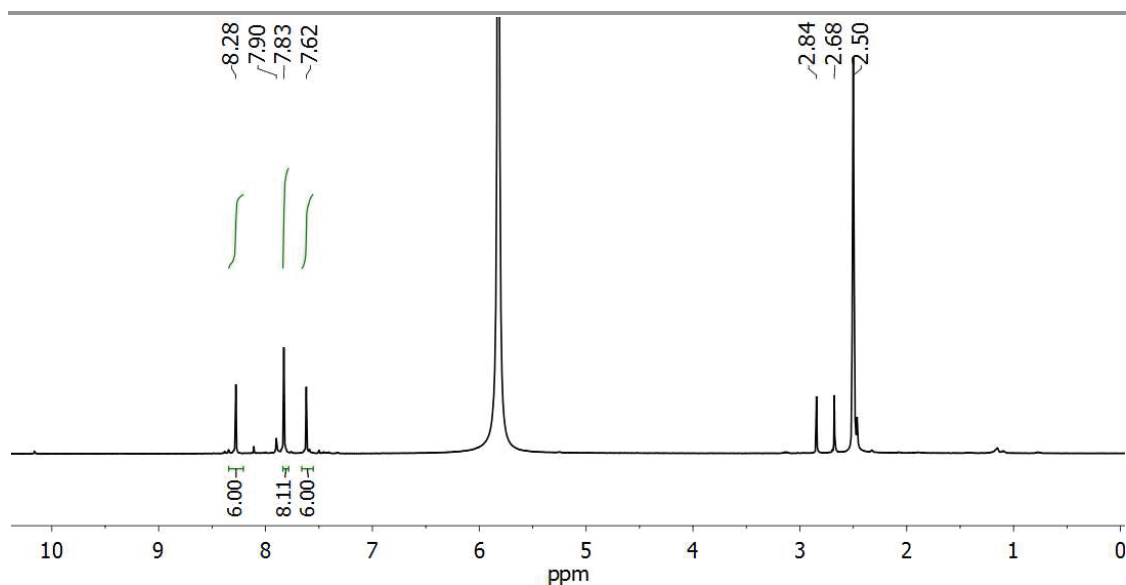
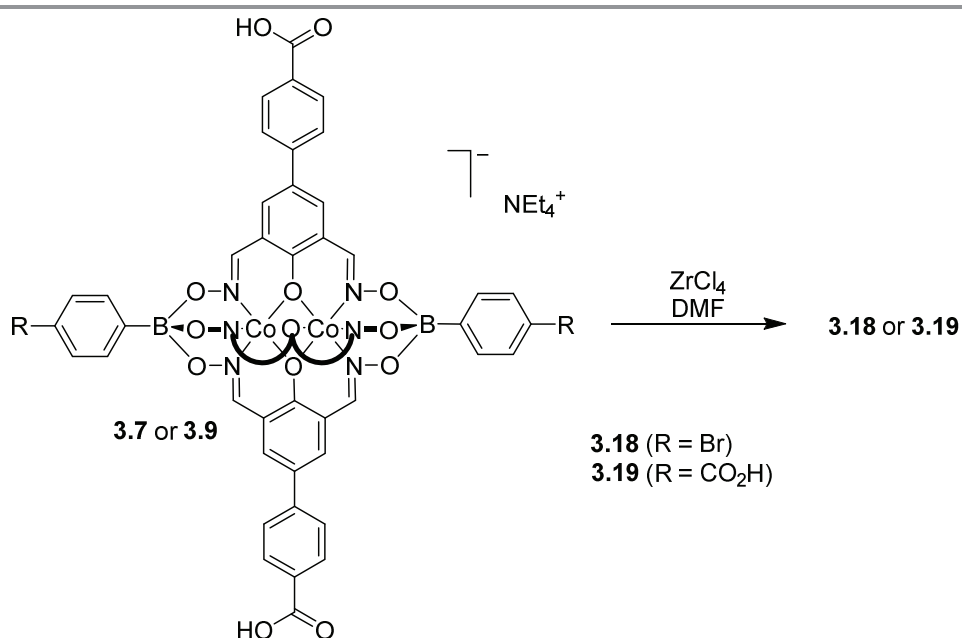


Figure 3.13 – ^1H -NMR spectrum of **3.17** after digestion upon addition of DCl in D_2O (residual DMF denoted as *). Absence of tetraethylammonium cation is unambiguously confirmed.

Encouraged by the successful synthesis of **3.16** and **3.17**, we have subsequently investigated the utilization of the tri- and the pentatopic metalloligands **3.7** and **3.9**. The observations were similar as before: after 3 days (DMF, 120°C), we were able to collect orange, amorphous powders (**3.18** and **3.19**, Scheme 3.8). The absence of NEt_4^+ cations in **3.18** and **3.19** was again confirmed by digestion NMR experiments.



Scheme 3.9 – Synthesis of the Zr-MOFs **3.18** and **3.19**.

In contrast to the Zn-based MOFs **3.10–3.15**, the Zr-based MOFs were all found to display substantial permanent porosity after removal of the solvent by heating at 150°C under dynamic vacuum (Figure 3.14a,b). BET (N_2 , 77K) measurements revealed specific surface areas of 410 m^2g^{-1} (**3.16**), 955 m^2g^{-1} (**3.17**), 535 m^2g^{-1} (**3.18**), and 546 m^2g^{-1} (**3.19**). It is worth noting that the surface area of **3.17** is more than twice of that of **3.16**. Both, **3.16** and **3.17**, are based on the same type of ditopic metalloligand, differing only in terms of the equatorial group R (Br vs. *tert*-butyl). This result suggests that it is possible to use the lateral oximate ligands for modulating the porosity of the MOFs. CO_2 (273K) physisorption experiments revealed high capacities for all Zr-MOFs, with MOF **3.17** being able to take up 85 cm^3g^{-1} at 1 bar (Figure 3.14c). This value is slightly higher than what has been observed for UiO-66 derivatives.¹¹¹

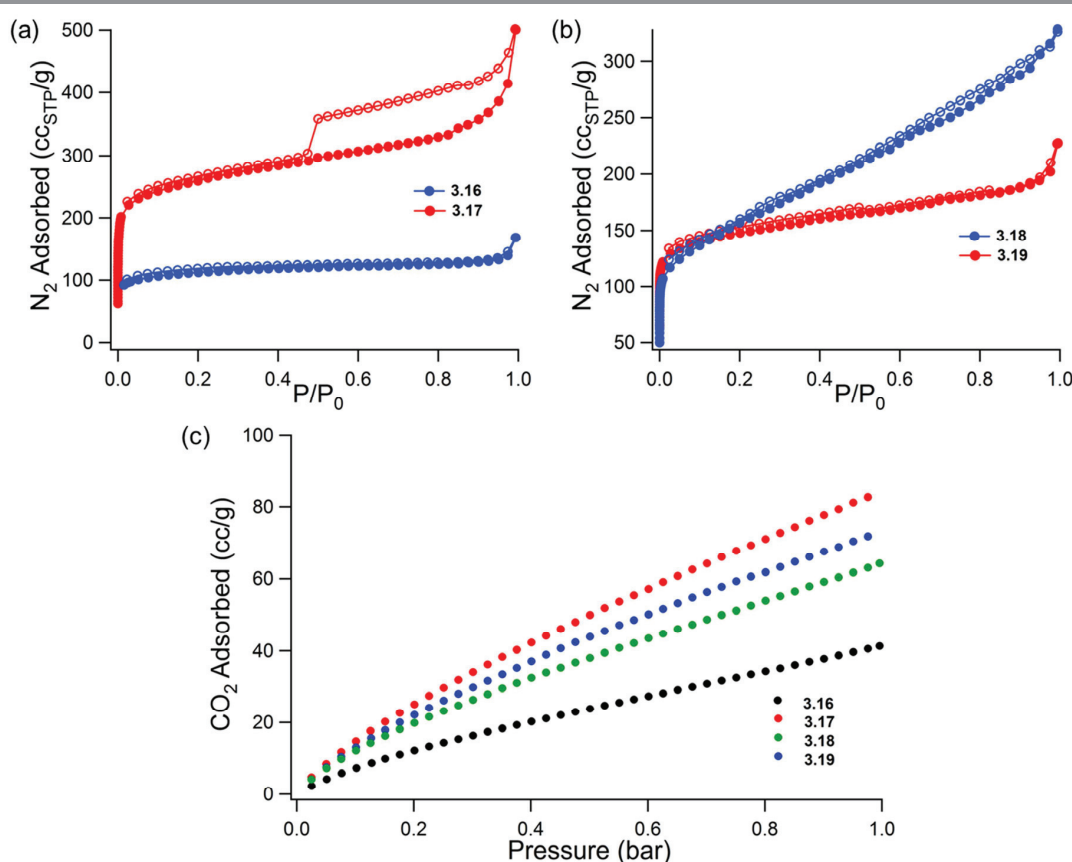


Figure 3.14 – N_2 full isotherm at 77 K for Zr-MOF **3.16**, **3.17** (a) and **3.18**, **3.19** (b). Full circles and open circles represent the adsorption, respectively desorption, points; (c) CO_2 adsorption isotherms at 273 K for ZrMOFs **3.16–3.19**.

To evaluate the thermal stability of the Zr-MOFs, we have performed thermogravimetric analyses. Degradation was observed at temperatures between 300°C and 340°C (Figure 3.15). This temperature range is lower than that what has been observed for Zr-MOFs such as UiO-66 (450°C). We thus conclude that decomposition onset is due to degradation of the metalloligand rather than carboxylate-cluster bond breakage. In line with this assumption is the observation that the

clathrochelate ligands alone undergo thermal degradation in the same temperature region. Nevertheless, a thermal stability of up to 300 °C is sufficient for many potential applications.

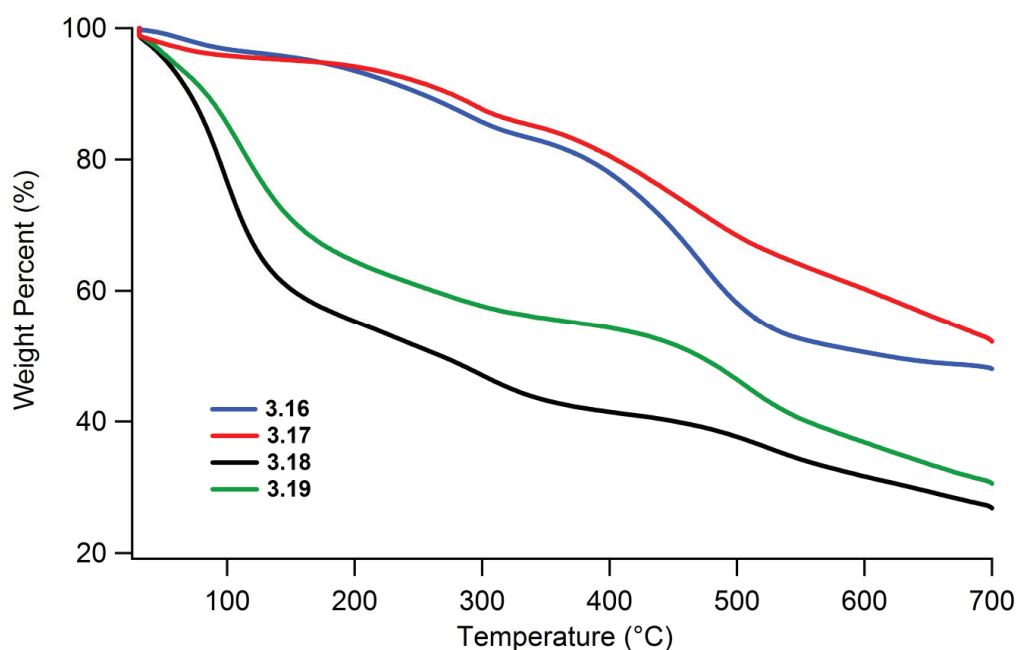


Figure 3.15 - Thermogravimetric analyses traces of the activated Zr-MOFs **3.16** (red) and **3.17** (blue) and of the as-synthesized Zr-MOFs **3.18** and **3.19**.

3.4 Conclusion

Mono- and dinuclear clathrochelate complexes with up to five pendent carboxylic acid groups have been synthesized by metal-templated reactions using easily accessible starting materials. These rigid and robust complexes represent interesting metalloligands for applications in metallasupramolecular chemistry and materials science. The carboxylic acid functions are oriented in a divergent fashion, with well-defined coordinate vectors. In terms of size, the clathrochelates are comparable to carboxylic acid-functionalized porphyrin ligands, which have found numerous applications in the past.¹¹² A unique feature of our new carboxylic-appended metalloligands is their trigonal bipyramidal geometry. Such geometry is difficult to access with purely organic scaffolds.

To demonstrate the utility of carboxylic acid-functionalized clathrochelates in MOF chemistry, we have synthesized three-dimensional network structures with zinc (**3.10–3.14**) or zirconium clusters as SBUs (**3.16–3.19**). Our results show that the metalloligands are compatible with reactions conditions employed for MOF synthesis, and that the steric bulk of the clathrochelates is not detrimental to the coordination of multiple metalloligands to one SBU. One should also note that the thermal and chemical stability of the clathrochelates is sufficient for many potential applications.

Chapter 4 Dinuclear clathrochelates functionalized with pendant cyano groups

The results presented in this chapter detail the synthesis of homometallic dinuclear Co^{2+} and Zn^{2+} clathrochelates decorated with cyano groups. Following two distinct synthetic strategies, we were able to prepare clathrochelates containing two, three, four, or five cyano groups which are oriented in a divergent fashion. The utility of these new metalloligands is demonstrated by the synthesis of one-, two-, and three-dimensional coordination polymers, in which the clathrochelate ligands are linked by Ag^+ ions. The results presented in this chapter were published in “Dinuclear Clathrochelate Complexes with Pendent Cyano Groups as Metalloligands”, Mathieu Marmier, Giacomo Cecot, Anna V. Vologzhanina, José L. Bila, Ivica Zivkovic, Henrik M. Ronnow, Balint Nafradi, Euro Solari, Philip Pattison, Rosario Scopelliti and Kay Severin, *Dalton Trans.*, **2016**, accepted.¹¹³

4.1 Introduction

Silver(I) ions tend to form labile complexes with a flexible coordination number and geometry.¹¹⁴ These features are attractive for the preparation of coordination polymers (CPs)¹¹⁵ because the reversible and malleable coordination chemistry facilitates crystallization, and thus characterization. A sizable fraction of the silver(I) CPs reported to date is based on polycyano ligands. Various ligands have been used in this context, including compounds with two,¹¹⁶ three,¹¹⁷ four,¹¹⁸ and more¹¹⁹ cyano groups. In addition to purely organic ligands, the utilization of metalloligands with cyano groups in the ligand periphery has been explored. Some selected examples are shown in Figure 4.1. The nature of the organic linkers used in these examples has been discussed in section 1.2.2.

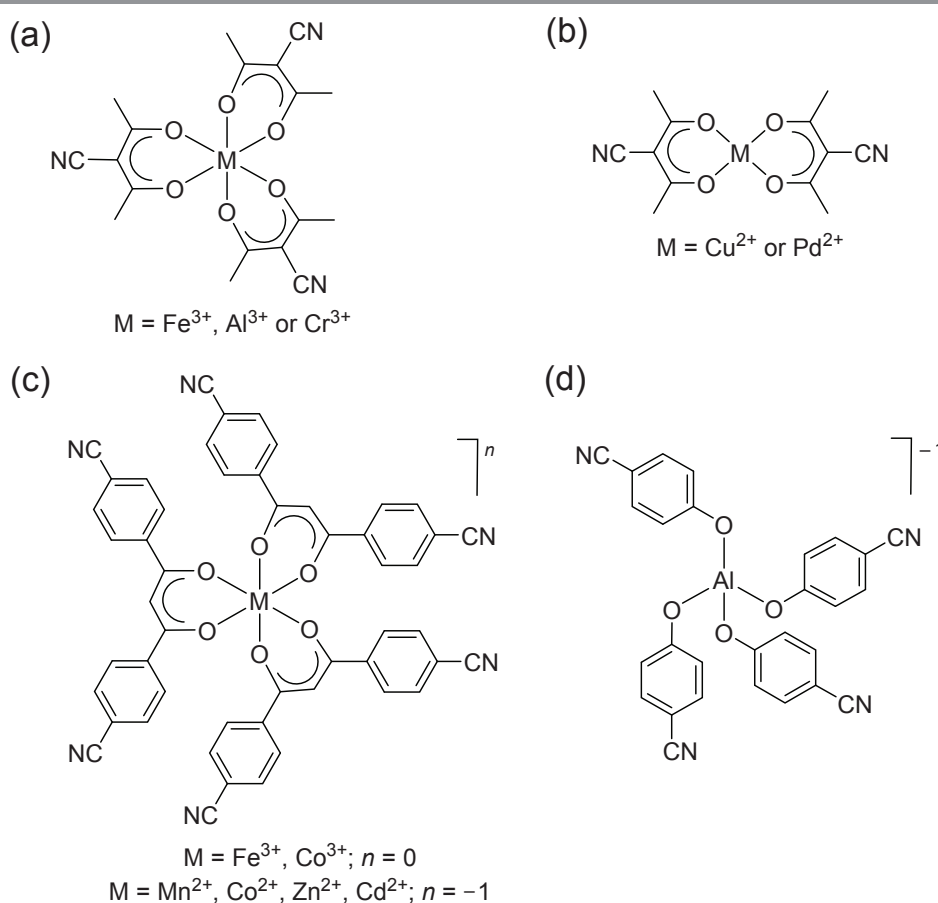


Figure 4.1 – Examples of neutral (a, b and c) and anionic (c and d) metalloligands with pendent cyanogroups. The complexes were used to prepare heterometallic coordination polymers with silver(I) salts.¹²⁰⁻¹²²

The groups of Englert, Hosseini, Burrows and Mahon used homo- and heteroleptic metalloligands containing 3-cyanoacetylacetonato ligands for the construction of silver(I) CPs.¹²⁰ Tritopic metalloligands were obtained with iron (III),^{120h} aluminum(III),^{120c} and chromium(III),^{120g} whereas ditopic metalloligands were formed with copper(II)^{120h} and palladium(II).^{120b} Visconti *et al.* have used

β -diketonate ligands with two benzonitrile groups to make hexadentate metalloligands.¹²¹ The complexes display an overall charge of zero or minus one, depending on the central metal ion. Very similar three-dimensional CPs were obtained with these metalloligands, despite the difference in overall charge. Notably, it was possible to perform anion exchange in single crystal to single crystal processes. Schulz and coworkers have prepared silver(I) CPs with a diamond-like topology using the tetrahedral $[\text{Al}(\text{OC}_6\text{H}_4\text{CN})_4]^{-1}$ anion.¹²² Due to network interpenetration, larger channels or pores were not observed.

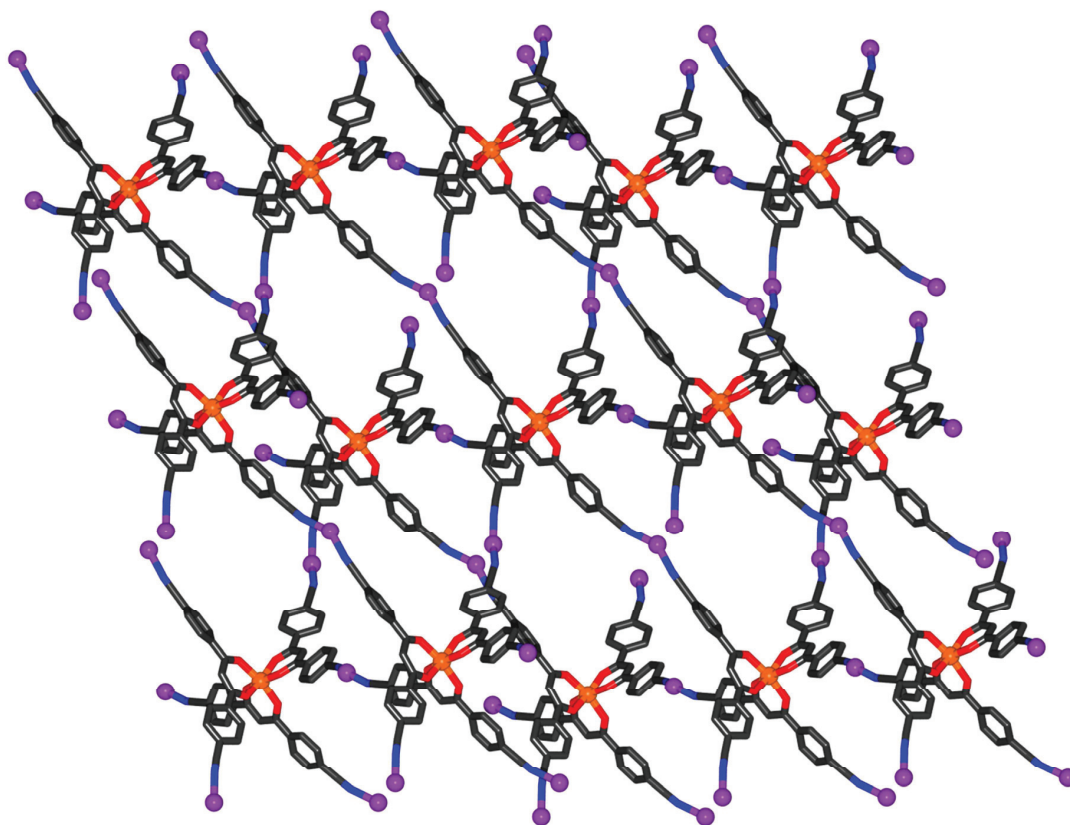
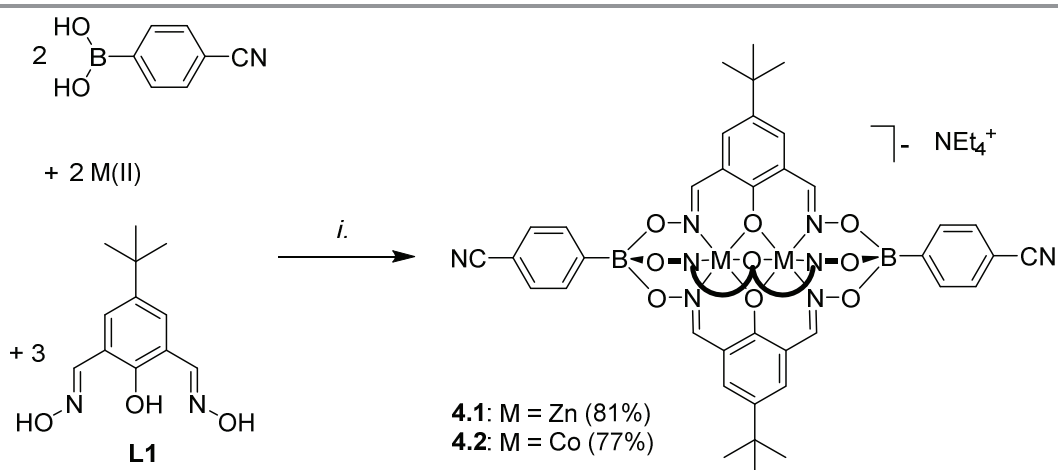


Figure 4.2 – Molecular representation of three-dimensional CP constructed from Fe(II)-based hexadentate neutral metalloligands and Ag(I) described by Visconti *et al.*¹²¹ Hydrogen atoms, anions (PF_6^-) and solvent molecules have been omitted for clarity. Color coding: C: gray; Ag: purple; Fe: orange; N: blue; O: red.

4.2 Direct synthesis of cyano-functionalized clathrochelates

In order to introduce cyano groups in apical position, we have followed our well-established reaction using commercially available 4-cyanophenylboronic acid in combination with 2,6-diformyl-4-*tert*-butylphenol dioxime (**L1**). As metal salts, we have employed either $[\text{Co}(\text{H}_2\text{O})_6](\text{NO}_3)_2$ or $\text{Zn}(\text{OTf})_2$. The reactions proceeded in a clean fashion, and the desired clathrochelates **4.1** and **4.2** could be isolated in high yield following addition of tetraethylammonium hydroxide (Scheme 4.1). Both complexes were analyzed by Fourier-transform infrared spectroscopy (FT-IR) and high-resolution mass spectrometry. The diamagnetic zinc complex **4.1** was also analyzed by NMR spectroscopy ($\text{DMSO-}d_6$). Only one set of signals for the protons of the phenolatodioximato ligand were observed, corroborating the expected *pseudo-C*₃ symmetry of the complex. The FT-IR spectra showed a characteristic band at 2220 cm^{-1} , which can be assigned to the absorption frequency of the cyano groups. In line with our earlier observations for Zn(II) clathrochelates described in Chapters 2 and 3, complex **4.1** was found to be luminescent with an emission maximum at 445 nm (DMF, $\lambda_{\text{ex}} = 335\text{ nm}$).



Scheme 4.1 – Synthesis of the ditopic clathrochelate complexes **4.1** and **4.2**. Reagents and conditions: (i.): $[\text{Co}(\text{H}_2\text{O})_6](\text{NO}_3)_2$ or $\text{Zn}(\text{OTf})_2$, EtOH/MeOH, 70°C , then NEt_4OH .

Previously, we had investigated the magnetic properties of dinuclear Co clathrochelates **3.2** and **3.4** with pendent carboxylic acid groups using the Evans method. The data suggested that the Co(II) centers have a high spin configuration. For complex **4.2**, we have now performed a more detailed analysis using a superconducting quantum interference device (SQUID) magnetometer (work carried out by Dr. Ivica Zivkovic and Prof. Henrik M. Rønnow, Institute of Physics, EPFL). A plot of the magnetic susceptibility vs. temperature reveals an increase of the susceptibility as temperature decreases and a broad maximum around 87 K below which a significant decrease of the susceptibility occurs (Figure 4.3). Given that the pair of cobalt ions are well separated from other magnetic ions, the inter-cluster interaction can be neglected and the Hamiltonian of the system can be written

simply as $H = -2J \cdot S_1 \cdot S_2$, where S_1 and S_2 are spins of two cobalt ions that form a pair and J is the intra-cluster exchange interaction. The room temperature value of the effective moment per Co ion reaches $5.0 \mu_B$, close to the theoretically maximum value for a high-spin cobalt(II) state with $L = 3$ orbital momentum included. The data has been analyzed using MagSaki software¹²³ which takes into account the magnetic exchange coupling J , spin-orbit coupling λ , an orbital reduction factor κ and the axial-splitting parameter Δ . Very good agreement with measured data has been achieved with $J = -20(3) \text{ cm}^{-1}$, $\lambda = -110(10) \text{ cm}^{-1}$, $\kappa = 1(0.1)$ and $\Delta = 286(30)$. These parameters correspond to significant g-factor anisotropy, $g_x = 4.9(0.3)$ and $g_z = 3.0(0.3)$, which is in agreement with preliminary ESR measurements. These values are similar to those reported for other di-nuclear Co-based compounds with much larger intra-cluster magnetic interaction.¹²⁴

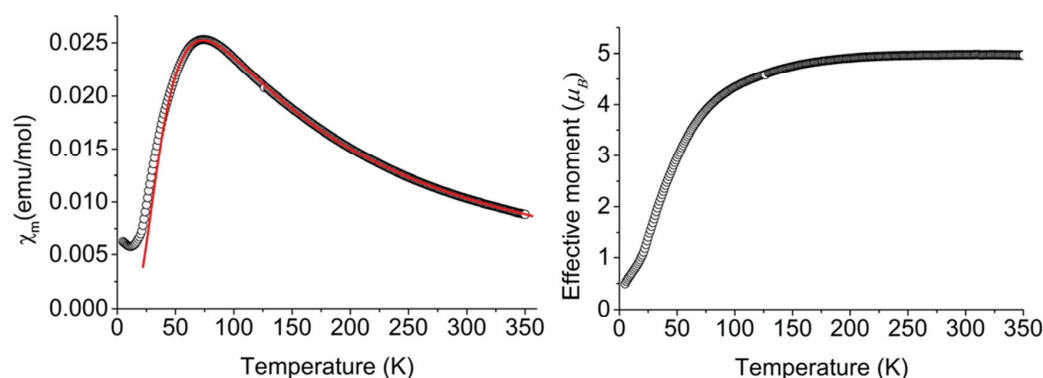
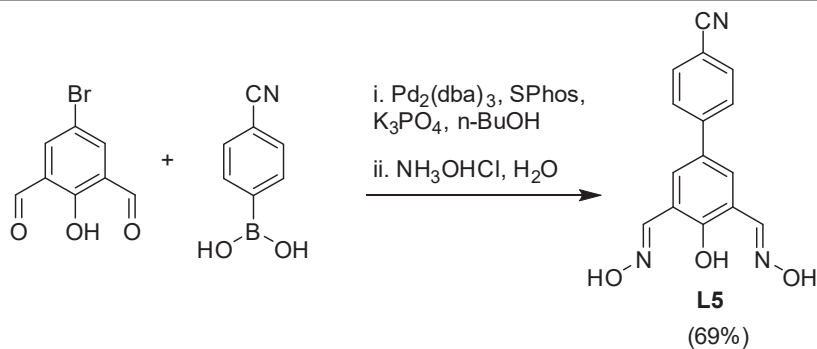


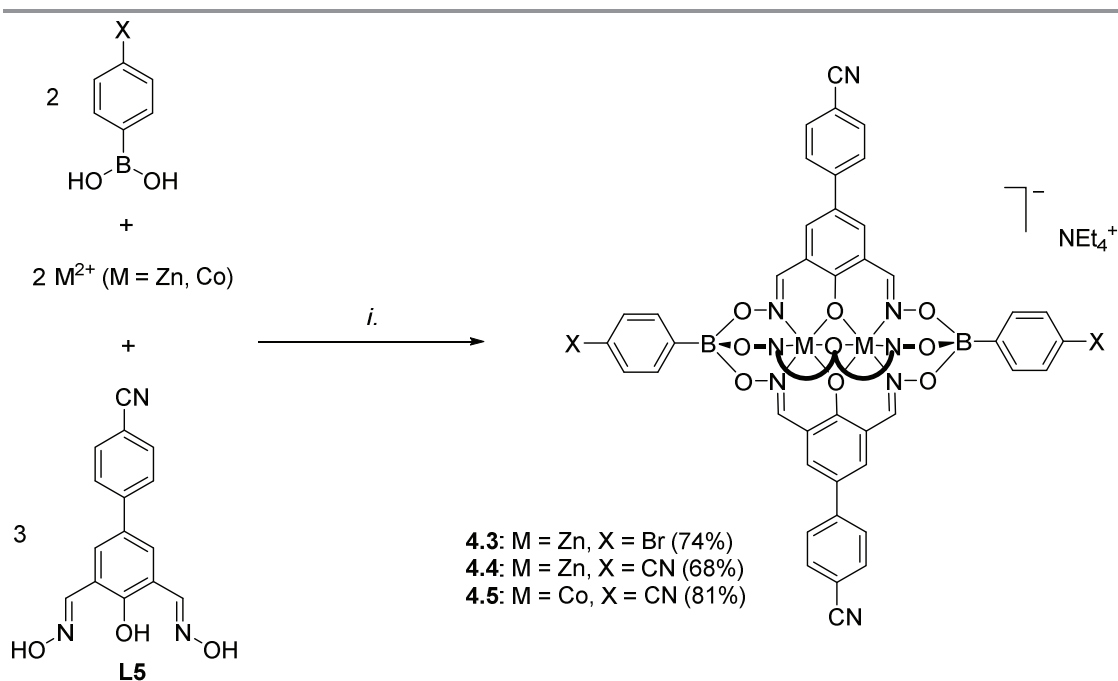
Figure 4.3 – The magnetic susceptibility and the effective magnetic moment of complex **4.2** as a function of temperature as determined by SQUID measurements.

In order to prepare clathrochelates with cyano groups in lateral position, we have prepared the phenoldioxime ligand **L5**. The synthesis of this ligand was accomplished by Pd-catalyzed cross-coupling of 4-cyanophenylboronic acid and 2,6-diformyl-4-bromophenol in presence of SPhos and $\text{Pd}_2(\text{dba})_3$,⁶⁴ followed by treatment of the crude dialdehyde with hydroxylamine hydrochloride (Scheme 4.2).



Scheme 4.2 – Synthesis of the dioxime ligand **L5**.

The tri- and pentatopic clathrochelates **4.3–4.5** were then obtained by using **L5** in combination of either 4-bromophenylboronic acid or 4-cyanophenylboronic following the standard protocol (Scheme 4.3). To the best of our knowledge, complexes **4.4** and **4.5** represent the first examples of polycyano ligands with trigonal bipyramidal geometry. Zn-based clathrochelates **4.3** and **4.4** are luminescent, with emission maxima at 450 nm (DMF, λ_{ex} = 335 nm). Their emissions are thus slightly red-shifted compared to what was observed for **4.1**. The analytical data for **4.3–4.5** are in line with the expected structures. The magnetic properties of **4.5** were expected to be similar to what was found for **4.2** and additional SQUID measurements were not performed.

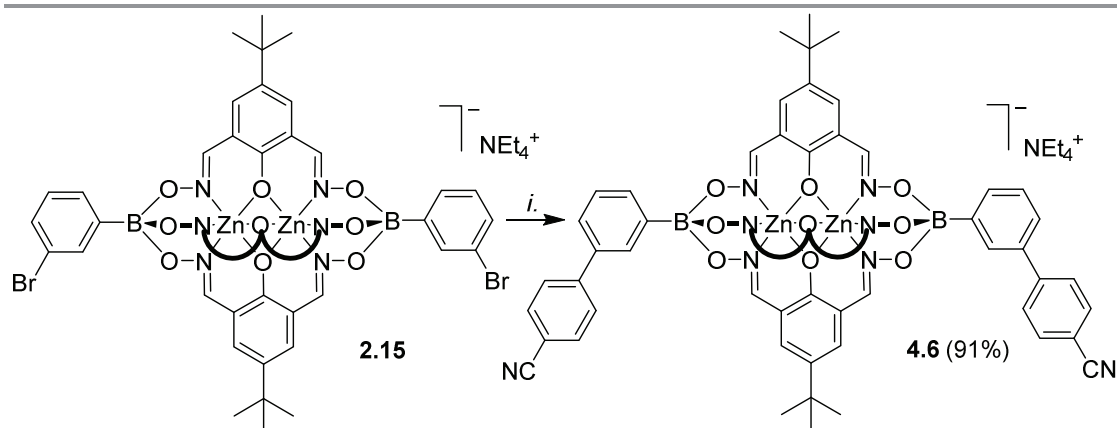


Scheme 4.3 – Synthesis of the tri- and pentatopic clathrochelate complexes **4.3–4.5**. Reagents and conditions: (i.): 4-bromo- or 4-cyanophenylboronic acid, dioxime ligand **L5**, $\text{Zn}(\text{OTf})_2$ or $[\text{Co}(\text{H}_2\text{O})_6](\text{NO}_3)_2$, MeOH/EtOH , 70°C , then NEt_4OH .

4.3 Synthesis of cyano-functionalized clathrochelates by postsynthetic cross-coupling reactions

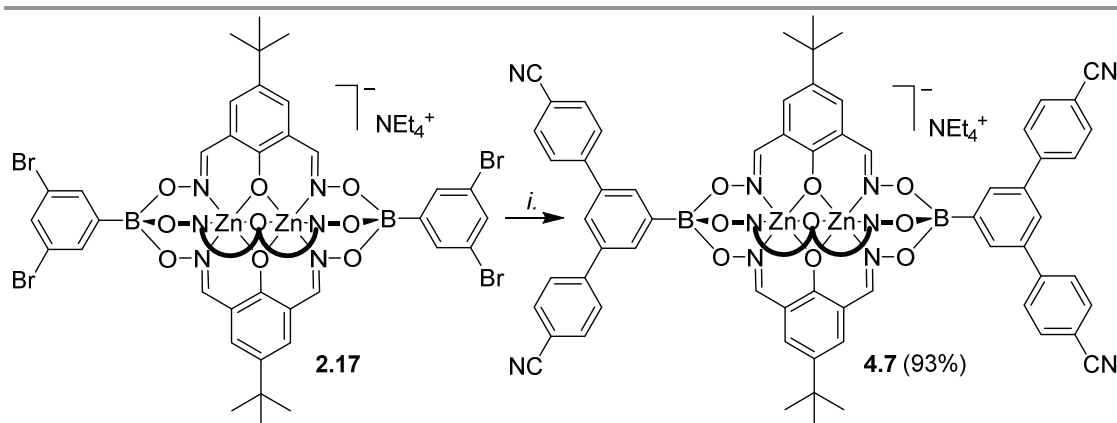
We have shown in section 2.3 that brominated clathrochelate complexes of Zn^{2+} and Co^{2+} are sufficiently stable to be used as substrates in Pd-catalyzed cross-coupling reactions, allowing the preparation of elongated polypyridyl ligands. We anticipated that a similar strategy could be used to prepare clathrochelate complexes with pendent benzonitrile groups. Indeed, the two-fold coupling of the previously described clathrochelate **2.15** featuring 3-bromophenylboronate ester caps with 4-cyanophenylboronic acid gave the desired complex **4.6** in 91% yield (Scheme 4.4). With regard to potential applications, it is worth noting that ditopic cyanoligands with a bent shape have been used

extensively for the preparation of silver(I) CPs.^{116a-g} Compared to the ligands used previously, clathrochelate stands out because of its size and its negative charge. Attempts to prepare a *linear* dicyano ligand by cross-coupling of a clathrochelate with terminal 4-bromophenylboronate ester groups were unfortunately not successful. Even though we were able to detect the desired product by mass spectrometry, we were not able to achieve a complete reaction, and separation of the side products was found to be difficult. This result indicates that coupling reactions in *para* position to the boronate ester function are more problematic.



Scheme 4.4 – Synthesis of the extended ditopic clathrochelate complex **4.6**. Reagents and conditions: (i.): **2.15** (1 eq.), 4-cyanophenylboronic acid (8 eq.), K_3PO_4 (4 eq.), $Pd_2(dba)_3$ (5 mol%), SPhos (10 mol%), n-BuOH/toluene (1:1), 90 °C, 14 h.

To further test the scope of the cross-coupling procedure, we used the tetrabrominated clathrochelate complex **2.17** as the brominated precursor. The subsequent four-fold coupling with 4-cyanophenylboronic acid in the presence of $Pd_2(dba)_3$ and SPhos was remarkably clean, providing the tetratopic complex **4.7** in 89% yield (Scheme 4.5).

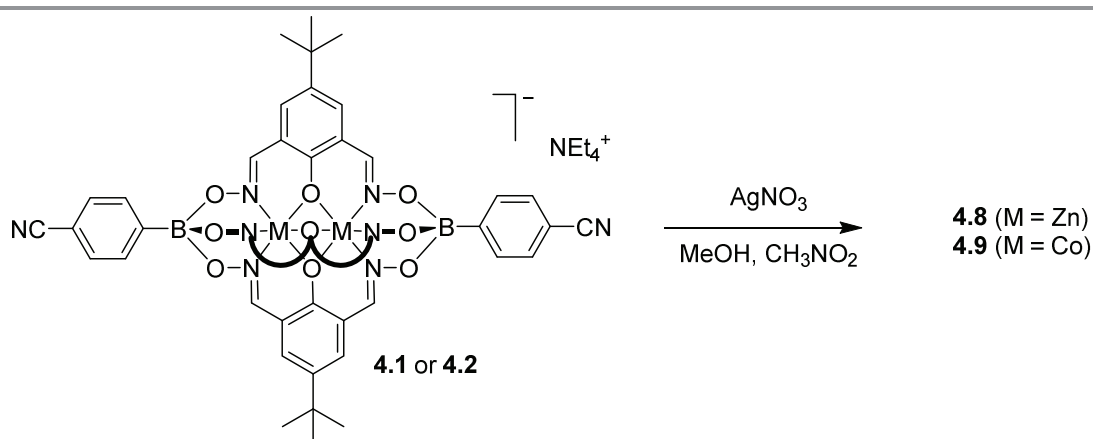


Scheme 4.5 – Synthesis of the tetratopic clathrochelate complex **4.7**. Reagents and conditions: (i.): **2.17** (1 eq.), 4-cyanophenylboronic acid (20 eq.), K_3PO_4 (10 eq.), $Pd_2(dba)_3$ (5 mol%), SPhos (10 mol%), n-BuOH/toluene (1:1), 90 °C, 14 h.

The elongated clathrochelates **4.6** and **4.7** are soluble in polar organic solvents such as DMSO, nitromethane and DMF, and the analytical data match the proposed structures. Both complexes are luminescent, with an emission maximum at 445 nm (DMF, λ_{ex} = 335 nm).

4.4 Coordination polymers with silver(I)

After having established efficient protocols for the synthesis of cyano-functionalized clathrochelate complexes, we started to explore their utilization as metalloligands in CPs. As outlined in the introduction, polycyano ligands are particularly suited for the preparation of silver(I) CPs, and we thus focused on reactions with Ag(I) salts. For some clathrochelate complexes, we were able to obtain crystalline CPs upon reaction with silver salts, and the results are detailed below. Single crystals of the CPs **4.8** and **4.9** were obtained by layering a solution of AgNO₃ in MeOH on top of a solution of **4.1** or **4.2** in nitromethane (Scheme 4.6). Crystallographic analyses revealed that both CPs are isostructural compounds having [Ag(**4.1**)](CH₃OH)_{2.5}(CH₃NO₂) and [Ag(**4.2**)](CH₃OH)_{2.25}(CH₃NO₂)_{1.5} stoichiometry, respectively. The terminal cyano groups coordinate to the Ag⁺ ions in a slightly bent fashion (N–Ag–N = 154° and 155°) forming an infinite chain. The Ag⁺ ions display a trigonal pyramidal geometry, with one of the coordination sites being occupied by a methanol ligand. The fourth coordination site is occupied by the oxygen atom of an adjacent boronate ester group. It should be noted that coordination of a metal ion to the oxygen atom of clathrochelate complexes has not been observed before. As a result of this cross-linking, we observe an unusual double chain architecture (Figure 4.4).^{116d} A summary of the bond distances of the connecting silver complexes is given in Table 4.1.



Scheme 4.6 – Synthesis of the heterometallic coordination polymer **4.8** and **4.9**.

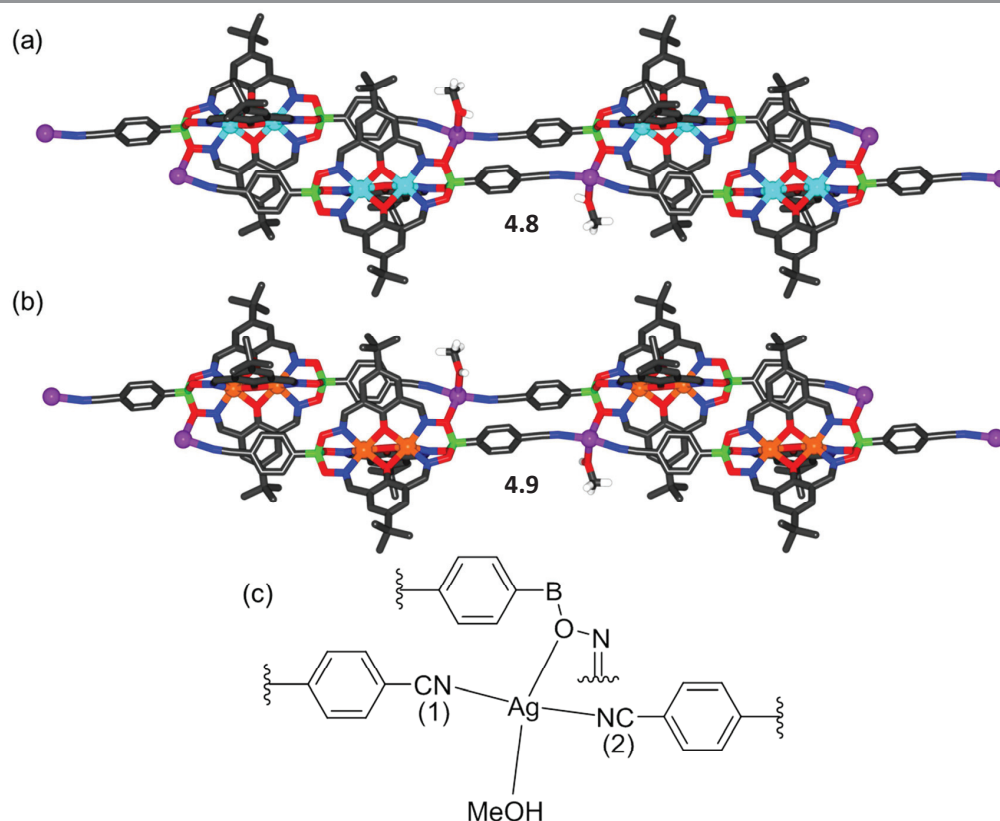
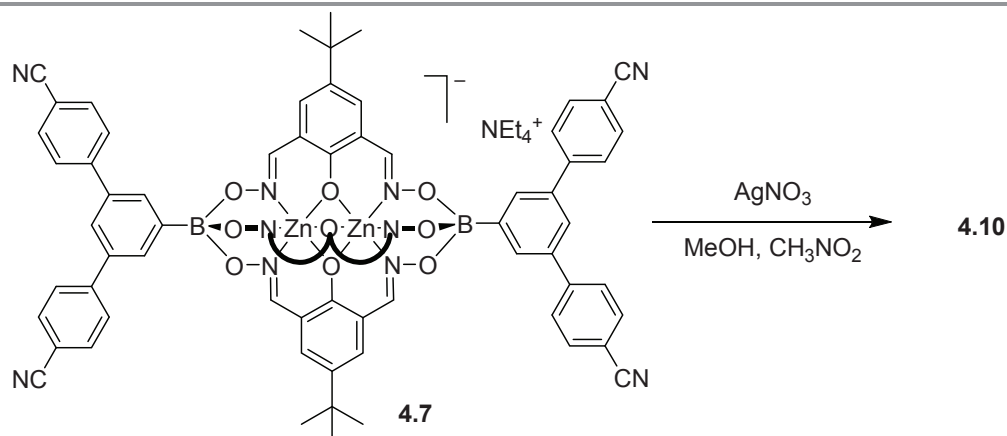


Figure 4.4 – Graphical representations of the double chain structure of (a) coordination polymer **4.8** and (b) **4.9**; (c) Representation of the first coordination sphere of the Ag^+ ions (bottom). Most hydrogen atoms and unbound solvent molecules have been omitted for clarity. Color coding: C: gray; H: white; Ag: purple; B: green; N: blue; O: red; Zn: cyan.

Table 4.1 – Selected bond lengths (Å) and angles (°) for the complexes **4.8** and **4.9**.

Complex	Ag–N(1)	Ag–N(2)	Ag–O _{MeOH}	Ag–O _{Oxime}
4.8	2.158(6) Å	2.132(6) Å	2.627(4) Å	2.586(4) Å
4.9	2.171(3) Å	2.155(3) Å	2.526(5) Å	2.577(3) Å

The structures of CPs **4.8** and **4.9** do not contain nitrate anions from the silver salt because the charge compensation is achieved by the metalloligand itself. It should be noted that for previously reported silver(I) CPs, the anion derived from the silver salt was often found to influence the final structure.^{116d,117a,d,118b,g} We were also successful in preparing a CP using the tetratopic metalloligand **4.7**. Layering a solution of AgOTs in MeOH on top of a solution of **4.7** in nitromethane led to the formation of transparent, plate-like crystals of coordination polymer **4.10** (Scheme 4.7).



Scheme 4.7 – Synthesis of the heterometallic coordination polymer **4.10**.

Single crystal X-ray analysis of **4.10** revealed the formation of a two-dimensional network structure with the stoichiometry $[\text{Ag}_2(\mathbf{4.7})_2](\text{CH}_3\text{OH})_{1.5}(\text{CH}_3\text{NO}_2)_3$. A graphical representation of the structure is depicted in Figure 4.5. One can observe two distinct clathrochelate metalloligands in the structure. The first one is coordinated via all of its cyano groups to silver ions Ag(1) and Ag(2), thereby forming an infinite double chain. The second clathrochelate is coordinated via only one of the four cyano groups to silver ions Ag(2). The latter display a trigonal pyramidal geometry ($\text{Ag}(2)\text{-N}_{\text{av.}} = 2.281 \text{ \AA}$), with the fourth coordination site being occupied by the oxygen atom of a boronate ester group from an adjacent clathrochelate ($\text{Ag}(2)\text{-O} = 2.587(6) \text{ \AA}$). The Ag(1) ions display approximate trigonal planar geometry, with coordination of Ag(1) to two cyano groups ($\text{Ag}(1)\text{-N}_{\text{av.}} = 2.173 \text{ \AA}$) and one oxygen atom of a boronate ester ($\text{Ag}(1)\text{-O} = 2.390(5) \text{ \AA}$). The Ag-O-B linkages connect the double chains, resulting in an overall two-dimensional 3,6-coordinated network structure, where silver atoms act as three-connected nodes and clathrochelates as six-connected nodes (through four cyano and two boronate groups). The underlying net of this CP has the **kgd** topology (kagome dual, given in terms of the RCSR notation,¹²⁵ see Figure 4.5c) which is the most widespread topology for 3,6-coordinated two-dimensional CPs.¹²⁶ As it was observed for CP **4.8** and **4.9**, the charge compensation is achieved by the metalloligands, and tosylate anions from the silver salt are not found in the structure.

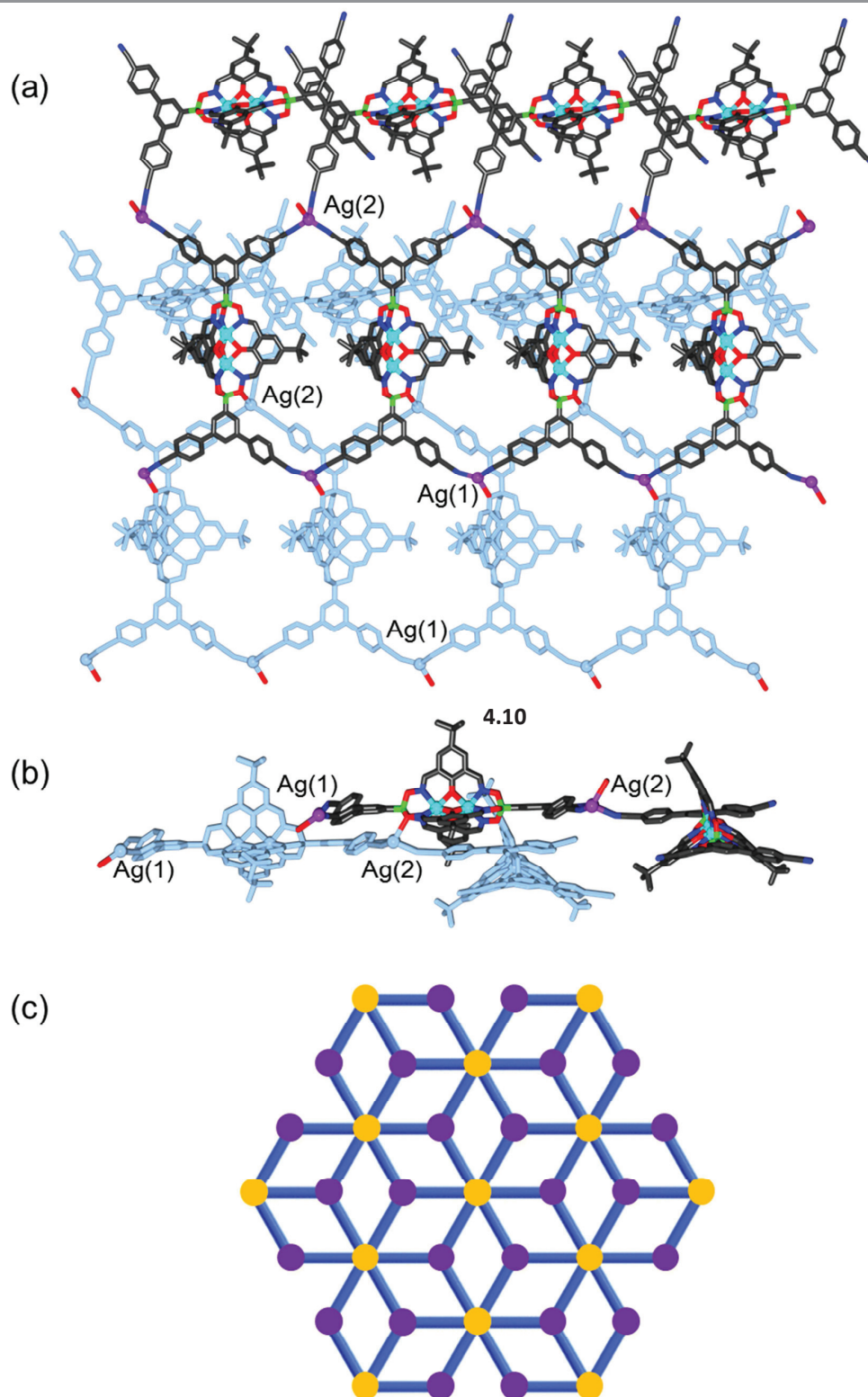
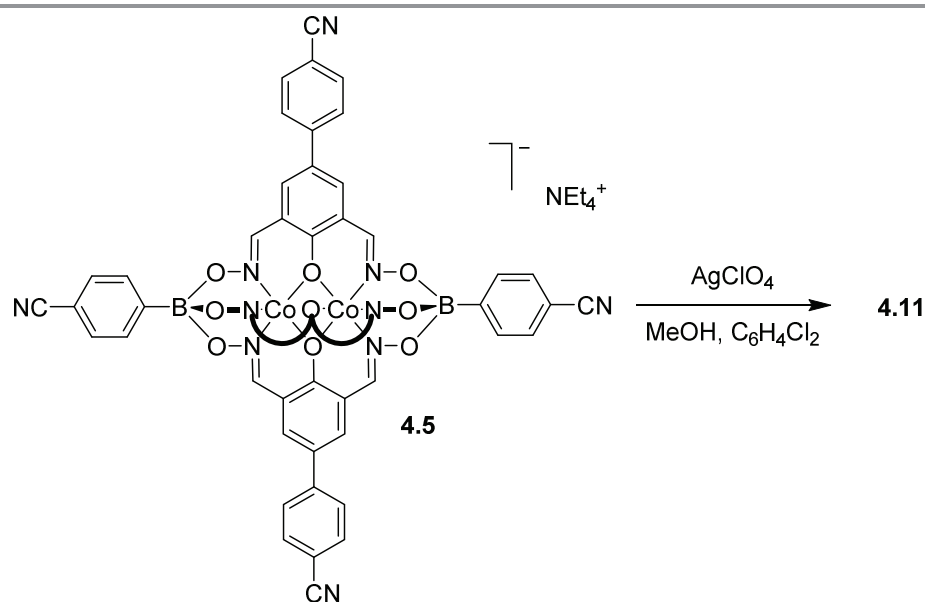


Figure 4.5 – Part of the structure of coordination polymer **4.10** with top (a) and side views (b). (c) Representation of the underlying **kgd** net, with **4.7** subunits represented as orange spheres and Ag(I) centers in purple. The shaded pale blue part of the structure is connected via Ag-O bonds. Hydrogen atoms and solvent molecules have been omitted for clarity. Color coding: C: gray; Ag: purple; B: green; N: blue; O: red; Zn: cyan.

Silver(I) CPs based on pentacyano ligands with a trigonal bipyramidal geometry are – to the best of our knowledge – not known. We were thus particularly interested to obtain CPs with the pentatopic metalloligands **4.4** and **4.5**. After several attempts, we were able to crystallize CP **4.11** using metalloligand **4.5** in combination with AgClO_4 in the presence of MeOH, DMF and 1,2-dichlorobenzene as solvents (Scheme 4.8). Single crystal X-ray analysis of **4.11** showed that a three-dimensional network with the stoichiometry $[\text{Ag}_3(\mathbf{4.5})_2(\text{OMe})](\text{C}_6\text{H}_4\text{Cl}_2)(\text{MeOH})(\text{sol.})_n$ had formed (Figure 4.6). The asymmetric unit of the crystal contains three silver ions and two clathrochelate complexes **4.5**. Although the ratio of Ag to **4.5** is equal to 3 : 2, the overall network is neutral due to presence of disordered methoxy groups which are coordinated to Ag(2) ions. Absence of perchlorate within CP was further proved by FT-IR analysis, which excluded its presence (Figure 4.7). Besides, the Ag(2) ions act as linker between two cobalt-containing metalloligands ($\text{Ag}(2)\text{-N}_{\text{av.}} = 2.119 \text{ \AA}$). The Ag(1) and Ag(3) ions, on the other hand, are coordinated in a trigonal planar fashion to three cyano groups, with Ag(1)-N distances varying from 2.11(2) to 2.30(2) \AA . Both metalloligands act as four-connected nodes through both of the apical and two of the three lateral cyano groups (one cyano group is ‘free’). The first crystallographically independent metalloligand coordinates to one Ag(2) and three Ag(1) ions, and the second one to one Ag(2) and three Ag(3) ions. As a result, the Ag(2) ions links two interpenetrating CPs of the stoichiometry $[\text{Ag}(\mathbf{4.5})]$ and the **utp** topology (widespread among 3-coordinated CP nets)¹²⁷ to form a three-dimensional net.



Scheme 4.8 – Synthesis of coordination polymer **4.11** using pentatopic clathrochelate **4.5**.

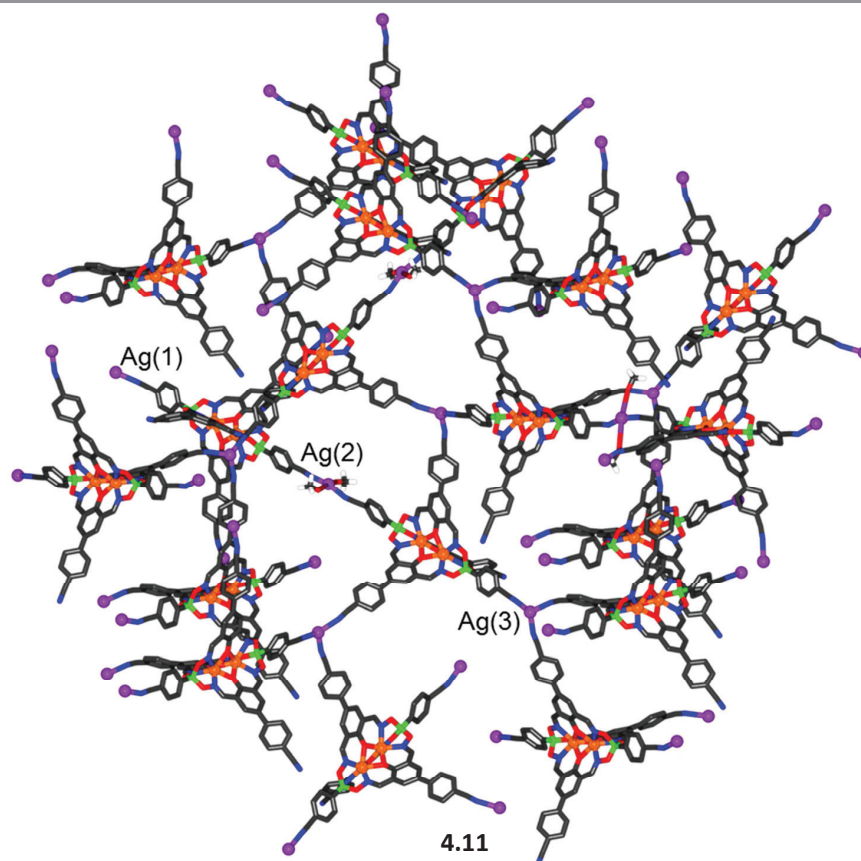


Figure 4.6 – Part of the structure of the three-dimensional coordination polymer **4.11**. Most hydrogen atoms and unbound solvent molecules have been omitted for clarity. Color coding: C: gray; H: white; Ag: purple; B: green; Co: orange; N: blue; O: red.

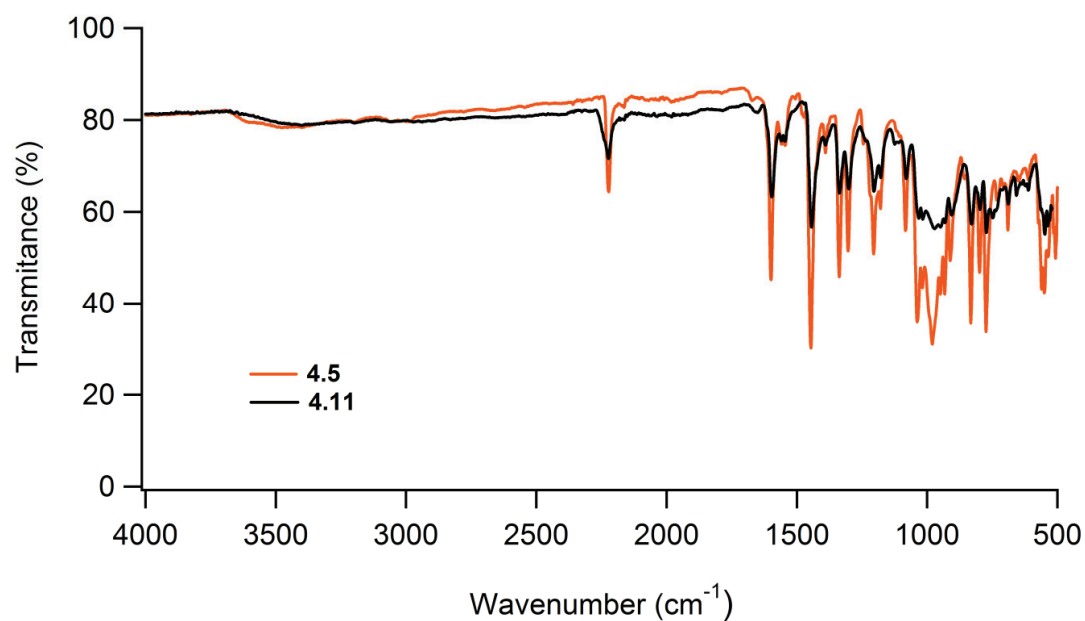


Figure 4.7 – FT-IR spectra of **4.5** and CP **4.11**, indicating the absence of perchlorate within the CP structure.

A topological analysis of the resulting architecture by means of the *ToposPro* package¹²⁸ revealed that the net has a point symbol $(8 \cdot 10^2)(8^2 \cdot 10^4)(8^2 \cdot 10)(8^3 \cdot 10^3)$. To the best of our knowledge, such a network topology has not been observed in crystals before. The structure was deposited to the Topos TTD collection under the abbreviation **epf1**. An intriguing structural feature of **4.11** is that all eight- and ten-membered circuits of the nodes are crossed by other rings, resulting in self-catenation (Figure 4.8). Self-catenated structures are single networks with regions in which chains from the same net pass through the smallest topological circuits in a fashion similar to that of interpenetrated systems. The observation of self-catenation in **4.11** is unusual because most of reported self-catenated nets are constructed from flexible ligands.¹²⁹ The catenation in **4.11** is very dense from a topological point of view: the eight-membered rings are crossed by 42 other rings and the ten-membered rings are crossed by at least 57 other rings. The topological density of the net can be given as $TD_{10} = 3127$, which is the number of nodes within the first 10 coordination spheres of a given node. According to the RCSR database,¹²⁵ this value represents the highest topological density among all known 3,3,4,4-coordinated nets, and is almost as high as $TD_{10} = 3245$ for a recently published 3,4-coordinated **mhq-z** net.¹³⁰ Despite the high topological density, CP **4.11** displays a very large solvent-accessible volume of 53% according to calculations with *Mercury*.¹³¹ These voids are occupied by highly disordered solvent molecules, some of which could not be located from difference Fourier maps. The attempted desolvation of CP **13** resulted in rapid degradation of the material.

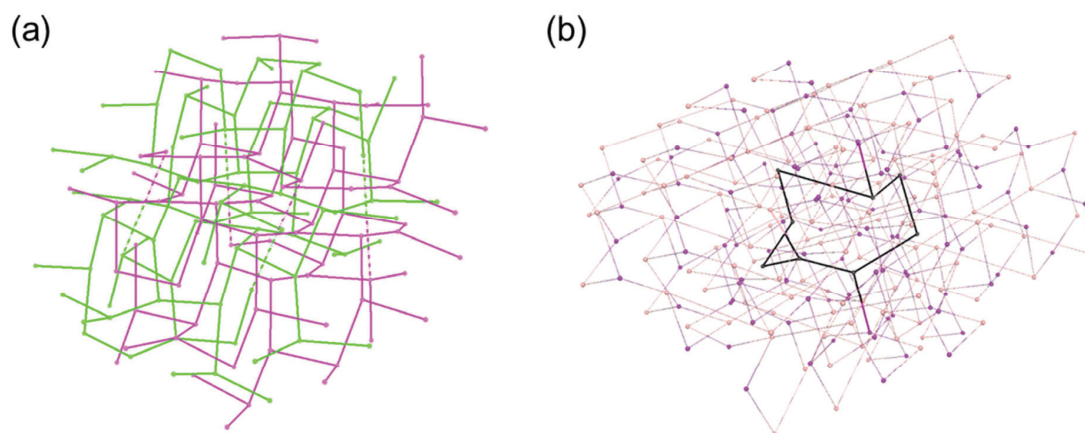


Figure 4.8 – (a) The underlying net of the three-dimensional coordination polymer **4.11**. Interpenetrating **utp** nets are shown in green and fuchsia, and the connections by Ag(2) atoms are depicted with dashed lines; (b) The 8-membered ring (black) catenated by 42 other 8- and 10-rings in the underlying net of coordination polymer **4.11**.

4.5 Conclusion

We have shown that dinuclear clathrochelate complexes with a trigonal bipyramidal shape can be decorated with cyano groups in apical and/or lateral position by using cyano-functionalized starting materials for the clathrochelate synthesis. Alternatively, we have been able to prepare elongated clathrochelates with pendent benzonitrile groups by post-synthetic modification of brominated clathrochelates in Pd-catalyzed cross-coupling reactions. The functionalized clathrochelates can be used as metalloligands for the preparation of heterometallic $\text{Co}^{2+}/\text{Ag}^+$ and $\text{Zn}^{2+}/\text{Ag}^+$ coordination polymers, as evidenced by the synthesis of one-, two-, and three-dimensional CPs in reactions with silver salts. Due to the negative charge of the metalloligands, the CPs are devoid of anions derived from the silver salt. A structure-directing role of the anion, as observed for many silver(I) CPs, is thereby avoided. The three-dimensional CP **4.11** is of special interest because it displays an unprecedented network topology and a very high topological density.

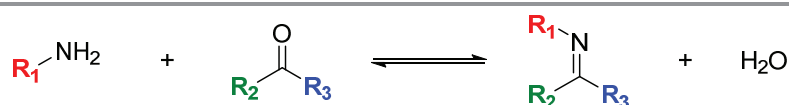
Potential applications of the CN-functionalized clathrochelate complexes described above are not restricted to the formation of polymeric networks. Polycyanoligands have also been employed for the constructions of molecularly defined nanostructures using coordination-based self-assembly,¹³² and our new metalloligands should be useful building blocks in this context as well.

Chapter 5 Miscellaneous structural variations of dinuclear clathrochelates

The results presented in this chapter detail firstly the synthesis of dinuclear clathrochelates with pendent formyl or amine groups. Attempts to perform polycondensation reactions with these new clathrochelates are discussed. Secondly, the synthesis of clathrochelates complexes sharing two different functional groups on their scaffold will be described, followed by the analysis of clathrochelate mixtures of increased complexity. Last but not least, studies on the relative stability of dinuclear clathrochelates are reported.

5.1 Introduction

The imine bond is created by the reaction between an aldehyde (or a ketone) and an amine (Scheme 5.1). This condensation reaction can be catalyzed by an acid (Lewis or Brønsted acids) as discovered by Schiff in 1864.¹³³ The reaction is reversible and therefore allows an error-correction process to occur, which makes imine-based self-assembly of great interest in dynamic covalent chemistry (DCC).¹³⁴ Conversely to coordination-driven self-assembly, imine bonds are based on the formation of covalent bonds.



Scheme 5.1 – Imine condensation reaction.

Since this reaction is reversible, the equilibrium can be influenced by several parameters. Firstly, the removal of water during the imine formation reaction (e.g. with a Dean-Stark apparatus or a drying agent), favors the formation of the imine bond. Nevertheless, the hydrolytic sensitivity of imine bonds can vary from one system to another. The equilibrium is also affected by the electronic properties of both the amine and the aldehyde counterparts. Aldehydes with electron-withdrawing groups, leading to an enhanced electrophilic character on the carbonyl center, are pushing the equilibrium to the formation of the imine.¹³⁵ Similarly, electron-rich amines favor product formation. Since the topic of imine-based self-assembly is extremely wide, ranging from the formation of discrete two-dimensional¹³⁶ or three-dimensional¹³⁷ structures to polymeric materials,¹³⁸ only selected examples will be discussed here.

Recently, Severin *et al.* reported a series of large cages constructed from bowl-shaped ruthenium trimer complexes functionalized with aldehyde groups and different amines.¹³⁹ The rational use of different amines led to the formation of [4+4] tetrahedral, [2+3] cylindrical or even [1+1] cages (Figure 5.1.). Their work also highlighted the dynamic nature of the imine bond, as they observed the conversion of one of their tetrahedral cages into a smaller cylindrical one, *via* an imine exchange mechanism.

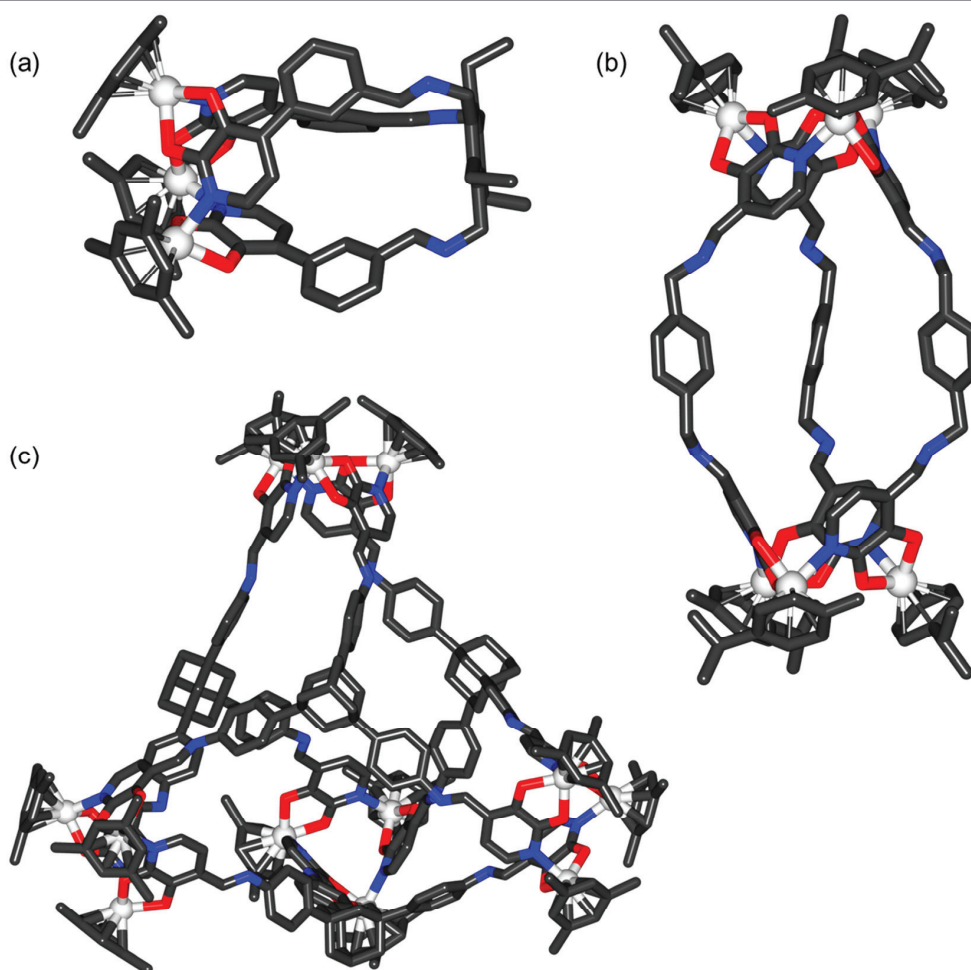


Figure 5.1 – Molecular structure of the imine-based cages obtained from the (a) [1+1], (b) [3+2] and (c) [4+4] condensation reactions. Hydrogen atoms and solvent molecules have been omitted for clarity. Color coding: C: gray; N: blue; O: red; Ru: light grey.

Imine-based self-assembly can also be combined with other reversible covalent bonds (boronic ester formation,¹⁴⁰ olefin or alkyne metathesis, disulfide bonds,¹⁴¹ etc.) or coordination bonds. The group of Nitschke is well-known for combining metal-ligand interactions and imine bond formation. Typically, they react a formylpyridine-functionalized ligand with an amine to form a N,N-ditopic ligand, that further binds to a metal center. Following this approach, they synthesized a vast library of molecularly defined nanostructures, from simple helicates¹⁴² to cubes or other polyhedra.¹⁴³ Interestingly, several of these complexes display high stability towards water, and some of them were even soluble in it. Selected representative examples of cages obtained by this approach are shown in Figure 5.2. More particularly, joint of the with Severin and Nitschke groups showed that tris(dioxime)-based clathrochelates functionalized with formylpyridyl or amine groups could be successfully incorporated into tetrahedral cages upon sub-component self-assembly with Fe(II) salts (Figure 5.2c).⁵³

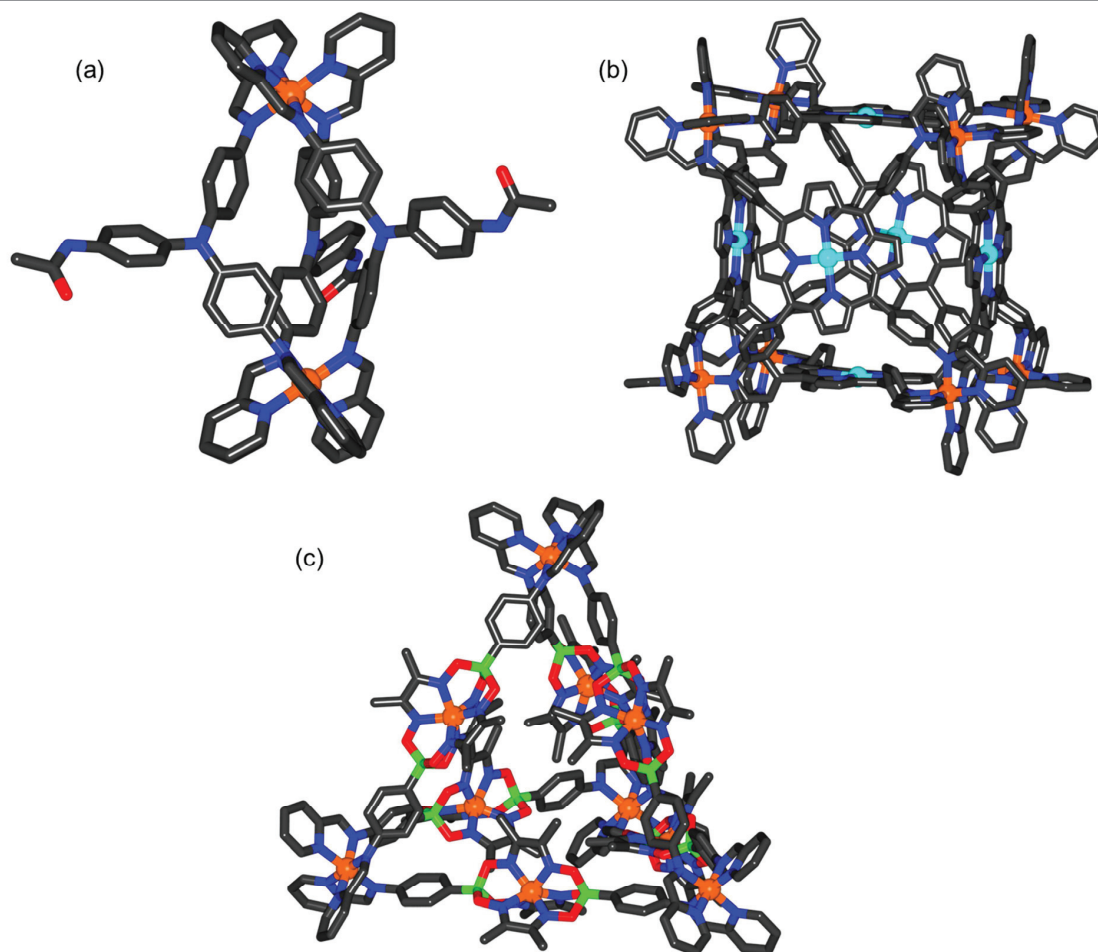
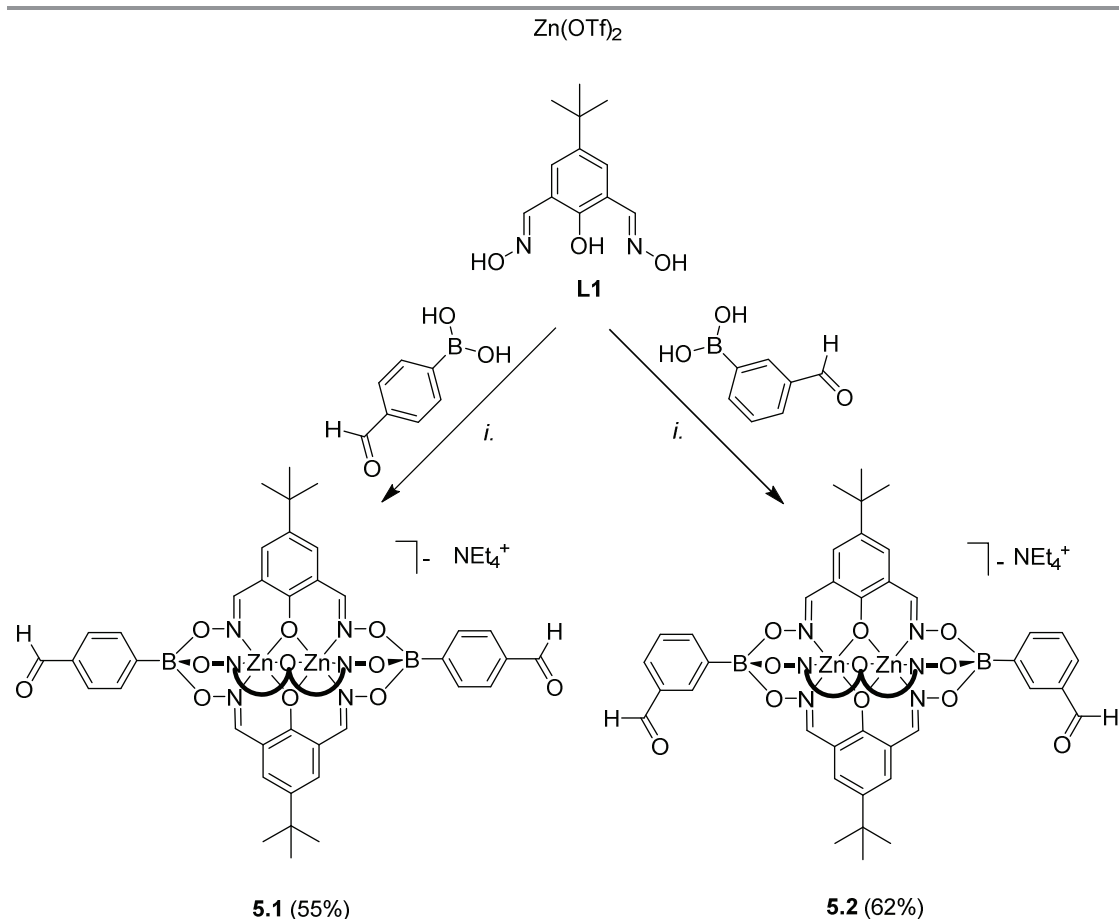


Figure 5.2 – Molecular structure of selected (a) helicate, (b) cube or (c) tetrahedral cage complexes obtained combining metal-ligand interactions and imine bond formation. Hydrogen atoms, counterions and solvent molecules have been omitted for clarity. Color coding: C: gray; B: green; Fe: orange; N: blue; Ni: cyan; O: red.

5.2 Synthesis of formyl- and amine-functionalized dinuclear clathrochelates

Following the synthetic strategy described in previous chapters, we were able to prepare dinuclear clathrochelates **5.1** and **5.2** bearing formyl substituents in *para* or *meta* position using commercially available 4- or 3-formylphenylboronic acids in combination with 2,6-diformyl-4-*tert*-butylphenol dioxime (**L1**) and $\text{Zn}(\text{OTf})_2$ (Scheme 5.2). The dialdehydes were obtained in moderate yields upon the addition of tetraethylammonium hydroxide to the reaction mixture. ^1H -NMR analysis of complexes **5.1** and **5.2** (Figure 5.3) unambiguously confirmed the presence of the unprotected aldehyde on the clathrochelate core, as evidenced by a characteristic NMR signal at $\delta = 9.99$ ppm (**5.1**) and 10.04 ppm (**5.2**). Despite several attempts of crystallization, we were not able to isolate single-crystals neither for **5.1** or **5.2**. Nevertheless, the analytical results (NMR, FT-IR and HRMS) confirmed the structures.



Scheme 5.2 – Synthesis of the ditopic clathrochelate complexes **5.1** and **5.2**. Reagents and conditions: (*i.*): EtOH/ CH_2Cl_2 , RT, then NEt_4OH .

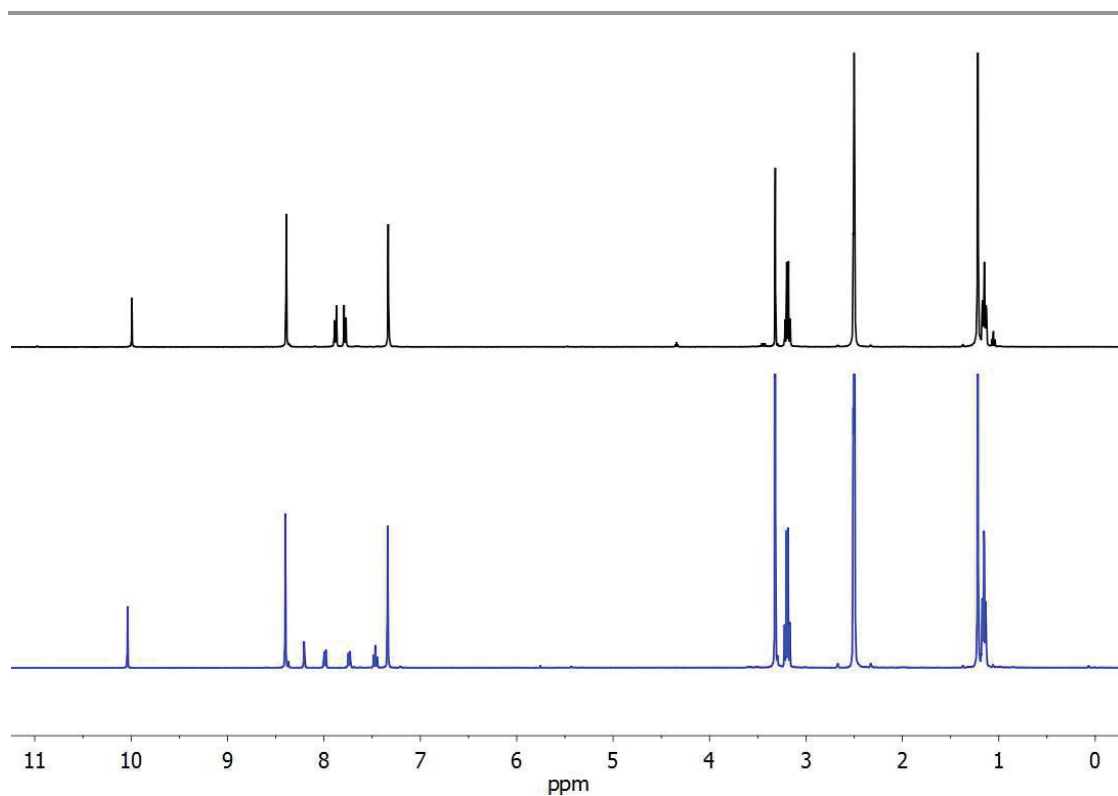
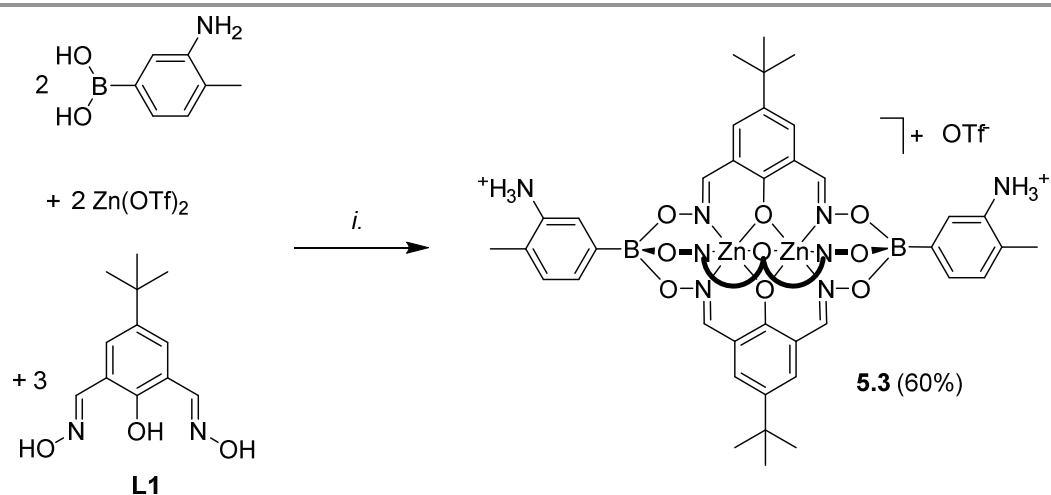


Figure 5.3 – NMR spectra of **5.1** (top, black curve) and **5.2** (bottom, blue curve) in DMSO- d_6 .

Similarly to the synthesis of dialdehyde-decorated clathrochelates, clathrochelate **5.3** with an apical 3-amino-4-methylphenyl group was obtained in its diprotonated form upon reaction of a commercially available boronic acid, **L1** and $\text{Zn}(\text{OTf})_2$ (Scheme 5.3). The complex was kept protonated because of enhanced stability compared to the free, deprotonated diamine analogue.



Scheme 5.3 – Synthesis of clathrochelate complex **5.3**. Reagents and conditions: (*i.*): EtOH, RT.

Despite all our efforts, we were not successful in synthesizing the 4-aminophenyl-decorated clathrochelate. Due to the cost of 4-aminophenylboronic acid, the direct synthetic route was not envisaged. Relying on the work of Dr. Matthew Wise, we attempted the synthesis of a benzyl protected 4-amino derivative. However, solubility problems led to the premature stop of this route.

5.3 Formyl- and amine-functionalized dinuclear clathrochelates as building blocks

Clathrochelate complexes **5.1** and **5.2** were tested individually in combination with several di- or triamine-based ligands depicted in Figure 5.4, in order to synthesize discrete macrocycles or cage compounds. Some of these ligands have aliphatic amines, whereas others have aromatic ones. The reactions were performed on NMR-scale, by dissolving complexes **5.1** or **5.2** in dry solvents such as CDCl_3 or CD_2Cl_2 . NMR spectra were recorded before the addition of the corresponding amine and the reaction was followed by NMR.

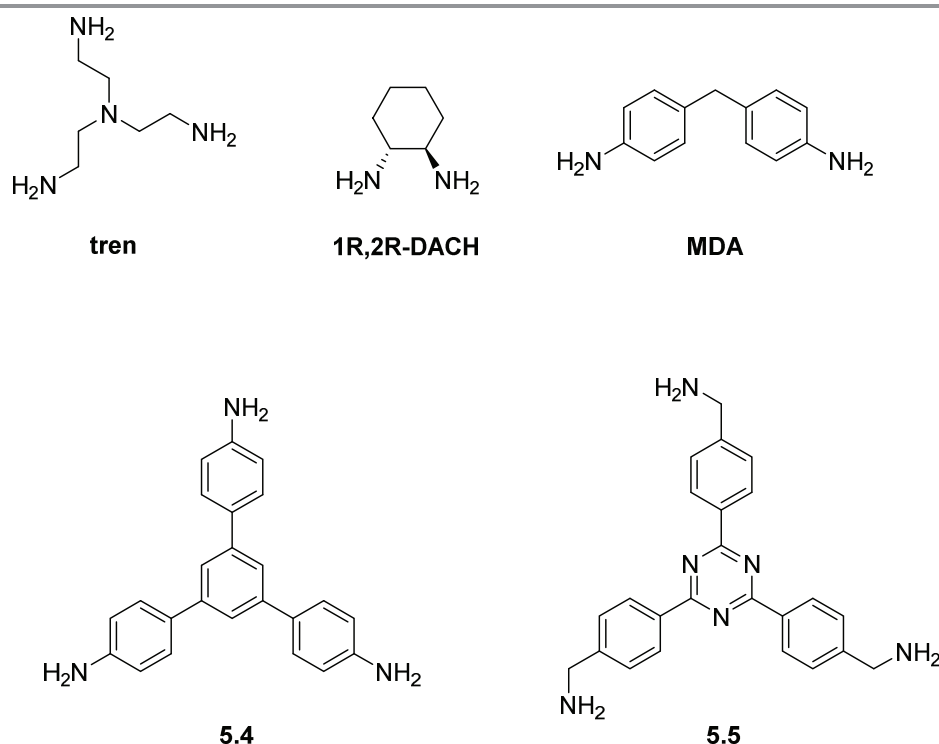


Figure 5.4 – Structure of the polyamines used in this study. Tren = tris(2-aminoethyl)amine; DACH = diaminocyclohexane; MDA = methylenedianiline.

While combining **5.1** with tritopic **tren** in CD_2Cl_2 , the complete disappearance of the aldehyde signal of **5.1** at $\delta = 9.99$ was observed within the course of 3 hours (Figure 5.5). Interestingly, the formation of a broad peak of unknown multiplicity was observed at $\delta = 8.3$ ppm, which can be

attributed to the signals of imine protons. Based on symmetry considerations, we assume that multiple species were formed. Moreover, a precipitate was observed over the course of the reaction. HRMS analysis failed to confirm the presence of discrete structures. However, this first example showed that reactions of diformylated clathrochelates with aliphatic amines are feasible.

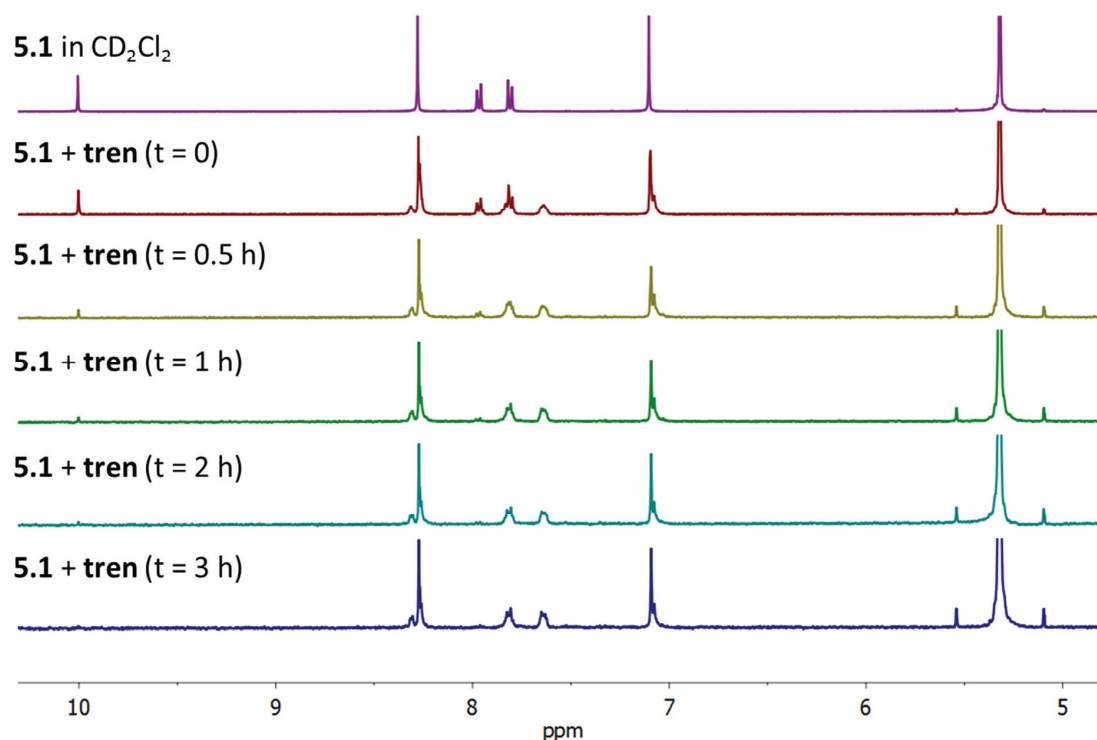


Figure 5.5 – Evolution of the ^1H NMR spectrum of a mixture of **tren** and **5.1** in CD_2Cl_2 . For clarity, only the aromatic region of the spectrum is shown.

On the other hand, combining the same dialdehyde clathrochelate **5.1** with aromatic triamine **5.4**, a completely different behavior was observed. Whilst **tren** was reacting quickly with **5.1**, leading to the complete disappearance of the aldehyde peak, a very low conversion was found for **5.4** (Figure 5.6). Even after 48 hours of reaction, only 12 % of the initial **5.1** had reacted with **5.4**, as evidenced by the appearance of a complex series of new peaks, the most characteristic of which being the signals of the imine protons. The reaction mixture was kept several extra days, but no major changes were observed. This result indicates that aromatic amines tend to be less suitable candidates for imine condensations with our dinuclear clathrochelates. All other attempts of reaction between polyamines depicted in Figure 5.4 and ditopic clathrochelates **5.1** or **5.2** showed similar behavior (i.e.: no reaction, or formation of a complex mixture of species).

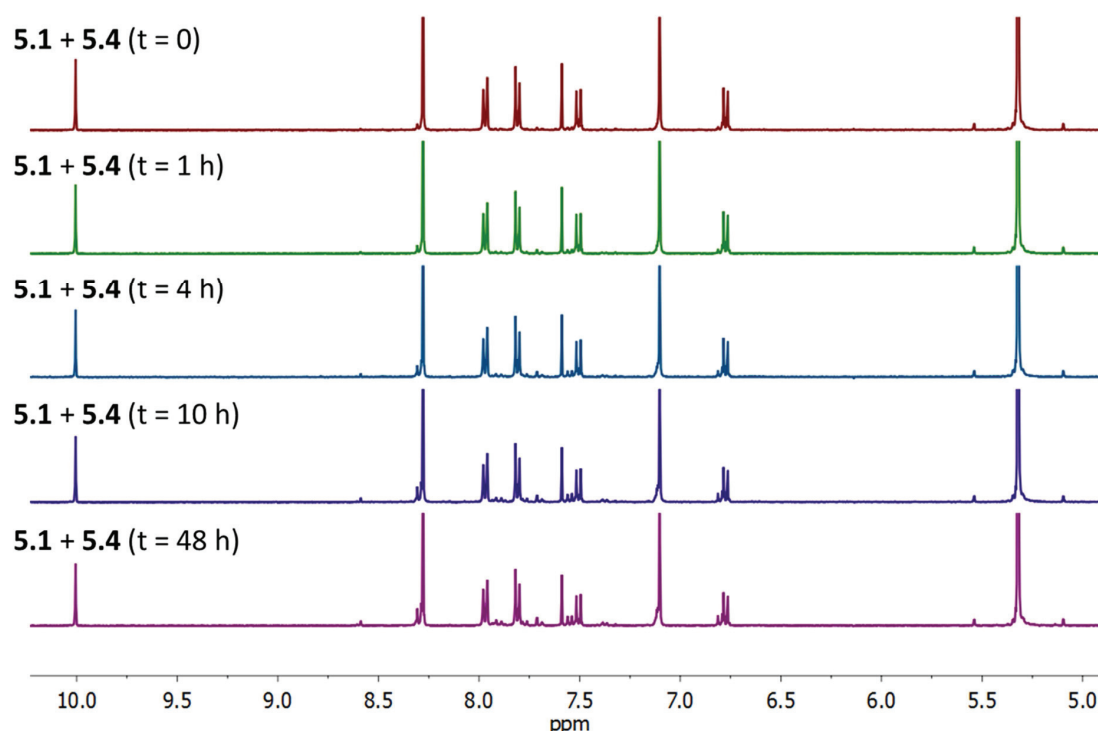
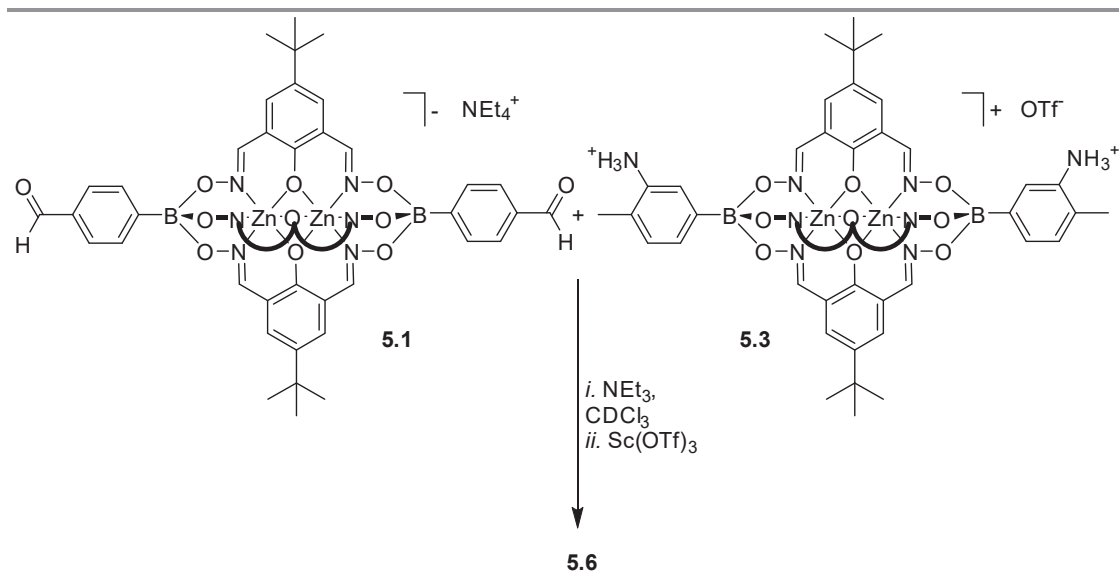


Figure 5.6 – Evolution of the ^1H NMR spectrum of a mixture of **5.4** and **5.1** in CD_2Cl_2 . For clarity, only the aromatic region of the spectrum is shown.

We also attempted to perform a direct reaction between the dinuclear clathrochelates **5.1** and **5.3** (Scheme 5.4). The diamine clathrochelate **5.3** was first deprotonated in CDCl_3 by addition of triethylamine, and clathrochelate **5.1** was subsequently added and the reaction was monitored by ^1H NMR. Capitalizing on the rigid character of our clathrochelate core, we were expecting to form a discrete [3+3] macrocycle, or a polymeric material. Regrettably, no changes were observed by NMR, even after 2 weeks of reaction. $\text{Sc}(\text{OTf})_3$ (10 mol %) was then added to the mixture, and minor changes were observed, as evidenced in Figure 5.7. An imine peak at $\delta = 8.6$ ppm slowly appeared, but the conversion of the aldehyde to the imine was found to be extremely slow (25 % conversion after 48 hours) and incomplete. Overall, the results show that amine- or aldehyde-functionalized clathrochelate are not very suited as building blocks in dynamic covalent chemistry.



Scheme 5.4 – Reaction between dialdehyde complex **5.1** and diamine-functionalized clathrochelate **5.3**.

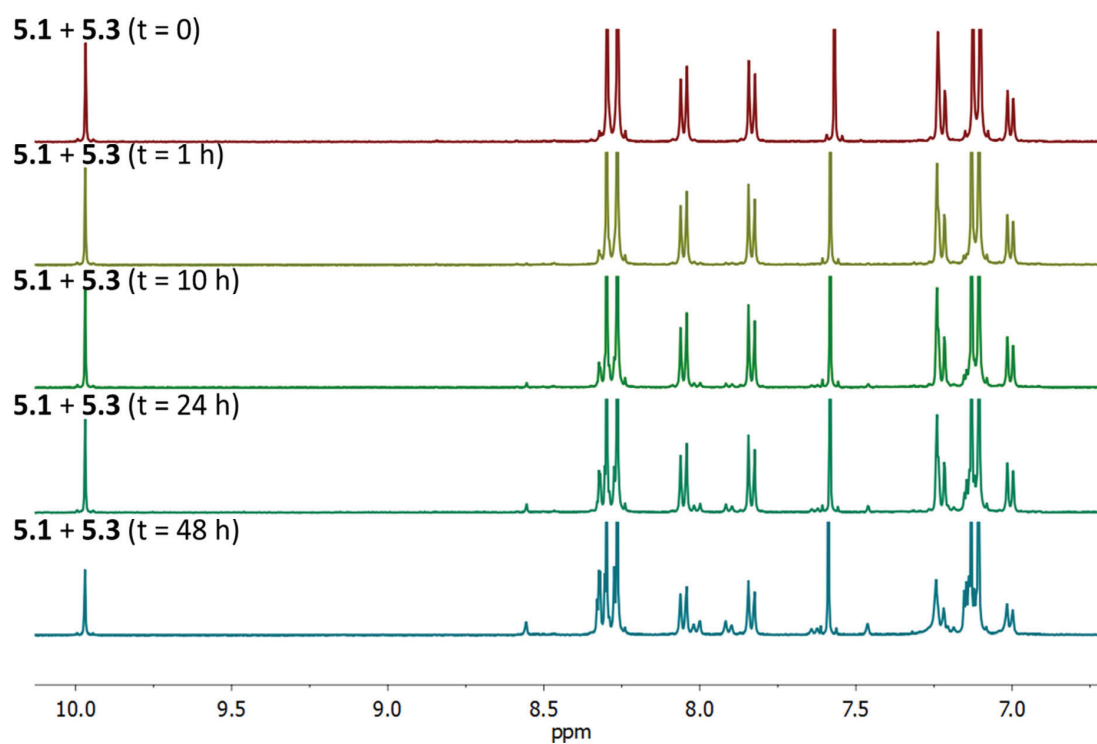
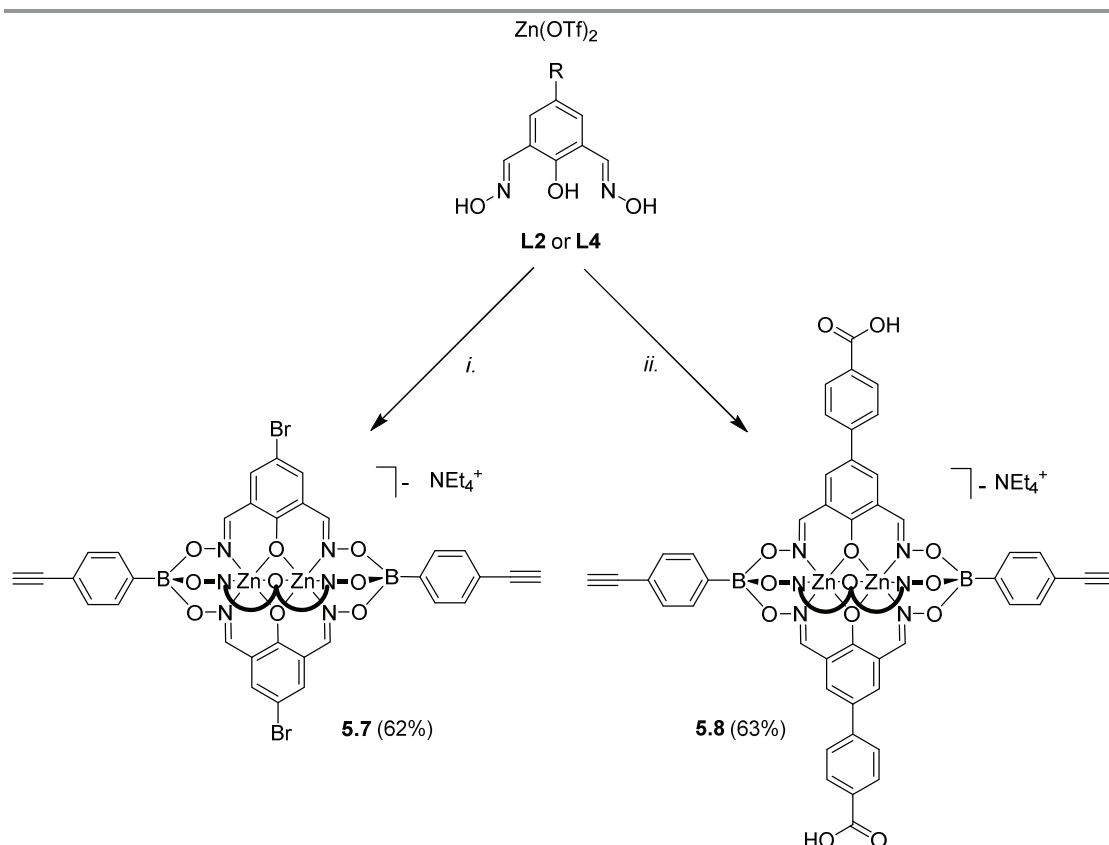


Figure 5.7 – Evolution of the ^1H NMR spectrum of a mixture of **5.3** and **5.1** in CDCl_3 after the addition of $\text{Sc}(\text{OTf})_3$ (10 mol %). For clarity, only the aromatic region of the spectrum is shown.

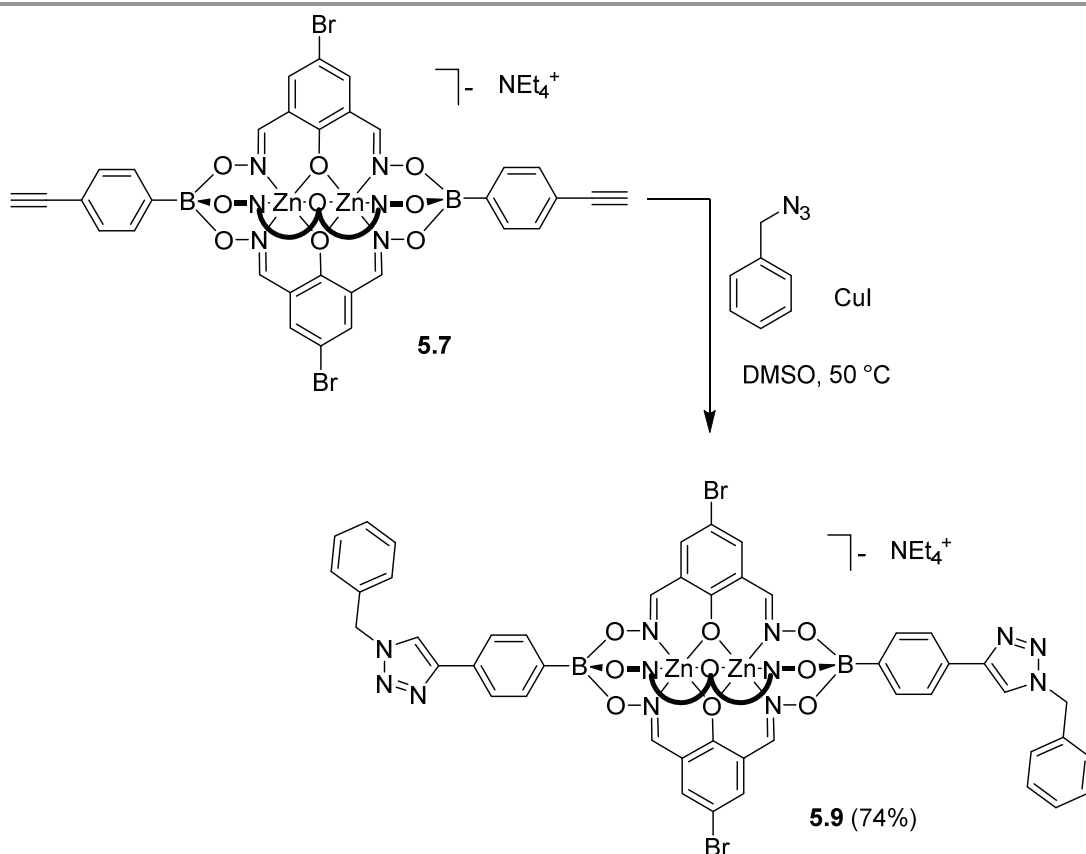
5.4 Synthesis of clathrochelates decorated with terminal acetylene groups, and their use in “click” chemistry

While exploring the potential functional groups that could be placed on our clathrochelate scaffold, we synthesized clathrochelates with terminal acetylene groups by reaction of 4-(dihydroxyborophenyl)acetylene, $\text{Zn}(\text{OTf})_2$ and the dioxime ligands **L2** or **L4** (Scheme 5.5). The acetylene moiety was found to be robust enough to withstand the mild reaction conditions, and the complexes **5.7** and **5.8** were isolated in good yields (**5.7**: 62%, **5.8**: 63%).



Scheme 5.5 – Synthesis of acetylene-decorated clathrochelates **5.7** and **5.8**. Reagents and conditions: (i.): Dioxime **L2**, EtOH/MeOH, 50 °C, then NEt₄OH; (ii.): Dioxime **L4**, EtOH/MeOH, 50 °C, then NEt₄OH.

NMR analyses unambiguously confirmed the presence of the terminal acetylene groups, with a ¹H NMR characteristic signal at $\delta = 4.03$ ppm (**5.7**) or $\delta = 4.05$ ppm (**5.8**). In order to assess the feasibility of “click” reactions with our dinuclear clathrochelates, we attempted the synthesis of an adduct between **5.7** and benzylazide in presence of copper iodide in DMSO (Scheme 5.6). The reaction was monitored by ESI-MS. After 16 hours, no trace of the starting material was found. Aqueous workup led to the isolation of the pure product **5.9**, whose structure was confirmed by HRMS and NMR spectroscopy (74% yield).

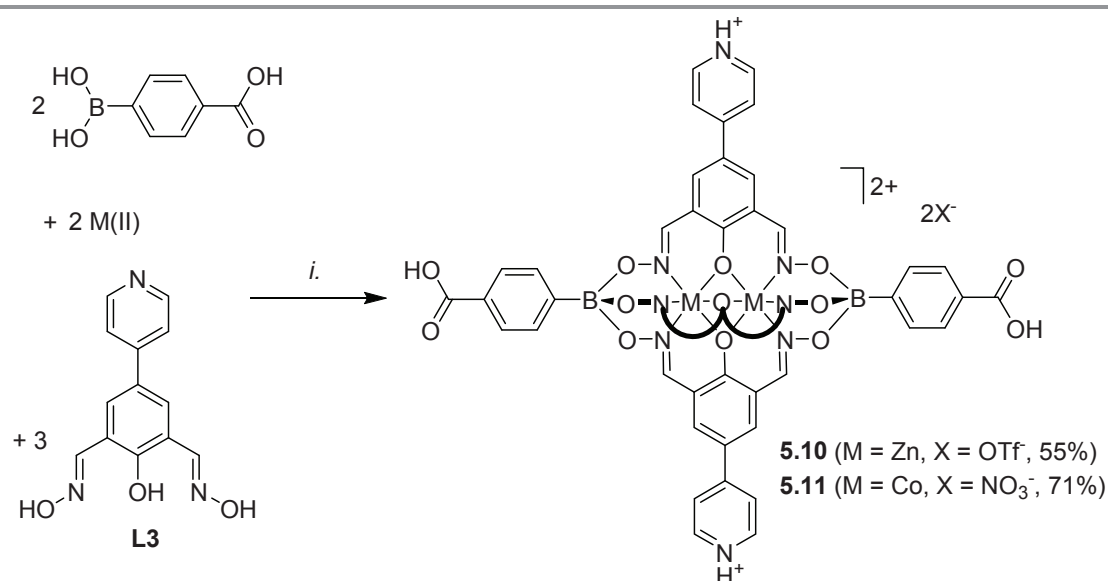


Scheme 5.6 – Synthesis of “click” adduct **5.9** between clathrochelate **5.7** and benzylazide in presence of CuI (25 mol %).

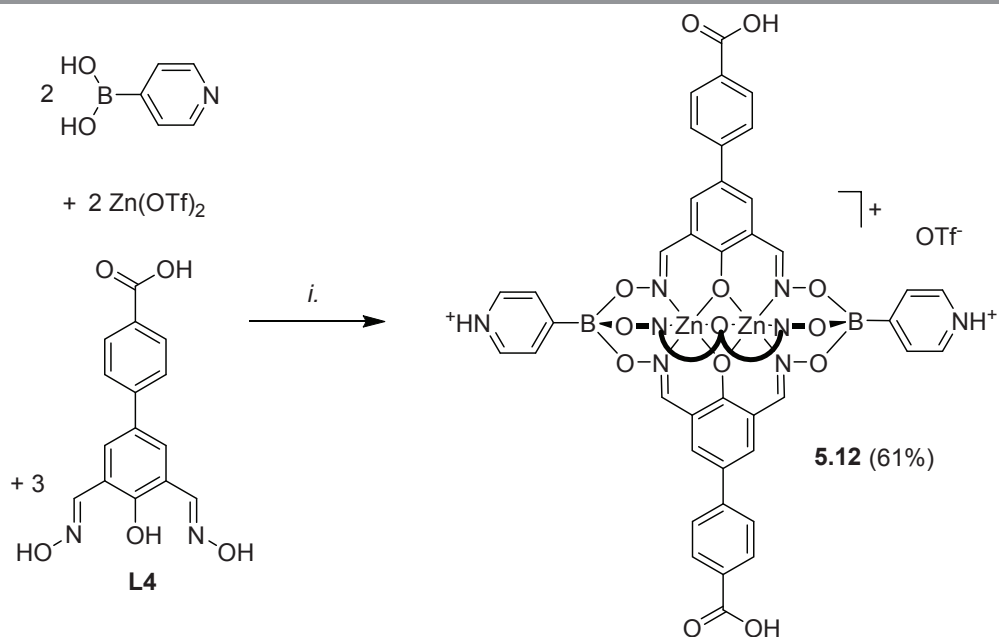
Several attempts were performed to incorporate clathrochelate **5.8** within a MOF structure. Indeed, MOF based on this tritopic subunit bearing free acetylene groups inside its cavity would be a perfect candidate for post-synthetic modifications (PSM).¹⁴⁴ Unfortunately, all attempts to obtain a crystalline MOF structure failed, and this approach was ultimately abandoned.

5.5 Synthesis of clathrochelates appended with different functional groups

So far, syntheses of clathrochelates bearing pyridyl (Chapter 2), carboxylic acid (Chapter 3), cyano (Chapter 4), aldehyde, amine or acetylene groups (Chapter 5) have been described. With the exception of **5.8**, the complexes feature only one type of functional group. We saw that it is possible to incorporate apical functional groups through the proper choice of the boronic acid, or lateral groups using functionalized dioxime ligands (e.g. **L3**, **L4** or **L5**). It appeared evident that combining these two approaches would allow synthesizing clathrochelate complexes with different functional groups. Combining 4-carboxyphenylboronic acid together with pyridyl-functionalized dioxime **L3** led to the formation of clathrochelates **5.10** (M = Zn) and **5.11** (M = Co) having two apical carboxylic acid groups and three lateral protonated pyridyl moieties (Scheme 5.7). On the other hand, reaction between 4-pyridylboronic acid and carboxylic acid-functionalized dioxime **L4** afforded the clathrochelate **5.12** with two apical pyridyl groups and three lateral carboxylic acid groups (Scheme 5.8). Their structures were confirmed by NMR spectroscopy and HRMS analyses.

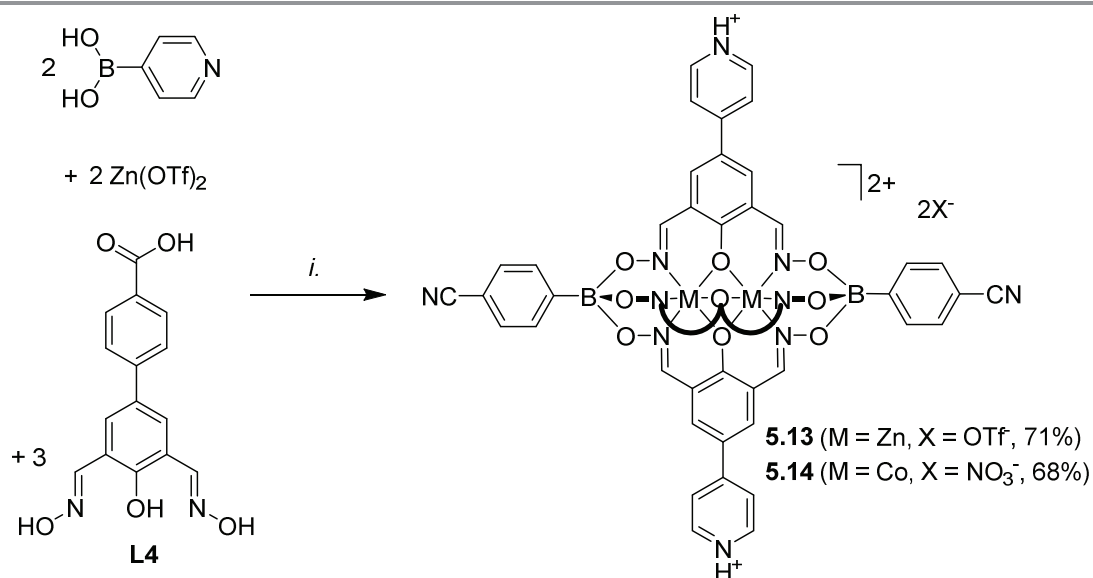


Scheme 5.7 – Synthesis of clathrochelates **5.10** and **5.11** with carboxylic acid and pyridyl groups. Reagents and conditions: (i): Dioxime **L3**, [Co(H₂O)₆](NO₃)₂ or Zn(OTf)₂, EtOH/MeOH, 70 °C.



Scheme 5.8 – Synthesis of clathrochelate **5.12** with carboxylic acid and pyridyl functional groups. Reagents and conditions: (i.): Dioxime **L4**, $\text{Zn}(\text{OTf})_2$, EtOH/MeOH, 70 °C.

Following a similar strategy, clathrochelates **5.13** and **5.14** were isolated from the reaction of 4-cyanophenylboronic acid and dioxime ligand **L3** (Scheme 5.9). The diamagnetic zinc complex **5.13** was also analyzed by NMR spectroscopy ($\text{DMSO-}d_6$). Single crystal X-ray structural analysis of **5.14** revealed the presence of the expected dinuclear clathrochelate core with protonated lateral pyridyl groups and apical 4-cyanophenyl groups (Figure 5.8).



Scheme 5.9 – Synthesis of clathrochelate **5.13–5.14** with cyano and pyridyl groups. Reagents and conditions: (i.): Dioxime **L4**, $[\text{Co}(\text{H}_2\text{O})_6](\text{NO}_3)_2$ or $\text{Zn}(\text{OTf})_2$, EtOH/MeOH, 70 °C.

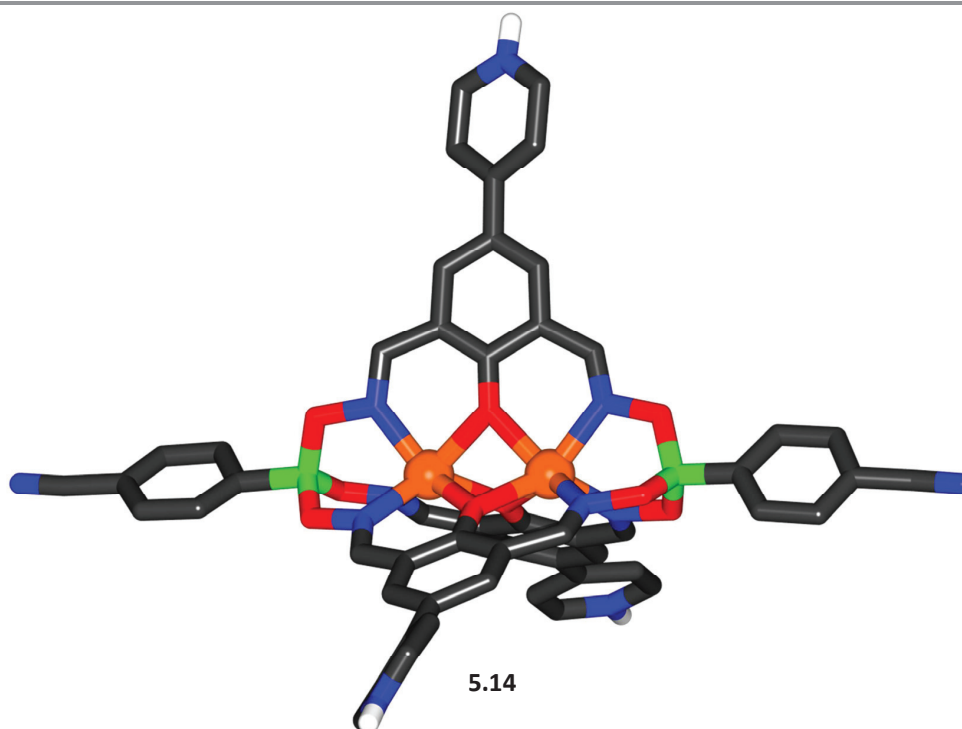
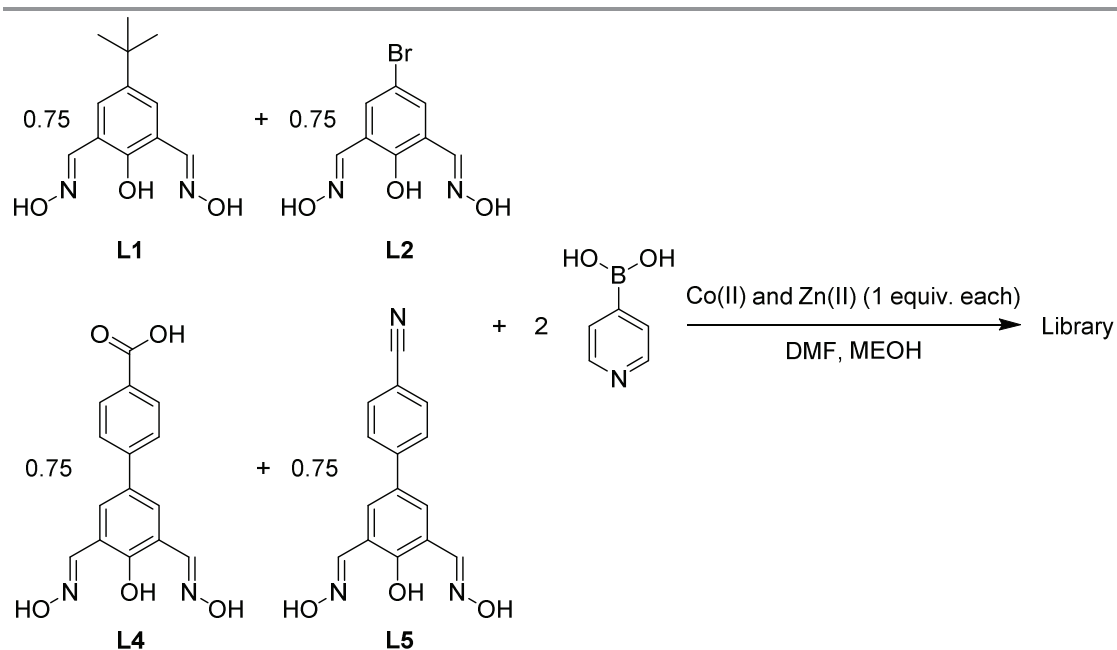


Figure 5.8 – Molecular structure of metalloligand **5.14** in the crystal. Most hydrogen atoms, counter ions (NO_3^-), and solvent molecules have been omitted for clarity. Color coding: C: gray; B: green; Co: orange; N: blue; O: red.

This approach highlights the versatility of our clathrochelate core, which can be decorated with multiple functional groups. One can easily imagine combining other functional groups together, resulting in a library of metalloligands with various functionalities.

5.6 MS analysis of clathrochelate mixtures

The clathrochelates presented so far all display *pseudo-C₃* symmetry. We were wondering if it would be possible to synthesize dinuclear clathrochelates bearing different dioxime ligands, therefore breaking this symmetry. Purely qualitative analysis of a mixture of clathrochelates obtained by the one-pot reaction of four dioxime ligands (**L1**, **L2**, **L4** and **L5**), 4-pyridylboronic acid, $\text{Zn}(\text{OTf})_2$ and $[\text{Co}(\text{H}_2\text{O})_6](\text{NO}_3)_2$ in MeOH and DMF was performed by high-resolution mass spectrometry (Scheme 5.10). We were interested in investigating whether some preferential combinations of dioximato ligands and/or metals would arise from this study. The stoichiometry of all compounds was chosen to have no limiting reagents, which would introduce an experimental bias.



Scheme 5.10 – One-pot reaction between dioxime ligands **L1**, **L2**, **L4**, **L5**, 4-pyridylboronic acid, Zn(OTf)_2 and $[\text{Co(H}_2\text{O)}_6](\text{NO}_3)_2$.

For sake of clarity, the clathrochelate complexes present in the mixture will be designated by the metal (M) present in their core, followed by their different oximato substituents, using the nomenclature $(\text{M1M2})(\text{L})(\text{L}')(\text{L}'')$. Based on a simple combinatorial analysis, 20 different oximato ligand combinations are possible. Since the dinuclear core can be homometallic ($\text{M1} = \text{M2} = \text{Co}$ or Zn) or heterometallic ($\text{M1} = \text{Co}$; $\text{M2} = \text{Zn}$), we can theoretically observe the formation of 60 different clathrochelate complexes. These complexes would be spread over only circa 200 Da, since the clathrochelate with the lowest m/z is $(\text{Co})_2(\text{L1})_3$ ($m/z = 995.2317$) and the one with the highest m/z is $(\text{Zn})_2(\text{L4})_3$ ($m/z = 1197.0991$). Analysis of this mixture, whose mass spectrum is shown in Figure 5.9, was performed by Dr. Konstantine O. Zhurov, using a hybrid linear ion trap Fourier transform ion cyclotron resonance (FT-ICR) mass spectrometer, with aliquots diluted to a concentration of circa 20 μM in MeOH. Isotopic pattern of all calculated clathrochelate complexes were then compared with the experimental results.

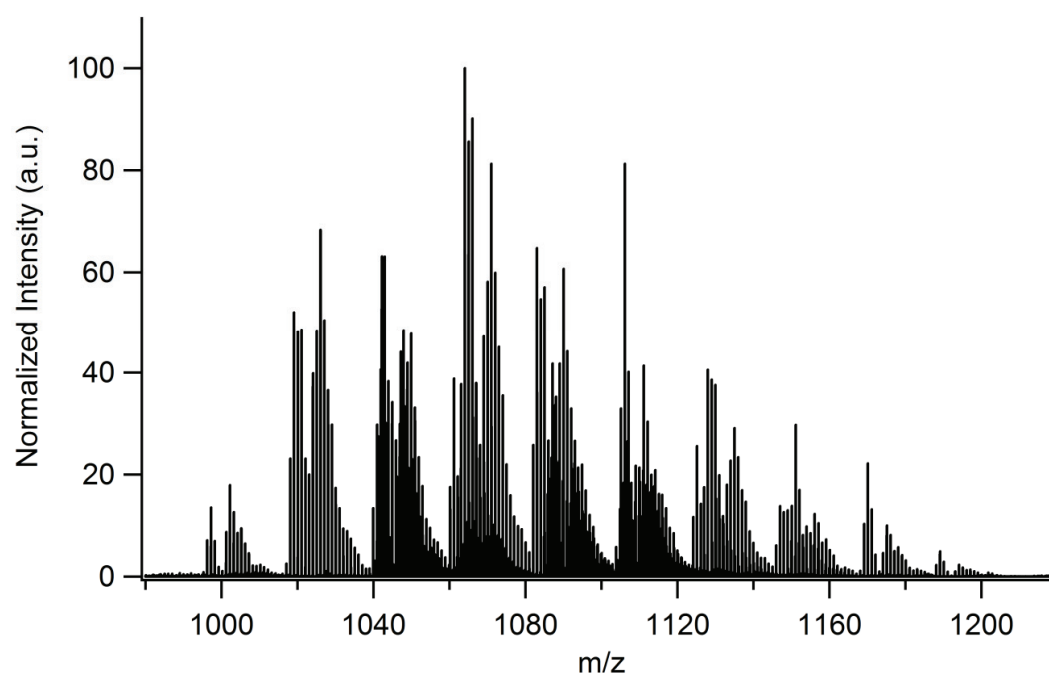


Figure 5.9 – Part of the ESI FT-ICR mass spectrum of the complex mixture obtained from the one-pot reaction between dioxime ligands **L1**, **L2**, **L4**, **L5**, 4-pyridylboronic acid, $\text{Zn}(\text{OTf})_2$ and $[\text{Co}(\text{H}_2\text{O})_6](\text{NO}_3)_2$.

Selected attributions of the experimental pattern to clathrochelate complexes are shown in Figure 5.10. The low m/z region shows the presence of homometallic dinuclear $\text{Zn}(\text{II})$ and $\text{Co}(\text{II})$ clathrochelates, as well as the heteronuclear $\text{Co}(\text{II})\text{Zn}(\text{II})$ complex. No quantitative analysis was performed on the relative intensities between $(\text{Co})_2(\text{L1})_3$, $(\text{CoZn})(\text{L1})_3$ and $(\text{Zn})_2(\text{L1})_3$. It is therefore not possible to calculate the ratio of the different complexes. One can also observe the formation of clathrochelates with different oximato ligands (Figure 5.10b), resulting in a spectrum of high complexity. The presence of different oximes does not affect the distribution of the metals, and both heterometallic and homometallic assemblies are observed. Careful analysis of the whole spectrum allowed us to assign the peaks to all of the 60 possible clathrochelate complexes. No preference for any specific combination of dioximato ligands and/or metal is observed. This result highlights the extreme modular behavior of this scaffold, allowing synthesizing clathrochelates with up to three different functional groups on the oxime part. An extension of this approach to an even more complex mixture by adding a second boronic acid was not attempted due to a tremendous increase of the required time to analyze the mass spectrum. Nevertheless, based on our previous observations, it would certainly be possible to create clathrochelate complexes sharing five different substituents. It should be noted that the mixture was only studied in solution, and that none of the complexes present in this mixture were isolated and further characterized.

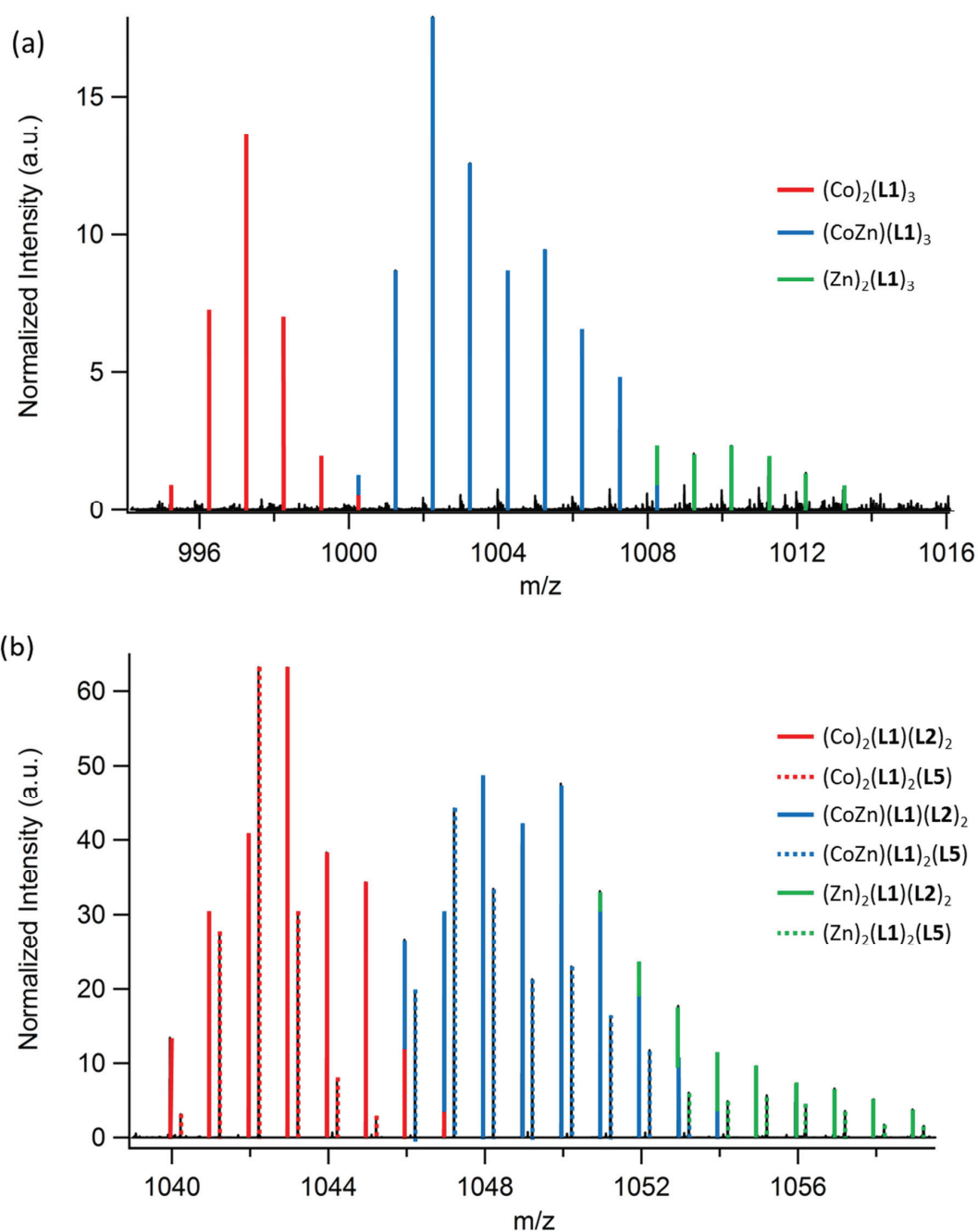
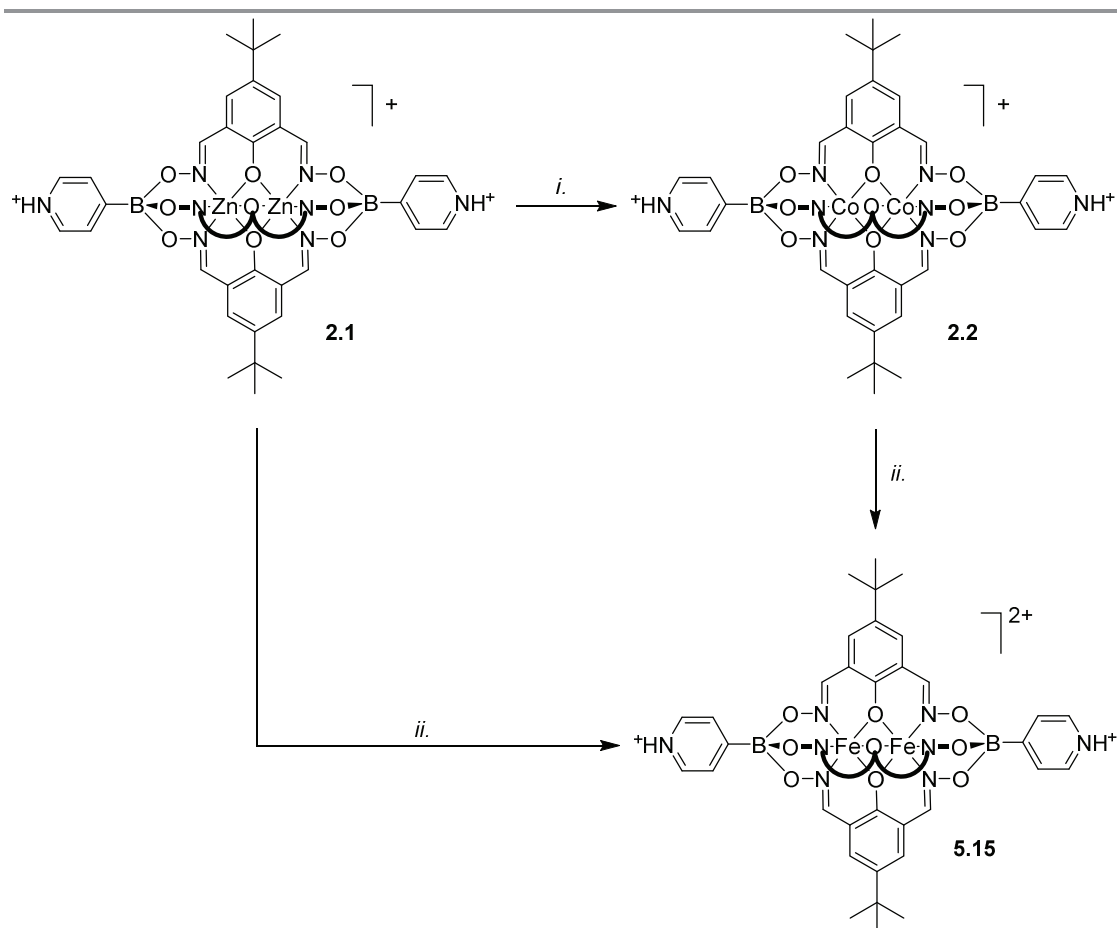


Figure 5.10 – Selected isotopic distributions of complex clathrochelates mixture. The red, blue and green lines are guidelines for the eyes to recognize peaks from the homometallic Co(II), heterometallic Co(II)Zn(II) and homometallic Zn(II) complexes, respectively.

5.7 Studies on the relative stability of clathrochelate complexes

Encouraged by the results of the MS analysis and the successful observation of all possible products, we explored the potential of high-resolution mass spectrometry for studying the relative stability of dinuclear clathrochelates. Empirical observations revealed that Co(II)-based clathrochelates seemed to be slightly more robust than their Zn(II) analogues. Indeed, the Zr-based MOFs described in Chapter 3 were obtained exclusively with Co(II) complexes, whilst Zn(II) clathrochelates did not give satisfactory results. We therefore examined metal-exchange with our clathrochelates complexes. A solution of Zn(II)-based **2.1** in MeOH was heated overnight in presence of an excess of $[\text{Co}(\text{H}_2\text{O})_6](\text{NO}_3)_2$ (Scheme 5.11). The resulting solution was subsequently analyzed by HRMS, using the same experimental setup as described in section 5.6. Surprisingly, the analysis of the mass spectrum revealed a complete metal exchange to give the Co(II) clathrochelate **2.2** (Figure 5.11a).



Scheme 5.11 – Metal exchange reactions of clathrochelates. Reagents and conditions: (i.): $[\text{Co}(\text{H}_2\text{O})_6](\text{NO}_3)_2$ (20 equiv.), MeOH, 80°C, 12h; (ii.): $[\text{Fe}(\text{H}_2\text{O})_6](\text{ClO}_4)_2$ (20 equiv.), MeOH, 80°C, 12h.

Subsequent studies revealed that the exchange could also be performed on the dinuclear Co(II) clathrochelate **2.2**. Overnight heating of a methanolic solution of **2.2** in presence of excess $[\text{Fe}(\text{H}_2\text{O})_6](\text{ClO}_4)_2$ led to the complete disappearance of the peaks corresponding to the homometallic Co(II) complex, and the exclusive formation of a new specie (Figure 5.11b). The new clathrochelate features a mixed-valence Fe(II)Fe(III) core, despite the fact that only Fe(II) was used during the synthesis. One of the Fe(II) centers is oxidized to Fe(III) during the reaction, leading to the formation of the doubly-charged species **5.15**, as evidenced by its isotopic distribution. Similarly, the direct exchange from homometallic Zn(II) **2.1** to Fe(II)Fe(III) **5.15** was performed using similar reaction conditions (Scheme 5.11). Interestingly, the reverse reaction (i.e. exchange from homometallic Co(II) to Zn(II) clathrochelate) was not observed by HRMS analysis. Moreover, only one of the Fe(II) centers is oxidized to Fe(III). Attempts to synthesize homometallic Fe(III) were not successful. In order to determine whether the mechanism followed a dissociative pathway, where dioximato ligands are partially removed from the clathrochelate core, we performed the scrambling experiment depicted in Scheme 5.12. Zn(II)-based clathrochelates **2.1** and **5.16**, were heated in presence of $[\text{Fe}(\text{H}_2\text{O})_6](\text{ClO}_4)_2$ overnight. As expected, the complete exchange of the Zn(II) centers to their Fe(II)Fe(III) analogues was observed, as evidenced by the doubly-charged state in the mass spectrum (Figure 5.12). Metal exchange occurred along with scrambling of the oximato ligands, since MS peaks corresponding to clathrochelates of the composition $(\text{Fe})_2(\text{L1})_3$, $(\text{Fe})_2(\text{L1})_2(\text{L2})$, $(\text{Fe})_2(\text{L1})(\text{L2})_2$ and $(\text{Fe})_2(\text{L2})_3$ were observed (here $(\text{Fe})_2$ refers to Fe(II)Fe(III) for sake of clarity). We therefore conclude that the exchange mechanism follows a dissociative pathway, where at least one of the dioximato ligands is removed from the clathrochelate core.

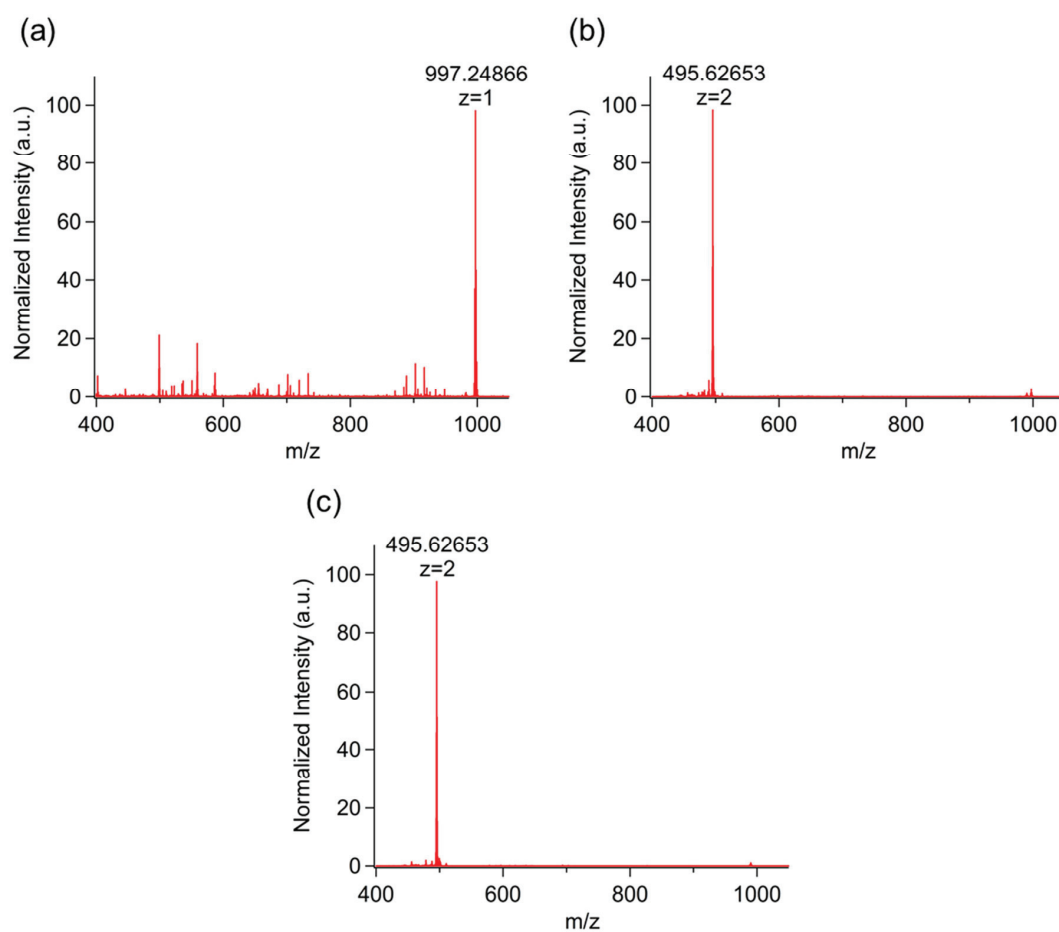
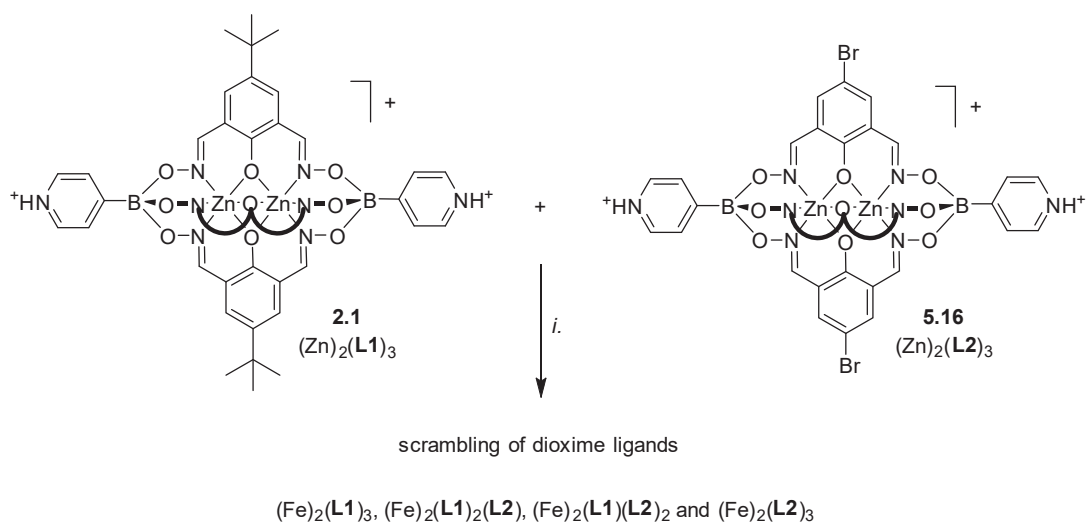


Figure 5.11 – ESI FT-ICR mass spectrum of exchange experiments (a) from Zn(II) to Co(II), (b) from Co(II) to Fe(II)Fe(III) and (c) from Zn(II) to Fe(II)Fe(III).



Scheme 5.12 – Scrambling experiments between L₁-functionalized clathrochelate **2.1** and L₂-functionalized complex **5.16** upon addition of Fe(II) salt. Reagents and conditions: (i.): [Fe(H₂O)₆](ClO₄)₂, MeOH, 80 °C, 12 h.

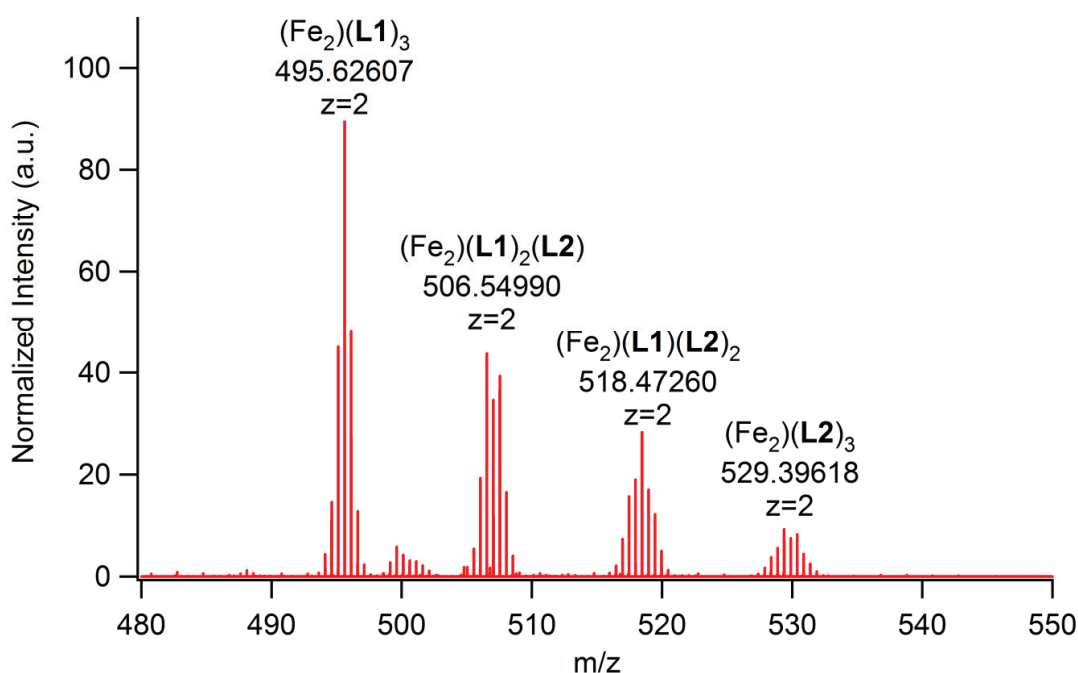
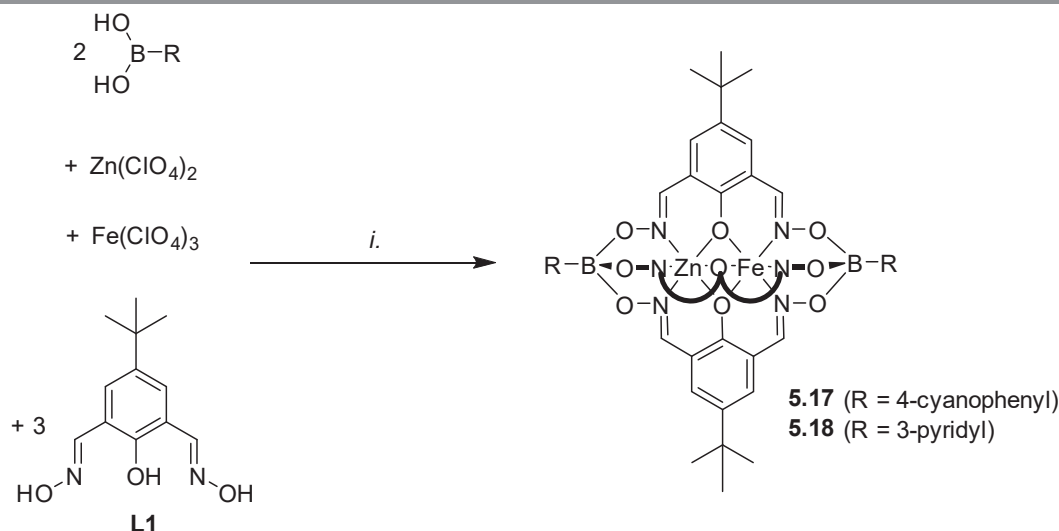


Figure 5.12 – Part of the ESI FT-ICR mass spectrum of the scrambling experiment between clathrochelates **2.1** and **5.16** upon addition of $[\text{Fe}(\text{H}_2\text{O})_6](\text{ClO}_4)_2$

5.8 Deliberate synthesis of heterometallic, dinuclear clathrochelates

The HRMS experiments described in sections 5.6 and 5.7 have shown that heterometallic dinuclear complexes can be obtained. In the complex mixture analysis, Co(II)Zn(II) cores were observed for all combinations of dioxime ligands. Nevertheless, the deliberate synthesis of heterometallic dinuclear, anionic clathrochelates was not expected to give major differences in the clathrochelates properties, and the tedious purification steps inferred with this approach were limiting its interest. On the other hand, stability experiments showed that Fe(II)Fe(III) clathrochelates were formed preferentially. These clathrochelates, provided that they do not possess protonated groups, would give neutral metalloligands, and major differences in the reactivity can be naturally expected. Therefore, we decided to investigate whether the synthesis of neutral heterometallic clathrochelates is feasible. By using simultaneously Fe(III) salts and Zn(II) salts during the clathrochelate synthesis, we observed the formation of a homometallic dinuclear Zn(II) complex as well as its Zn(II)Fe(III) analogue (Scheme 5.13). Since the heterometallic clathrochelate is neutral, purification was achieved by column chromatography, and clathrochelates **5.17** and **5.18** were obtained in 31% and 29% yield, respectively. These low yields are explained by the statistical distribution of products, and it is one of the limitation of this approach. Single crystal X-ray structural

analysis of complexes **5.17** and **5.18** confirmed the presence of Fe(III) and Zn(II) metal centers, and the neutral character of the clathrochelates was unambiguously confirmed by the absence of any counterion in the crystal structure (Figure 5.13).



Scheme 5.13 – Synthesis of heterometallic clathrochelates **5.17** and **5.18**. Reagents and conditions: (*i.*): $[\text{Fe}(\text{H}_2\text{O})_6](\text{ClO}_4)_2$ (1.0 equiv.), $[\text{Zn}(\text{H}_2\text{O})_6](\text{ClO}_4)_2$ (1.0 equiv.), dioxime **L1** (3.0 equiv.), 4-pyridylboronic acid (2.0 equiv.) or 4-cyanophenylboronic acid (2.0 equiv.), MeOH, 50 °C, 2 h, then base (**5.17**: NEt_4OH ; **5.18**: K_2CO_3).

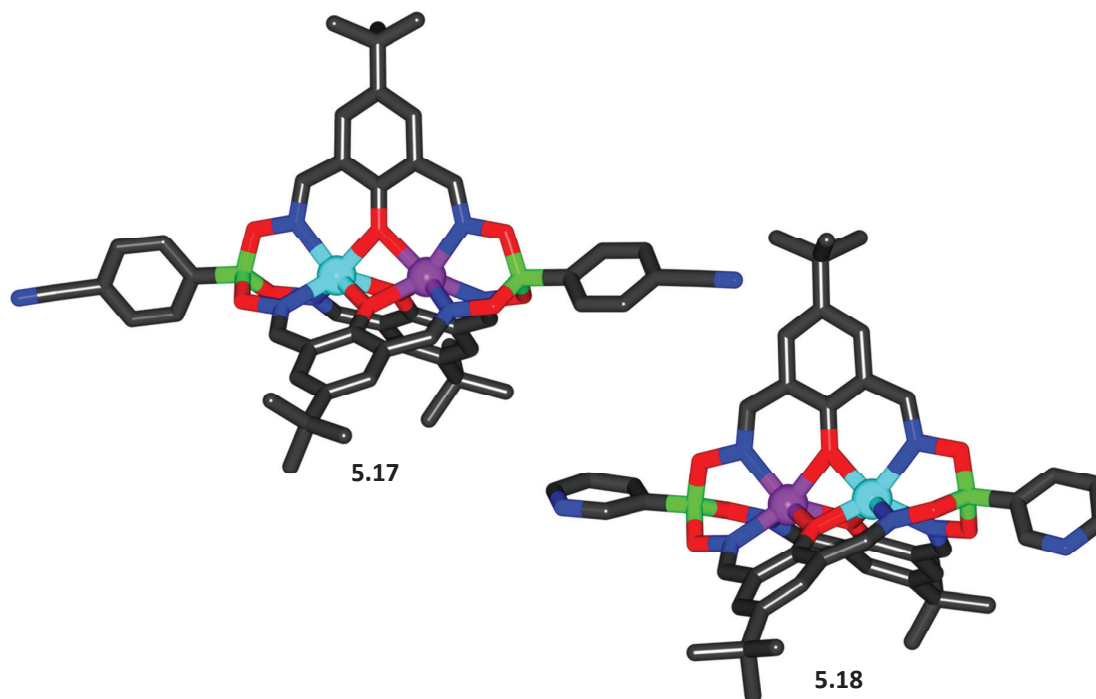


Figure 5.13 – Molecular structure of clathrochelates **5.17** (left) and **5.18** (right) in the crystal. Hydrogen atoms and solvent molecules have been omitted for clarity. Color coding: C: gray; B: green; Fe: purple; N: blue; O: red; Zn: cyan.

The results presented in this very last section are only preliminary, and were used as a starting point for a new research project in our group. The opportunities of this new class of clathrochelates are various, from the exploration of the possible heterometallic combination to the deliberate synthesis of neutral Fe(II)Fe(III) or anionic Fe(II)Fe(II) complexes. For the latter, we believe that they could possess intrinsic redox properties. Preliminary investigations in this direction have been performed in our lab and they confirm this hypothesis.

5.9 Conclusion

In this chapter, the syntheses of formyl- and amine-functionalized clathrochelates are described, along with their unsuccessful incorporation into discrete structures by DCC. We hypothesize that this is partly due to the electron-rich character of the aldehydes, leading to a reduced electrophilicity of clathrochelates **5.1** and **5.2**. The synthesis of acetylene-functionalized clathrochelates, as well as preliminary results about their successful use in “click” chemistry is also described. Studies on the diversity-oriented synthesis of clathrochelates showed that metalloligands with different functional groups could be obtained, and that clathrochelates with different dioximato ligands are accessible. Stability studies revealed that neutral Fe(II)Fe(III) complexes tended to be more stable than their anionic Co(II) and Zn(II) analogues. These last results serve as the basis for a new research topic, whose exciting preliminary results show that dinuclear clathrochelates still have a lot of potential for applications in supramolecular chemistry.

Chapter 6 Conclusions and Outlook

In this thesis, the syntheses and the characterization of novel dinuclear clathrochelate complexes are described. The complexes represent easy-to-access metalloligands, whose syntheses are generally high-yielding. Apart from being easily accessible, these clathrochelates display interesting characteristics for applications in metallasupramolecular chemistry and materials science: they are rigid, large, robust, and they can show additional functions (e.g. fluorescence or extra charge) depending on the metal ions that are present in the clathrochelate core. The successful incorporations of these dinuclear complexes into discrete structures or polymeric assemblies are described.

In Chapter 2, the syntheses of polypyridyl clathrochelate complexes are reported. Two distinct approaches have been employed: a direct synthesis or the postsynthetic functionalization of brominated clathrochelates *via* Pd-catalyzed cross-coupling reactions. Functionalization of clathrochelates with 3- or 4-pyridyl groups resulted in the formation of metalloligands with up to seven pyridyl groups. Linear, ditopic clathrochelates were successfully incorporated into two-dimensional CPs, whereas pentatopic metalloligands were shown to form MOFs of novel topologies. Furthermore, we have demonstrated that tetratopic clathrochelates can be used to build pentameric $M_{10}L_5$ barrel structures.

Carboxylic acid-decorated clathrochelates, with up to five functional groups, are discussed in Chapter 3. The utility of these new metalloligands in MOF chemistry was demonstrated by the synthesis of three-dimensional coordination polymers, in which the clathrochelate ligands are linked by Zn- or Zr-clusters. Whilst the MOFs displaying MOF-5 topology were shown to have no permanent porosities, Zr-MOFs based on linear, ditopic clathrochelates showed interesting surface areas and excellent CO₂ uptake. Interestingly, the gas sorption properties of the Zr-based MOFs were strongly influenced by the steric bulk induced by the lateral dioximato substituents, indicating that modulating the gas sorption properties of clathrochelates-based MOFs could be feasible through the dioxime functionalization. Several MOFs presented in this chapter showed unusual SBUs, leading to pronounced changes in the overall geometry of the networks.

Chapter 4 was dedicated to cyano-appended clathrochelates. The new clathrochelate complexes were used as metalloligands for the construction of heterometallic Zn(II)/Ag(I) and Co(II)/Ag(I) coordination polymers. A one-dimensional double-chain CP was observed for linear, ditopic clathrochelates, whereas two- and three-dimensional CPs were generated from tetra- and pentatopic metalloligands. The three-dimensional network is unique as it displays an unprecedented network topology, and showed self-catenation with an extremely high topological density. The 1D and 2D CPs are neutral, conversely to most of the Ag(I)-based CPs reported to date, the charge balance being accomplished by the intrinsic anionic character of the clathrochelates.

In Chapter 5, attempts towards the incorporation of formyl- and amine-functionalized clathrochelates into imine-based structures are discussed. The modular nature of our clathrochelate ligands was demonstrated through the analysis of a complex mixture obtained from different metal ions and dioximato ligands. Interestingly, we showed that it was possible to incorporate different metal centers in the clathrochelate core, leading to heterometallic clathrochelate complexes. Neutral dinuclear clathrochelates containing an Fe(II)Fe(III) core were also observed while performing metal exchange experiments. The latter showed that Zn(II)-based clathrochelates could be post-synthetically exchanged to their Co(II), respectively Fe(II)Fe(III) analogues. HRMS experiments showed that this process occurred *via* a dissociative mechanism.

Preliminary studies performed in our lab show that neutral Fe(II)Fe(III) clathrochelates are redox-responsive metalloligands. Finding a way to switch from the neutral to the anionic, or vice versa, would be of great interest. Moreover, due to the increased stability of neutral Fe(II)Fe(III) clathrochelates, we expect them to be useful for the preparation of more robust MOFs. The absence of counterions could lead to materials with greater porosities, and the redox character of the MOFs would be an additional interesting feature. I strongly believe that many chapters have still to be written, and that inspiration from recent literature applied to dinuclear clathrochelates can enable the preparation of novel materials with exciting functionalities.

Chapter 7 Experimental Part

7.1 General

Unless specified, all commercially available chemicals were used without further purification. Unless explicitly stated, yields refer to the products containing only trace amounts of solvents or impurities, as judged by ^1H NMR spectroscopy. Dried solvents were obtained using a solvent purification system from Innovative Technologies, Inc.

NMR Spectroscopy: ^1H , ^{13}C , ^{19}F and ^{31}P spectra were obtained on a Bruker AvanceIII spectrometer (^1H : 400 MHz, ^{13}C : 100.6 MHz, ^{31}P : 161 MHz, ^{19}F : 376 MHz) equipped with a 5 mm BBFO-Plus_z probe, or on a Bruker Avance spectrometer (^1H : 400 MHz, ^{13}C : 100.6 MHz, ^{31}P : 161 MHz, ^{19}F : 376 MHz) equipped with a 5 mm BBHz probe. DOSY, HSQC, HMBC, ROESY experiments were conducted on the two spectrometers described before and on a Bruker DRX-400 (^1H : 400 MHz) equipped with a 5 mm BBO probe. ^1H and ^{13}C chemical shifts are reported in parts per million δ (ppm) referenced to the internal solvent. Unless specified, all spectra were recorded at RT.

UV-VIS spectroscopy: Absorption spectra were recorded with a Cary 60 UV-Vis from Agilent Technologies.

Fluorescence spectroscopy: Emission spectra were recorded with a Varian Cary Eclipse spectrofluorimeter from Agilent Technologies.

Mass spectrometry: Electrospray-ionisation MS data were acquired on a Q-ToF Ultima mass spectrometer (Waters) operated in the negative or positive ionization modes and data were processed using the MassLynx 4.1 software. APPI-FT-ICR experiments were performed on a hybrid linear ion trap Fourier transform ion cyclotron resonance mass spectrometer (LTQ FT-ICR MS, Thermo Scientific, Bremen, Germany) equipped with a 10 T superconducting magnet (Oxford Instruments Nanoscience, Abingdon, UK). Data analysis was carried out using XCalibur software (Thermo Scientific, Bremen, Germany).

Thermogravimetric analysis: Thermogravimetric analysis was performed on a Perkin-Elmer TGA 4000 equipped with an AS 6000 autosampler. Data were collected using the PYRIS software and processed in IGOR PRO. The sample was heated from 30 °C to 700 °C at a rate of 15 °C per minute in an aluminum oxide crucible under a 20 mL·min⁻¹ flow of N₂.

Gas sorption: Gas sorption measurements were performed on a Quantachrome Autosorb iQ surface area analyzer. Before the measurements, CPs were dried under a high vacuum for 4h at 100 °C, then 6 h at 120 °C and 4 h at 150 °C. The N₂ multi-point BET and full isotherm analyses were performed at 77.3 K using liquid nitrogen bath. CO₂ sorption isotherms were performed at 273.15 K using a water/ice bath.

Fourier-Transform Infrared Spectroscopy: IR spectra were recorded on a Perkin Elmer Spectrum One Golden Gate FTIR spectrometer.

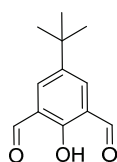
Powder X-Ray Diffraction: Powder diagram of **3.11** was recorded, from 2 to 32° in 2 θ in symmetric ω : θ configuration on an MPD PRO from PANalytical, equipped with copper radiation, a Ni-foil and an X'Celerator multi-strip detector. We used a step-size of 0.008° and an acquisition-time of 620 s per step. The powder was strewn, as is, on a thin Vaseline layer spread on an appropriately cut silicon single crystal, which was rotated about its normal during the data collection. By means of an automatic divergence slit, we irradiated an area of 10mm and limited the beam laterally by a corresponding beam-mask. The files were then converted to a fixed divergence slit of 0.5° and the background subtracted with the help of the HighScore program. The powder data of **3.17** was measured in capillary mode using the beamline BM01A (SNBL) at the ESRF. The images were collected using a Pilatus2M pixel area detector from Dectris Ltd (Switzerland). The powder patterns were then integrated using the program FIT2D.¹⁴⁵

Single crystal X-ray diffraction crystallography: Intensity data were collected using a Bruker APEX II CCD system, using graphite monochromatized Mo-K α radiation (λ = 0.71073 Å) at 100(2) K, 120(2) K or 180(2) K, a μ mx system using a Genix micro-source sealed tube with Mo-K α radiation (λ = 0.71073 Å) at 140(2) K. Complicated structures (MOFs, disordered crystals) were collected at the Swiss Norwegian beamline BM01A at the ESRF in Grenoble (France) using synchrotron radiation on the Pilatus@SNBL kappa goniometer from Huber Diffractionstechnik GmbH equipped with a Pilatus2M pixel detector from Dectris Ltd. Data collection was performed at low temperature (100 K) using a Cryostream 700 Series from Oxford Cryosystems Ltd. Data integration and empirical absorption corrections were carried out using CrysAlis Pro.¹⁴⁶ Data reduction was carried out using XPREP. All structures were solved by direct methods or charge flipping using SHELXT¹⁴⁷ or SUPERFLIP¹⁴⁸ and refined with SHELXL¹⁴⁸ using full-matrix least-squares routines on F^2 . Techniques commonly applied for macromolecular structures were employed to generate a molecular model and increase robustness of the refinement. Stereochemical restraints for the organic parts and counter ions of the structure were generated by the GRADE program using the GRADE Web Server (<http://grade.globalphasing.org>)⁹⁶ and applied in the refinement. A GRADE dictionary for SHELXL contains target values and standard deviations for 1.2-distances (DFIX) and 1.3-distances (DANG), as well as restraints for planar groups (FLAT). GRADE restraint dictionaries of disordered moieties were loaded into the database of DSR.¹⁴⁹ DSR was subsequently employed to place and refine those disordered moieties in a semi-automatic fashion by starting with a rigid body refinement followed by a restrained refinement using restraints from GRADE dictionaries. Additionally, local structural similarity was exploited in some of the structures to make the geometries of several clathrochelate ligands in the asymmetric unit similar to each other using non-crystallographic symmetry restraints (NCSY) for 1,4 distances. The refinement of ADP's for non-hydrogen atoms was enabled by using the new rigid bond restraint (RIGU) in the SHELXL program. Carbon-bound hydrogen atoms were

included in idealized positions and refined using a riding model. The contribution of the electron density associated with disordered counterions and solvent molecules, which could not be modelled with discrete atomic positions were handled using the SQUEEZE¹⁵⁰ routine in PLATON.¹⁵¹ Solvent masks (.fab files) generated by PLATON were included in the SHELXL refinement via the ABIN instruction in order to leave the original structure factors untouched. The same atom names are used for different disorder components, which only differ in the part numbers. Therefore, the TABS keyword behind the ACTA instruction was employed to generate the CIF.¹⁴⁸ Details of crystals, CCDC numbers, data collections and structure refinements are available in Chapter 8.

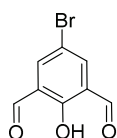
7.2 Experimental Procedures

7.2.1 2,6-Diformyl-4-*tert*-butylphenol



The procedure of Lindoy¹⁵² was followed to obtain the titled compound. 4-*tert*-butylphenol (5.14 g, 34.2 mmol, 1.0 equiv.) and urotropine (9.60 g, 68.5 mmol, 2.0 equiv.) were dissolved in TFA (60 ml) under inert atmosphere. The yellow solution was refluxed for 48 h, with a color change from yellow to orange. The solution was cooled down, and poured into 4M HCl (200 ml). After stirring for 20 min, the solution was extracted with CH₂Cl₂ (2 x 150 ml). The combined organic extracts were washed with 4 M HCl (2 x 200 ml), water (200 ml), brine (200 ml) and dried over Na₂SO₄. The yellow crystalline residue was purified by column chromatography (CH₂Cl₂). Traces of monoformylated product were removed by recrystallization in cyclohexane, yielding 2,6-diformyl-4-*tert*-butylphenol as yellowish needles (4.12 g, 19.9 mmol, 58%). ¹H-NMR (400 MHz, CDCl₃): δ = 11.47 (s, 1H, Ar-OH), 10.24 (s, 2H, CHO), 7.98 (s, 2H, Ar-H), 1.35 (s, 9H, (CH₃)₃). ¹³C-NMR (101 MHz, CDCl₃): δ = 192.50, 161.87, 143.29, 134.82, 122.83, 34.48, 31.27. HRMS-ESI: Calcd for C₁₂H₁₄O₃: 205.0865; found: 205.0858. IR: 2960, 2865, 1685, 1655, 1615, 1595, 1470, 1445, 1420, 1400, 1380, 1365, 1345, 1315, 1280, 1270, 1220, 1120, 1035, 980, 940, 910, 830, 800, 755, 730, 630, 615, 555 cm⁻¹.

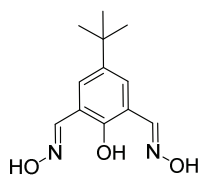
7.2.2 2,6-Diformyl-4-bromophenol



The procedure described by Lindoy¹⁵² was followed with the following modifications. Urotropine (9.75 g, 69.2 mmol, 4.0 equiv.) was dissolved in TFA (33 ml). 4-bromophenol (3.0 g, 17.3 mmol, 1.0 equiv.) was added in one portion, and the yellow solution was stirred at 120 °C under inert atmosphere for 48 h. The reaction mixture was then cooled down to RT, H₂O (21 ml) and H₂SO₄ 50% (10.5ml) were added and the reaction mixture was stirred 2 h at RT. The mixture was poured into H₂O (210 ml) and the precipitate was isolated by filtration and washed with H₂O (800 ml). The yellow precipitate was then dissolved in EtOAc (100 ml) and dried over MgSO₄.

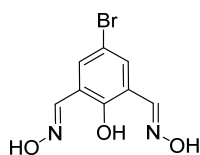
Purification by column chromatography (15 to 40% EtOAc in petroleum ether) afforded the dialdehyde in the form of yellow needles (2.11 g, 9.22 mmol, 54%). **¹H-NMR** (400 MHz, CDCl₃): δ = 11.54 (s, 1H, Ar-OH), 10.19 (s, 2H, CHO), 8.05 (s, 2H, Ar-H). **¹³C-NMR** (101 MHz, CDCl₃): δ = 191.03, 162.38, 139.88, 124.74, 112.29. **HRMS-APPI**: calcd for C₈H₅BrO₃: 228.94948; found: 228.94892. **IR**: 3300, 3060, 2875, 1675, 1660, 1600, 1575, 1435, 1400, 1375, 1325, 1280, 1260, 1200, 1120, 1095, 1005, 970, 900, 885, 745, 705, 605 cm⁻¹.

7.2.3 2,6-Diformyl-4-*tert*-butylphenoldioxime (L1)



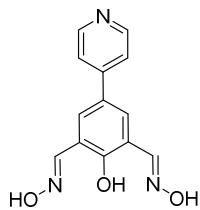
The procedure of Chaudhuri⁵⁸ was followed with the following modifications. In a 100 ml round bottom flask, 2,6-diformyl-4-*tert*-butylphenol (2.0 g, 9.7 mmol, 1.0 equiv.) and hydroxylamine hydrochloride (1.52 g, 21.8 mmol, 2.25 equiv.) were suspended in H₂O (25 ml), and the mixture was heated at 85 °C. MeOH was then added until all solids dissolve, and the clear yellow solution was stirred at 85°C for 1.5 h. H₂O was then added dropwise until the solution becomes slightly turbid. The solution was cooled to RT, and kept at this temperature for 24 h. The crystalline material was then filtered, washed with H₂O (3 x 50 ml) and dried under vacuum to afford the corresponding oxime **L1** as a crystalline, beige solid (1.84 g, 7.79 mmol, 80%). **¹H-NMR** (400 MHz, Acetone-*d*₆): δ = 10.50 (s, 1H, NOH), 10.47 (s, 1H, Ar-OH), 8.44 (s, 2H, CHNOH), 7.65 (s, 2H, Ar-H), 1.31 (s, 9H, (CH₃)₃). **¹³C-NMR** (101 MHz, Acetone-*d*₆): δ = 154.02, 148.84, 142.96, 127.12, 119.40, 34.70, 31.61. **HRMS-ESI**: calcd. for C₁₂H₁₆N₂O₃: 237.1239; found: 237.1238. **IR**: 3400, 3260, 2950, 2865, 1625, 1610, 1460, 1375, 1355, 1320, 1290, 1260, 1215, 1060, 1035, 1025, 1015, 990, 955, 940, 900, 870, 825, 740, 705, 675, 640 cm⁻¹. **Elem. anal.** For C₁₂H₁₆N₂O₃: calc. (%) C 61.00, H 6.83, N 11.86; found C 62.10, H 6.90, N 12.15.

7.2.4 2,6-Diformyl-4-bromophenol dioxime (L2)



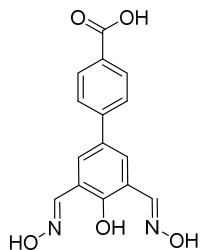
2,6-Diformyl-4-bromophenol (2.1 g, 9.2 mmol, 1.0 equiv.) was dissolved in a mixture of MeOH (15 ml) and H₂O (30 ml) and hydroxylamine hydrochloride (1.6 g, 23 mmol, 2.5 equiv.) was added. The solution was heated for 1 h at 85 °C, and H₂O was added until the solution became turbid. The mixture was cooled down to RT, and the product was allowed to crystallize overnight. The white precipitate was isolated by filtration, washed with H₂O (3 x 100 ml) and dried under vacuum to afford the dioxime **L2** as an off-white powder (2.0 g, 7.7 mmol, 84%). **¹H-NMR** (400 MHz, DMSO-*d*₆): δ = 11.70 (s, 2H), 10.89 (s, 1H), 8.34 (s, 2H), 7.68 (s, 2H). **¹³C-NMR** (101 MHz, DMSO-*d*₆): δ = 153.46, 145.78, 130.32, 121.36, 110.87. **HRMS-ESI**: calcd. for C₈H₇BrN₂O₃: 256.9562; found: 256.9562. **IR**: 3240, 3090, 2995, 1620, 1485, 1440, 1385, 1325, 1285, 1255, 1220, 1020, 1000, 930, 870, 690, 650, 585 cm⁻¹.

7.2.5 Dioxime L3



Under inert atmosphere, 2,6-diformyl-4-bromophenol (586 mg, 2.56 mmol, 1.0 equiv.), 4-pyridylboronic acid (2.52 g, 20.5 mmol, 8.0 equiv.) and K_3PO_4 (2.17 g, 10.2 mmol, 4.0 equiv.) were suspended in *n*-BuOH (300 ml) degassed with N_2 . SPhos (53 mg, 0.13 mmol, 0.05 equiv.) and $Pd_2(dba)_3$ (59 mg, 0.06 mmol, 0.025 equiv.) were added, and the mixture was stirred at 80 °C under N_2 atmosphere for 24 h. The mixture was cooled down to RT, and the yellow precipitate that formed was filtered, washed with *n*-BuOH (2 x 70 ml) and dried under vacuum. The resulting adduct of the corresponding 2,6-diformyl-4-pyridine-phenol and K_3PO_4 was then dissolved in H_2O (100 ml), and the yellow solution was heated at 85 °C. Hydroxylamine hydrochloride (445 mg, 6.4 mmol, 2.25 equiv.) was added all at once, and the reaction was stirred at 85 °C for 2 h. The suspension was cooled down to RT, filtered, washed with H_2O (4 x 50 ml) and dried under vacuum to afford the oxime **L3** as a pale yellow powder (375 mg, 1.45 mmol, 57%). 1H -NMR (400 MHz, $DMSO-d_6$): δ = 11.65 (s, 2H, NOH), 11.07 (s, 1H, Ar-OH), 8.62 (d, J = 4.6 Hz, 2H, Py-H), 8.45 (s, 2H, CHNOH), 7.98 (s, 2H, Ar-H), 7.65 (d, J = 4.9 Hz, 2H, Py-H). ^{13}C -NMR (101 MHz, $DMSO-d_6$): δ = 155.21, 150.25, 146.75, 145.88, 128.61, 127.01, 120.60, 119.82. HRMS-ESI: calcd. for $C_{13}H_{11}N_3O_3$: 258.0879; found: 258.0882. IR: 3265, 2460, 1810, 1605, 1560, 1450, 1315, 1270, 1230, 1215, 1055, 1035, 1015, 975, 935, 815, 755, 705, 610 cm^{-1} . Elem. Anal. for $C_{13}H_{11}N_3O_3$: calc. (%) C 60.70, H 4.31, N 16.33; found C 59.23, H 4.42, N 16.02.

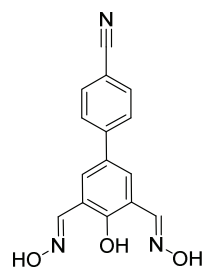
7.2.6 Dioxime L4



Under inert atmosphere, 2,6-diformyl-4-bromophenol (900 mg, 3.93 mmol, 1.0 equiv.), 4-carboxyphenylboronic acid (5.22 g, 31.5 mmol, 8.0 equiv.) and K_3PO_4 (3.33 g, 15.7 mmol, 4.0 equiv.) were suspended in degassed *n*-BuOH (250 ml). SPhos (81 mg, 0.2 mmol, 0.05 equiv.) and $Pd_2(dba)_3$ (90 mg, 0.09 mmol, 0.025 equiv.) were added, and the mixture was stirred overnight at 85 °C under an atmosphere of N_2 . The reaction mixture was cooled down to RT, and the yellow precipitate that formed was isolated by filtration, washed with *n*-BuOH (2 x 60 ml) and dried under vacuum. The yellow powder was then dissolved in H_2O (200 ml) and the resulting solution was heated at 85 °C for 15 min. $NH_2OH \cdot HCl$ (1.092 g, 15.72 mmol, 4.0 equiv) was added and the pale yellow suspension was heated 2 h at 85 °C. After cooling down to RT, the suspended product was isolated by filtration, washed with H_2O (4 x 100 ml) and dried under vacuum to afford the dioxime **L4** as a pale yellow powder (950 mg, 3.16 mmol, 81%). 1H -NMR (400 MHz, $DMSO-d_6$): δ = 12.94 (s, 1H), 11.61 (s, 2H), 10.99 (s, 1H), 8.45 (s, 2H), 8.02 (d, J = 8.3 Hz, 2H), 7.93 (s, 2H), 7.75 (d, J = 8.2 Hz, 2H). ^{13}C -NMR (101 MHz, $DMSO-d_6$): δ = 167.06, 154.55, 146.84, 143.12, 130.49, 130.04, 129.29, 127.09,

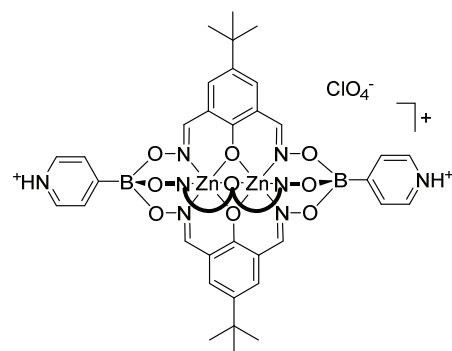
126.15, 119.69. **HRMS-ESI:** calcd. for $C_{15}H_{11}N_2O_5$: 299.0668; found: 299.0670. **IR:** 3545, 3355, 2905, 1675, 1610, 1500, 1450, 1410, 1270, 1230, 1200, 1175, 1105, 1030, 990, 850, 775, 725, 700 cm^{-1} .

7.2.7 Dioxime ligand L5



Under inert atmosphere, 2,6-diformyl-4-bromophenol (600 mg, 2.62 mmol, 1.0 equiv.), 4-cyanophenylboronic acid (3.06 g, 20.83 mmol, 8.0 equiv.) and K_3PO_4 (2.23 g, 10.48 mmol, 4.0 equiv.) were suspended in degassed *n*-BuOH (250 ml). SPhos (54 mg, 0.13 mmol, 0.05 equiv.) and $Pd_2(dba)_3$ (60 mg, 0.06 mmol, 0.025 equiv.) were added, and the mixture was stirred overnight at 85 °C under N_2 atmosphere. The reaction mixture was cooled down to RT, and the yellow precipitate that formed was filtered, washed with *n*-BuOH (2 x 60 ml) and dried under vacuum. The yellow powder was then dissolved in H_2O (200 ml) and the resulting solution was heated at 85 °C for 30 min. $NH_2OH \cdot HCl$ (728 mg, 10.48 mmol, 4.0 equiv) was added and the white suspension was heated 2 h at 85 °C. After cooling down to RT, the suspended product was isolated by filtration, washed with H_2O (2 x 100 ml) and dried under vacuum to afford the dioxime **L5** as an off-white powder (510 mg, 1.81 mmol, 69%). **1H -NMR** (400 MHz, $DMSO-d_6$): δ = 11.64 (s, 2H), 11.04 (s, 1H), 8.44 (s, 2H), 7.93 (s, 2H), 7.92 (d, J = 8.6 Hz, 2H), 7.84 (d, J = 8.5 Hz, 2H). **^{13}C -NMR** (101 MHz, $DMSO-d_6$): δ = 154.88, 146.79, 143.53, 132.93, 129.78, 127.28, 126.97, 119.78, 118.91, 109.65. **HRMS-ESI:** Calcd. for $C_{15}H_{11}N_3O_3$: 282.0879; found: 282.0885. **IR:** 3250, 2225, 1735, 1630, 1605, 1455, 1280, 1200, 1180, 1030, 1000, 975, 940, 835, 700, 660, 600 cm^{-1} .

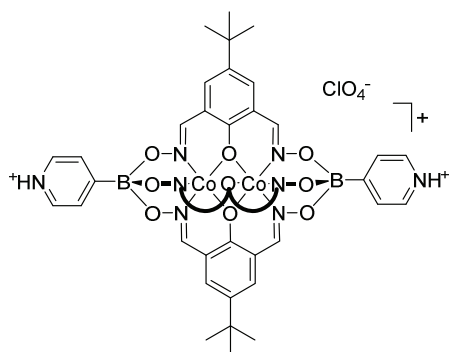
7.2.8 Clathrochelate 2.1



Dioxime **L1** (500 mg, 2.12 mmol, 1.5 equiv.) and 4-pyridylboronic acid (173 mg, 1.41 mmol, 1.0 equiv.) were dissolved in EtOH (20 ml) and CH_2Cl_2 (20 ml). The solution was stirred under air at RT until all solids dissolved. $[Zn(H_2O)_6](ClO_4)_2$ (525 mg, 1.41 mmol, 1.0 equiv.) was added to the solution, and the mixture was stirred at RT for 2 h. The yellow precipitate that formed was filtered, washed with CH_2Cl_2 (2 x 10 ml) and EtOH (2 x 20 ml), and the product was dried under vacuum, affording complex **2.1** as a yellow powder (695 mg, 0.63 mmol, 89%). Single crystals suitable for X-Rays analysis were grown by slow evaporation of the reaction mixture in absence of stirring. **1H -NMR** (400 MHz, $DMSO-d_6$): δ = 8.79 (d, J = 6.5 Hz, 4H, $N_{py}CH$), 8.44 (s, 6H, ONCH), 8.20 (d, J = 6.5 Hz, 4H, $N_{py}CHCH$), 7.37 (s, 6H, Ar-H), 1.22 (s, 27H, $(CH_3)_3$). **^{13}C -NMR** (101 MHz, $DMSO-d_6$): δ = 162.56, 155.10, 139.17, 137.36, 132.97, 129.46, 117.99, 33.44, 31.11. **HRMS-ESI:**

calcd. for $C_{46}H_{49}B_2N_8O_9Zn_2$: 1009.2387; found: 1009.2392. **IR**: 2950, 1610, 1550, 1445, 1395, 1365, 1325, 1285, 1220, 1200, 1075, 1035, 1000, 940, 875, 840, 770, 695, 630, 620 cm^{-1} .

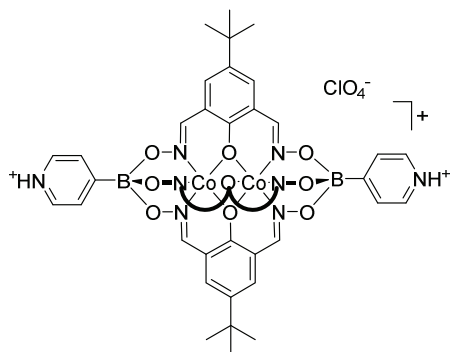
7.2.9 Clathrochelate 2.2



Dioxime **L1** (400 mg, 1.7 mmol, 1.5 equiv.) and 4-pyridylboronic acid (140 mg, 1.13 mmol, 1.0 equiv.) were dissolved in EtOH (20 ml) and CH_2Cl_2 (20 ml). The solution was stirred under air at RT until all solids dissolved. $[Co(H_2O)_6](ClO_4)_2$ (416 mg, 1.13 mmol, 1.0 equiv.) was added to the solution, and the mixture was stirred at RT for 1 h. The orange precipitate that formed was filtered, washed with CH_2Cl_2 (2 x 10 ml) and EtOH (2 x 20 ml), and

the product was dried under vacuum, affording complex **2.2** as an orange powder (550 mg, 0.50 mmol, 89%). Single crystals suitable for X-Rays analysis were grown by slow evaporation of the reaction mixture in absence of stirring. **HRMS-ESI**: calcd. for $C_{46}H_{49}B_2N_8O_9Co_2$: 499.1283 ($M+H$)²⁺; found: 499.1277. **IR**: 2955, 1610, 1550, 1445, 1365, 1325, 1285, 1225, 1200, 1080, 1035, 940, 880, 840, 780, 770, 700, 625, 575, 545, 525 cm^{-1} .

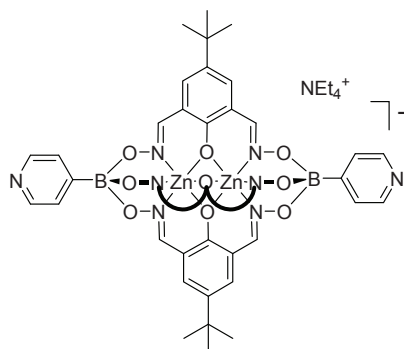
7.2.10 Clathrochelate 2.3



Dioxime **L1** (50 mg, 0.21 mmol, 1.5 equiv.) and 4-pyridylboronic acid (17.3 mg, 0.14 mmol, 1.0 equiv.) were dissolved in EtOH (5 ml) and CH_2Cl_2 (5 ml). The solution was stirred under air at RT until all solids dissolved. $[Mn(H_2O)_6](ClO_4)_2$ (51 mg, 0.14 mmol, 1.0 equiv.) was added to the solution, and the mixture was stirred at RT for 1 h. The yellow precipitate that formed was filtered, washed with CH_2Cl_2 (2 x 5 ml) and EtOH (2 x 5 ml), and the

product was dried under vacuum, affording clathrochelate **2.2** as a yellow powder (50 mg, 46 μ mol, 65%). Single crystals suitable for X-Rays analysis were grown by slow evaporation of the reaction mixture in absence of stirring. **HRMS-ESI**: calcd. for $C_{46}H_{49}B_2N_8O_9Mn_2$: 989.2564; found: 989.2579. **IR**: 2955, 1630, 1605, 1580, 1545, 1445, 1365, 1330, 1280, 1220, 1195, 1115, 1065, 1020, 990, 935, 840, 805, 780, 690, 625, 570, 550, 540 cm^{-1} .

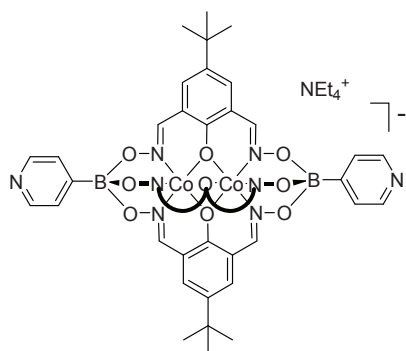
7.2.11 Clathrochelate 2.4



Clathrochelate **2.1** (980 mg, 0.88 mmol, 1.0 equiv.) was suspended in a mixture of MeOH (10 ml) and MeCN (10 ml). Tetraethylammonium hydroxide (25 % in MeOH, 1.3 ml, 1.94 mmol, 2.2 equiv.) was added, leading to the complete dissolution of the clathrochelate. The pale clear solution was stirred at RT for 1 h, and the precipitate that formed was filtered, washed with MeCN (2 x 5 ml) and cold MeOH (3 ml) and dried under vacuum to afford **2.4** as a pale yellow powder

(921 mg, 0.809 mmol, 92 %). ¹H-NMR (400 MHz, DMSO-*d*₆): δ = 8.41 (d, *J* = 5.5 Hz, 4H), 8.39 (s, 6H), 7.57 (d, *J* = 5.5 Hz, 4H), 7.33 (s, 6H), 3.17 (q, *J* = 7.2 Hz, 8H), 1.22 (s, 27H), 1.16 – 1.11 (m, 12H). ¹³C-NMR (101 MHz, DMSO-*d*₆): δ = 162.43, 154.28, 147.61, 137.06, 132.38, 127.19, 118.20, 51.39, 51.35, 51.32, 33.40, 31.14, 7.04. HRMS-ESI: Calcd for C₄₆H₄₈B₂N₈O₉Zn₂1009.2387; found: 1009.2386. IR: 2965, 1620, 1550, 1445, 1425, 1360, 1330, 1200, 1150, 1080, 1035, 920, 875, 855, 840, 785, 755, 700, 645 cm⁻¹.

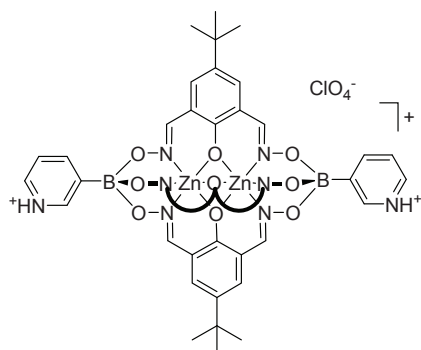
7.2.12 Clathrochelate 2.5



Clathrochelate **2.2** (200 mg, 0.18 mmol, 1.0 equiv.) was suspended in a mixture of MeCN (10 ml) and MeOH (10 ml). Tetraethylammonium hydroxide (25 % in MeOH, 267 µl, 0.40 mmol, 2.2 equiv.) was added, leading to the complete dissolution of the clathrochelate. The orange solution was stirred at RT for 2 h, concentrated to approximately 4 ml, and the orange precipitate was washed with cold MeCN (3 x 4 ml) and dried under vacuum to afford the clathrochelate **2.5** as a

crystalline orange material (178 mg, 0.16 mmol, 88 %). HRMS-ESI: calcd. for C₄₆H₄₈B₂N₈O₉Co₂: 997.2488; found: 997.2484. IR: 2950, 1610, 1590, 1550, 1450, 1395, 1365, 1330, 1285, 1220, 1205, 1140, 1085, 1035, 995, 925, 875, 840, 815, 785, 770, 700, 650, 565, 550 cm⁻¹.

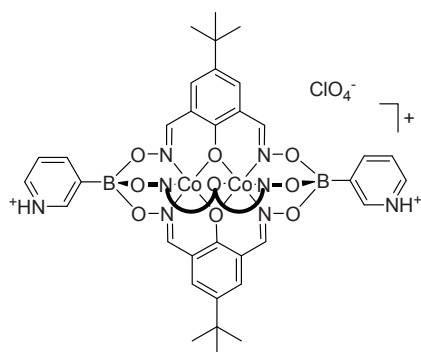
7.2.13 Clathrochelate 2.6



Dioxime **L1** (200 mg, 0.85 mmol, 1.5 equiv.) and 4-pyridylboronic acid (70 mg, 0.56 mmol, 1.0 equiv.) were dissolved in EtOH (10 ml) and CH₂Cl₂ (10 ml). The solution was stirred under air at RT until all solids dissolved. [Zn(H₂O)₆](ClO₄)₂ (210 mg, 0.56 mmol, 1.0 equiv.) was added to the solution, and the mixture was stirred at RT for 3 h. The yellow precipitate that formed was filtered, washed with CH₂Cl₂ (2 x 10 ml) and EtOH (1 x 20 ml), and the product was

dried under vacuum, affording complex **2.6** as a yellow powder (250 mg, 0.23 mmol, 82%). Single crystals suitable for X-Rays analysis were grown by slow evaporation of the reaction mixture in absence of stirring. **¹H-NMR** (400 MHz, DMSO-*d*₆): δ = 8.84 (m, 2H, BCCHNH), 8.83 (m, 2H, BCCHNHCH) 8.74 (dt, *J* = 7.7, 1.4 Hz, 2H, BCCH), 8.45 (s, 6H, ONCH), 8.04 (dd, *J* = 7.6, 6.3 Hz, 2H, NHCHCH), 7.37 (s, 6H, Ar-*H*), 1.22 (s, 27H, (CH₃)₃). **¹³C-NMR** (101 MHz, DMSO-*d*₆): δ = 162.55, 155.06, 149.25, 144.61, 142.86, 139.76, 137.36, 132.91, 126.01, 118.01, 33.44, 31.11. **HRMS-ESI**: calcd. for C₄₆H₄₉B₂N₈O₉Zn₂: 1007.2408; found: 1007.2404. **IR**: 2955, 1615, 1555, 1445, 1360, 1330, 1315, 1275, 1215, 1105, 1075, 1000, 935, 885, 835, 780, 770, 700, 685, 620 cm⁻¹.

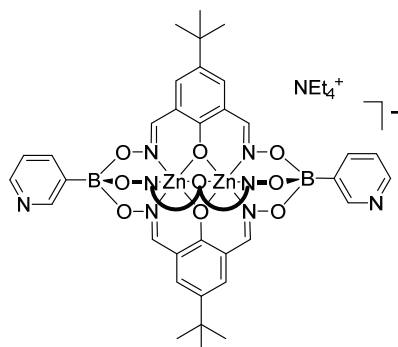
7.2.14 Clathrochelate 2.7



Dioxime **L1** (30 mg, 0.13 mmol, 1.5 equiv.) and 4-pyridylboronic acid (10.4 mg, 0.09 mmol, 1.0 equiv.) were dissolved in EtOH (5 ml) and CH₂Cl₂ (5 ml). The solution was stirred under air at RT until all solids dissolved. [Co(H₂O)₆](ClO₄)₂ (31 mg, 0.09 mmol, 1.0 equiv.) was added to the solution, and the mixture was stirred at RT for 1 h. The orange precipitate that formed was filtered, washed with CH₂Cl₂ (2 x 4 ml) and EtOH (1 x 10 ml), and the product was

dried under vacuum, affording complex **2.7** as an orange crystalline solid (45 mg, 0.04 mmol, 96%). Single crystals suitable for X-Rays analysis were grown by slow evaporation of the reaction mixture in absence of stirring. **HRMS-ESI**: calcd. for C₄₆H₄₉B₂N₈O₉Co₂: 997.2488; found: 997.2319. **IR**: 2955, 2865, 1610, 1550, 1445, 1395, 1365, 1320, 1280, 1215, 1080, 995, 935, 880, 840, 805, 780, 770, 700, 680, 620, 575, 540 cm⁻¹.

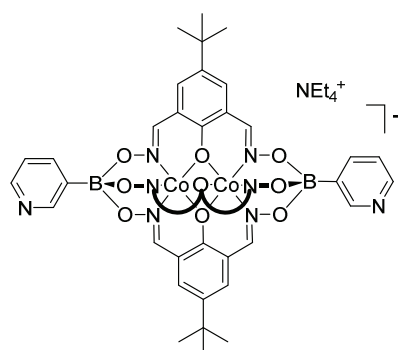
7.2.15 Clathrochelate 2.8



2.6 (300 mg, 0.27 mmol, 1.0 equiv) was suspended in a mixture of MeCN (10 ml) and MeOH (10 ml). Tetraethylammonium hydroxide (25 % in MeOH, 400 μ l, 0.60 mmol, 2.2 equiv.) was added, and the clear solution was stirred at RT for 3 h. The solution was then concentrated to \sim 5 ml, and the precipitate was filtered, washed with cold MeCN (3 x 3 ml) and dried under vacuum to afford **2.8** as a yellow crystalline material (233 mg, 0.203 mmol, 75 %). **¹H-NMR** (400 MHz, DMSO-*d*₆): δ =

8.77 (dd, *J* = 1.8, 1.0 Hz, 2H), 8.38 (s, 6H), 7.94 (dt, *J* = 7.4, 1.9 Hz, 2H), 7.33 (s, 6H), 7.23 (ddd, *J* = 7.5, 4.8, 1.0 Hz, 2H), 3.16 (q, *J* = 7.2 Hz, 8H), 1.21 (s, 27H), 1.17 – 1.09 (m, 12H). **¹³C-NMR** (101 MHz, DMSO): δ = 162.50, 154.31, 152.89, 147.26, 139.24, 137.17, 132.42, 122.40, 51.45, 33.47, 31.21, 7.09. **HRMS-ESI**: Calcd for C₄₆H₄₈B₂N₈O₉Zn₂: 1008.2416; found: 1008.2432. **IR**: 2955, 1610, 1585, 1550, 1445, 1395, 1365, 1330, 1285, 1220, 1185, 1140, 1080, 1050, 980, 920, 840, 780, 775, 725, 705, 635, 555, 525 cm⁻¹.

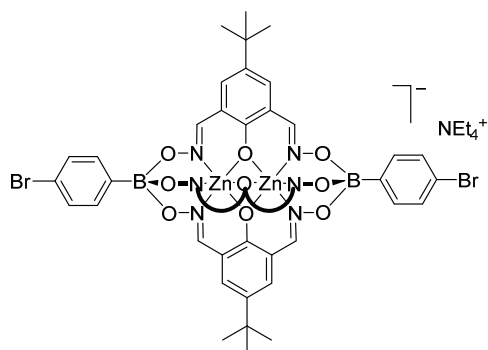
7.2.16 Clathrochelate 2.9



2.7 (540 mg, 0.49 mmol, 1.0 equiv.) was suspended in a mixture of MeCN (10 ml) and MeOH (10 ml). Tetraethylammonium hydroxide (25 % in MeOH, 725 μ l, 1.09 mmol, 2.2 equiv.) was added, leading to the complete dissolution of the clathrochelate. The orange solution was stirred at RT for 2 h, filtered and the orange precipitate was washed with MeCN (3 x 8 ml) and dried under vacuum to afford **2.9** as a crystalline orange material (460 mg, 0.41 mmol,

84 %). **HRMS-ESI**: calcd. for C₄₆H₄₉B₂N₈O₉Co₂: 997.2488; found: 997.2484. **IR**: 2950, 2865, 1610, 1585, 1550, 1445, 1395, 1365, 1325, 1280, 1220, 1080, 1050, 1020, 985, 925, 840, 780, 770, 705, 635, 570 cm⁻¹.

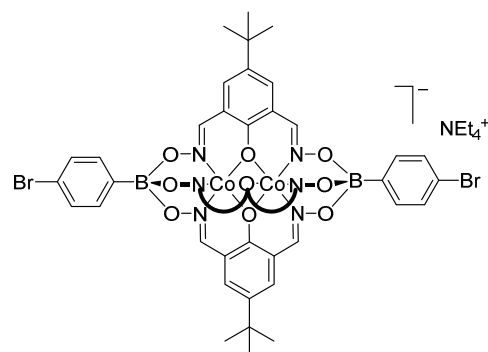
7.2.17 Clathrochelate **2.10**



A mixture dioxime **L1** (400 mg, 1.69 mmol, 3.0 equiv.), 4-bromophenylboronic acid (228 mg, 1.13 mmol, 2.0 equiv.) and $\text{Zn}(\text{OTf})_2$ (412 mg, 1.13 mmol, 2.0 equiv.) in MeOH (30 ml) was heated to 70 °C until all solid dissolved. Tetraethylammonium hydroxide (565 μl , 0.84 mmol, 25% in MeOH) was added, and the solution was stirred at 70 °C for 10 min. After a second addition

of tetraethylammonium hydroxide (565 μl , 0.84 mmol, 25% in MeOH), the solution was cooled down to RT, and the solvent was removed under reduced pressure. The yellow solid was suspended in EtOH (10 ml), isolated by filtration, washed with EtOH (3 x 10 ml) and Et_2O (2 x 50 ml) and dried under vacuum to afford **2.10** as a yellow powder (469 mg, 0.36 mmol, 64%). **$^1\text{H-NMR}$** (400 MHz, $\text{DMSO-}d_6$): δ = 8.35 (s, 6H), 7.59 (d, J = 8.0 Hz, 4H), 7.40 (d, J = 8.1 Hz, 4H), 7.31 (s, 6HH), 3.19 (q, J = 7.2 Hz, 8H), 1.21 (s, 27H), 1.15 (t, J = 7.2 Hz, 12H). **$^{13}\text{C-NMR}$** (101 MHz, $\text{DMSO-}d_6$): δ = 162.38, 154.00, 136.98, 134.09, 132.21, 129.12, 119.56, 118.24, 51.32, 33.37, 31.13, 7.02 (C-B not detected). **HRMS-ESI**: calcd. for $\text{C}_{48}\text{H}_{47}\text{B}_2\text{Br}_2\text{N}_6\text{O}_9\text{Zn}_2$: 1163.0518; found: 1163.0504. **IR**: 2955, 2860, 1610, 1580, 1550, 1445, 1395, 1365, 1330, 1280, 1240, 1220, 1195, 1080, 1040, 980, 925, 840, 815, 780, 730, 705, 675, 635, 560, 520 cm^{-1} .

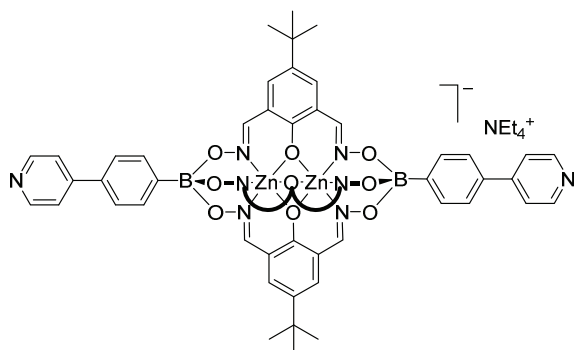
7.2.18 Clathrochelate **2.11**



A mixture of dioxime **L1** (300 mg, 1.27 mmol, 3.0 equiv.), 4-bromophenylboronic acid (170 mg, 0.85 mmol, 2.0 equiv.) and $[\text{Co}(\text{H}_2\text{O})_6](\text{NO}_3)_2$ (246 mg, 0.85 mmol, 2.0 equiv.) in MeOH (30 ml) was heated to 70 °C until all solid dissolved. Tetraethylammonium hydroxide (423 μl , 0.64 mmol, 25% in MeOH) was added, and the solution was stirred at 70 °C for 10 min. After a second addition of tetraethylammonium

hydroxide (423 μl , 0.64 mmol, 25% in MeOH), the solution was cooled down to RT, and the solvent was removed under reduced pressure. The orange solid was suspended in EtOH (10 ml), isolated by filtration, washed with EtOH (3 x 10 ml) and Et_2O (2 x 50 ml) and dried under vacuum to afford **2.11** as a bright orange powder (390 mg, 0.31 mmol, 73%). **HRMS-ESI**: calcd. for $\text{C}_{48}\text{H}_{47}\text{B}_2\text{Br}_2\text{Co}_2\text{N}_6\text{O}_9$: 1151.0621; found: 1151.0637. **IR**: 2960, 2860, 1610, 1580, 1550, 1445, 1390, 1360, 1330, 1285, 1240, 1225, 1195, 1170, 1080, 1040, 1010, 995, 930, 840, 820, 785, 770, 705, 680, 635, 570 cm^{-1} .

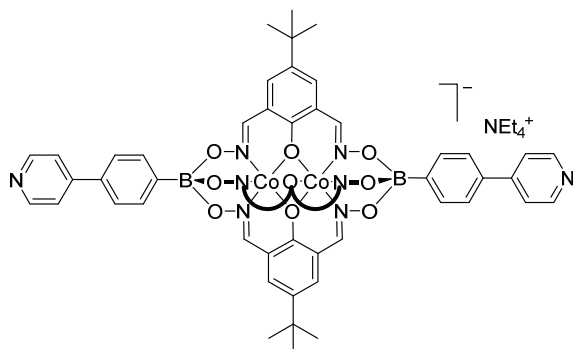
7.2.19 Clathrochelate **2.12**



To a 25 ml pyrex vial containing **2.10** (90 mg, 69 μmol , 1.0 equiv.), 4-pyridylboronic acid hydrate (58 mg, 0.41 mmol, 6 equiv.) and K_3PO_4 (44 mg, 0.21 mmol, 3.0 equiv.) under inert atmosphere were added degassed *n*-BuOH (10 ml) and degassed toluene (10 ml). $\text{Pd}_2(\text{dba})_3$ (3.21 mg, 3.5 μmol , 0.05 equiv.) and SPhos (2.85 mg, 7 μmol , 0.1

equiv.) were then added and the system was cycled two times with nitrogen, and the sealed vial was heated for 12 h at 120 $^\circ\text{C}$. After cooling to RT, the reaction mixture was filtered through Celite, and washed with *n*-BuOH (5 ml), MeOH (20 ml) and H_2O (200 ml). The filtrate was then concentrated to half its volume and the resulting precipitate was isolated by filtration, washed with H_2O (2 x 50 ml) and Et_2O (100 ml). The crude product was suspended in a mixture of MeOH (10 ml) and MeCN (10 ml) and tetraethylammonium hydroxide (46 μl , 69 μmol , 25% in MeOH) was added, leading to a complete dissolution of all material. The solvents were removed under reduced pressure and the solid was suspended in EtOH (8 ml), isolated by filtration, washed with EtOH (2 x 5 ml) and Et_2O (2 x 30 ml) and dried under vacuum to afford **2.12** as a pale-yellow powder (60 mg, 47 μmol , 68%). X-ray quality, light yellow crystals were obtained by slow diffusion of Et_2O into a solution of the complex in DCM. $^1\text{H-NMR}$ (400 MHz, $\text{DMSO}-d_6$): δ = 8.62 (d, J = 5.1 Hz, 4H), 8.39 (s, 6H), 7.81 (d, J = 7.7 Hz, 4H), 7.74 (d, J = 5.2 Hz, 4H), 7.68 (d, J = 7.9 Hz, 4H), 7.33 (s, 6H), 3.18 (q, J = 7.2 Hz, 8H), 1.23 (s, 27H), 1.14 (t, J = 7.2 Hz, 12H). $^{13}\text{C-NMR}$ (101 MHz, $\text{DMSO}-d_6$): δ = 162.43, 153.98, 150.08, 147.91, 136.97, 134.57, 132.70, 132.18, 124.71, 120.96, 118.30, 51.36, 33.40, 31.16, 7.04 (C-B not detected). **HRMS-ESI**: calcd. for $\text{C}_{58}\text{H}_{55}\text{B}_2\text{N}_8\text{O}_9\text{Zn}_2$: 1161.2845; found: 1161.2885. **IR**: 2955, 2865, 1610, 1595, 1550, 1445, 1410, 1390, 1365, 1330, 1285, 1225, 1200, 1140, 1075, 1040, 995, 930, 840, 810, 780, 775, 755, 690, 635, 565, 555, 525, 505 cm^{-1} .

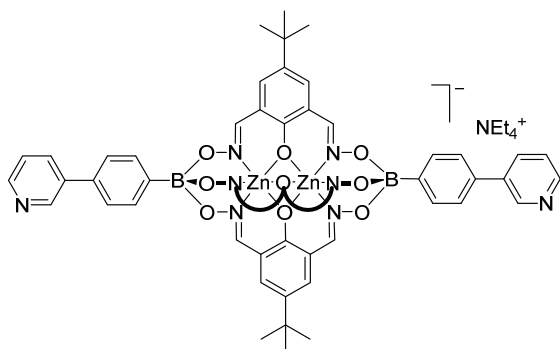
7.2.20 Clathrochelate **2.13**



To a 25 ml pyrex vial containing **2.11** (100 mg, 78 μ mol, 1.0 equiv.), 4-pyridylboronic acid hydrate (65 mg, 0.47 mmol, 6 equiv.) and K_3PO_4 (50 mg, 0.23 mmol, 3.0 equiv.) under inert atmosphere were added degassed *n*-BuOH (10 ml) and degassed toluene (10 ml). $Pd_2(dba)_3$ (3.57 mg, 3.9 μ mol, 0.05 equiv.) and SPhos (3.2 mg, 7.8 μ mol, 0.1

equiv.) were then added and the system was cycled two times with nitrogen, and the sealed vial was heated for 12 h at 120 $^{\circ}C$. After cooling to RT, the reaction mixture was filtered through Celite, and washed with *n*-BuOH (5 ml), MeOH (20 ml) and H_2O (200 ml). The filtrate was then concentrated to half its volume and the resulting precipitate was isolated by filtration, washed with H_2O (2 x 50 ml) and Et_2O (100 ml). The crude product was suspended in a mixture of MeOH (10 ml) and MeCN (10 ml) and tetraethylammonium hydroxide (52 μ l, 78 μ mol, 25% in MeOH) was added, leading to a complete dissolution of all material. The solvents were removed under reduced pressure and the solid was suspended in EtOH (10 ml), isolated by filtration, washed with EtOH (2 x 7 ml) and Et_2O (2 x 30 ml) and dried under vacuum to afford **2.13** as an orange powder (77 mg, 60 μ mol, 77%). **HRMS-ESI**: calcd. for $C_{58}H_{55}B_2Co_2N_8O_9$: 1147.2942 ; found: 1147.2981. **IR**: 2965, 2860, 1605, 1595, 1550, 1530, 1450, 1410, 1365, 1330, 1285, 1225, 1200, 1080, 1040, 1025, 995, 935, 880, 840, 810, 785, 770, 755, 695, 635, 570, 535 cm^{-1} .

7.2.21 Clathrochelate **2.14**

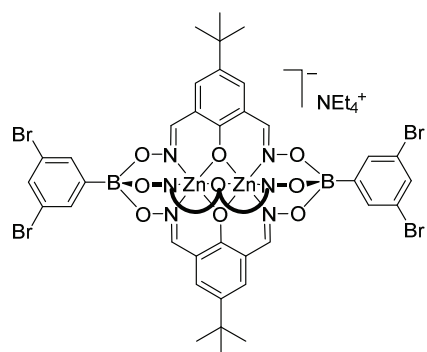


To a 25 ml pyrex vial containing **2.10** (90 mg, 69 μ mol, 1.0 equiv.), 3-pyridylboronic acid hydrate (58 mg, 0.41 mmol, 6 equiv.) and K_3PO_4 (44 mg, 0.21 mmol, 3.0 equiv.) under inert atmosphere were added degassed *n*-BuOH (10 ml) and degassed toluene (10 ml). $Pd_2(dba)_3$ (3.21 mg, 3.5 μ mol, 0.05 equiv.) and SPhos (2.85 mg, 7 μ mol, 0.1 equiv.) were then added and the

system was cycled two times with nitrogen, and the sealed vial was heated for 12 h at 120 $^{\circ}C$. After cooling to RT, the reaction mixture was filtered through Celite, and was washed with *n*-BuOH (5 ml), MeOH (20 ml) and H_2O (200 ml). The filtrate was then concentrated to half its volume and the

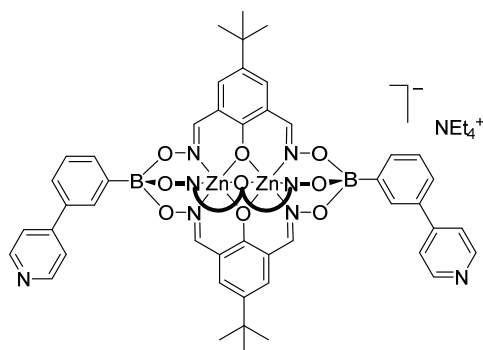
resulting precipitate was isolated by filtration, washed with H₂O (2 x 50 ml) and Et₂O (100 ml). The crude product was suspended in a mixture of MeOH (10 ml) and MeCN (10 ml) and tetraethylammonium hydroxide (46 µl, 69 µmol, 25% in MeOH) was added, leading to a complete dissolution of all material. The solvents were removed under reduced pressure and the solid was suspended in EtOH (8 ml), isolated by filtration, washed with EtOH (2 x 5 ml) and Et₂O (2 x 30 ml) and dried under vacuum to afford **2.14** as a pale-yellow powder (87 mg, 67 µmol, 98%). ¹H-NMR (400 MHz, DMSO-*d*₆): δ = 8.93 (s, 2H), 8.56 (d, *J* = 4.0 Hz, 2H), 8.40 (s, 6H), 8.10 (d, *J* = 7.9 Hz, 2H), 7.80 (d, *J* = 7.6 Hz, 4H), 7.60 (d, *J* = 7.7 Hz, 4H), 7.50 (dd, *J* = 7.2, 5.1 Hz, 2H), 7.34 (s, 6H), 3.18 (q, *J* = 7.2 Hz, 8H), 1.24 (s, 27H), 1.14 (t, *J* = 6.4 Hz, 12H). ¹³C-NMR (101 MHz, DMSO-*d*₆): δ = 162.43, 153.95, 147.85, 147.51, 136.98, 136.50, 134.55, 133.78, 132.68, 132.16, 124.85, 123.81, 118.32, 51.35, 33.41, 31.17, 7.03 (C-B not detected). HRMS-ESI: calcd. for C₅₈H₅₅B₂N₈O₉Zn₂: 1161.2845; found: 1161.2844. IR: 2960, 2870, 1610, 1590, 1550, 1445, 1390, 1365, 1330, 1285, 1225, 1200, 1080, 1040, 1020, 995, 930, 840, 810, 780, 775, 705, 695, 635, 620, 656, 525 cm⁻¹.

7.2.22 Clathrochelate **2.15**



A mixture of dioxime **L1** (400 mg, 1.69 mmol, 3.0 equiv.), 3-bromophenylboronic acid (228 mg, 1.13 mmol, 2.0 equiv.) and Zn(OTf)₂ (412 mg, 1.13 mmol, 2.0 equiv.) in MeOH (30 ml) was heated to 70 °C until all solid dissolved. Tetraethylammonium hydroxide (565 µl, 0.84 mmol, 25% in MeOH) was added, and the solution was stirred at 70 °C for 10 min. After a second addition of tetraethylammonium hydroxide (565 µl, 0.84 mmol, 25% in MeOH), the solution was cooled down to RT, and the solvent was removed under reduced pressure. The yellow solid was suspended in EtOH (10 ml), isolated by filtration, washed with EtOH (3 x 10 ml) and Et₂O (2 x 50 ml) and dried under vacuum to afford **2.15** as a yellow powder (486 mg, 0.38 mmol, 67%). ¹H-NMR (400 MHz, DMSO-*d*₆): δ = 8.39 (s, 6H), 7.78 – 7.75 (m, 2H), 7.62 (d, *J* = 7.2 Hz, 2H), 7.36 (d, *J* = 8.0 Hz, 2H), 7.34 (s, 6H), 7.20 (t, *J* = 7.6 Hz, 2H), 3.17 (q, *J* = 7.2 Hz, 8H), 1.22 (s, 27H), 1.14 (t, *J* = 7.2 Hz, 12H). ¹³C-NMR (101 MHz, DMSO-*d*₆): δ = 162.41, 154.15, 137.03, 134.38, 132.31, 130.58, 128.85, 128.64, 120.96, 118.24, 51.35, 33.40, 31.15, 7.02 (C-B not detected). HRMS-ESI: calcd. for C₄₈H₄₇B₂Br₂N₆O₉Zn₂: 1163.0518; found: 1163.0525. IR: 2955, 2860, 1610, 1550, 1445, 1395, 1365, 1330, 1285, 1240, 1190, 1080, 1035, 990, 960, 930, 890, 835, 775, 715, 640, 560, 520, 510 cm⁻¹.

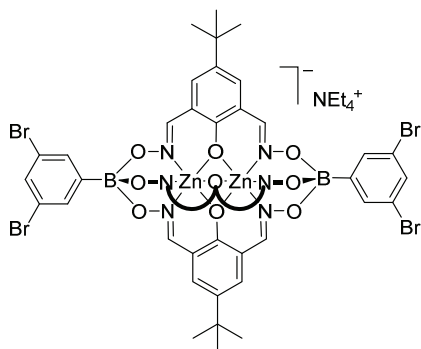
7.2.23 Clathrochelate 2.16



To a 25 ml pyrex vial containing **2.15** (90 mg, 69 μ mol, 1.0 equiv.), 4-pyridylboronic acid hydrate (58 mg, 0.41 mmol, 6 equiv.) and K_3PO_4 (44 mg, 0.21 mmol, 3.0 equiv.) under inert atmosphere were added degassed *n*-BuOH (10 ml) and degassed toluene (10 ml). $Pd_2(dba)_3$ (3.21 mg, 3.5 μ mol, 0.05 equiv.) and SPhos (2.85 mg, 7 μ mol, 0.1 equiv.) were then added and the system was cycled two times with nitrogen, and the

sealed vial was heated for 12 h at 120 $^{\circ}C$. After cooling to RT, the reaction mixture was filtered through Celite, and was washed with *n*-BuOH (5 ml), MeOH (20 ml) and H_2O (200 ml). The filtrate was then concentrated to half its volume and the resulting precipitate was isolated by filtration, washed with H_2O (2 x 50 ml) and Et_2O (100 ml). The crude product was suspended in a mixture of MeOH (10 ml) and MeCN (10 ml) and tetraethylammonium hydroxide (46 μ l, 69 μ mol, 25% in MeOH) was added, leading to a complete dissolution of all material. The solvents were removed under reduced pressure and the solid was suspended in EtOH (8 ml), isolated by filtration, washed with EtOH (2 x 5 ml) and Et_2O (2 x 30 ml) and dried under vacuum to afford **2.16** as a pale-yellow powder (81 mg, 62 μ mol, 91%). **1H -NMR** (400 MHz, $DMSO-d_6$): δ = 8.64 (d, J = 3.6 Hz, 4H), 8.41 (s, 6H), 8.05 (s, 2H), 7.77 (d, J = 7.1 Hz, 2H), 7.72 (d, J = 4.1 Hz, 4H), 7.61 (d, J = 7.1 Hz, 2H), 7.39 (t, J = 7.4 Hz, 2H), 7.33 (s, 6H), 3.17 (q, J = 6.8 Hz, 8H), 1.22 (s, 27H), 1.13 (m, 12H). **^{13}C -NMR** (101 MHz, $DMSO-d_6$): δ = 162.44, 154.06, 150.09, 148.59, 136.99, 135.12, 133.08, 132.19, 130.13, 127.26, 124.54, 121.21, 118.32, 51.38, 33.41, 31.16, 7.04 (C-B not detected). **HRMS-ESI**: calcd. for $C_{58}H_{55}B_2N_8O_9Zn_2$: 1161.2845; found: 1161.2878. **IR**: 2955, 2870, 1610, 1605, 1550, 1445, 1395, 1365, 1330, 1285, 1240, 1195, 1080, 1035, 995, 980, 930, 900, 835, 775, 725, 695, 650, 615, 555, 525 cm^{-1} .

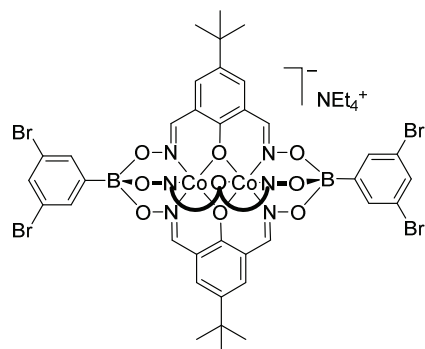
7.2.24 Clathrochelate 2.17



A mixture of doxime **L1** (400 mg, 1.69 mmol, 3.0 equiv.), 3,5-dibromophenylboronic acid (315 mg, 1.13 mmol, 2.0 equiv.) and $Zn(OTf)_2$ (412 mg, 1.13 mmol, 2.0 equiv.) in MeOH (30 ml) was heated to 70 $^{\circ}C$ until all solid dissolved. Tetraethylammonium hydroxide (565 μ l, 0.84 mmol, 25 % in methanol) was added, and the solution was stirred at 70 $^{\circ}C$ for 10 min. After a second addition of tetraethylammonium hydroxide (565 μ l, 0.84 mmol, 25 % in methanol), the

solution was cooled down to RT, and the solvent was removed under reduced pressure. The yellow solid was suspended in EtOH (10 ml), filtered, washed with EtOH (3 x 10 ml) and Et₂O (2 x 50 ml) and dried under vacuum to afford **2.17** as a yellow powder (600 mg, 0.41 mmol, 74 %). **¹H-NMR** (400 MHz, DMSO-*d*₆): δ = 8.42 (s, 6H), 7.74 (d, *J* = 1.9 Hz, 4H), 7.62 (t, *J* = 1.9 Hz, 2H), 7.36 (s, 6H), 3.16 (q, *J* = 7.2 Hz, 8H), 1.22 (s, 27H), 1.13 (t, *J* = 7.2 Hz, 12H). **¹³C-NMR** (101 MHz, DMSO-*d*₆): δ = 162.44, 154.47, 137.10, 133.32, 132.52, 130.68, 121.55, 118.17, 51.32, 33.41, 31.13, 7.03. **HRMS-ESI**: calcd. for C₄₈H₄₅B₂Br₄N₆O₉Zn₂: 1320.8707; found: 1320.8702. **IR**: 2955, 2860, 1610, 1540, 1445, 1390, 1365, 1330, 1285, 1225, 1190, 1100, 1080, 1045, 990, 925, 880, 855, 840, 785, 775, 735, 720, 680, 635, 560, 520, 510 cm⁻¹

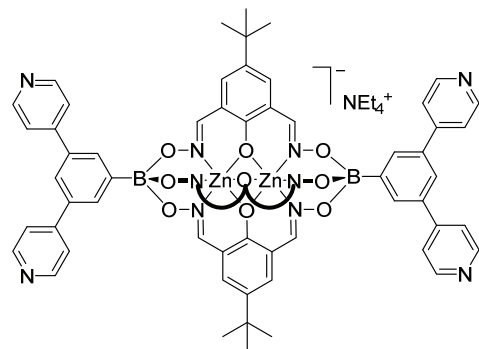
7.2.25 Clathrochelate 2.18



A mixture of dioxime **L1** (400 mg, 1.27 mmol, 3.0 equiv.), 3,5-dibromophenylboronic acid (316 mg, 0.85 mmol, 2.0 equiv.) and [Co(H₂O)₆](NO₃)₂ (329 mg, 0.85 mmol, 2.0 equiv.) in MeOH (30 ml) was heated to 70 °C until all solid dissolved. Tetraethylammonium hydroxide (564 μ l, 0.64 mmol, 25% in MeOH) was added, and the solution was stirred at 70 °C for 10 min. After a second addition of tetraethylammonium hydroxide (564 μ l, 0.64 mmol, 25% in MeOH), the solution

was cooled down to RT, and the solvent was removed under reduced pressure. The orange solid was suspended in EtOH (10 ml), filtered, washed with EtOH (3 x 10 ml) and Et₂O (2 x 50 ml) and dried under vacuum to afford **2.18** as an orange powder (660 mg, 0.45 mmol, 82 %). **HRMS-ESI**: calcd. for C₄₈H₄₅B₂Br₄N₆O₉Co₂: 1308.8785; found: 1308.8807. **IR**: 2955, 2860, 1605, 1540, 1390, 1365, 1330, 1285, 1190, 1085, 1045, 995, 925, 880, 855, 785, 770, 720, 680, 565, 530 cm⁻¹.

7.2.26 Clathrochelate 2.19

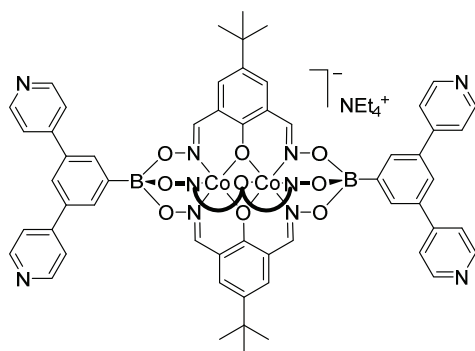


To a 25 ml pyrex vial containing **2.17** (100 mg, 69 μ mol, 1.0 equiv.), 4-pyridylboronic acid hydrate (193 mg, 1.37 mmol, 20 equiv.) and K₃PO₄ (146 mg, 0.69 mmol, 10 equiv.) under inert atmosphere were added degassed *n*-BuOH (10 ml) and degassed toluene (10 ml). Pd₂(dba)₃ (3.21 mg, 3.5 μ mol, 0.05 equiv.) and SPhos (2.85 mg, 7 μ mol, 0.1 equiv.) were then added and the system was cycled two times with nitrogen, and the sealed vial was

heated for 12 h at 120 °C. After cooling to RT, the reaction mixture was filtered through Celite, and

the plug was washed with *n*-BuOH (5 ml), MeOH (20 ml) and H₂O (200 ml). The filtrate was then concentrated to half its volume and the resulting precipitate was filtered, washed with H₂O (2 x 50 ml) and Et₂O (100 ml). The crude product was suspended in a mixture of MeOH (10 ml) and MeCN (10 ml) and tetraethylammonium hydroxide (46 μ l, 69 μ mol, 25 % in methanol) was added, leading to a complete dissolution of all material. The solvents were removed and the solid was suspended in EtOH (8 ml), filtered, washed with EtOH (2 x 5 ml) and Et₂O (2 x 30 ml) and dried under vacuum to afford **2.19** as a pale-yellow powder (92 mg, 64 μ mol, 93 %). **¹H-NMR** (400 MHz, DMSO-*d*₆): δ = 8.69 (d, *J* = 5.6 Hz, 8H), 8.45 (s, 6H), 8.14 (d, *J* = 1.4 Hz, 4H), 8.00 (s, 2H), 7.86 (d, *J* = 5.7 Hz, 8H), 7.35 (s, 6H), 3.18 (q, *J* = 7.2 Hz, 8H), 1.22 (s, 27H), 1.14 (t, *J* = 7.2 Hz, 12H). **¹³C-NMR** (101 MHz, DMSO-*d*₆): δ = 162.50, 154.28, 150.16, 148.08, 137.05, 136.33, 132.30, 131.23, 123.32, 121.52, 118.31, 51.36, 33.43, 31.17, 7.05. **HRMS-ESI**: calcd. for C₆₈H₆₁B₂N₁₀O₉Zn₂: 1315.3383; found: 1315.3357. **IR**: 2950, 2860, 1600, 1590, 1545, 1445, 1395, 1330, 1285, 1245, 1225, 1185, 1075, 1035, 990, 930, 890, 835, 820, 780, 770, 760, 685, 635, 615, 560, 525, 510 cm⁻¹.

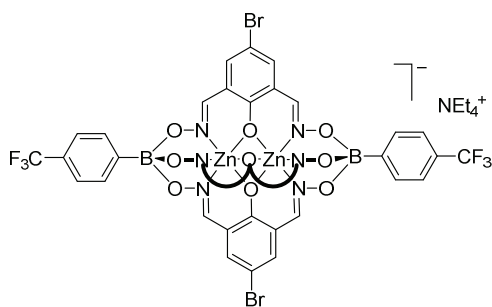
7.2.27 Clathrochelate **2.20**



To a 25 ml pyrex vial containing **2.18** (100 mg, 69 μ mol, 1.0 equiv.), 4-pyridylboronic acid hydrate (193 mg, 1.37 mmol, 20 equiv.) and K₃PO₄ (146 mg, 0.69 mmol, 10 equiv.) under inert atmosphere were added degassed *n*-BuOH (10 ml) and degassed toluene (10 ml). Pd₂(dba)₃ (3.21 mg, 3.5 μ mol, 0.05 equiv.) and SPhos (2.85 mg, 7 μ mol, 0.1 equiv.) were then added and the system was cycled two times with nitrogen, and the sealed vial was

heated for 12 h at 120 °C. After cooling to RT, the reaction mixture was filtered through Celite, and the plug was washed with *n*-BuOH (5 ml), MeOH (20 ml) and H₂O (200 ml). The filtrate was then concentrated to half its volume and the resulting precipitate was filtered, washed with H₂O (2 x 50 ml) and Et₂O (100 ml). The crude product was suspended in a mixture of MeOH (10 ml) and MeCN (10 ml) and tetraethylammonium hydroxide (50 μ l, 75 μ mol, 25 % in methanol) was added, leading to a complete dissolution of all material. The solvents were removed and the solid was suspended in EtOH (8 ml), filtered, washed with EtOH (2 x 5 ml) and Et₂O (2 x 30 ml) and dried under vacuum to afford **2.20** as an orange powder (95 mg, 65 μ mol, 95 %). **HRMS-ESI**: calcd. for C₆₈H₆₁B₂N₁₀O₉Co₂: 1301.3468; found: 1301.3474. **IR**: 2955, 2865, 1600, 1550, 1445, 1400, 1365, 1330, 1285, 1245, 1225, 1190, 1080, 1035, 990, 935, 890, 840, 820, 785, 775, 760, 690, 640, 615, 565, 530 cm⁻¹.

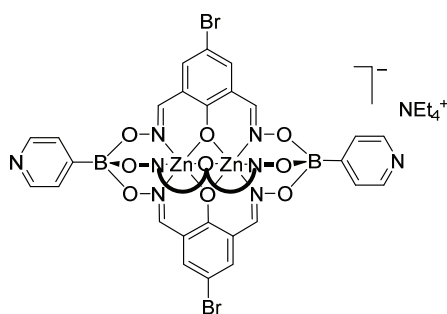
7.2.28 Clathrochelate 2.21



A mixture of dioxime **L2** (400 mg, 1.54 mmol, 3.0 equiv.), 4-(trifluoromethyl)phenylboronic acid (200 mg, 1.03 mmol, 2.0 equiv.) and $\text{Zn}(\text{OTf})_2$ (376 mg, 1.03 mmol, 2.0 equiv.) in MeOH (30 ml) was heated to 70 °C until all solid dissolved. Tetraethylammonium hydroxide (515 μl , 0.77 mmol, 25% in MeOH) was added, and the solution was stirred at 70 °C for 10

min. After a second addition of tetraethylammonium hydroxide (515 μl , 0.77 mmol, 25% in MeOH), the solution was cooled down to RT, and the solvent was removed under reduced pressure. The yellow solid was suspended in EtOH (10 ml), isolated by filtration, washed with EtOH (3 x 10 ml) and Et_2O (2 x 50 ml) and dried under vacuum to afford **2.21** as a yellow powder (540 mg, 0.40 mmol, 78%). **$^1\text{H-NMR}$** (400 MHz, $\text{DMSO-}d_6$): δ = 8.39 (s, 6H), 7.83 (d, J = 7.7 Hz, 4H), 7.57 (d, J = 7.8 Hz, 4H), 7.53 (s, 6H), 3.19 (q, J = 7.2 Hz, 8H), 1.15 (ddt, J = 7.3, 5.4, 2.1 Hz, 12H). **$^{13}\text{C-NMR}$** (101 MHz, $\text{DMSO-}d_6$): δ = 163.32, 153.41, 136.95, 132.27, 127.00, 124.94, 122.99, 120.83, 105.08, 51.36, 7.05 (C-B not detected). **$^{19}\text{F-NMR}$** (376 MHz, $\text{DMSO-}d_6$): δ = -60.51. **HRMS-ESI**: calcd. for $\text{C}_{38}\text{H}_{20}\text{B}_2\text{Br}_3\text{F}_6\text{N}_6\text{O}_9\text{Zn}_2$: 1210.7468; found: 1210.7467. **IR**: 1605, 1550, 1515, 1435, 1395, 1320, 1220, 1205, 1155, 1090, 1075, 1060, 1040, 1020, 980, 965, 950, 935, 890, 870, 845, 830, 780, 745, 700, 665, 640, 630, 600, 545, 530, 510 cm^{-1} .

7.2.29 Clathrochelate 2.22



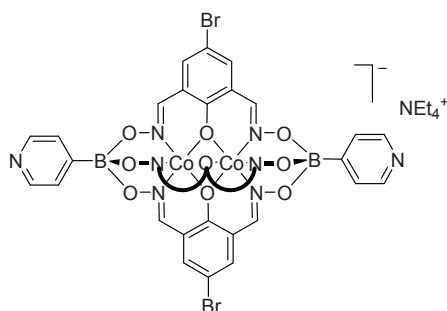
A mixture of dioxime **L2** (200 mg, 0.77 mmol, 3.0 equiv.) and 4-pyridylboronic acid hydrate (72 mg, 0.51 mmol, 2.0 equiv.) were dissolved in MeOH (30 ml). $\text{Zn}(\text{OTf})_2$ (187 mg, 0.51 mmol, 2.0 equiv.) was added and the yellow solution was heated at 50 °C for 15 min. The solvent was removed under reduced pressure and the yellow solid was suspended in EtOH (10 ml), isolated by filtration and

washed with EtOH (10 ml) and Et_2O (20 ml). The yellow solid was then suspended in a mixture of MeOH (10 ml) and MeCN (10 ml) and tetraethylammonium hydroxide (345 μl , 0.51 mmol, 25% in MeOH) was added, and the solution was stirred at RT for 10 min. After removal of the solvents under reduced pressure the solid was suspended in EtOH (8 ml), isolated by filtration, washed with cold EtOH (3 x 5 ml) and Et_2O (2 x 50 ml) and dried under vacuum to afford **2.22** as a yellow powder (270 mg, 0.22 mmol, 87%). **$^1\text{H-NMR}$** (400 MHz, $\text{DMSO-}d_6$): δ = 8.41 (d, J = 5.7 Hz, 4H), 8.39 (s, 6H), 7.54 (d,

$J = 5.7$ Hz, 4H), 7.52 (s, 6H), 3.20 (q, $J = 7.2$ Hz, 8H), 1.20 – 1.10 (m, 12H). $^{13}\text{C-NMR}$ (101 MHz, $\text{DMSO-}d_6$): $\delta = 163.32, 153.52, 147.73, 137.00, 127.09, 120.80, 105.09, 51.37, 7.05$ (C-B not detected).

HRMS-ESI: calcd. for $\text{C}_{34}\text{H}_{20}\text{B}_2\text{Br}_3\text{N}_8\text{O}_9\text{Zn}_2$: 1076.7623; found: 1076.7626. **IR:** 1605, 1550, 1485, 1435, 1325, 1205, 1075, 1035, 970, 945, 890, 875, 810, 780, 745, 700, 685, 650, 540, 520, 515 cm^{-1}

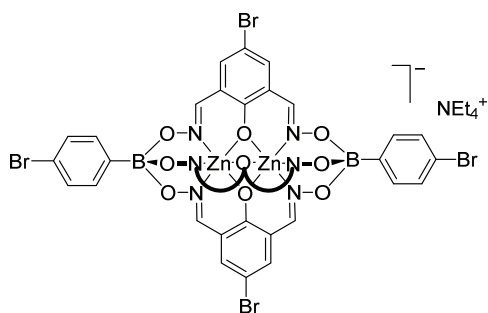
7.2.30 Clathrochelate **2.23**



A mixture of dioxime **L2** (200 mg, 0.77 mmol, 3.0 equiv.) and 4-pyridylboronic acid hydrate (72 mg, 0.51 mmol, 2.0 equiv.) were dissolved in MeOH (30 ml). $[\text{Co}(\text{H}_2\text{O})_6](\text{NO}_3)_2$ (150 mg, 0.51 mmol, 2.0 equiv.) was added and the orange solution was heated at 50 °C for 15 min. The solvent was removed under reduced pressure and the orange solid was suspended in EtOH (10 ml), isolated by

filtration and washed with EtOH (10 ml) and Et_2O (20 ml). The orange solid was then suspended in a mixture of MeOH (10 ml) and MeCN (10 ml) and tetraethylammonium hydroxide (345 μl , 0.51 mmol, 25% in MeOH) was added, and the solution was stirred at RT for 10 min. After removal of the solvents under reduced pressure the solid was suspended in EtOH (8 ml), isolated by filtration, washed with cold EtOH (3 x 5 ml) and Et_2O (2 x 50 ml) and dried under vacuum to afford **2.23** as an orange powder (250 mg, 0.21 mmol, 82%). **HRMS-ESI:** calcd. for $\text{C}_{34}\text{H}_{20}\text{B}_2\text{Br}_3\text{Co}_2\text{N}_8\text{O}_9$: 1164.7731; found: 1164.7717. **IR:** 1600, 1550, 1485, 1435, 1330, 1245, 1210, 1175, 1080, 1035, 970, 945, 895, 870, 810, 780, 770, 750, 700, 690, 650, 540, 520, 510 cm^{-1} .

7.2.31 Clathrochelate **2.24**

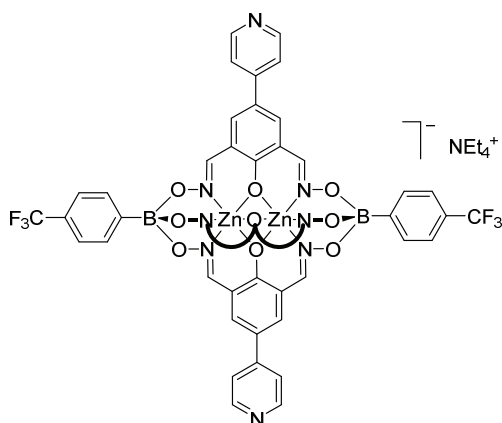


A mixture of dioxime **L2** (400 mg, 1.54 mmol, 3.0 equiv.), 4-bromophenylboronic acid (206 mg, 1.03 mmol, 2.0 equiv.) and $\text{Zn}(\text{OTf})_2$ (380 mg, 1.03 mmol, 2.0 equiv.) in MeOH (30 ml) was heated to 70 °C until all solid dissolved. Tetraethylammonium hydroxide (515 μl , 0.77 mmol, 25% in MeOH) was added, and the solution was stirred at 70 °C for 10 min. After a second

addition of tetraethylammonium hydroxide (515 μl , 0.77 mmol, 25% in MeOH), the solution was cooled down to RT, and the solvent was removed under reduced pressure. The yellow solid was suspended in EtOH (10 ml), isolated by filtration, washed with EtOH (3 x 10 ml) and Et_2O (2 x 50 ml) and dried under vacuum to afford **2.24** as a yellow powder (551 mg, 0.40 mmol, 79%). $^1\text{H-NMR}$ (400 MHz, $\text{DMSO-}d_6$): $\delta = 8.37$ (s, 6H), 7.56 (d, $J = 8.0$ Hz, 4H), 7.51 (s, 6H), 7.40 (d, $J = 8.0$ Hz, 4H), 3.18 (q, J

= 7.2 Hz, 8H), 1.15 (t, J = 6.2 Hz, 12H). **$^{13}\text{C-NMR}$** (101 MHz, $\text{DMSO-}d_6$): δ = 163.27, 153.23, 136.83, 134.02, 129.25, 120.84, 119.81, 105.02, 51.36, 7.04 (C-B not detected). **HRMS-ESI**: calcd. for $\text{C}_{36}\text{H}_{20}\text{B}_2\text{Br}_5\text{N}_6\text{O}_9\text{Zn}_2$: 1232.5909; found: 1232.5892. **IR**: 1605, 1550, 1480, 1430, 1390, 1325, 1240, 1220, 1200, 1065, 1040, 1010, 975, 950, 930, 890, 855, 820, 780, 700, 670, 560, 535, 510 cm^{-1} .

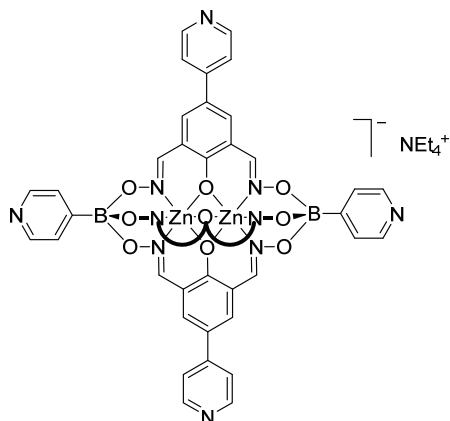
7.2.32 Clathrochelate 2.25



To a 25 ml pyrex vial containing **2.21** (100 mg, 74 μmol , 1.0 equiv.), 4-pyridylboronic acid hydrate (156 mg, 1.12 mmol, 15 equiv.) and K_3PO_4 (118 mg, 0.56 mmol, 7.5 equiv.) under inert atmosphere were added degassed n -BuOH (10 ml) and degassed toluene (10 ml). $\text{Pd}_2(\text{dba})_3$ (3.41 mg, 3.7 μmol , 0.05 equiv.) and SPhos (3.06 mg, 7.4 μmol , 0.1 equiv.) were then added and the system was cycled two times with nitrogen, and the sealed vial was heated

for 12 h at $120\text{ }^\circ\text{C}$. After cooling to RT, the reaction mixture was filtered through Celite, and was washed with n -BuOH (5 ml), MeOH (20 ml) and H_2O (200 ml). The filtrate was then concentrated to half its volume and the resulting precipitate was isolated by filtration, washed with H_2O (2 x 50 ml) and Et_2O (100 ml). The crude product was suspended in a mixture of MeOH (10 ml) and MeCN (10 ml) and tetraethylammonium hydroxide (50 μl , 74 μmol , 25% in MeOH) was added, leading to a complete dissolution of all material. The solvents were removed under reduced pressure and the solid was suspended in EtOH (8 ml), isolated by filtration, washed with EtOH (2 x 5 ml) and Et_2O (2 x 30 ml) and dried under vacuum to afford **2.25** as a pale-yellow powder (81 mg, 61 μmol , 82%). **$^1\text{H-NMR}$** (400 MHz, $\text{DMSO-}d_6$): δ = 8.56 (d, J = 5.9 Hz, 6H), 8.56 (s, 6H), 7.95 (s, 6H), 7.90 (d, J = 7.6 Hz, 4H), 7.65 (d, J = 5.5 Hz, 6H), 7.61 (d, J = 7.8 Hz, 4H), 3.18 (q, J = 7.2 Hz, 8H), 1.14 (t, J = 6.4 Hz, 12H). **$^{13}\text{C-NMR}$** (101 MHz, $\text{DMSO-}d_6$): δ = 165.19, 154.20, 150.10, 145.53, 133.79, 132.28, 123.59, 123.04, 119.73, 119.50, 51.39, 7.06 (C-B, CF_3 and C- CF_3 not detected). **$^{19}\text{F-NMR}$** (376 MHz, $\text{DMSO-}d_6$): δ = -60.47. **HRMS-ESI**: calcd. for $\text{C}_{53}\text{H}_{32}\text{B}_2\text{F}_6\text{N}_9\text{O}_9\text{Zn}_2$: 1206.0978; found: 1206.1001. **IR**: 1705, 1595, 1560, 1445, 1395, 1335, 1320, 1305, 1240, 1220, 1205, 1150, 1120, 1080, 1065, 1040, 995, 980, 955, 915, 830, 820, 795, 775, 760, 730, 695, 670, 610, 600, 565, 520 cm^{-1} .

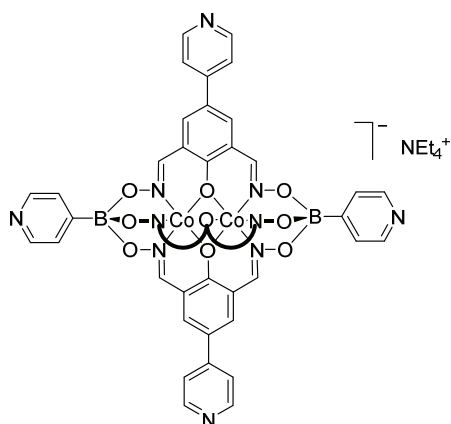
7.2.33 Clathrochelate **2.26**



To a 25 ml pyrex vial containing **2.22** (100 mg, 83 μ mol, 1.0 equiv.), 4-pyridylboronic acid hydrate (174 mg, 1.24 mmol, 15 equiv.) and K_3PO_4 (132 mg, 0.62 mmol, 7.5 equiv.) under inert atmosphere were added degassed *n*-BuOH (10 ml) and degassed toluene (10 ml). $Pd_2(dba)_3$ (3.79 mg, 4.1 μ mol, 0.05 equiv.) and SPhos (3.40 mg, 8.3 μ mol, 0.1 equiv.) were then added and the system was cycled two times with nitrogen, and the sealed vial was heated for 12 h at 120 °C. After cooling to RT, the reaction

mixture was filtered through Celite, and was washed with *n*-BuOH (5 ml), MeOH (20 ml) and H_2O (200 ml). The filtrate was then concentrated to half its volume and the resulting precipitate was isolated by filtration, washed with H_2O (2 x 50 ml) and Et_2O (100 ml). The crude product was suspended in a mixture of MeOH (10 ml) and MeCN (10 ml) and tetraethylammonium hydroxide (55 μ l, 83 μ mol, 25% in MeOH) was added, leading to a complete dissolution of all material. The solvents were removed under reduced pressure and the solid was suspended in EtOH (8 ml), isolated by filtration, washed with EtOH (2 x 5 ml) and Et_2O (2 x 30 ml) and dried under vacuum to afford **2.26** as a pale-yellow powder (85 mg, 71 μ mol, 85%). X-ray quality, light yellow crystals were obtained by slow diffusion of iPr_2O into a solution of the complex in DCM. **1H -NMR** (400 MHz, $DMSO-d_6$): δ = 8.57 (d, J = 6.0 Hz, 6H), 8.56 (s, 6H), 8.45 (d, J = 5.5 Hz, 4H), 7.94 (s, 6H), 7.65 (d, J = 6.2 Hz, 6H), 7.61 (d, J = 5.5 Hz, 4H), 3.18 (q, J = 7.2 Hz, 8H), 1.19 – 1.10 (m, 12H). **^{13}C -NMR** (101 MHz, $DMSO-d_6$): δ = 165.20, 154.33, 150.12, 147.78, 145.53, 133.85, 127.15, 123.64, 119.74, 119.49, 51.38, 7.06 (C-B not detected). **HRMS-ESI**: calcd. for $C_{49}H_{32}B_2N_{11}O_9Zn_2$: 1072.1133; found: 1072.1174. **IR**: 1605, 1590, 1560, 1445, 1400, 1340, 1310, 1220, 1205, 1080, 1035, 995, 975, 945, 915, 825, 795, 775, 765, 735, 695, 655, 610, 656, 545, 520, 510 cm^{-1} .

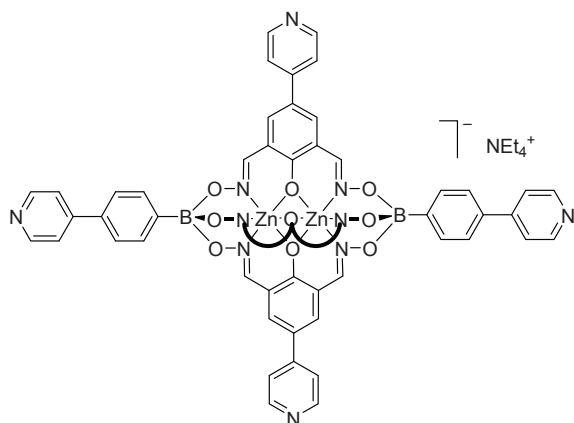
7.2.34 Clathrochelate **2.27**



To a 25 ml pyrex vial containing **2.23** (100 mg, 84 μ mol, 1.0 equiv.), 4-pyridylboronic acid hydrate (175 mg, 1.25 mmol, 15 equiv.) and K_3PO_4 (134 mg, 0.63 mmol, 7.5 equiv.) under inert atmosphere were added degassed *n*-BuOH (10 ml) and degassed toluene (10 ml). $Pd_2(dba)_3$ (3.83 mg, 4.2 μ mol, 0.05 equiv.) and SPhos (3.44 mg, 8.4 μ mol, 0.1 equiv.) were then added and the system was cycled two times with nitrogen, and the sealed vial was heated for 12 h at 120 $^{\circ}C$. After cooling to RT, the reaction

mixture was filtered through Celite, and was washed with *n*-BuOH (5 ml), MeOH (20 ml) and H_2O (200 ml). The filtrate was then concentrated to half its volume and the resulting precipitate was isolated by filtration, washed with H_2O (2 x 50 ml) and Et_2O (100 ml). The crude product was suspended in a mixture of MeOH (10 ml) and MeCN (10 ml) and tetraethylammonium hydroxide (55 μ l, 84 μ mol, 25% in MeOH) was added, leading to a complete dissolution of all material. The solvents were removed under reduced pressure and the solid was suspended in EtOH (8 ml), isolated by filtration, washed with EtOH (2 x 5 ml) and Et_2O (2 x 30 ml) and dried under vacuum to afford **2.27** as an orange powder (82 mg, 69 μ mol, 82%). **HRMS-ESI:** calcd. for $C_{49}H_{32}B_2Co_2N_{11}O_9Zn_2$: 1058.1250; found: 1058.1267. **IR:** 1600, 1560, 1450, 1405, 1335, 1310, 1220, 1205, 1085, 1035, 995, 975, 915, 825, 800, 775, 740, 700, 670, 655, 615, 570, 550, 530, 510 cm^{-1} .

7.2.35 Clathrochelate **2.28**

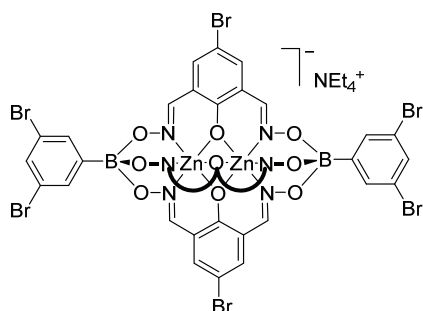


To a 25 ml pyrex vial containing **2.24** (100 mg, 73 μ mol, 1.0 equiv.), 4-pyridylboronic acid hydrate (205 mg, 1.47 mmol, 20 equiv.) and K_3PO_4 (156 mg, 0.73 mmol, 10 equiv.) under inert atmosphere were added degassed *n*-BuOH (10 ml) and degassed toluene (10 ml). $Pd_2(dba)_3$ (5.04 mg, 5.5 μ mol, 0.075 equiv.) and SPhos (4.52 mg, 11 μ mol, 0.15 equiv.) were then added and the system was cycled

two times with nitrogen, and the sealed vial was heated for 12 h at 120 $^{\circ}C$. After cooling to RT, the reaction mixture was filtered through Celite, and was washed with *n*-BuOH (5 ml), MeOH (20 ml) and H_2O (200 ml). The filtrate was then concentrated to half its volume and the resulting precipitate was

isolated by filtration, washed with H₂O (2 x 50 ml) and Et₂O (100 ml). The crude product was suspended in a mixture of MeOH (10 ml) and MeCN (10 ml) and tetraethylammonium hydroxide (49 µl, 73 µmol, 25% in MeOH) was added, leading to a complete dissolution of all material. The solvents were removed and the solid was suspended in EtOH (8 ml), isolated by filtration, washed with EtOH (2 x 5 ml) and Et₂O (2 x 30 ml) and dried under vacuum to afford **2.24** as a pale-yellow powder (81 mg, 60 µmol, 82%). X-ray quality, light yellow crystals were obtained by slow diffusion of Et₂O into a solution of the complex in DCM. **¹H-NMR** (400 MHz, DMSO-*d*₆): δ = 8.63 (d, *J* = 5.4 Hz, 4H), 8.57 (d, *J* = 4.8 Hz, 6H), 8.56 (s, 6H), 7.94 (s, 6H), 7.84 (d, *J* = 8.0 Hz, 4H), 7.75 (d, *J* = 5.9 Hz, 4H), 7.71 (d, *J* = 8.1 Hz, 4H), 7.66 (d, *J* = 6.0 Hz, 6H), 3.19 (q, *J* = 7.2 Hz, 8H), 1.19 – 1.10 (m, 12H). **¹³C-NMR** (101 MHz, DMSO-*d*₆): δ = 165.21, 154.02, 150.12, 147.86, 145.58, 134.81, 133.65, 132.68, 124.89, 124.85, 123.55, 121.00, 119.74, 119.59, 51.37, 7.06 (C-B not detected). **HRMS-ESI**: calcd. for C₆₁H₄₀B₂N₁₁O₉Zn₂: 1224.1765; found: 1224.1733. **IR**: 1595, 1560, 1445, 1335, 1305, 1205, 1075, 1040, 995, 970, 935, 910, 815, 795, 775, 755, 690, 610, 565, 530, 520 cm⁻¹.

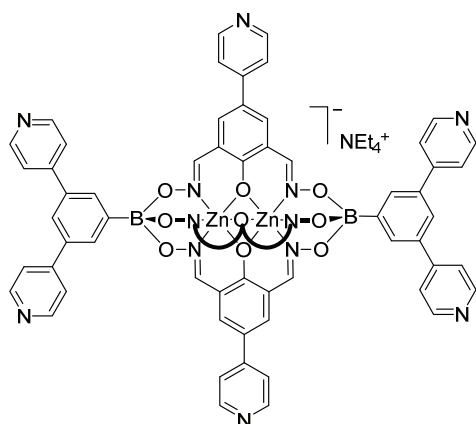
7.2.36 Clathrochelate **2.29**



A mixture of dioxime **L2** (438 mg, 1.69 mmol, 3.0 equiv.), 3,5-dibromophenylboronic acid (315 mg, 1.13 mmol, 2.0 equiv.) and Zn(OTf)₂ (410 mg, 1.13 mmol, 2.0 equiv.) in MeOH (30 ml) was heated to 70 °C until all solid dissolved. Tetraethylammonium hydroxide (565 µl, 0.84 mmol, 25% in MeOH) was added, and the solution was stirred at 70 °C for 10 min. After a second addition of tetraethylammonium

hydroxide (565 µl, 0.84 mmol, 25% in MeOH), the solution was cooled down to RT, and the solvent was removed under reduced pressure. The yellow solid was suspended in EtOH (10 ml), isolated by filtration, washed with EtOH (3 x 10 ml) and Et₂O (2 x 50 ml) and dried under vacuum to afford **2.29** as a yellow powder (590 mg, 0.39 mmol, 69%). **¹H-NMR** (400 MHz, DMSO-*d*₆): δ = 8.43 (s, 6H), 7.70 (d, *J* = 1.6 Hz, 4H), 7.63 (s, 2H), 7.53 (s, 6H), 3.19 (q, *J* = 7.2 Hz, 8H), 1.15 (t, *J* = 7.1 Hz, 12H). **¹³C-NMR** (101 MHz, DMSO-*d*₆): δ = 163.27, 153.23, 136.83, 134.02, 129.25, 120.84, 119.81, 105.02, 51.36, 7.04 (C-B not detected). **HRMS-ESI**: calcd. for C₃₆H₁₈B₂Br₇N₆O₉Zn₂: 1390.4099; found: 1390.4065. **IR**: 1605, 1575, 1540, 1480, 1470, 1435, 1390, 1350, 1335, 1325, 1220, 1205, 1190, 1090, 1070, 1045, 990, 980, 950, 895, 870, 850, 780, 730, 715, 675, 550, 520, 510 cm⁻¹.

7.2.37 Clathrochelate **2.30**



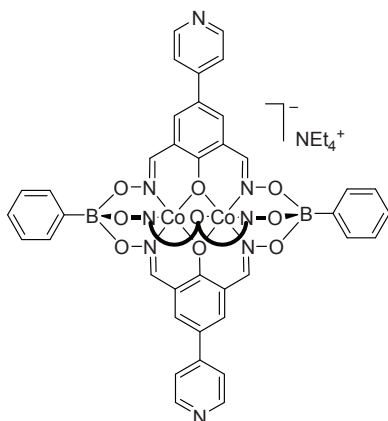
To a 25 ml pyrex vial containing **2.29** (100 mg, 66 μ mol, 1.0 equiv.), 4-pyridylboronic acid hydrate (258 mg, 2.3 mmol, 28 equiv.) and K_3PO_4 (195 mg, 0.92 mmol, 14 equiv.) under inert atmosphere were added degassed *n*-BuOH (10 ml) and degassed toluene (10 ml). $Pd_2(dba)_3$ (6.04 mg, 6.6 μ mol, 0.1 equiv.) and SPhos (5.41 mg, 13.2 μ mol, 0.2 equiv.) were then added and the system was cycled two times with nitrogen, and the sealed vial was heated for 12 h at 120 $^{\circ}C$. After cooling to RT, the

reaction mixture was filtered through Celite, and was washed with *n*-BuOH (5 ml), MeOH (20 ml) and H_2O (200 ml). The filtrate was then concentrated to half its volume and the resulting precipitate was isolated by filtration, washed with H_2O (2 x 50 ml) and Et_2O (100 ml). The crude product was suspended in a mixture of MeOH (10 ml) and MeCN (10 ml) and tetraethylammonium hydroxide (44 μ l, 66 μ mol, 25% in MeOH) was added, leading to a complete dissolution of all material. The solvents were removed under reduced pressure and the solid was suspended in EtOH (8 ml), isolated by filtration, washed with EtOH (2 x 5 ml) and Et_2O (2 x 30 ml) and dried under vacuum to afford **2.30** as a pale-yellow powder (84 mg, 56 μ mol, 85%). **1H -NMR** (400 MHz, $DMSO-d_6$): δ = 8.70 (d, J = 5.8 Hz, 8H), 8.62 (s, 6H), 8.56 (d, J = 5.8 Hz, 6H), 8.19 – 8.12 (m, 4H), 8.03 (s, 2H), 7.96 (s, 6H), 7.87 (d, J = 5.9 Hz, 8H), 7.65 (d, J = 6.0 Hz, 6H), 3.19 (q, J = 7.2 Hz, 8H), 1.15 (t, J = 7.1 Hz, 12H). **^{13}C -NMR** (101 MHz, $DMSO-d_6$): δ = 165.26, 154.31, 150.19, 150.11, 148.03, 145.56, 136.51, 133.74, 131.18, 123.61, 123.50, 121.54, 119.72, 119.59, 51.37, 7.05 (C-B not detected). **HRMS-ESI**: calcd. for $C_{71}H_{46}B_2N_{13}O_9Zn_2$: 1378.2302; found: 1378.2233. **IR**: 1595, 1555, 1445, 1400, 1335, 1305, 1215, 1190, 1075, 1035, 970, 915, 885, 820, 795, 775, 750, 685, 635, 615, 585, 565, 530, 520, 510 cm^{-1} .

7.2.38 Coordination polymer **2.31**

CP **2.31** was prepared in multiple batches. The individual reactions were carried out in sealed 7 ml microwave vials as follows: $[Zn(H_2O)_6](ClO_4)_2$ (20 mg, 54 μ mol) was added to a solution of complex **2.1** (30 mg, 27 μ mol) in DMF (5.0 mL). The resulting mixture was briefly sonicated before the vial was placed for 48 h into an oil bath at 120 $^{\circ}C$. The vial was then allowed to cool to room temperature to induce crystallization. After 2 days, the resulting yellow crystals were washed with DMF (3 x 5 mL) before being isolated by filtration and dried under vacuum for 3 days (31 mg, 89%). **IR**: 2950, 1670, 1610, 1445, 1385, 1329, 1220, 1202, 1080, 1035, 995, 931, 838, 785, 770, 700, 660 cm^{-1} .

7.2.39 Clathrochelate 2.32



A mixture of dioxime **L3** (50 mg, 0.19 mmol, 3.0 equiv.) and phenylboronic acid (16 mg, 0.13 mmol, 2.0 equiv.) were dissolved in MeOH (10 ml). $[\text{Co}(\text{H}_2\text{O})_6](\text{ClO}_4)_2$ (60 mg, 0.13 mmol, 2.0 equiv.) was added and the orange solution was heated at 50 °C for 15 min. The solvent was removed under reduced pressure and the yellow solid was suspended in EtOH (10 ml), isolated by filtration and washed with EtOH (10 ml) and Et₂O (20 ml). The yellow solid was then suspended in a mixture of MeOH (10 ml) and MeCN (10 ml) and tetraethylammonium

hydroxide (405 µl, 0.61 mmol, 25% in MeOH) was added, and the solution was stirred at RT for 1 h. After removal of the solvents under reduced pressure the solid was suspended in EtOH (8 ml), isolated by filtration, washed with cold EtOH (3 x 5 ml) and Et₂O (2 x 50 ml) and dried under vacuum to afford **2.32** as an orange powder (57 mg, 0.05 mmol, 76%). **HRMS-ESI:** Calcd for C₅₁H₃₄B₂N₉O₉Co₂: 1056.1346; Found : 1056.1329.

7.2.40 Complex 2.33

In a 5-mm NMR tube, a solution of $[\text{Pt}(\text{dppp})](\text{OTf})_2$ (2 mg) in MeOH (1 ml) was layered onto a solution of **2.32** (5 mg, 4.2 µmol) in a mixture of 1,2,4-trichlorobenzene (1 ml) and DMF (0.7 ml). X-ray quality, transparent plate crystals were obtained over the course of 2 weeks.

7.2.41 Complex 2.34

In a NMR tube, $[\text{Pt}(\text{dcpm})](\text{OTf})_2$ (6.55 mg, 7.26 µmol, 2.1 equiv.) was added to a solution of **2.19** (5.0 mg, 3.46 µmol, 1.0 equiv.) in DMSO-*d*₆ (0.75 ml). The solution was kept at 50 °C for 12 hours, and the reaction was monitored by ¹H and ³¹P NMR by recording a NMR spectrum every hour. **¹H-NMR** (400 MHz, DMSO-*d*₆): δ = 9.29 (s, 4H), 9.18 (s, 4H), 8.65 – 8.26 (m, 16H), 8.09 (s, 2H), 7.88 (s, 2H), 7.35 (s, 2H), 6.88 (s, 2H), 6.30 (s, 2H), 4.21 (s, 4H), 2.44 – 1.30 (m, 91H), 1.27 (s, 9H), 0.58 (s, 9H), -0.12 (s, 9H). **³¹P-NMR** (162 MHz, DMSO-*d*₆): δ = -49.54 (dd, J = 1316.2 Hz).

7.2.42 Complex 2.35

In a NMR tube, $[\text{Pt}(\text{dppm})](\text{OTf})_2$ (6.37 mg, 7.26 µmol, 2.1 equiv.) was added to a solution of **2.19** (5.0 mg, 3.46 µmol, 1.0 equiv.) in DMSO-*d*₆ (0.75 ml). The solution was kept at 50 °C for 12 hours, and the reaction was monitored by ¹H and ³¹P NMR by recording a NMR spectrum every hour. **¹H-NMR** (400 MHz, DMSO-*d*₆): δ = 9.15 (s, 4H), 9.08 (s, 4H), 8.47 – 7.84 (m, 27H), 7.83 – 7.41 (m, 25H), 7.32 (s,

2H), 6.80 (s, 2H), 6.23 (s, 2H), 5.57 (s, 4H), 1.26 (s, 9H), 0.52 (s, 9H), -0.20 (s, 9H). ³¹P-NMR (162 MHz, DMSO-*d*₆): δ = -57.44 (dd, J = 1391 Hz).

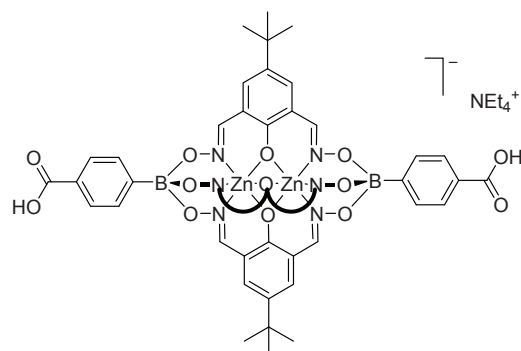
7.2.43 Coordination polymers 2.36 and 2.37

In a 5-ml pyrex vial, **2.26** (10 mg, 8.4 μmol, 1.0 equiv.) and [Co(H₂O)₆](NO₃)₂ (10 mg, 34 μmol, 4.0 equiv.) were dissolved in DMF (4 ml). The tube was sealed and was heated at 120 °C for 4 d. After cooling to RT, the solvent was carefully removed with a syringe and fresh DMF (5 ml) was slowly added to immerse all crystals. This operation was repeated every 12 hours for four times. The single-crystals of **2.36** were then harvested by filtration, washed with DMF (2 x 100 ml) and dried in air for 6 hours to yield **2.36** and/or **2.37** as bright red single-crystals (6 mg).

7.2.44 Coordination polymer 2.38

In a 5-mm NMR tube, a solution of CoCl₂ (5 mg) in MeOH (1 ml) was layered onto a solution of **2.26** (5 mg, 4.2 μmol) in a mixture of 1,2-dichlorobenzene (1 ml) and DMF (0.7 ml). X-ray quality, bright orange crystals were obtained over the course of 3 weeks.

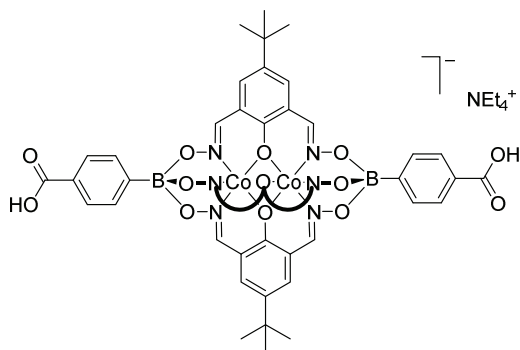
7.2.45 Clathrochelate 3.1



A mixture of oxime **L1** (1.0 g, 4.23 mmol, 3.0 equiv.), 4-carboxyphenylboronic acid (470 mg, 2.83 mmol, 2.0 equiv.) and Zn(OTf)₂ (1.025 g, 2.83 mmol, 2.0 equiv.) in a mixture of MeOH (30 ml) and EtOH (30 ml) was heated to 70 °C until all solid dissolved. Tetraethylammonium hydroxide (1.41 ml, 2.11 mmol, 25% in MeOH) was added, and the solution was stirred at 70 °C for 10 min. After a

second addition of tetraethylammonium hydroxide (1.41 ml, 2.11 mmol, 25% in MeOH), the solution was cooled down to RT, and was concentrated to 20 ml. The yellow precipitate was isolated by filtration, washed with EtOH (3 x 10 ml) and Et₂O (2 x 50 ml) and dried under vacuum to afford **3.1** as a pale yellow powder (1.0 g, 0.82 mmol, 87%). ¹H-NMR (400 MHz, DMSO-*d*₆): δ = 12.56 (s, 2H), 8.38 (s, 6H), 7.83 (d, J = 8.2 Hz, 4H), 7.76 (d, J = 8.3 Hz, 4H), 7.33 (s, 6H), 3.18 (q, J = 7.2 Hz, 8H), 1.22 (s, 27H), 1.18 – 1.09 (m, 12H). ¹³C-NMR (101 MHz, DMSO-*d*₆): δ = 168.13, 162.42, 154.08, 137.04, 132.26, 131.83, 128.35, 127.40, 118.27, 51.37, 33.40, 31.15, 7.01 (C-B not detected). HRMS-ESI: calcd. for C₅₀H₄₉B₂N₆O₁₃Zn₂: 1093.2124; found: 1093.2112. IR: 2960, 2865, 1680, 1610, 1550, 1445, 1395, 1365, 1330, 1285, 1225, 1200, 1180, 1080, 1035, 1020, 980, 930, 855, 840, 785, 765, 725, 640, 555, 540, 525 cm⁻¹.

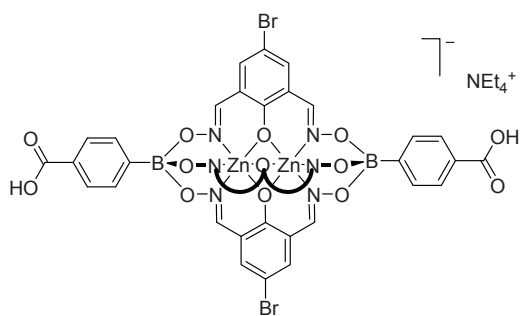
7.2.46 Clathrochelate **3.2**



A mixture of oxime **L1** (2.0 g, 8.46 mmol, 3.0 equiv.), 4-carboxyphenylboronic acid (940 mg, 5.66 mmol, 2.0 equiv.) and $[\text{Co}(\text{H}_2\text{O})_6](\text{NO}_3)_2$ (1.64 g, 5.66 mmol, 2.0 equiv.) in a mixture of MeOH (40 ml) and EtOH (40 ml) was heated to 70 °C until all solid dissolved. Tetraethylammonium hydroxide (1.41 ml, 2.11 mmol, 25% in MeOH) was added, and the solution

was stirred at 70 °C for 10 min. After a second addition of tetraethylammonium hydroxide (1.41 ml, 2.11 mmol, 25% in MeOH), the orange suspension was cooled down to RT, and was concentrated to 30 ml. The orange microcrystalline precipitate was isolated by filtration, washed with EtOH (3 x 20 ml) and Et₂O (2 x 50 ml) and dried under vacuum to afford **2** as a bright orange powder (3.13 g, 2.6 mmol, 92%). X-ray quality single crystals of **3.2** were obtained from a solution of the compound in a mixture of MeOH and toluene (1:1). **HRMS-ESI**: calcd. for $\text{C}_{50}\text{H}_{49}\text{B}_2\text{N}_6\text{O}_{13}\text{Co}_2$: 1081.2224; found: 1081.2225. **IR**: 2960, 2865, 1680, 1610, 1555, 1445, 1395, 1365, 1330, 1285, 1225, 1200, 1180, 1085, 1035, 1015, 985, 930, 855, 840, 790, 765, 725, 570, 540, 520 cm^{-1} .

7.2.47 Clathrochelate **3.3**

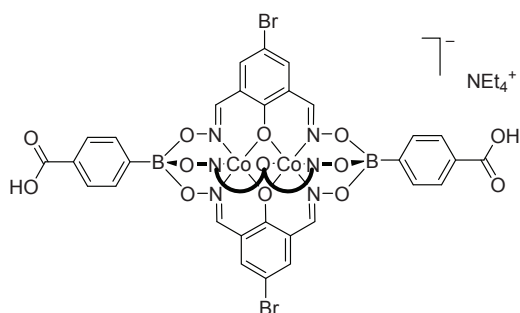


A mixture of oxime **L2** (500 mg, 1.93 mmol, 3.0 equiv.), 4-carboxyphenylboronic acid (213 mg, 1.29 mmol, 2.0 equiv.) and $\text{Zn}(\text{OTf})_2$ (467 mg, 1.29 mmol, 2.0 equiv.) in a mixture of MeOH (30 ml) and EtOH (30 ml) was heated to 70 °C until all solid dissolved. Tetraethylammonium hydroxide (645 μl , 0.97 mmol, 25% in MeOH) was added, and the

solution was stirred at 70 °C for 10 min. After a second addition of tetraethylammonium hydroxide (645 μl , 0.97 mmol, 25% in MeOH), the solution was cooled down to RT, and was concentrated to 20 ml. The yellow precipitate was isolated by filtration, washed with EtOH (3 x 10 ml) and Et₂O (2 x 50 ml) and dried under vacuum to afford **3.3** as a pale yellow powder (580 mg, 0.47 mmol, 74%). **¹H-NMR** (400 MHz, DMSO-*d*₆): δ = 12.59 (s, 4H), 8.39 (s, 6H), 7.83 (d, *J* = 7.7 Hz, 4H), 7.74 (d, *J* = 7.6 Hz, 4H), 7.52 (s, 6H), 3.19 (q, *J* = 7.2 Hz, 8H), 1.22 – 1.08 (m, 12H). **¹³C-NMR** (101 MHz, DMSO-*d*₆): δ = 163.31, 153.31, 136.88, 131.78, 127.50, 120.88, 105.06, 51.37, 7.06 (C-B not detected). **HRMS-ESI**:

calcd. for $C_{38}H_{22}B_2Br_3N_6O_{13}Zn_2$: 1162.7517; found: 1162.7533. **IR**: 2980, 1715, 1675, 1600, 1550, 1430, 1320, 1300, 1205, 1040, 1000, 970, 930, 890, 850, 765, 690, 535 cm^{-1} .

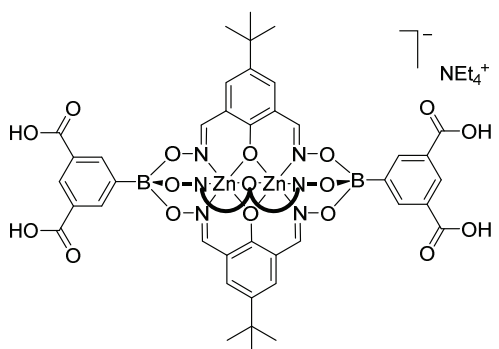
7.2.48 Clathrochelate 3.4



A mixture of oxime **L2** (500 mg, 1.93 mmol, 3.0 equiv.), 4-carboxyphenylboronic acid (213 mg, 1.29 mmol, 2.0 equiv.) and $[Co(H_2O)_6](NO_3)_2$ (375 mg, 1.29 mmol, 2.0 equiv.) in a mixture of MeOH (30 ml) and EtOH (30 ml) was heated to 70 °C until all solid dissolved. Tetraethylammonium hydroxide (645 μ l, 0.97 mmol, 25% in MeOH) was added, and

the solution was stirred at 70 °C for 10 min. After a second addition of tetraethylammonium hydroxide (645 μ l, 0.97 mmol, 25% in MeOH), the solution was cooled down to RT, and was concentrated to 20 ml. The orange precipitate was isolated by filtration, washed with EtOH (3 x 10 ml) and Et_2O (2 x 50 ml) and dried under vacuum to afford **3.4** as a bright orange powder (600 mg, 0.49 mmol, 77%). **HRMS-ESI**: calcd. for $C_{38}H_{22}B_2Br_3Co_2N_6O_{13}$: 1148.7642; found: 1148.7638. **IR**: 2975, 1675, 1600, 1550, 1505, 1480, 1430, 1315, 1285, 1200, 1175, 1120, 1080, 1040, 1020, 975, 930, 895, 855, 785, 765, 700, 665, 560, 540 cm^{-1} .

7.2.49 Clathrochelate 3.5

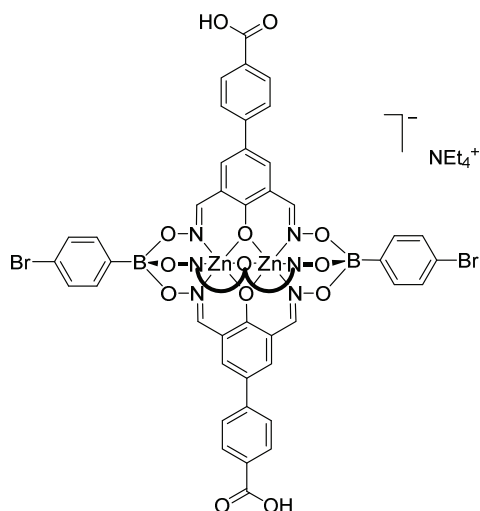


A mixture of oxime **L1** (500 mg, 2.12 mmol, 3.0 equiv.), 3,5-dicarboxyphenylboronic acid (296 mg, 1.41 mmol, 2.0 equiv.) and $Zn(OTf)_2$ (512 mg, 1.41 mmol, 2.0 equiv.) in a mixture of MeOH (30 ml) and EtOH (30 ml) was heated to 70 °C until all solid dissolved. Tetraethylammonium hydroxide (705 μ l, 1.06 mmol, 25% in MeOH) was added, and the solution was stirred at 70 °C for 10 min. After a second addition of

tetraethylammonium hydroxide (705 μ l, 1.06 mmol, 25% in MeOH), the solution was cooled down to RT, and was concentrated to 5 ml. The precipitate was isolated by filtration, washed with EtOH (3 x 10 ml) and Et_2O (2 x 30 ml) and dried under vacuum to afford **3.5** as a pale yellow powder (400 mg, 0.31 mmol, 44%). **¹H-NMR** (400 MHz, $DMSO-d_6$): δ = 12.85 (s, 4H), 8.48 (s, 4H), 8.42 (s, 6H), 8.37 (s, 2H), 7.38 (s, 6H), 3.18 (q, J = 7.3 Hz, 8H), 1.21 (s, 27H), 1.15 (ddd, J = 9.3, 5.5, 1.9 Hz, 12H). **¹³C-NMR** (101 MHz, $DMSO-d_6$): δ = 167.74, 162.45, 154.25, 137.09, 132.49, 129.15, 128.38, 118.24, 51.37, 33.44, 31.16, 7.06 (C-B not detected). **HRMS-ESI**: calcd. for $C_{52}H_{49}B_2N_6O_{17}Zn_2$: 1181.1921; found:

1181.1931. IR: 2955, 1680, 1640, 1610, 1545, 1445, 1410, 1360, 1325, 1225, 1140, 1080, 1040, 985, 935, 905, 835, 775, 720 cm^{-1} .

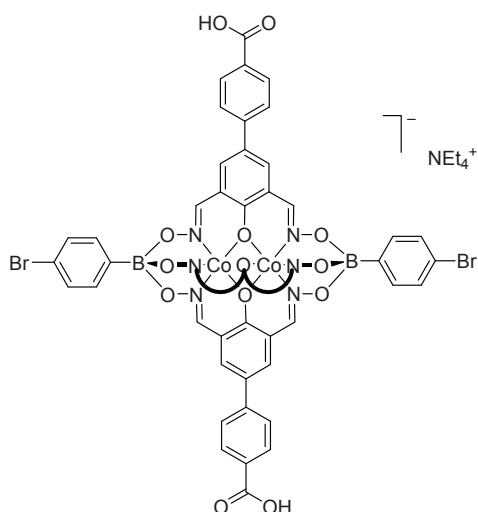
7.2.50 Clathrochelate **3.6**



A mixture of oxime **L4** (100 mg, 0.33 mmol, 3.0 equiv.), 4-bromophenylboronic acid (45 mg, 0.22 mmol, 2.0 equiv.) and $\text{Zn}(\text{OTf})_2$ (81 mg, 0.22 mmol, 2.0 equiv.) in a mixture of MeOH (15 ml) and EtOH (15 ml) was heated to 70 °C until all solid dissolved. Tetraethylammonium hydroxide (112 μl , 0.167 mmol, 25% in MeOH) was added, and the solution was stirred at 70 °C for 10 min. After a second addition of tetraethylammonium hydroxide (112 μl , 0.167 mmol, 25% in MeOH), the solution was cooled down to RT, and was concentrated to 5 ml. The yellow precipitate

was isolated by filtration, washed with EtOH (3 x 8 ml) and Et_2O (2 x 50 ml) and dried under vacuum to afford **3.6** as a bright yellow powder (580 mg, 0.47 mmol, 74%). $^1\text{H-NMR}$ (400 MHz, $\text{DMSO-}d_6$): δ = 12.91 (s, 3H), 8.52 (s, 6H), 7.97 (d, J = 8.3 Hz, 6H), 7.85 (s, 6H), 7.75 (d, J = 8.2 Hz, 6H), 7.64 (d, J = 8.2 Hz, 4H), 7.48 – 7.20 (m, 4H), 3.19 (q, J = 7.3 Hz, 8H), 1.19 – 1.11 (m, 5H). $^{13}\text{C-NMR}$ (101 MHz, $\text{DMSO-}d_6$): δ = 167.77, 164.51, 154.11, 142.97, 134.10, 133.81, 129.94, 129.29, 125.71, 125.37, 119.78, 119.44, 51.33, 7.06 (C-B not detected). HRMS-ESI: calcd. for $\text{C}_{57}\text{H}_{35}\text{B}_2\text{Br}_2\text{N}_6\text{O}_{15}\text{Zn}_2$: 1354.9277; found: 1354.9266. IR: 2975, 1720, 1690, 1600, 1550, 1480, 1445, 1335, 1300, 1195, 1100, 1075, 1040, 975, 930, 905, 855, 825, 770, 705, 535 cm^{-1} .

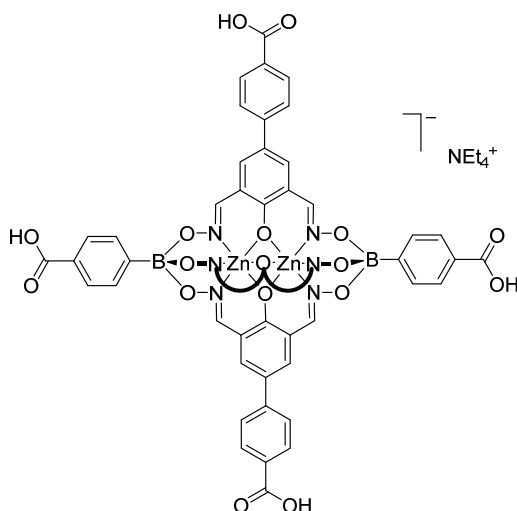
7.2.51 Clathrochelate 3.7



A mixture of oxime **L4** (436 mg, 1.45 mmol, 3.0 equiv.), 4-bromophenylboronic acid (192 mg, 0.97 mmol, 2.0 equiv.) and $[\text{Co}(\text{H}_2\text{O})_6](\text{NO}_3)_2$ (278 mg, 0.97 mmol, 2.0 equiv.) in a mixture of MeOH (30 ml) and EtOH (30 ml) was heated to 70 °C until all solid dissolved. Tetraethylammonium hydroxide (485 μl , 0.73 mmol, 25% in MeOH) was added, and the solution was stirred at 70 °C for 30 min. After a second addition of tetraethylammonium hydroxide (485 μl , 0.73 mmol, 25% in MeOH), the solution was cooled down to RT, and was concentrated to 30 ml. The orange precipitate

was isolated by filtration, washed with EtOH (3 x 20 ml) and Et_2O (2 x 50 ml) and dried under vacuum to afford **3.7** as a bright orange powder (485 mg, 0.33 mmol, 68%). **HRMS-ESI**: calcd. for $\text{C}_{57}\text{H}_{35}\text{B}_2\text{Br}_2\text{Co}_2\text{N}_6\text{O}_{15}$: 1342.9382; found: 1342.9375. **IR**: 3000, 1720, 1685, 1600, 1550, 1480, 1445, 1335, 1305, 1195, 1085, 1040, 975, 930, 905, 855, 770, 705 cm^{-1} .

7.2.52 Clathrochelate 3.8

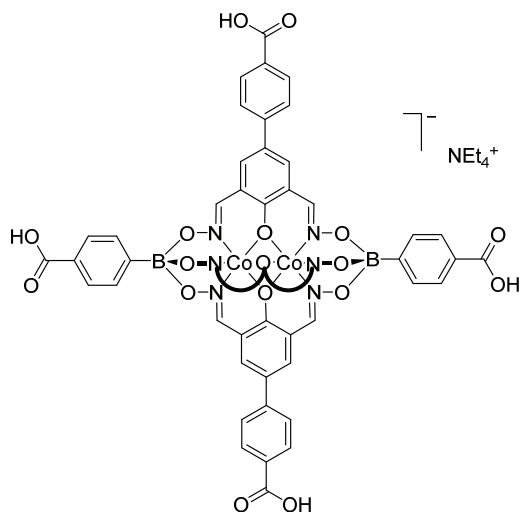


A mixture of oxime **L4** (300 mg, 1 mmol, 3.0 equiv.), 4-carboxyphenylboronic acid (108 mg, 0.66 mmol, 2.0 equiv.) and $\text{Zn}(\text{OTf})_2$ (246 mg, 0.66 mmol, 2.0 equiv.) in a mixture of MeOH (30 ml) and EtOH (30 ml) was heated to 70 °C until all solid dissolved. Tetraethylammonium hydroxide (335 μl , 0.5 mmol, 25% in MeOH) was added, and the solution was stirred at 70 °C for 10 min. After a second addition of tetraethylammonium hydroxide (335 μl , 0.5 mmol, 25% in MeOH), the solution was cooled down to RT, and was concentrated to 15 ml. The

yellow precipitate was isolated by filtration, washed with EtOH (3 x 10 ml) and Et_2O (3 x 40 ml) and dried under vacuum to afford **14** as a pale yellow powder (360 mg, 0.25 mmol, 76%). **$^1\text{H-NMR}$** (400 MHz, $\text{DMSO-}d_6$): δ = 12.77 (s, 5H), 8.54 (s, 6H), 7.97 (d, J = 8.5 Hz, 6H), 7.87 (d, J = 8.2 Hz, 4H), 7.85 (s, 6H), 7.81 (d, J = 8.3 Hz, 4H), 7.75 (d, J = 8.6 Hz, 6H), 3.18 (q, J = 7.2 Hz, 8H), 1.21 – 1.09 (m, 12H). **$^{13}\text{C-NMR}$** (101 MHz, $\text{DMSO-}d_6$): δ = 168.12, 167.14, 154.17, 143.10, 133.86, 131.83, 129.94, 128.55,

125.69, 125.39, 119.80, 119.47, 99.51, 51.34, 7.06 (C-B not detected). **HRMS-ESI:** Calcd for $C_{59}H_{37}B_2N_6O_{19}Zn_2$: 1287.0869; found: 1287.0889. **IR:** 3085, 1710, 1675, 1605, 1555, 1450, 1320, 1290, 1215, 1080, 1035, 1020, 970, 930, 905, 855, 770, 740, 705 cm^{-1} .

7.2.53 Clathrochelate **3.9**



A mixture of oxime **L4** (150 mg, 0.5 mmol, 3.0 equiv.), 4-carboxyphenylboronic acid (55 mg, 0.33 mmol, 2.0 equiv.) and $[Co(H_2O)_6](NO_3)_2$ (97 mg, 0.33 mmol, 2.0 equiv.) in a mixture of MeOH (10 ml) and EtOH (30 ml) was heated to 70 °C until all solid dissolved. Tetraethylammonium hydroxide (167 μ l, 0.25 mmol, 25% in MeOH) was added, and the solution was stirred at 70 °C for 10 min. After a second addition of tetraethylammonium hydroxide (167 μ l, 0.5 mmol, 25% in MeOH), the solution was cooled down to RT,

and was concentrated to 10 ml. The yellow precipitate was isolated by filtration, washed with EtOH (3 x 10 ml) and Et₂O (3 x 40 ml) and dried under vacuum to afford **3.9** as an orange powder (161 mg, 0.11 mmol, 69%). **HRMS-ESI:** Calcd for $C_{59}H_{37}B_2Co_2N_6O_{19}$: 1273.0981; found: 1273.0973. **IR:** 2985, 1710, 1600, 1550, 1445, 1390, 1335, 1300, 1205, 180, 1085, 1035, 1015, 955, 930, 910, 855, 765, 705, 655, 565, 540 cm^{-1} .

7.2.54 MOF **3.10**

In a 5-ml pyrex vial, **3.1** (10 mg, 8.2 μ mol, 1.0 equiv.) and $[Zn(H_2O)_6](NO_3)_2$ (9.8 mg, 32.8 μ mol, 3.7 equiv.) were dissolved in DMF (2 ml) and 1,2,4-trichlorobenzene (2 ml). The tube was sealed and was heated at 120 °C for 2 d. After cooling to RT, the single-crystals were harvested by filtration, washed with DMF (3 x 100 ml) and air-dried for 4 h to yield **3.10** as yellow powder (11.1 mg, approx. 72% based on **3.1**). **IR:** 2950, 2865, 1655, 1610, 1540, 1445, 1395, 1365, 1325, 1280, 1220, 1200, 1140, 1075, 1035, 1020, 980, 925, 860, 840, 770, 730, 680, 635, 565 cm^{-1} .

7.2.55 MOF **3.11**

In a 5-ml pyrex vial, **3.1** (10 mg, 8.2 μ mol, 1.0 equiv.) and $[Zn(H_2O)_6](NO_3)_2$ (9.8 mg, 32.8 μ mol, 3.7 equiv.) were dissolved in DMF (2 ml) and 1,2-dichlorobenzene (2 ml). The tube was sealed and was heated at 120 °C for 2 d. After cooling to RT, the single-crystals were harvested by filtration, washed with DMF (3 x 100 ml) and air-dried for 4 h to yield **3.11** as yellow powder (10.6 mg, approx.

75% based on **3.1**). IR: 2960, 2865, 1610, 1585, 1445, 1395, 1365, 1325, 1280, 1240, 1225, 1205, 1140, 1080, 1035, 1015, 990, 930, 860, 840, 775, 730, 680, 635, 535 cm⁻¹.

7.2.56 MOF 3.12

In a 5-ml pyrex vial, **3.2** (10 mg, 8.2 μmol, 1.0 equiv.) and [Zn(H₂O)₆](NO₃)₂ (9.8 mg, 32.8 μmol, 4 equiv.) were dissolved in DMF (2 ml) and 1,2-dichlorobenzene (2 ml). The tube was sealed and was heated at 120 °C for 2 d. After cooling to RT, the single-crystals were harvested by filtration, washed with DMF (3 x 100 ml) and air-dried for 4 h to yield **3.12** as bright orange powder (9.9 mg, approx. 80% based on **3.2**). IR: 3420, 2935, 2865, 1650, 1600, 1545, 1500, 1445, 1405, 1385, 1330, 1285, 1255, 1225, 1200, 1175, 1140, 1085, 1040, 1020, 990, 930, 860, 840, 775, 730, 685, 660, 565 cm⁻¹.

7.2.57 MOF 3.13

In a 5-ml pyrex vial, **3.2** (10 mg, 8.2 μmol, 1.0 equiv.) and [Zn(H₂O)₆](NO₃)₂ (9.8 mg, 32.8 μmol, 4 equiv.) were dissolved in DMF (2 ml) and 1,2,4-trichlorobenzene (2 ml). The tube was sealed and was heated at 120 °C for 2 d. After cooling to RT, the single-crystals were harvested by filtration, washed with DMF (3 x 100 ml) and air-dried for 4 h to yield **3.13** as bright orange powder (10.6 mg, 82% based on **3.2**). IR: 3420, 2950, 2865, 1650, 1605, 1545, 1500, 1445, 1385, 1330, 1285, 1255, 1200, 1175, 1140, 1085, 1040, 1020, 985, 930, 860, 840, 775, 730, 685, 660, 570 cm⁻¹.

7.2.58 MOF 3.14

In a 5-ml pyrex vial, **3.4** (10 mg, 7.8 μmol, 1.0 equiv.) and [Zn(H₂O)₆](NO₃)₂ (9.3 mg, 31.2 μmol, 4 equiv.) were dissolved in DMF (2 ml) and DEF (2 ml). The tube was sealed and was heated at 120 °C for 2 d. After cooling to RT, the single-crystals were harvested by filtration, washed with DEF (100 ml) and DMF (2 x 100 ml) and air-dried for 4 h to yield **3.14** as bright orange crystals (10.5 mg, approx. 55% based on **3.4**). IR: 3400, 2930, 2870, 1650, 1600, 1540, 1500, 1435, 1385, 1325, 1255, 1205, 1375, 1145, 1095, 1080, 1035, 1020, 975, 930, 895, 860, 840, 770, 720, 700, 660, 555, 535 cm⁻¹.

7.2.59 MOF 3.15

In a 5-ml pyrex vial, **3.6** (10 mg, 6.7 μmol, 1.0 equiv.) and [Zn(H₂O)₆](NO₃)₂ (7.8 mg, 26.9 μmol, 4 equiv.) were dissolved in DMF (2 ml) and DMSO (2 ml). The tube was sealed and was heated at 120 °C for 5 d. After cooling to RT, the single-crystals were harvested by filtration, washed with DMF (100 ml) and air-dried for 2 h to yield **3.15** as yellow powder (7.2 mg, approx. 55% based on **3.6**).

7.2.60 Zr-MOF 3.16

In a 5-ml pyrex vial, ZrCl_4 (25 mg, 0.107 mmol, 1.05 equiv.) was suspended in DMF (2 ml) and was ultrasonically dissolved. **3.2** (125 mg, 0.103 mmol, 1.0 equiv.) in DMF (2 ml) was added, and the tube was sealed. After 3 d at 120 °C, the precipitate was isolated by filtration, washed with DMF (3 x 100 ml) and air-dried for 4 h to yield **3.16** as an orange powder (106 mg). IR: 2950, 2865, 1650, 1610, 1555, 1445, 1410, 1365, 1330, 1280, 1205, 1180, 1140, 1080, 1040, 1020, 990, 930, 840, 770, 720, 635, 570 cm^{-1} .

7.2.61 Zr-MOF 3.17

In a 5-ml pyrex vial, ZrCl_4 (24 mg, 0.103 mmol, 1.09 equiv.) was suspended in DMF (2 ml) and was ultrasonically dissolved. **3.4** (120 mg, 0.094 mmol, 1.0 equiv.) in DMF (2 ml) was added, and the tube was sealed. After 3 d at 120 °C, the precipitate was isolated by filtration, washed with DMF (3 x 100 ml) and air-dried for 4 h to yield **3.17** as an orange powder (110 mg). IR: 2925, 1650, 1600, 1540, 1500, 1435, 1410, 1385, 1325, 1255, 1205, 1180, 1145, 1080, 1035, 1020, 975, 935, 895, 860, 770, 700, 660, 550, 535 cm^{-1} .

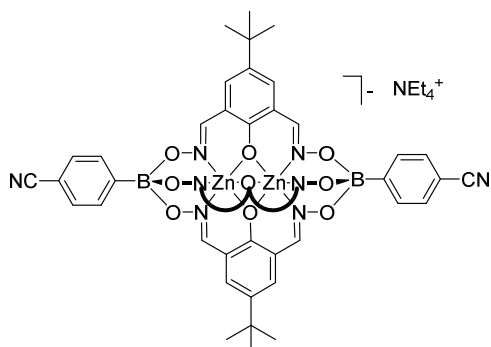
7.2.62 Zr-MOF 3.18

In a 5-ml pyrex vial, ZrCl_4 (22 mg, 0.094 mmol, 1.05 equiv.) was suspended in DMF (2 ml) and was ultrasonically dissolved. **3.7** (120 mg, 0.089 mmol, 1.0 equiv.) in DMF (2 ml) was added, and the tube was sealed. After 3 d at 120 °C, the precipitate was isolated by filtration, washed with DMF (3 x 100 ml) and air-dried for 4 h to yield **3.18** as an orange powder (96 mg). IR : 3435, 2930, 2865, 1650, 1600, 1545, 1495, 1435, 1405, 1385, 1335, 1305, 1255, 1220, 1200, 1090, 1060, 1040, 1010, 980, 930, 910, 865, 820, 785, 710, 660, 565 cm^{-1} .

7.2.63 Zr-MOF 3.19

In a 5-ml pyrex vial, ZrCl_4 (21 mg, 0.090 mmol, 1.05 equiv.) was suspended in DMF (2 ml) and was ultrasonically dissolved. **3.9** (120 mg, 0.085 mmol, 1.0 equiv.) in DMF (2 ml) was added, and the tube was sealed. After 3 d at 120 °C, the precipitate was isolated by filtration, washed with DMF (3 x 100 ml) and air-dried for 4 h to yield **3.19** as an orange powder (80 mg). IR : 3420, 2930, 2865, 1650, 1600, 1540, 1500, 1435, 1405, 1385, 1335, 1300, 1255, 1215, 1180, 1150, 1095, 1060, 1040, 1020, 980, 935, 910, 865, 780, 710, 660 cm^{-1} .

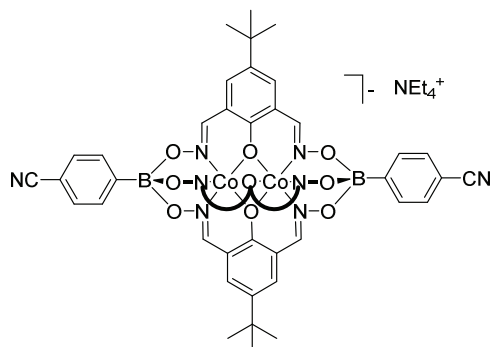
7.2.64 Clathrochelate 4.1



A mixture of dioxime **L1** (100 mg, 0.423 mmol, 3.0 equiv.), 4-cyanophenylboronic acid (41.5 mg, 0.283 mmol, 2.0 equiv.) and $\text{Zn}(\text{OTf})_2$ (105.5 mg, 0.283 mmol, 2.0 equiv.) in a mixture of MeOH (30 ml) and EtOH (30 ml) was heated to 70 °C until all solids had dissolved. Tetraethylammonium hydroxide (141 μl , 0.211 mmol, 25% in MeOH) was added, and the solution was stirred at 70 °C for 20 min. After a second

addition of tetraethylammonium hydroxide (141 μl , 0.211 mmol, 25% in MeOH), the solution was cooled down to RT and concentrated to 5 ml. The yellow precipitate was isolated by filtration, washed with EtOH (3 x 5 ml) and Et_2O (2 x 50 ml) and dried under vacuum to afford **4.1** as a yellow powder (135 mg, 0.114 mmol, 81%). **$^1\text{H-NMR}$** (400 MHz, $\text{DMSO-}d_6$): δ = 8.39 (s, 6H), 7.83 (d, J = 7.7 Hz, 4H), 7.67 (d, J = 7.8 Hz, 4H), 7.33 (s, 6H), 3.13 (q, J = 7.2 Hz, 8H), 1.21 (s, 27H), 1.15 (t, J = 7.1 Hz, 12H). **$^{13}\text{C-NMR}$** (101 MHz, $\text{DMSO-}d_6$): δ = 162.51, 154.40, 137.23, 132.64, 132.50, 130.17, 119.99, 118.27, 108.72, 51.456, 33.47, 31.21, 7.07 (C-B not detected). **HRMS-ESI**: Calcd. for $\text{C}_{50}\text{H}_{47}\text{B}_2\text{N}_8\text{O}_9\text{Zn}_2$: 1057.2216; found: 1057.2269. **IR**: 2960, 2865, 2220, 1610, 1550, 1445, 1395, 1365, 1330, 1285, 1225, 1205, 1150, 1080, 1040, 1000, 930, 840, 785, 775, 690, 635, 625, 565, 525 cm^{-1} .

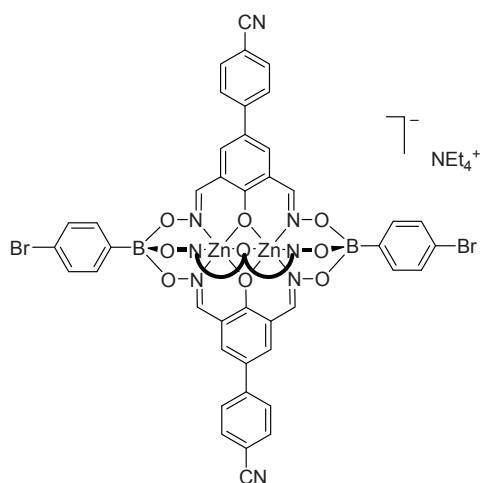
7.2.65 Clathrochelate 4.2



A mixture of dioxime **L1** (200 mg, 0.846 mmol, 3.0 equiv.), 4-cyanophenylboronic acid (83 mg, 0.564 mmol, 2.0 equiv.) and $[\text{Co}(\text{H}_2\text{O})_6](\text{NO}_3)_2$ (164 mg, 0.564 mmol, 2.0 equiv.) in a mixture of MeOH (30 ml) and EtOH (30 ml) was heated to 70 °C until all solids had dissolved. Tetraethylammonium hydroxide (282 μl , 0.423 mmol, 25% in MeOH) was added, and the solution was stirred at 70 °C for 20 min. After a second

addition of tetraethylammonium hydroxide (282 μl , 0.423 mmol, 25% in MeOH), the solution was cooled down to RT, and was concentrated to 5 ml. The orange precipitate was isolated by filtration, washed with EtOH (3 x 8 ml) and Et_2O (2 x 50 ml) and dried under vacuum to afford **4.2** as an orange powder (254 mg, 0.216 mmol, 77%). **HRMS-ESI**: Calcd. for $\text{C}_{50}\text{H}_{47}\text{B}_2\text{Co}_2\text{N}_8\text{O}_9$: 1043.2332; found: 1043.2307. **IR**: 2960, 2220, 1740, 1610, 1550, 1450, 1395, 1365, 1330, 1285, 1225, 1205, 1085, 1040, 1020, 995, 930, 840, 785, 775, 690, 635, 625, 565, 535 cm^{-1} .

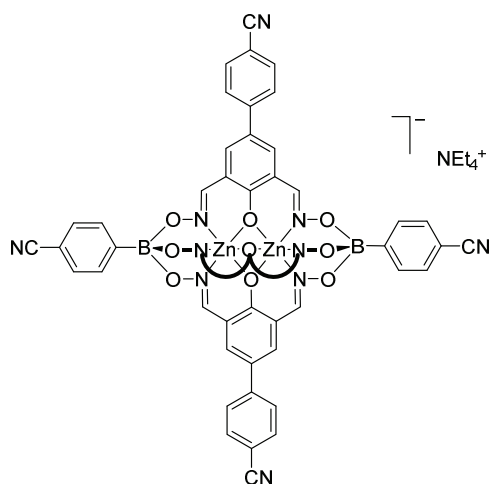
7.2.66 Clathrochelate **4.3**



A mixture of dioxime **L5** (100 mg, 0.355 mmol, 3.0 equiv.), 4-bromophenylboronic acid (47.6 mg, 0.237 mmol, 2.0 equiv.) and $\text{Zn}(\text{OTf})_2$ (86.2 mg, 0.237 mmol, 2.0 equiv.) in MeOH (40 ml) was heated to 70 °C until all solids had dissolved. Tetraethylammonium hydroxide (118 μl , 0.178 mmol, 25% in MeOH) was added, and the solution was stirred at 70 °C for 1 h. After a second addition of tetraethylammonium hydroxide (118 μl , 0.178 mmol, 25% in MeOH), the solution was cooled down to RT, and the solvent was

removed under reduced pressure. The yellow precipitate was suspended in EtOH (8 ml), isolated by filtration, washed with EtOH (3 x 10 ml) and Et_2O (2 x 50 ml) and dried under vacuum to afford **4.3** as a yellow powder (125 mg, 0.088 mmol, 74%). $^1\text{H-NMR}$ (400 MHz, $\text{DMSO}-d_6$): δ = 8.51 (s, 6H), 7.91 – 7.85 (m, 12H), 7.82 (d, J = 8.3 Hz, 6H), 7.62 (d, J = 7.9 Hz, 4H), 7.43 (d, J = 7.8 Hz, 4H), 3.19 (q, J = 7.3 Hz, 8H), 1.15 (tt, J = 7.0, 2.9 Hz, 12H). $^{13}\text{C-NMR}$ (101 MHz, $\text{DMSO}-d_6$): δ = 164.83, 154.07, 143.33, 134.05, 133.94, 132.79, 129.31, 126.03, 124.81, 119.81, 119.53, 119.05, 108.62, 51.37, 7.04. (C-B not detected). **HRMS-ESI**: Calcd. for $\text{C}_{57}\text{H}_{32}\text{B}_2\text{Br}_2\text{N}_9\text{O}_9\text{Zn}_2$: 1297.9440; found: 1297.9434. **IR**: 2985, 2225, 1600, 1545, 1445, 1340, 1305, 1200, 1180, 1080, 1040, 975, 930, 905, 840, 820, 795, 770, 735, 705, 680, 615, 545, 535 cm^{-1} .

7.2.67 Clathrochelate **4.4**

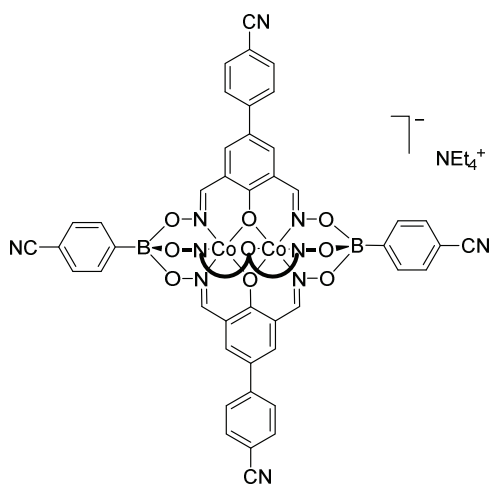


A mixture of dioxime **L5** (100 mg, 0.355 mmol, 3.0 equiv.), 4-cyanophenylboronic acid (35 mg, 0.237 mmol, 2.0 equiv.) and $\text{Zn}(\text{OTf})_2$ (86.2 mg, 0.237 mmol, 2.0 equiv.) in MeOH (40 ml) was heated to 70 °C until all solids had dissolved. Tetraethylammonium hydroxide (118 μl , 0.178 mmol, 25% in MeOH) was added, and the solution was stirred at 70 °C for 1 h. After a second addition of tetraethylammonium hydroxide (118 μl , 0.178 mmol, 25% in MeOH), the solution was cooled down to RT, and the solvent was

removed under reduced pressure. The yellow precipitate was suspended in EtOH (8 ml), isolated by filtration, washed with EtOH (3 x 8 ml) and Et_2O (2 x 50 ml) and dried under vacuum to afford **4.4** as a

yellow powder (106 mg, 0.08 mmol, 68%). **¹H-NMR** (400 MHz, DMSO-*d*₆): δ = 8.54 (s, 6H), 7.92 – 7.78 (m, 22H), 7.69 (d, *J* = 7.6 Hz, 4H), 3.19 (q, *J* = 7.2 Hz, 8H), 1.15 (t, *J* = 6.7 Hz, 12H). **¹³C-NMR** (101 MHz, DMSO-*d*₆): δ = 164.89, 154.38, 143.33, 134.14, 132.85, 132.56, 130.26, 126.10, 124.94, 119.87, 119.51, 119.10, 108.90, 108.70, 51.41, 7.08 (C-B not detected). **HRMS-ESI**: Calcd. for C₅₉H₃₂B₂N₁₁O₉Zn₂: 1192.1139; found: 1192.1090. **IR**: 2985, 2220, 1600, 1555, 1545, 1480, 1445, 1390, 1335, 1305, 1245, 1205, 1180, 1075, 1035, 1020, 975, 930, 910, 830, 795, 775, 735, 690, 645, 615, 560, 545, 530 cm⁻¹.

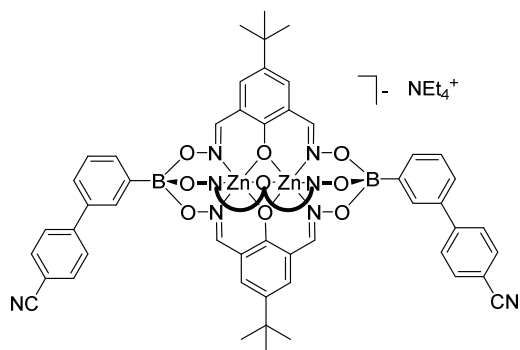
7.2.68 Clathrochelate 4.5



A mixture of dioxime **L5** (120 mg, 0.426 mmol, 3.0 equiv.), 4-cyanophenylboronic acid (42 mg, 0.284 mmol, 2.0 equiv.) and [Co(H₂O)₆](NO₃)₂ (82 mg, 0.284 mmol, 2.0 equiv.) in MeOH (40 ml) was heated to 70 °C until all solids had dissolved. Tetraethylammonium hydroxide (142 μ l, 0.213 mmol, 25% in MeOH) was added, and the solution was stirred at 70 °C for 1 h. After a second addition of tetraethylammonium hydroxide (142 μ l, 0.213 mmol, 25% in MeOH), the solution was cooled down to RT, and the solvent was

removed under reduced pressure. The orange precipitate was suspended in EtOH (10 ml), isolated by filtration, washed with EtOH (3 x 12 ml) and Et₂O (2 x 50 ml) and dried under vacuum to afford **4.5** as an orange powder (150 mg, 0.114 mmol, 81%). **HRMS-ESI**: Calcd for C₅₉H₃₂B₂Co₂N₁₁O₉: 1178.1254; found: 1178.1234. **IR**: 3450, 2970, 2225, 1735, 1600, 1545, 1445, 1365, 1340, 1305, 1205, 1080, 1040, 1020, 985, 935, 910, 835, 800, 775, 735, 690, 615, 550 cm⁻¹.

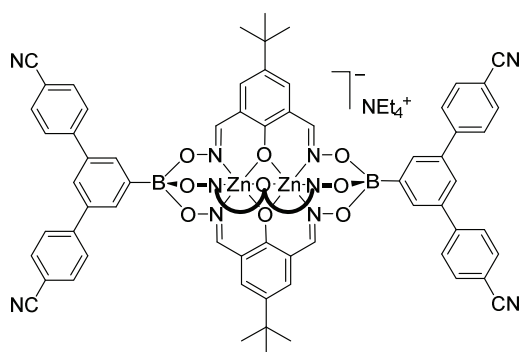
7.2.69 Clathrochelate 4.6



Under inert atmosphere, degassed *n*-BuOH (10 ml) and degassed toluene (10 ml) were added to a 25 ml pyrex vial containing **2.15** (100 mg, 77 μ mol, 1.0 equiv.), 4-cyanophenylboronic acid (91 mg, 0.62 mmol, 8 equiv.) and K₃PO₄ (66 mg, 0.31 mmol, 4.0 equiv.). Pd₂(dba)₃ (3.54 mg, 3.9 μ mol, 0.05 equiv.) and SPhos (3.2 mg, 7.7 μ mol, 0.1 equiv.) were then added, and the system was cycled two times with nitrogen. The sealed vial was then heated for 12 h at 90 °C. After cooling to RT, the reaction mixture

was filtered through Celite, and washed with *n*-BuOH (5 ml), acetone (20 ml) and H₂O (200 ml). The filtrate was then concentrated to half its volume and the resulting precipitate was isolated by filtration, washed with H₂O (2 x 50 ml) and Et₂O (100 ml), and dried under vacuum to afford **4.6** as a yellow powder (85 mg, 70 μ mol, 91%). **¹H-NMR** (400 MHz, DMSO-*d*₆): δ = 8.40 (s, 6H), 7.99 (s, 2H), 7.91 (dd, *J* = 8.4 Hz, 8H), 7.74 (d, *J* = 7.2 Hz, 2H), 7.56 (d, *J* = 7.5 Hz, 2H), 7.38 (t, *J* = 7.5 Hz, 2H), 7.33 (s, 6H), 3.18 (q, *J* = 7.2 Hz, 8H), 1.22 (s, 27H), 1.14 (t, *J* = 7.2 Hz, 12H). **¹³C-NMR** (101 MHz, DMSO-*d*₆): δ = 162.44, 154.04, 146.39, 136.98, 136.30, 132.75, 132.60, 132.19, 130.46, 127.45, 127.24, 124.84, 119.09, 118.31, 109.23, 51.35, 33.41, 31.16, 7.05 (C-B not detected). **HRMS-ESI**: Calcd. for C₆₂H₅₅B₂N₈O₉Zn₂: 1209.2848; found: 1209.2838. **IR**: 2955, 2870, 2225, 1605, 1550, 1505, 1445, 1395, 1365, 1325, 1280, 1240, 1225, 1185, 1140, 1075, 1050, 1035, 995, 980, 950, 900, 840, 780, 720, 685, 635, 595, 555, 525 cm⁻¹.

7.2.70 Clathrochelate 4.7



Under inert atmosphere, degassed *n*-BuOH (10 ml) and degassed toluene (10 ml) were added to a 25 ml pyrex vial containing **2.17** (100 mg, 69 μ mol, 1.0 equiv.), 4-cyanophenylboronic acid (202 mg, 1.37 mmol, 20 equiv.) and K₃PO₄ (146 mg, 0.687 mmol, 10.0 equiv.). Pd₂(dba)₃ (6.4 mg, 6.9 μ mol, 0.1 equiv.) and SPhos (5.7 mg, 13.8 μ mol, 0.2 equiv.) were then added, and the system was cycled two times with nitrogen. The sealed vial was then heated for 12 h at 90 °C. After cooling to RT, the reaction mixture was filtered through Celite, and washed with *n*-BuOH (5 ml), acetone (20 ml) and H₂O (200 ml). The filtrate was then concentrated to half its volume and the resulting precipitate was isolated by filtration, washed with H₂O (2 x 50 ml) and Et₂O (100 ml), and dried under vacuum to afford **4.7** as a yellow powder (87 mg, 70 μ mol, 89%). **¹H-NMR** (400 MHz, DMSO-*d*₆): δ = 8.44 (s, 6H), 8.07 (s, 4H), 8.04 (d, *J* = 8.1 Hz, 8H), 7.97 (d, *J* = 8.1 Hz, 8H), 7.90 (s, 2H), 7.34 (s, 6H), 3.18 (q, *J* = 7.2 Hz, 8H), 1.22 (s, 27H), 1.14 (t, *J* = 7.0 Hz, 12H). **¹³C-NMR** (101 MHz, DMSO-*d*₆): δ = 162.48, 154.24, 145.83, 137.41, 137.02, 132.76, 132.27, 131.08, 128.05, 127.80, 119.03, 118.29, 109.62, 51.36, 33.41, 31.15, 7.04 (C-B not detected). **HRMS-ESI**: Calcd. for C₇₆H₆₁B₂N₁₀O₉Zn₂: 1411.3386; found: 1411.3365. **IR**: 2955, 2865, 2225, 1675, 1605, 1555, 1505, 1450, 1395, 1365, 1330, 1285, 1240, 1225, 1180, 1140, 1070, 1035, 995, 930, 890, 835, 785, 725, 680, 635, 605, 590, 565, 555 cm⁻¹.

7.2.71 Coordination polymer 4.8

In a 5 mm-wide glass tube, a solution of AgNO_3 (10 mg) in MeOH (1.5 ml) was layered on top of a solution of **4.1** (10 mg) in nitromethane (1.5 ml) covered by a buffer layer of a 1:1 mixture of MeOH and nitromethane (2 ml). Transparent yellowish needles of **4.8** (7.4 mg) were obtained within one week. IR: 2960, 2865, 2245, 2165, 1615, 1550, 1445, 1395, 1365, 1330, 1280, 1220, 1200, 1080, 1035, 1000, 930, 875, 840, 815, 785, 775, 690, 635, 560, 540, 530 cm^{-1} .

7.2.72 Coordination polymer 4.9

In a 5 mm-wide glass tube, a solution of AgNO_3 (10 mg) in MeOH (1.5 ml) was layered on top of a solution of **4.2** (10 mg) in nitromethane (1.5 ml) covered by a buffer layer of a 1:1 mixture of MeOH and nitromethane (2 ml). Orange needles of **4.9** (8.1 mg) were obtained within one week. IR: 2955, 2860, 2250, 2225, 2165, 1610, 1555, 1450, 1395, 1365, 1330, 1265, 1210, 1090, 1020, 970, 930, 840, 825, 785, 765, 695, 655, 635, 610, 570, 560 cm^{-1} .

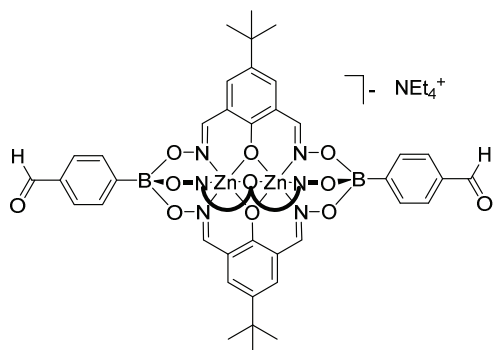
7.2.73 Coordination polymer 4.10

In a 5 mm-wide glass tube, a solution of AgOTs (10 mg) in MeOH (1.5 ml) was layered on top of a solution of **4.7** (10 mg) in nitromethane (1.5 ml) covered by a buffer layer of a 1:1 mixture of MeOH and nitromethane (2 ml). Transparent pale-yellow plates of **4.10** (4.1 mg) were obtained within one week. IR: 2955, 2865, 2235, 1680, 1610, 1555, 1505, 1450, 1395, 1365, 1330, 1285, 1240, 1225, 1185, 1145, 1070, 1035, 995, 930, 890, 835, 785, 725, 680, 640, 605, 590, 570, 555 cm^{-1} .

7.2.74 Coordination polymer 4.11

In a 5 mm-wide glass tube, a solution of AgClO_4 (10 mg) in MeOH (1.5 ml) was layered on top of a solution of **4.5** (10 mg) in 1,2-dichlorobenzene (1.5 ml) covered by a buffer layer of a 1:1 mixture of MeOH and 1,2-dichlorobenzene (2 ml). Orange plates of **4.11** (9.8 mg) were obtained within one week. IR: 3390, 2225, 1600, 1560, 1545, 1445, 1390, 1340, 1305, 1205, 1180, 1080, 1035, 1020, 980, 935, 910, 830, 800, 775, 750, 690, 655, 610, 550, 535 cm^{-1} .

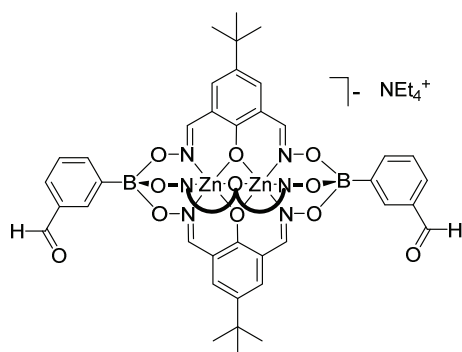
7.2.75 Clathrochelate 5.1



4-formylphenylboronic acid (85 mg, 0.56 mmol, 2.0 equiv.) and dioxime **L1** (200 mg, 0.84 mmol, 3.0 equiv.) were dissolved in EtOH (10 ml) and CH₂Cl₂ (10 ml). Zn(OTf)₂ (204 mg, 0.56 mmol, 2.0 equiv.) was added, followed by tetraethylammonium hydroxide (1.5 M in MeOH, 0.47 ml, 0.71 mmol, 2.5 equiv.), and the solution was stirred at RT for 4 h. The precipitate that formed was isolated by filtration, washed with

EtOH (4 x 5 ml) and Et₂O (50 ml) and dried under vacuum to yield **5.1** as an off-yellow powder (183 mg, 0.153 mmol, 55%). **¹H-NMR** (400 MHz, DMSO-*d*₆): δ = 9.99 (s, 2H, CHO), 8.39 (s, 6H, ONCH), 7.88 (d, *J* = 8.0 Hz, 4H, CHOCCH), 7.78 (d, *J* = 8.1 Hz, 4H, BCCCH), 7.33 (s, 6H, Ar-*H*), 3.19 (q, *J* = 7.3 Hz, 8H, NCH₂CH₃), 1.22 (s, 27H, (CH₃)₃), 1.19 – 1.11 (m, 12H, NCH₂CH₃). **¹³C-NMR** (101 MHz, DMSO-*d*₆): δ = 193.44, 162.44, 154.19, 137.04, 134.60, 132.37, 132.33, 127.78, 118.24, 51.33, 33.40, 31.15, 7.06. **HRMS-ESI**: Calcd for C₅₀H₄₉B₂N₆O₁₁Zn₂: 1059.2246; found: 1059.2037. **IR**: 2955, 2900, 2865, 1690, 1610, 1590, 1575, 1555, 1450, 1395, 1365, 1330, 1315, 1285, 1240, 1225, 1140, 1080, 1035, 990, 935, 910, 835, 775, 725, 700, 635, 625, 560, 525 cm⁻¹.

7.2.76 Clathrochelate 5.2

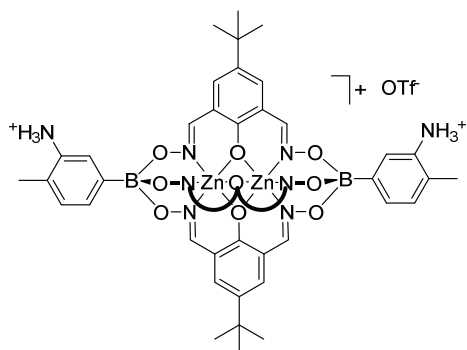


3-formylphenylboronic acid (85 mg, 0.56 mmol, 2.0 equiv.) and dioxime **L1** (200 mg, 0.84 mmol, 3.0 equiv.) were dissolved in EtOH (10 ml) and CH₂Cl₂ (10 ml). Zn(OTf)₂ (204 mg, 0.56 mmol, 2.0 equiv.) was added, followed by tetraethylammonium hydroxide (1.5 M in MeOH, 0.47 ml, 0.71 mmol, 2.5 equiv.), and the solution was stirred at RT for 4 h. The precipitate that formed was isolated by filtration, washed with EtOH (4 x 5 ml) and

Et₂O (50 ml) and dried under vacuum to yield **5.2** as an off-yellow powder (206 mg, 0.172 mmol, 62%). **¹H-NMR** (400 MHz, DMSO-*d*₆): δ = 10.04 (s, 2H), 8.40 (s, 6H), 8.21 (s, 2H), 7.99 (d, *J* = 7.3 Hz, 2H), 7.74 (d, *J* = 7.6 Hz, 2H), 7.47 (t, *J* = 7.4 Hz, 2H), 7.34 (s, 6H), 3.19 (q, *J* = 7.3 Hz, 8H), 1.22 (s, 27H), 1.19 – 1.11 (m, 12H, NCH₂CH₃). **¹³C-NMR** (101 MHz, DMSO-*d*₆): δ = 194.03, 162.43, 154.15, 138.31, 137.04, 134.78, 133.54, 132.32, 127.18, 118.26, 51.39, 33.41, 31.15, 7.06. **HRMS-ESI**: Calcd for C₅₀H₄₉B₂N₆O₁₁Zn₂: 1059.2246; found: 1059.2222. **IR**: 2955, 2900, 2865, 1690, 1610, 1590, 1575, 1555,

1450, 1395, 1365, 1330, 1315, 1285, 1240, 1225, 1140, 1080, 1035, 990, 935, 910, 835, 775, 725, 700, 635, 625, 560, 525 cm⁻¹.

7.2.77 Clathrochelate **5.3**



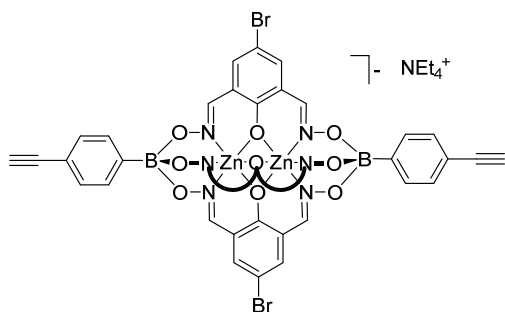
Dioxime **L1** (500 mg, 2.12 mmol, 3.0 equiv.) and 3-amino-4-methylbenzeneboronic acid (213 mg, 1.41 mmol, 2.0 equiv.) were dissolved in EtOH (20 ml). The solution was stirred under air at RT until all solids dissolved. Zn(OTf)₂ (512 mg, 1.41 mmol, 2.0 equiv.) was added to the solution, and the mixture was stirred at RT for 4 h. The orange precipitate that formed was filtered, washed with EtOH (2 x 8 ml) and Et₂O (2 x 30 ml), and

the product was dried under vacuum, affording complex **5.3** as a beige solid (514 mg, 0.423 mmol, 60%). ¹H-NMR (400 MHz, DMSO-*d*₆): δ = 9.60 (s, 6H), 8.33 (s, 6H), 7.62 (d, *J* = 1.2 Hz, 2H), 7.59 (dd, *J* = 7.5, 1.2 Hz, 2H), 7.30 (s, 6H), 7.20 (d, *J* = 7.6 Hz, 2H), 2.32 (s, 6H), 1.22 (s, 27H). ¹³C-NMR (101 MHz, DMSO-*d*₆): δ = 162.40, 153.97, 137.07, 132.23, 131.10, 129.54, 129.45, 128.07, 126.18, 118.24, 33.40, 31.15, 16.69. HRMS-ESI: Calcd for C₅₀H₅₇B₂N₈O₉Zn₂: 1065.3015; found: 1065.3025. IR: 2955, 2865, 1615, 1555, 1505, 1445, 1395, 1335, 1280, 1240, 1225, 1170, 1080, 1030, 995, 925, 840, 785, 775, 690, 640, 560, 530 cm⁻¹.

7.2.78 Complex **5.6**

In a 5-mm NMR tube, **5.3** (5.0 mg, 4.11 mmol, 1.0 equiv.) was suspended in CDCl₃ (0.75 ml), and tetraethylammonium hydroxide (1.5 M in MeOH, 5.5 μl, 8.22 mmol, 2.0 equiv.), was added. Once all solids dissolved, **5.1** (4.91 mg, 4.11 mmol, 1.0 equiv.) was added, and a NMR spectrum was recorded every hour. After 2 weeks of reaction, since no changes were observed, Sc(OTf)₃ (0.20 mg, 0.41 mmol, 0.1 equiv.) was added and the reaction was monitored by NMR.

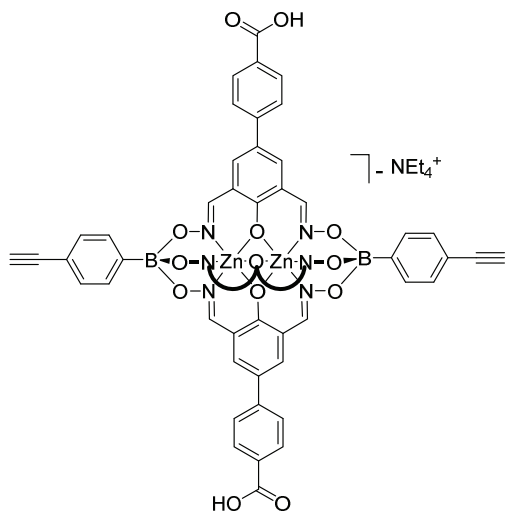
7.2.79 Clathrochelate **5.7**



A mixture of dioxime **L2** (200 mg, 0.772 mmol, 3.0 equiv.), 4-dihydroxyborophenylacetylene (75 mg, 0.515 mmol, 2.0 equiv.) and $\text{Zn}(\text{OTf})_2$ (188 mg, 0.515 mmol, 2.0 equiv.) in a mixture of MeOH (10 ml) and EtOH (10 ml) was heated to 50 °C until all solids had dissolved. Tetraethylammonium hydroxide (257 μl , 0.386 mmol, 25% in MeOH) was added, and the

solution was stirred at 50 °C for 20 min. After a second addition of tetraethylammonium hydroxide (257 μl , 0.386 mmol, 25% in MeOH), the solution was cooled down to RT, and was concentrated to 5 ml. The yellow precipitate was isolated by filtration, washed with EtOH (3 x 5 ml) and Et_2O (2 x 50 ml) and dried under vacuum to afford **5.7** as a yellow powder (200 mg, 0.159 mmol, 62%). **$^1\text{H-NMR}$** (400 MHz, $\text{DMSO-}d_6$): δ = 8.37 (s, 6H), 7.63 (d, J = 8.0 Hz, 4H), 7.51 (s, 6H), 7.34 (d, J = 8.0 Hz, 4H), 4.03 (s, 2H), 3.19 (q, J = 7.2 Hz, 8H), 1.24 – 1.04 (m, 12H). **$^{13}\text{C-NMR}$** (101 MHz, $\text{DMSO-}d_6$): δ = 163.28, 153.22, 136.80, 131.90, 129.80, 120.86, 119.30, 105.02, 84.67, 79.45, 51.37, 7.04. **HRMS-ESI**: Calcd. for $\text{C}_{40}\text{H}_{22}\text{B}_2\text{Br}_3\text{N}_6\text{O}_9\text{Zn}_2$: 1122.7721; found: 1122.7732.

7.2.80 Clathrochelate **5.8**

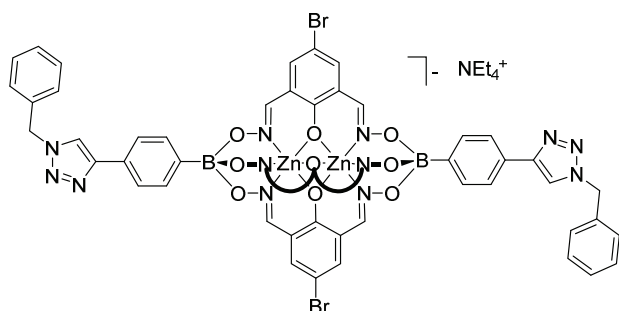


A mixture of dioxime **L4** (200 mg, 0.66 mmol, 3.0 equiv.), 4-dihydroxyborophenylacetylene (65 mg, 0.44 mmol, 2.0 equiv.) and $\text{Zn}(\text{OTf})_2$ (160 mg, 0.44 mmol, 2.0 equiv.) in a mixture of MeOH (20 ml) and EtOH (20 ml) was heated to 50 °C until all solid dissolved. Tetraethylammonium hydroxide (222 μl , 0.33 mmol, 25% in MeOH) was added, and the solution was stirred at 50 °C for 30 min. After a second addition of tetraethylammonium hydroxide (222 μl , 0.33 mmol, 25% in MeOH), the solution was cooled down to RT, and was concentrated to 5 ml.

The yellow precipitate was isolated by filtration, washed with EtOH (3 x 5 ml) and Et_2O (2 x 50 ml) and dried under vacuum to afford **5.8** as a yellow powder (190 mg, 0.138 mmol, 63%). **$^1\text{H-NMR}$** (400 MHz, $\text{DMSO-}d_6$): δ = 12.85 (s, 3H), 8.53 (s, 6H), 7.97 (d, J = 8.1 Hz, 6H), 7.84 (s, 6H), 7.75 (d, J = 8.2 Hz, 6H), 7.69 (d, J = 7.7 Hz, 4H), 7.37 (d, J = 7.6 Hz, 4H), 4.05 (s, 2H), 3.18 (q, J = 7.3 Hz, 8H), 1.20 – 1.11

(m, 12H). $^{13}\text{C-NMR}$ (101 MHz, $\text{DMSO-}d_6$): δ = 167.17, 164.53, 154.08, 143.06, 133.79, 131.95, 130.06, 129.91, 129.84, 125.66, 125.37, 119.45, 119.24, 84.71, 79.42, 51.37, 7.04.

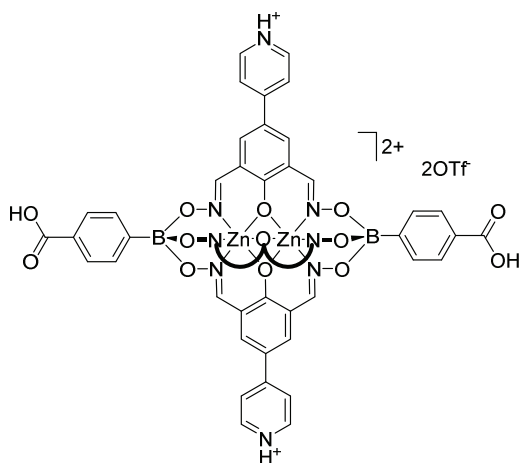
7.2.81 Clathrochelate **5.9**



In a 25 ml pyrex vial, **5.7** (50 mg, 40 μmol , 1.0 equiv.) was dissolved in DMSO (20 ml). CuI (1.9 mg, 10 μmol , 0.25 equiv.) and benzylazide (10 μl , 80 μmol , 2.0 equiv.) were added and the solution was stirred at 50 $^{\circ}\text{C}$ for 16 h. After cooling to RT, MeOH (20 ml) was added and the precipitate was

filtered off. To the filtrate was added H_2O (200 ml), and the solution was concentrated to approximately 100 ml under reduced pressure. The precipitate that formed was isolated by filtration, washed with EtOH (3 x 8 ml) and Et_2O (2 x 30 ml) and the product was dried under vacuum, yielding **5.9** as a pale yellow powder (45 mg, 30 μmol , 74%). $^1\text{H-NMR}$ (400 MHz, $\text{DMSO-}d_6$): δ = 8.56 (s, 2H), 8.39 (s, 6H), 7.84 – 7.64 (m, 8H), 7.52 (s, 6H), 7.48 – 7.30 (m, 10H), 5.64 (s, 4H), 3.18 (q, J = 7.2 Hz, 8H), 1.20 – 1.08 (m, 12H). $^{13}\text{C-NMR}$ (101 MHz, $\text{DMSO-}d_6$): δ = 163.28, 153.10, 147.57, 136.72, 136.09, 132.22, 128.77, 128.44, 128.11, 127.93, 123.38, 120.92, 120.86, 104.99, 52.96, 51.36, 7.03. **HRMS-ESI**: Calcd. for $\text{C}_{54}\text{H}_{36}\text{B}_2\text{Br}_3\text{N}_{12}\text{O}_9\text{Zn}_2$: 1388.9008; found: 1388.8961. **IR**: 2925, 1605, 1550, 1480, 1435, 1320, 1210, 1075, 1040, 995, 970, 935, 890, 840, 780, 770, 725, 700, 675, 565, 545, 525 cm^{-1} .

7.2.82 Clathrochelate **5.10**

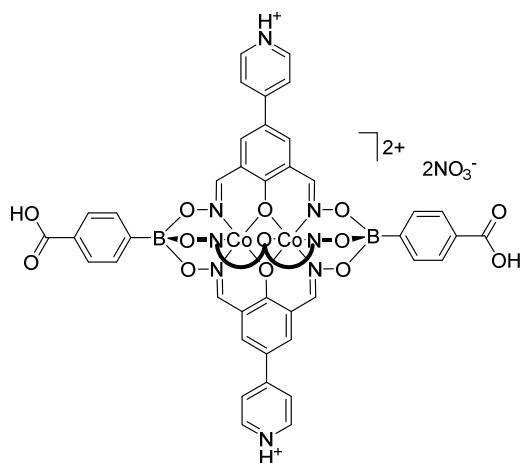


A mixture of dioxime **L3** (50 mg, 0.194 mmol, 3.0 equiv.), 4-carboxyphenylboronic acid (21 mg, 0.13 mmol, 2.0 equiv.) and $\text{Zn}(\text{OTf})_2$ (47 mg, 0.13 mmol, 2.0 equiv.) in a mixture of MeOH (30 ml) and EtOH (30 ml) was heated to 70 $^{\circ}\text{C}$ for 4 h. After cooling to RT, the solution was concentrated to 10 ml. The yellow precipitate was isolated by filtration, washed with EtOH (3 x 8 ml) and Et_2O (2 x 50 ml) and dried under vacuum to afford **5.10** as a bright yellow powder (48 mg, 0.036 mmol, 55%). $^1\text{H-NMR}$ (400

MHz, $\text{DMSO-}d_6$): δ = 8.82 (d, J = 6.3 Hz, 6H), 8.60 (s, 6H), 8.23 (s, 6H), 8.20 (d, J = 6.4 Hz, 6H), 7.88 (d, J = 8.2 Hz, 4H), 7.80 (d, J = 7.8 Hz, 4H). $^{13}\text{C-NMR}$ (101 MHz, $\text{DMSO-}d_6$): δ = 168.10, 166.89, 154.02, 143.09, 135.21, 134.09, 131.75, 128.74, 127.66, 121.11, 121.02, 120.05. **HRMS-ESI**: Calcd. for

$C_{53}H_{37}B_2N_9O_{13}Zn_2$: 579.5639 (M^{2+}); found: 579.5638. IR: 1680, 1640, 1590, 1555, 1510, 1445, 1375, 1350, 1310, 1225, 1205, 1165, 1080, 1030, 980, 935, 910, 855, 795, 775, 745, 700, 670, 635, 615, 565, 535 cm^{-1} .

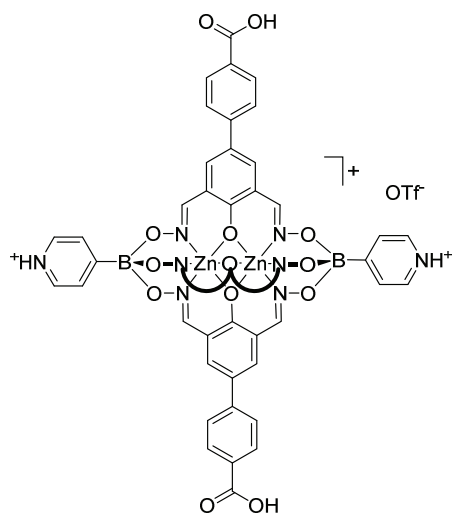
7.2.83 Clathrochelate 5.11



A mixture of dioxime **L3** (50 mg, 0.194 mmol, 3.0 equiv.), 4-carboxyphenylboronic acid (21 mg, 0.13 mmol, 2.0 equiv.) and $[Co(H_2O)_6](NO_3)_2$ (38 mg, 0.13 mmol, 2.0 equiv.) in a mixture of MeOH (30 ml) and EtOH (30 ml) was heated to 70 °C for 4 h. After cooling to RT, the solution was concentrated to 10 ml. The orange precipitate was isolated by filtration, washed with EtOH (3 x 7 ml) and Et₂O (2 x 50 ml) and dried under vacuum to afford **5.11** as a bright orange powder (58 mg, 0.046 mmol, 55%). HRMS-

ESI: Calcd. for $C_{53}H_{37}B_2N_9O_{13}Co_2$: 573.5689 (M^{2+}); found: 573.5697. IR: 1690, 1340, 1600, 1510, 1445, 1345, 1310, 1225, 1205, 1080, 1040, 1020, 980, 910, 825, 800, 775, 745, 715, 700, 615, 545, 525 cm^{-1} .

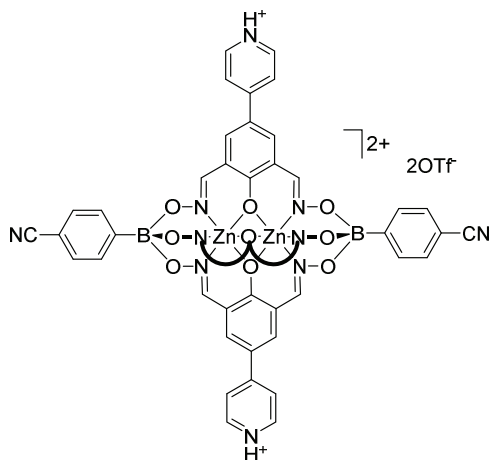
7.2.84 Clathrochelate 5.12



A mixture of dioxime **L4** (50 mg, 0.166 mmol, 3.0 equiv.), 4-pyridylboronic acid (14 mg, 0.111 mmol, 2.0 equiv.) and $Zn(OTf)_2$ (41 mg, 0.111 mmol, 2.0 equiv.) in a mixture of MeOH (10 ml) and EtOH (10 ml) was heated to 70 °C for 4 h. After cooling to RT, the solution was concentrated to 2 ml. The yellow precipitate was isolated by filtration, washed with EtOH (3 x 5 ml) and Et₂O (2 x 50 ml) and dried under vacuum to afford **5.12** as a yellow powder (45 mg, 0.034 mmol, 61%). ¹H-NMR (400 MHz, DMSO-*d*₆): δ = 8.77 (d, J = 6.1 Hz, 4H), 8.58 (s, 6H), 8.22 (d, J = 6.0 Hz, 4H), 7.97 (d, J = 8.5 Hz, 6H), 7.87 (s, 6H), 7.75 (d, J = 8.6

Hz, 6H). ¹³C-NMR (101 MHz, DMSO-*d*₆): δ = 157.33, 155.16, 142.89, 139.64, 134.53, 129.95, 129.40, 128.64, 126.02, 125.53, 125.48, 119.18. HRMS-ESI: Calcd. for $C_{55}H_{37}B_2N_8O_{15}Zn_2$: 1201.1147; found: 1201.1158. IR: 3060, 1715, 1685, 1605, 1550, 1490, 1445, 1390, 1325, 1290, 1205, 1160, 1115, 1065, 1045, 1025, 1000, 980, 940, 910, 855, 805, 775, 700, 635, 610, 575, 535 cm^{-1} .

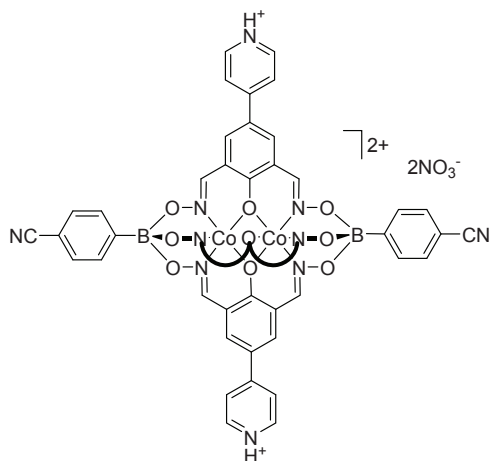
7.2.85 Clathrochelate **5.13**



A mixture of dioxime **L3** (50 mg, 0.194 mmol, 3.0 equiv.), 4-cyanophenylboronic acid (19 mg, 0.13 mmol, 2.0 equiv.) and $\text{Zn}(\text{OTf})_2$ (47 mg, 0.13 mmol, 2.0 equiv.) in a mixture of MeOH (10 ml) and EtOH (10 ml) was heated to 70 °C for 4 h. After cooling to RT, the solution was concentrated to 5 ml. The yellow precipitate was isolated by filtration, washed with EtOH (3 x 5 ml) and Et₂O (2 x 30 ml) and dried under vacuum to afford **5.13** as a bright yellow powder (65 mg, 0.046 mmol, 71%). **¹H-NMR** (400 MHz, DMSO-*d*₆):

δ = 8.85 (d, *J* = 6.2 Hz, 6H), 8.61 (s, 6H), 8.24 (s, 6H), 8.19 (d, *J* = 6.6 Hz, 6H), 7.85 (d, *J* = 8.0 Hz, 4H), 7.72 (d, *J* = 8.1 Hz, 4H). **¹³C-NMR** (101 MHz, DMSO-*d*₆): δ = 166.95, 154.17, 142.62, 135.38, 132.39, 130.29, 121.12, 120.81, 119.95, 119.73, 109.02. **HRMS-ESI**: Calcd. for $\text{C}_{53}\text{H}_{35}\text{B}_2\text{N}_{11}\text{O}_9\text{Zn}_2$: 561.5685 (M^{2+}); found: 561.5692. **IR**: 2225, 1640, 1605, 1590, 1560, 1510, 1445, 1375, 1350, 1310, 1225, 1205, 1165, 1080, 1030, 975, 910, 825, 795, 780, 755, 690, 640, 615, 560, 530 cm^{-1} .

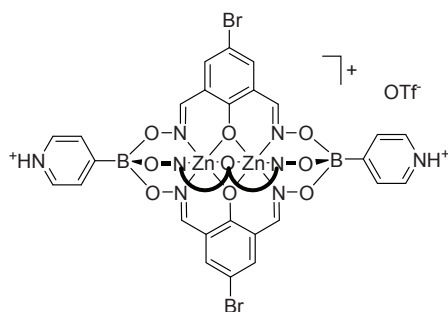
7.2.86 Clathrochelate **5.14**



A mixture of dioxime **L3** (50 mg, 0.194 mmol, 3.0 equiv.), 4-cyanophenylboronic acid (19 mg, 0.13 mmol, 2.0 equiv.) and $[\text{Co}(\text{H}_2\text{O})_6](\text{NO}_3)_2$ (38 mg, 0.13 mmol, 2.0 equiv.) in a mixture of MeOH (10 ml) and EtOH (10 ml) was heated to 70 °C for 4 h. After cooling to RT, the solution was concentrated to 5 ml. The orange precipitate was isolated by filtration, washed with EtOH (3 x 7 ml) and Et₂O (2 x 50 ml) and dried under vacuum to afford **5.14** as an orange powder (54 mg, 0.044 mmol, 68%). X-ray quality single crystals of

5.14 were obtained from the slow evaporation of a solution of the compound in a mixture of MeOH and CH_2Cl_2 (1:1). **HRMS-ESI**: Calcd. for $\text{C}_{53}\text{H}_{35}\text{B}_2\text{N}_{11}\text{O}_9\text{Co}_2$: 554.5743 (M^{2+}); found: 554.5742. **IR**: 2225, 1635, 1590, 1560, 1510, 1445, 1375, 1345, 1310, 1225, 1205, 1080, 1040, 1020, 975, 935, 910, 825, 795, 775, 755, 695, 615, 565, 535 cm^{-1} .

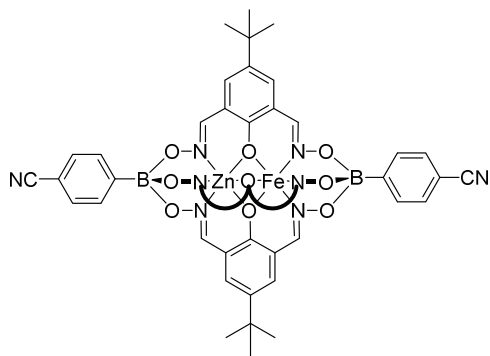
7.2.87 Clathrochelate **5.16**



A mixture of dioxime **L2** (200 mg, 0.77 mmol, 3.0 equiv.) and 4-pyridylboronic acid hydrate (72 mg, 0.51 mmol, 2.0 equiv.) were dissolved in MeOH (30 ml). Zn(OTf)₂ (187 mg, 0.51 mmol, 2.0 equiv.) was added and the yellow solution was heated at 50 °C for 15 min. The solvent was removed under reduced pressure and the yellow solid was suspended in EtOH (5 ml), isolated by filtration and

washed with EtOH (2 x 5 ml) and Et₂O (20 ml) and dried in vacuo to afford **5.16** as a bright yellow solid (241 mg, 0.196 mmol, 76%). ¹H-NMR (400 MHz, DMSO-*d*₆): δ = 8.78 (d, *J* = 5.8 Hz, 4H), 8.43 (s, 6H), 8.17 (d, *J* = 5.7 Hz, 4H), 7.58 (s, 6H). ¹³C-NMR (101 MHz, DMSO-*d*₆): δ = 163.42, 154.30, 139.42, 137.57, 129.42, 120.54, 105.30. HRMS-ESI: Calcd. for C₃₄H₂₂B₂Br₃N₈O₉Zn₂: 1076.7794; found: 1076.7785. IR: 1610, 1550, 1485, 1440, 1325, 1205, 1075, 1035, 975, 950, 890, 880, 810, 785, 745, 700, 680, 645, 540, 520 cm⁻¹.

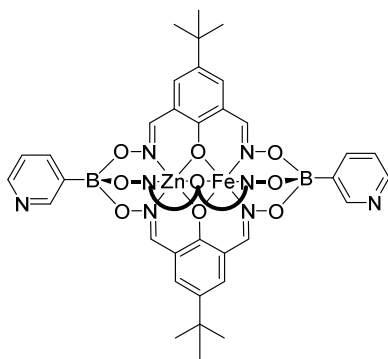
7.2.88 Clathrochelate **5.17**



A mixture of dioxime **L1** (50 mg, 0.211 mmol, 3.0 equiv.), 4-cyanophenylboronic acid (23 mg, 0.141 mmol, 2.0 equiv.), [Zn(H₂O)₆](ClO₄)₂ (26 mg, 0.07 mmol, 1.0 equiv.) and [Fe(H₂O)](ClO₄)₃ (26 mg, 0.07 mmol, 1.0 equiv.) in a mixture of MeOH (10 ml) and EtOH (10 ml) was heated to 50 °C until all solid dissolved. Tetraethylammonium hydroxide (70 μl, 0.105 mmol, 25% in MeOH) was added, and the

solution was stirred at 50 °C for 30 min. After a second addition of tetraethylammonium hydroxide (70 μl, 0.105 mmol, 25% in MeOH), the solution was cooled down to RT, and the solvent was evaporated under reduced pressure. The black residue was purified by column chromatography (eluent: DCM) to afford **5.17** as a black microcrystalline powder (23 mg, 0.022 mmol, 31%). X-ray quality single crystals of **5.17** were obtained from the slow diffusion of Et₂O into a solution of **5.17** in CH₂Cl₂. IR: 2955, 2865, 2230, 1615, 1585, 1560, 1450, 1395, 1365, 1310, 1275, 1245, 1230, 1215, 1100, 1090, 1045, 1020, 1000, 985, 960, 940, 920, 840, 830, 790, 765, 720, 690, 640, 560, 540, 530 cm⁻¹.

7.2.89 Clathrochelate **5.18**



A mixture of dioxime **L1** (50 mg, 0.211 mmol, 3.0 equiv.) and 3-pyridylboronic acid (21 mg, 0.141 mmol, 2.0 equiv.) in EtOH (10 ml) was heated to 50 °C until all solid dissolved. A mixture of $[\text{Zn}(\text{H}_2\text{O})_6](\text{ClO}_4)_2$ (26 mg, 0.07 mmol, 1.0 equiv.) and $[\text{Fe}(\text{H}_2\text{O})](\text{ClO}_4)_3$ (26 mg, 0.07 mmol, 1.0 equiv.) in MeOH (10 ml) was added to the first solution, and the reaction was stirred at 50 °C for 2 h. The black precipitate was filtered and washed with EtOH (2 x 10 ml). The crude protonated mixture was

suspended in MeOH (20 ml) and MeCN (20 ml), and K_2CO_3 (28 mg, 0.211 mmol, 3.0 equiv.) was added in one portion. The suspension was stirred at RT for 2h, solvent were removed under reduced pressure and the black residue was purified by column chromatography (eluent: acetone/ CH_2Cl_2 20:80) to afford **5.18** as a black microcrystalline powder (20 mg, 0.020 mmol, 29%). X-ray quality single crystals of **5.18** were obtained from the slow diffusion of Et_2O into a solution of **5.18** in CHCl_3 . IR: 2955, 2865, 1610, 1585, 1560, 1450, 1405, 1365, 1310, 1275, 1230, 1215, 1095, 1045, 985, 925, 840, 790, 765, 725, 695, 665, 650, 600, 565, 545, 530 cm^{-1} .

Chapter 8 Appendix

8.1 Crystallographic Tables

Table 8.1 – Crystallographic data and structure refinement details of clathrochelates **2.1** and **2.2**.

Structure, CCDC no.	2.1, 980630	2.2, 980631
Empirical formula	C ₄₇ H ₅₀ B ₂ Cl ₃ N ₈ O ₁₃ Zn ₂	C ₅₁ H ₆₃ B ₂ Cl ₃ Co ₂ N ₈ O ₁₅
Mol. Weight / g mol ⁻¹	1193.66	1273.92
Temperature / K	140(2)	140(2)
Wavelength / Å	0.71073	0.71073
Crystal system	Monoclinic	Monoclinic
Space group	<i>C2/c</i>	<i>P21/c</i>
<i>a</i> / Å	20.085(9)	11.866(4)
<i>b</i> / Å	26.915(9)	26.913(5)
<i>c</i> / Å	11.882(4)	17.852(5)
α / °	90	90
β / °	117.982(16)	97.484(18)
γ / °	90	90
Volume / Å ³	5672(4)	5652(3)
Z	4	4
Density / g cm ⁻³	1.398	1.497
Absorption Coeff. / mm ⁻¹	1.052	0.802
Crystal size / mm ³	0.269 x 0.201 x 0.119	0.369 x 0.279 x 0.219
Θ range / °	2.674 to 25.531	2.671 to 27.713
	-24 ≤ <i>h</i> ≤ 24	-15 ≤ <i>h</i> ≤ 15
Index ranges	-32 ≤ <i>k</i> ≤ 31	-32 ≤ <i>k</i> ≤ 35
	-14 ≤ <i>l</i> ≤ 14	-23 ≤ <i>l</i> ≤ 23
Reflections collected	9285	22063
Independent reflections	5261 [<i>R</i> (int) = 0.0400]	13046 [<i>R</i> (int) = 0.0432]
Completeness	99.7 % (to Θ = 25.242°)	99.5 % (to Θ = 25.242°)
Absorption correction	None	None
Max. & min. transmission	-	-
Data / restraints / parameters	5261 / 583 / 403	13046 / 1083 / 772
Goodness-of-fit on F ²	1.116	1.019
Final <i>R</i> indices [<i>I</i> > 2 s (<i>I</i>)]	<i>R</i> 1 = 0.0970, <i>wR</i> 2 = 0.2752	<i>R</i> 1 = 0.0667, <i>wR</i> 2 = 0.1649
<i>R</i> indices (all data)	<i>R</i> 1 = 0.1259, <i>wR</i> 2 = 0.3005	<i>R</i> 1 = 0.1265, <i>wR</i> 2 = 0.1970
Extinction coefficient	-	-
Larg. diff. peak/hole / eÅ ⁻³	2.001 and -1.001	0.703 and -0.833
Flack <i>x</i> (Parsons)	-	-

Table 8.2 – Crystallographic data of clathrochelates **2.3**, **2.6** and **2.7**.

Structure, experiment no.	2.3, MM094b	2.6, MM117	2.7, MM119
Empirical formula	C ₄₆ H ₄₉ B ₂ N ₈ O ₁₃ ClMn ₂	C ₄₆ H ₄₉ B ₂ ClN ₈ O ₁₃ Zn ₂	C ₄₆ H ₄₉ B ₂ ClCo ₂ N ₈ O ₁₃
Mol. Weight / g mol ⁻¹	1222.02	1109.74	1096.86
Temperature / K	140(2)	140(2)	140(2)
Wavelength / Å	0.71073	0.71073	0.71073
Crystal system	Monoclinic	Monoclinic	Monoclinic
Space group	<i>C2/c</i>	<i>P21/c</i>	<i>P21/c</i>
<i>a</i> / Å	19.952(7)	11.564(3)	11.551(3)
<i>b</i> / Å	26.909(8)	27.380(4)	27.292(4)
<i>c</i> / Å	11.900(3)	18.506(4)	18.513(4)
α / °	90	90	90
β / °	115.984(15)	101.438(16)	101.420(15)
γ / °	90	90	90
Volume / Å ³	5743(3)	5743(2)	5721(2)
<i>Z</i>	4	4	4
Density / g cm ⁻³	1.413	1.283	1.274
Absorption Coeff. / mm ⁻¹	0.746	0.944	0.689
Crystal size / mm ³	-	-	-
Θ range / °	5.4 to 50.7	5.16 to 55.4	5.16 to 55.36
Index ranges	-24 ≤ <i>h</i> ≤ 23	-15 ≤ <i>h</i> ≤ 15	-15 ≤ <i>h</i> ≤ 15
	-32 ≤ <i>k</i> ≤ 32	-35 ≤ <i>k</i> ≤ 35	-35 ≤ <i>k</i> ≤ 35
	-14 ≤ <i>l</i> ≤ 14	-24 ≤ <i>l</i> ≤ 23	-22 ≤ <i>l</i> ≤ 23
Reflections collected	10195	25631	23947
Independent reflections	5255 [<i>R</i> (int) = 0.0442]	13135 [<i>R</i> (int) = 0.0332]	12721 [<i>R</i> (int) = 0.0296]
Completeness	-	-	-
Absorption correction	-	-	-
Max. & min. transmission	-	-	-
Data / restraints / parameters	5255 / 0 / 335	13135 / 18 / 784	12721 / 53 / 856
Goodness-of-fit on <i>F</i> ²	2.119	1.069	1.050
Final <i>R</i> indices [<i>I</i> > 2 <i>s</i> (<i>I</i>)]	<i>R</i> 1 = 0.1298, <i>wR</i> 2 = 0.3356	<i>R</i> 1 = 0.0776, <i>wR</i> 2 = 0.2225	<i>R</i> 1 = 0.0613, <i>wR</i> 2 = 0.1783
<i>R</i> indices (all data)	<i>R</i> 1 = 0.1585, <i>wR</i> 2 = 0.3456	<i>R</i> 1 = 0.1040, <i>wR</i> 2 = 0.2449	<i>R</i> 1 = 0.0858, <i>wR</i> 2 = 0.1974
Extinction coefficient	-	-	-
Larg. diff. peak/hole / eÅ ⁻³	2.02 and -1.75	1.61 and -1.19	1.15 and -0.63
Flack <i>x</i> (Parsons)	-	-	-

Table 8.3 – Crystallographic data and structure refinement details of clathrochelates **2.12**, **2.26**, **2.28**.

Structure, CCDC no.	2.12, 1453506	2.26, 1453507	2.28, 1453508
Empirical formula	C ₆₆ H ₇₅ B ₂ N ₉ O ₉ Zn ₂	C ₅₇ H ₅₂ B ₂ N ₁₂ O ₉ Zn ₂	C ₆₅ H ₅₀ B ₂ N _{11.50} O ₉ Zn ₂
Mol. Weight / g mol ⁻¹	1290.71	1201.46	1288.52
Temperature / K	100(2)	100(2)	140(2)
Wavelength / Å	0.69791	0.69791	0.71073
Crystal system	Monoclinic	Orthorhombic	Monoclinic
Space group	<i>P</i> 21/ <i>c</i>	<i>C</i> 2221	<i>I</i> 2/ <i>a</i>
<i>a</i> / Å	17.9643(4)	16.9652(2)	24.0018(8)
<i>b</i> / Å	22.2539(9)	25.8649(2)	26.4540(8)
<i>c</i> / Å	20.8724(4)	14.1059(10)	25.9813(10)
α / °	90	90	90
β / °	108.065(2)	90	115.749(5)
γ / °	90	90	90
Volume / Å ³	7932.9(4)	6189.71(10)	14858.6(10)
<i>Z</i>	4	4	8
Density / g cm ⁻³	1.081	1.289	1.152
Absorption Coeff. / mm ⁻¹	0.656	0.800	0.702
Crystal size / mm ³	0.500 x 0.400 x 0.300	0.500 x 0.150 x 0.150	0.361 x 0.254 x 0.193
Θ range / °	1.569 to 21.549	1.991 to 26.855	3.381 to 29.517
	-18 ≤ <i>h</i> ≤ 18	-21 ≤ <i>h</i> ≤ 20	-32 ≤ <i>h</i> ≤ 32
Index ranges	-22 ≤ <i>k</i> ≤ 18	-33 ≤ <i>k</i> ≤ 33	-34 ≤ <i>k</i> ≤ 36
	-21 ≤ <i>l</i> ≤ 21	-18 ≤ <i>l</i> ≤ 17	-30 ≤ <i>l</i> ≤ 35
Reflections collected	56549	46615	81462
Independent reflections	9262 [<i>R</i> (int) = 0.0901]	6700 [<i>R</i> (int) = 0.0536]	18615 [<i>R</i> (int) = 0.0396]
Completeness	95.7 % (to Θ = 21.549°)	99.3 % (to Θ = 24.755°)	99.7 % (to Θ = 25.242°)
Absorption correction	Semi-empirical from equivalents	Semi-empirical from equivalents	Analytical
Max. & min. transmission	1.00000 and 0.43991	0.889 and 0.6916	0.898 and 0.821
Data / restraints / parameters	9262 / 566 / 919	6700 / 0 / 376	18615 / 0 / 809
Goodness-of-fit on <i>F</i> ²	1.039	1.081	1.022
Final <i>R</i> indices [<i>I</i> > 2 <i>s</i> (<i>I</i>)]	<i>R</i> 1 = 0.0834, <i>wR</i> 2 = 0.2197	<i>R</i> 1 = 0.0293, <i>wR</i> 2 = 0.0819	<i>R</i> 1 = 0.0492, <i>wR</i> 2 = 0.1314
<i>R</i> indices (all data)	<i>R</i> 1 = 0.0909, <i>wR</i> 2 = 0.2267	<i>R</i> 1 = 0.0293, <i>wR</i> 2 = 0.0819	<i>R</i> 1 = 0.0759, <i>wR</i> 2 = 0.1508
Extinction coefficient	-	-	-
Larg. diff. peak/hole / eÅ ⁻³	1.333 and -1.031	0.32 and -0.34	1.393 and -0.476
Flack <i>x</i> (Parsons)	-	0.051(4)	-

Table 8.4 – Crystallographic data and structure refinement details of coordination polymer **2.31**.

Structure, CCDC no.	2.31, 980635
Empirical formula	C ₁₂₈ H ₁₇₈ B ₄ N ₂₈ O ₃₀ Zn ₅
Mol. Weight / g mol ⁻¹	2959.18
Temperature / K	100(2)
Wavelength / Å	0.71073
Crystal system	Monoclinic
Space group	<i>C2/c</i>
<i>a</i> / Å	31.656(9)
<i>b</i> / Å	31.476(5)
<i>c</i> / Å	21.712(4)
α / °	90
β / °	115.962(7)
γ / °	90
Volume / Å ³	17876(7)
<i>Z</i>	4
Density / g cm ⁻³	1.100
Absorption Coeff. / mm ⁻¹	0.726
Crystal size / mm ³	0.495 x 0.395 x 0.304
Θ range / °	3.021 to 27.518
	-41 ≤ <i>h</i> ≤ 40
Index ranges	-40 ≤ <i>k</i> ≤ 40
	-28 ≤ <i>l</i> ≤ 26
Reflections collected	112893
Independent reflections	20236 [<i>R</i> (int) = 0.0454]
Completeness	99.2 % (to Θ = 25.242°)
Absorption correction	Semi-empirical from equivalents
Max. & min. transmission	0.7456 and 0.5750
Data / restraints / parameters	20236 / 2051 / 935
Goodness-of-fit on <i>F</i> ²	0.919
Final <i>R</i> indices [<i>I</i> > 2 <i>s</i> (<i>I</i>)]	<i>R</i> 1 = 0.0938, <i>wR</i> 2 = 0.2757
<i>R</i> indices (all data)	<i>R</i> 1 = 0.1357, <i>wR</i> 2 = 0.3234
Extinction coefficient	-
Larg. diff. peak/hole / eÅ ⁻³	1.528 and -1.124
Flack <i>x</i> (Parsons)	-

Table 8.5 – Crystallographic data of clathrochelate **2.32** and complexes **2.33** and **2.34**.

Structure, experiment no.	2.32, MM168C3	2.33, MM221-Pt	2.34, MM614H
Empirical formula	C ₅₁ H ₃₇ B ₂ N ₉ O ₁₇ Cl ₂ Zn ₂	C ₃₆₂ H ₂₈₆ B ₈ N ₃₆ O ₃₆ P ₁₂ Co ₈ Pt ₆ S ₁₀	C ₆₀₅ H ₇₆₅ B ₁₀ N ₅₀ O ₉₀ F ₄₅ P ₂₀ S ₁₅ Zn ₁₀ Pt ₁₀
Mol. Weight / g mol ⁻¹	1125.84	8136.95	14845.62
Temperature / K	140(2)	140(2)	140(2)
Wavelength / Å	1.54178	1.54178	1.54178
Crystal system	Monoclinic	Monoclinic	Monoclinic
Space group	<i>P</i> 21	<i>P</i> 21/ <i>n</i>	<i>P</i> 21/ <i>n</i>
<i>a</i> / Å	16.046(3)	25.2748(12)	12.249(2)
<i>b</i> / Å	30.0005(19)	16.7986(6)	26.275(5)
<i>c</i> / Å	18.6935(19)	25.2799(12)	41.732(8)
<i>α</i> / °	90	90	90
<i>β</i> / °	91.177(16)	109.223(5)	90.200(16)
<i>γ</i> / °	90	90	90
Volume / Å ³	8996.9(17)	10134.9(8)	13431(4)
<i>Z</i>	6	1	1
Density / g cm ⁻³	1.2466	1.333	1.835
Absorption Coeff. / mm ⁻¹	1.928	7.677	7.168
Crystal size / mm ³	-	-	0.328 x 0.271 x 0.133
Θ range / °	7.18 to 174.98	7.406 to 145.796	6.728 to 102.534
Index ranges	-20 ≤ <i>h</i> ≤ 19	-29 ≤ <i>h</i> ≤ 31	-8 ≤ <i>h</i> ≤ 12
	-36 ≤ <i>k</i> ≤ 33	-18 ≤ <i>k</i> ≤ 20	-26 ≤ <i>k</i> ≤ 26
	-22 ≤ <i>l</i> ≤ 18	-28 ≤ <i>l</i> ≤ 31	-41 ≤ <i>l</i> ≤ 42
Reflections collected	24777	19231	63375
Independent reflections	20317 [<i>R</i> (int) = 0.1247]	19231 [<i>R</i> (int) = 0.1288]	14396 [<i>R</i> (int) = 0.2879]
Completeness	-	-	-
Absorption correction	-	-	-
Max. & min. transmission	-	-	-
Data / restraints / parameters	20317 / 0 / 961	19231 / 0 / 917	14396 / 0 / 580
Goodness-of-fit on F ²	1.639	1.046	1.181
Final <i>R</i> indices [<i>I</i> > 2 <i>s</i> (<i>I</i>)]	<i>R</i> 1 = 0.2210, <i>wR</i> 2 = 0.4687	<i>R</i> 1 = 0.1257, <i>wR</i> 2 = 0.3188	<i>R</i> 1 = 0.1706, <i>wR</i> 2 = 0.4060
<i>R</i> indices (all data)	<i>R</i> 1 = 0.3001, <i>wR</i> 2 = 0.5401	<i>R</i> 1 = 0.1516, <i>wR</i> 2 = 0.3462	<i>R</i> 1 = 0.3384, <i>wR</i> 2 = 0.4929
Extinction coefficient	-	-	-
Larg. diff. peak/hole / eÅ ⁻³	3.019 and -1.47	4.63 and -2.45	1.75 and -0.78
Flack <i>x</i> (Parsons)	8.128(11)	-	-

Table 8.6 – Crystallographic data of coordination polymers **2.36**, **2.37** and **2.38**.

Structure, experiment no.	2.36, MM638A	2.37, MM674A	2.38, MM183D3
Empirical formula	C ₅₁ H ₃₂ B ₂ N ₁₁ O ₁₃ Co ₂ Cl _{0.63}	C ₅₂ H ₃₉ B ₂ CoN ₁₃ O ₁₂ Zn ₂	C _{39.25} HBCL ₄ Co ₂ N ₁₁ O ₉
Mol. Weight / g mol ⁻¹	642.6	1249.25	1029.16
Temperature / K	140(2)	100(2)	140(2)
Wavelength / Å	0.71073	0.69791	0.71073
Crystal system	Monoclinic	Monoclinic	Monoclinic
Space group	<i>P</i> 2 ₁ / <i>n</i>	<i>C</i> 2/ <i>c</i>	<i>P</i> 2 ₁ / <i>a</i>
<i>a</i> / Å	31.4677(7)	32.613(7)	20.940
<i>b</i> / Å	17.0376(6)	19.032(4)	31.920
<i>c</i> / Å	43.3674(10)	31.787(6)	32.810
α / °	90	90	90
β / °	109.254(2)	102.16(3)	93.56
γ / °	90	90	90
Volume / Å ³	21950.2(10)	19287(7)	21888
Z	16	8	16
Density / g cm ⁻³	0.7777	0.860	1.249
Absorption Coeff. / mm ⁻¹	0.617	0.934	0.855
Crystal size / mm ³	-	0.200 x 0.200 x 0.100	-
Θ range / °	6.64 to 56.92	2.96 to 59.96	3.24 to 53.96
	-41 ≤ <i>h</i> ≤ 39	-40 ≤ <i>h</i> ≤ 27	-26 ≤ <i>h</i> ≤ 26
Index ranges	-22 ≤ <i>k</i> ≤ 18	-23 ≤ <i>k</i> ≤ 23	-39 ≤ <i>k</i> ≤ 38
	-53 ≤ <i>l</i> ≤ 48	-34 ≤ <i>l</i> ≤ 39	-37 ≤ <i>l</i> ≤ 39
Reflections collected	109508	44059	239217
Independent reflections	43367 [<i>R</i> (int) = 0.0498]	18533 [<i>R</i> (int) = 0.0516]	41598 [<i>R</i> (int) = 0.0350]
Completeness	-	-	-
Absorption correction	-	-	-
Max. & min. transmission	-	-	-
Data / restraints / parameters	43367 / 0 / 1494	18533 / 1136 / 785	41598 / 0 / 1369
Goodness-of-fit on F ²	2.657	1.024	2.880
Final <i>R</i> indices [<i>I</i> > 2 <i>s</i> (<i>I</i>)]	<i>R</i> 1 = 0.1809, w <i>R</i> 2 = 0.4826	<i>R</i> 1 = 0.0516, w <i>R</i> 2 = 0.1426	<i>R</i> 1 = 0.1744, w <i>R</i> 2 = 0.5573
<i>R</i> indices (all data)	<i>R</i> 1 = 0.2423, w <i>R</i> 2 = 0.5069	<i>R</i> 1 = 0.0596, w <i>R</i> 2 = 0.1478	<i>R</i> 1 = 0.1790, w <i>R</i> 2 = 0.5664
Extinction coefficient	-	-	-
Larg. diff. peak/hole / eÅ ⁻³	4.35 and -2.31	0.54 and -0.82	5.85 and -1.28
Flack <i>x</i> (Parsons)	-	-	-

Table 8.7 – Crystallographic data and structure refinement details of clathrochelate **3.2**.

Structure, CCDC no.	3.2, 1441272
Empirical formula	C _{61.5} H ₇₃ B ₂ Co ₂ N ₇ O ₁₃
Mol. Weight / g mol ⁻¹	1257.74
Temperature / K	120(2)
Wavelength / Å	0.71073
Crystal system	Triclinic
Space group	<i>P</i> 1
<i>a</i> / Å	16.359(2)
<i>b</i> / Å	16.504(2)
<i>c</i> / Å	32.228(6)
α / °	79.278(12)
β / °	77.959(13)
γ / °	62.972(11)
Volume / Å ³	7539(2)
<i>Z</i>	4
Density / g cm ⁻³	1.108
Absorption Coeff. / mm ⁻¹	0.496
Crystal size / mm ³	0.459 x 0.302 x 0.296
Θ range / °	1.494 to 24.800
	-19 ≤ <i>h</i> ≤ 19
Index ranges	-18 ≤ <i>k</i> ≤ 19
	-38 ≤ <i>l</i> ≤ 37
Reflections collected	66550
Independent reflections	41354 [<i>R</i> (int) = 0.0669]
Completeness	95.4 % (to Θ = 24.800°)
Absorption correction	Semi-empirical from equivalents
Max. & min. transmission	0.7451 and 0.4868
Data / restraints / parameters	41354 / 5589 / 3020
Goodness-of-fit on <i>F</i> ²	1.037
Final <i>R</i> indices [<i>I</i> > 2 <i>s</i> (<i>I</i>)]	<i>R</i> 1 = 0.0953, <i>wR</i> 2 = 0.2407
<i>R</i> indices (all data)	<i>R</i> 1 = 0.1252, <i>wR</i> 2 = 0.2661
Extinction coefficient	-
Larg. diff. peak/hole / eÅ ⁻³	1.004 and -0.817
Flack <i>x</i> (Parsons)	-

Table 8.8 – Crystallographic data and structure refinement details for MOFs **3.10**, **3.11** and **3.12**.

Structure, CCDC no.	3.10, 1439994	3.11, 1439995	3.12, 1439996
Empirical formula	C ₁₅₀ H ₁₄₁ B ₆ N ₁₈ O ₄₀ Zn ₁₀	C ₃₂₄ H ₃₄₀ B ₁₂ N ₄₁ O ₈₄ Zn ₂₀	C ₁₅₀ H ₁₄₁ B ₆ Co ₆ N ₁₈ O ₄₁ Zn ₄
Mol. Weight / g mol ⁻¹	3554.36	7589.47	3531.72
Temperature / K	180(2)	100(2)	100(2)
Wavelength / Å	0.71073	0.69633	0.71073
Crystal system	Trigonal	Monoclinic	Trigonal
Space group	<i>R</i> -3 <i>m</i>	<i>C</i> 2/ <i>c</i>	<i>R</i> -3 <i>m</i>
<i>a</i> / Å	27.750(5)	35.8409(2)	31.837(8)
<i>b</i> / Å	27.750(5)	42.7516(2)	31.837(8)
<i>c</i> / Å	27.750(5)	50.8130(5)	62.41(2)
α / °	70.755(7)	90	90
β / °	70.755(7)	91.5280(10)	90
γ / °	70.755(7)	90	120
Volume / Å ³	18454(11)	77830.8(10)	54787(34)
<i>Z</i>	2	4	6
Density / g cm ⁻³	0.640	0.648	0.642
Absorption Coeff. / mm ⁻¹	0.673	0.641	0.559
Crystal size / mm ³	0.466 x 0.431 x 0.360	0.400 x 0.350 x 0.300	0.297 x 0.269 x 0.150
Θ range / °	1.267 to 17.222	1.453 to 20.375	1.279 to 15.872
Index ranges	-23 ≤ <i>h</i> ≤ 23	-35 ≤ <i>h</i> ≤ 35	-23 ≤ <i>h</i> ≤ 24
	-23 ≤ <i>k</i> ≤ 23	-42 ≤ <i>k</i> ≤ 42	-24 ≤ <i>k</i> ≤ 24
	-23 ≤ <i>l</i> ≤ 23	-50 ≤ <i>l</i> ≤ 50	-48 ≤ <i>l</i> ≤ 48
Reflections collected	84372	229579	33033
Independent reflections	4054 [<i>R</i> (int) = 0.1109]	40637 [<i>R</i> (int) = 0.0527]	3173 [<i>R</i> (int) = 0.2496]
Completeness	99.1 % (to Θ = 8.500°)	99.7 % (to Θ = 20.375°)	99.5 % (to Θ = 15.872°)
Absorption correction	Semi-empirical from equivalents	Semi-empirical from equivalents	Semi-empirical from equivalents
Max. & min. transmission	0.7444 and 0.4938	0.6979 and 0.4316	0.6979 and 0.4316
Data / restraints / parameters	4054 / 1110 / 468	40637 / 7798 / 2628	3173 / 1447 / 452
Goodness-of-fit on <i>F</i> ²	1.806	2.002	1.305
Final <i>R</i> indices [<i>I</i> > 2 <i>s</i> (<i>I</i>)]	<i>R</i> 1 = 0.1036, <i>wR</i> 2 = 0.3446	<i>R</i> 1 = 0.1118, <i>wR</i> 2 = 0.4136	<i>R</i> 1 = 0.1038, <i>wR</i> 2 = 0.2752
<i>R</i> indices (all data)	<i>R</i> 1 = 0.1327, <i>wR</i> 2 = 0.3878	<i>R</i> 1 = 0.1192, <i>wR</i> 2 = 0.4229	<i>R</i> 1 = 0.1677, <i>wR</i> 2 = 0.3461
Extinction coefficient	-	-	-
Larg. diff. peak/hole / eÅ ⁻³	0.857 and -1.195	1.159 and -0.695	0.610 and -0.694
Flack <i>x</i> (Parsons)		-	-

Table 8.9 – Crystallographic data and structure refinement details for MOFs **3.13** and **3.14**.

Structure, CCDC no.	MOF 3.13, 1439997	MOF 3.14, 1439998
Empirical formula	C ₁₅₀ H ₁₄₁ B ₆ Co ₆ N ₁₈ O ₄₀ Zn ₄	C ₁₁₄ H ₆₀ B ₆ Br ₉ Co ₆ N ₁₈ O ₄₀ Zn ₄
Mol. Weight / g mol ⁻¹	3515.72	3720.91
Temperature / K	100(2)	100(2)
Wavelength / Å	0.69561	0.69561
Crystal system	Trigonal	Monoclinic
Space group	<i>R</i> -3	<i>C2/m</i>
<i>a</i> / Å	31.473(5)	45.916(4)
<i>b</i> / Å	31.473(5)	30.605(2)
<i>c</i> / Å	62.316(13)	27.785(2)
α / °	90	90
β / °	90	100.851(8)
γ / °	120	90
Volume / Å ³	53458(19)	38347(5)
<i>Z</i>	6	4
Density / g cm ⁻³	0.655	0.645
Absorption Coeff. / mm ⁻¹	0.572	1.466
Crystal size / mm ³	0.250 x 0.200 x 0.100	0.200 x 0.150 x 0.100
Θ range / °	1.497 to 23.113	1.755 to 20.353
	-35 ≤ <i>h</i> ≤ 35	-45 ≤ <i>h</i> ≤ 43
Index ranges	-35 ≤ <i>k</i> ≤ 35	-30 ≤ <i>k</i> ≤ 30
	-57 ≤ <i>l</i> ≤ 69	-24 ≤ <i>l</i> ≤ 25
Reflections collected	204166	60275
Independent reflections	16743 [<i>R</i> (int) = 0.0378]	16940 [<i>R</i> (int) = 0.1056]
Completeness	93.5 % (to Θ = 23.113°)	82.3 % (to Θ = 20.353°)
Absorption correction	Semi-empirical from equivalents	Semi-empirical from equivalents
Max. & min. transmission	1.00000 and 0.26476	1.00000 and 0.36866
Data / restraints / parameters	16743 / 1619 / 755	16940 / 1911 / 937
Goodness-of-fit on <i>F</i> ²	1.935	1.200
Final <i>R</i> indices [<i>I</i> > 2 <i>s</i> (<i>I</i>)]	<i>R</i> 1 = 0.1386, <i>wR</i> 2 = 0.4374	<i>R</i> 1 = 0.1124, <i>wR</i> 2 = 0.3354
<i>R</i> indices (all data)	<i>R</i> 1 = 0.1506, <i>wR</i> 2 = 0.4473	<i>R</i> 1 = 0.1435, <i>wR</i> 2 = 0.3563
Extinction coefficient	-	-
Larg. diff. peak/hole / eÅ ⁻³	1.640 and -0.731 e.Å ⁻³	0.963 and -0.824 e.Å ⁻³
Flack <i>x</i> (Parsons)	-	-

Table 8.10 – Crystallographic data and structure refinement details for MOFs **3.15**.

Structure, CCDC no.	MOF 3.15, 1440000
Empirical formula	C ₁₂₁ H ₈₃ B ₄ Br ₄ N ₁₃ O ₃₄ S ₂ Zn ₈
Mol. Weight / g mol ⁻¹	3212.96
Temperature / K	100(2)
Wavelength / Å	0.71073
Crystal system	Monoclinic
Space group	C2/c
<i>a</i> / Å	40.845(5)
<i>b</i> / Å	42.367(5)
<i>c</i> / Å	34.547(9)
<i>α</i> / °	90
<i>β</i> / °	115.816(11)
<i>γ</i> / °	90
Volume / Å ³	53817(17)
<i>Z</i>	8
Density / g cm ⁻³	0.793
Absorption Coeff. / mm ⁻¹	1.349
Crystal size / mm ³	0.479 x 0.346 x 0.248
Θ range / °	1.108 to 18.800
	-37 ≤ <i>h</i> ≤ 37
Index ranges	-38 ≤ <i>k</i> ≤ 38
	-31 ≤ <i>l</i> ≤ 31
Reflections collected	123244
Independent reflections	20751 [<i>R</i> (int) = 0.0851]
Completeness	98.6 % (to Θ = 18.800°)
Absorption correction	Semi-empirical from equivalents
Max. & min. transmission	1.00000 and 0.36866
Data / restraints / parameters	20751 / 4467 / 1675
Goodness-of-fit on F ²	1.480
Final <i>R</i> indices [<i>I</i> > 2 <i>s</i> (<i>I</i>)]	<i>R</i> 1 = 0.1071, <i>wR</i> 2 = 0.3391
<i>R</i> indices (all data)	<i>R</i> 1 = 0.1701, <i>wR</i> 2 = 0.3958
Extinction coefficient	-
Larg. diff. peak/hole / eÅ ⁻³	1.055 and -0.922 e.Å ⁻³
Flack <i>x</i> (Parsons)	-

Table 8.11 – Crystallographic data and structure refinement details for CPs **4.8** and **4.9**.

Structure, CCDC no.	4.8, 1481126	4.9, 1481127
Empirical formula	C _{53.5} H ₆₀ AgB ₂ N ₉ O _{13.5} Zn ₂	C _{53.75} H _{60.5} AgB ₂ Co ₂ N _{9.5} O _{14.25}
Mol. Weight / g mol ⁻¹	1305.33	1314.96
Temperature / K	100(2)	100(2)
Wavelength / Å	1.54178	0.71073
Crystal system	Monoclinic	Monoclinic
Space group	<i>P</i> 2 ₁ / <i>c</i>	<i>P</i> 2 ₁ / <i>c</i>
<i>a</i> / Å	12.3180(2)	12.3035(11)
<i>b</i> / Å	19.2910(4)	19.295(4)
<i>c</i> / Å	27.0609(5)	27.164(3)
<i>α</i> / °	90	90
<i>β</i> / °	96.918(2)	97.324(7)
<i>γ</i> / °	90	90
Volume / Å ³	6383.6(2)	6395.9(15)
<i>Z</i>	4	4
Density / g cm ⁻³	1.358	1.366
Absorption Coeff. / mm ⁻¹	3.846	0.882
Crystal size / mm ³	0.8 x 0.2 x 0.1	0.7 x 0.2 x 0.1
Θ range / °	4.01 to 73.08	3.10 to 30.00
	-15 ≤ <i>h</i> ≤ 14	-17 ≤ <i>h</i> ≤ 17
Index ranges	-23 ≤ <i>k</i> ≤ 23	-25 ≤ <i>k</i> ≤ 27
	-33 ≤ <i>l</i> ≤ 25	-38 ≤ <i>l</i> ≤ 38
Reflections collected	46094	106504
Independent reflections	12520 [<i>R</i> (int) = 0.036]	18526 [<i>R</i> (int) = 0.031]
Completeness	99.5 % (to Θ = 67.5°)	99.2 % (to Θ = 26.00°)
Absorption correction	Semi-empirical from equivalents	Semi-empirical from equivalents
Max. & min. transmission	1.00 and 0.38	0.75 and 0.64
Data / restraints / parameters	12520 / 53 / 813	18526 / 48 / 815
Goodness-of-fit on F ²	1.01	1.08
Final <i>R</i> indices [<i>I</i> > 2 <i>s</i> (<i>I</i>)]	<i>R</i> 1 = 0.083, <i>wR</i> 2 = 0.179	<i>R</i> 1 = 0.065, <i>wR</i> 2 = 0.140
<i>R</i> indices (all data)	<i>R</i> 1 = 0.088, <i>wR</i> 2 = 0.181	<i>R</i> 1 = 0.083, <i>wR</i> 2 = 0.152
Extinction coefficient	-	-
Larg. diff. peak/hole / eÅ ⁻³	1.61 and -2.53	3.11 and -2.11
Flack <i>x</i> (Parsons)	-	-

Table 8.12 – Crystallographic data and structure refinement details for CPs **4.10** and **4.11**.

Structure, CCDC no.	4.10, 1481128	4.11, 1481129
Empirical formula	C _{78.25} H _{68.5} AgB ₂ N _{11.5} O _{12.75} Zn ₂	C ₁₂₅ H ₇₁ Ag ₃ B ₄ Cl ₂ Co ₄ N ₂₂ O ₁₉
Mol. Weight / g mol ⁻¹	1634.17	2858.50
Temperature / K	140(2)	120(2)
Wavelength / Å	0.71073	0.69791
Crystal system	Triclinic	Orthorhombic
Space group	<i>P</i> 1	<i>Pna</i> 2 ₁
<i>a</i> / Å	15.6943(3)	40.6211(2)
<i>b</i> / Å	17.8805(5)	14.7220(1)
<i>c</i> / Å	18.0418(4)	34.9798(3)
α / °	67.658(2)	90
β / °	78.0034(17)	90
γ / °	65.410(2)	90
Volume / Å ³	4250.72(19)	20918.8(3)
<i>Z</i>	2	4
Density / g cm ⁻³	1.277	0.908
Absorption Coeff. / mm ⁻¹	0.850	0.626
Crystal size / mm ³	0.7 x 0.5 x 0.1	0.50 x 0.03 x 0.02
Θ range / °	3.60 to 29.48	1.51 to 23.04
	-20 ≤ <i>h</i> ≤ 21	-43 ≤ <i>h</i> ≤ 45
Index ranges	-23 ≤ <i>k</i> ≤ 24	-11 ≤ <i>k</i> ≤ 15
	-23 ≤ <i>l</i> ≤ 19	-38 ≤ <i>l</i> ≤ 38
Reflections collected	55999	89199
Independent reflections	32067 [<i>R</i> (int) = 0.031]	25055
Completeness	99.6 % (to Θ = 26.00°)	68.0 % (to Θ = 24.725°)
Absorption correction	Semi-empirical from equivalents	Semi-empirical from equivalents
Max. & min. transmission	0.75 and 0.50	1.00 and 0.40
Data / restraints / parameters	32067 / 209 / 2059	25055 / 397 / 1558
Goodness-of-fit on <i>F</i> ²	1.01	1.29
Final <i>R</i> indices [<i>I</i> > 2 <i>s</i> (<i>I</i>)]	<i>R</i> 1 = 0.061, <i>wR</i> 2 = 0.151	<i>R</i> 1 = 0.088, <i>wR</i> 2 = 0.201
<i>R</i> indices (all data)	<i>R</i> 1 = 0.072, <i>wR</i> 2 = 0.159	<i>R</i> 1 = 0.095, <i>wR</i> 2 = 0.204
Extinction coefficient	-	-
Larg. diff. peak/hole / eÅ ⁻³	2.18 and -0.95	0.95 and -0.75
Flack <i>x</i> (Parsons)	0.011(6)	0.31(3)

Table 8.13 – Crystallographic data of clathrochelates **5.14**, **5.17** and **5.18**.

Structure, experiment no.	5.14, 4-CNCoHL2	5.17, CFR078-2	5.18, CFR061-A3
Empirical formula	C ₄₆ H ₃₅ B ₂ Co ₂ N ₁₃ O ₁₅	C ₄₆ H ₄₇ B ₂ FeN ₈ O ₉ Zn	C ₅₀ H ₅₀ B ₂ Cl ₄ FeN ₈ O ₉ Zn
Mol. Weight / g mol ⁻¹	1149.35	998.76	1202.43
Temperature / K	100(2)	100(2)	140(2)
Wavelength / Å	0.71073	0.71073	1.54178
Crystal system	Triclinic	Orthorhombic	Monoclinic
Space group	<i>P</i> -1	<i>Pbcn</i>	<i>P</i> 2 ₁ / <i>n</i>
<i>a</i> / Å	17.26(3)	14.766(6)	20.2039(2)
<i>b</i> / Å	20.02(4)	12.136(4)	12.8242(10)
<i>c</i> / Å	30.76(3)	25.910(15)	23.3006(3)
α / °	102.68(8)	90	90
β / °	91.75(14)	90	90.7090(10)
γ / °	94.02(10)	90	90
Volume / Å ³	10337(30)	4643(4)	6036.7(11)
<i>Z</i>	8	4	4
Density / g cm ⁻³	1.477	1.429	1.323
Absorption Coeff. / mm ⁻¹	0.722	0.893	4.507
Crystal size / mm ³	-	-	-
Θ range / °	2.22 to 36.8	6.28 to 46.8	7.58 to 154.22
	-15 ≤ <i>h</i> ≤ 15	-16 ≤ <i>h</i> ≤ 16	-25 ≤ <i>h</i> ≤ 25
Index ranges	-17 ≤ <i>k</i> ≤ 17	-13 ≤ <i>k</i> ≤ 13	-16 ≤ <i>k</i> ≤ 16
	-27 ≤ <i>l</i> ≤ 27	-28 ≤ <i>l</i> ≤ 28	-29 ≤ <i>l</i> ≤ 28
Reflections collected	50440	33300	172446
Independent reflections	14771 [<i>R</i> (int) = 0.1507]	3389 [<i>R</i> (int) = 0.1324]	12713 [<i>R</i> (int) = 0.0903]
Completeness	-	-	-
Absorption correction	-	-	-
Max. & min. transmission	-	-	-
Data / restraints / parameters	14771 / 0 / 1103	3389 / 24 / 331	12713 / 6 / 702
Goodness-of-fit on <i>F</i> ²	2.074	1.217	2.557
Final <i>R</i> indices [<i>I</i> > 2 <i>s</i> (<i>I</i>)]	<i>R</i> 1 = 0.1678, <i>wR</i> 2 = 0.3601	<i>R</i> 1 = 0.1141, <i>wR</i> 2 = 0.2421	<i>R</i> 1 = 0.0958, <i>wR</i> 2 = 0.2815
<i>R</i> indices (all data)	<i>R</i> 1 = 0.2815, <i>wR</i> 2 = 0.4178	<i>R</i> 1 = 0.1514, <i>wR</i> 2 = 0.2624	<i>R</i> 1 = 0.1045, <i>wR</i> 2 = 0.2991
Extinction coefficient	-	-	-
Larg. diff. peak/hole / eÅ ⁻³	1.40 and -1.22	1.09 and -0.85	2.96 and -1.30
Flack <i>x</i> (Parsons)	-	-	-

Chapter 9 References

- [1] J.-M. Lehn, *Pure Appl. Chem.*, 1978, **50**, 871.
- [2] Selected recent reviews: (a) W. Wang, Y.-X. Wang and H.-B. Yang, *Chem. Soc. Rev.*, 2016, **45**, 2656; (b) L. Li, D. J. Fanna, N. D. Shepherd, L. F. Lindoy and F. Li, *J. Incl. Phenom. Macrocycl. Chem.*, 2015, **82**, 3; (c) T. R. Cook and P. J. Stang, *Chem. Rev.*, 2015, **115**, 7001; (d) M. Han, D. M. Engelhard and G. H. Clever, *Chem. Soc. Rev.*, 2014, **43**, 1848; (e) H. Amouri, C. Desmarests and J. Moussa, *Chem. Rev.*, 2012, **112**, 2015; (f) J. G. Hardy, *Chem. Soc. Rev.*, 2013, **42**, 7881.
- [3] Selected examples: (a) M. Eddaoudi, D. F. Sava, J. F. Eubank, K. Adil and V. Guillerme, *Chem. Soc. Rev.*, 2015, **44**, 228; (b) W. Lu, Z. Wei, Z.-Y. Gu, T.-F. Liu, J. Park, J. Park, J. Tian, M. Zhang, Q. Zhang, T. Gentle III, M. Bosch and H.-C. Zhou, *Chem. Soc. Rev.*, 2014, **43**, 5561; (c) (d) H. Furukawa, K. E. Cordova, M. O'Keeffe and O. M. Yaghi, *Science*, 2013, **341**, 123044.
- [4] (a) T. R. Cook, Y. Zheng and P. J. Stang, *Chem. Rev.*, 2013, **113**, 734; (b) R. Chakrabarty, P. S. Mukherjee and P. J. Stang, *Chem. Rev.*, 2011, **111**, 6810.
- [5] P. J. Stang and D. H. Cao, *J. Am. Chem. Soc.*, 1994, **116**, 4981.
- [6] (a) M. Fujita, J. Yazaki, and K. Ogura, *Chem. Lett.*, 1991, 1031; (b) M. Fujita, J. Yazaki and K. Ogura, *J. Am. Chem. Soc.*, 1990, **112**, 5645.
- [7] C. J. Kuehl, S. D. Huang and P. J. Stang, *J. Am. Chem. Soc.*, 2001, **123**, 9634.
- [8] M. Fujita, Y. J. Kwon, S. Washizu and K. Ogura, *J. Am. Chem. Soc.*, 1994, **116**, 1151.
- [9] G. Kumar and R. Gupta, *Chem. Soc. Rev.*, 2013, **42**, 9403.
- [10] Selected examples: (a) H. Li, Z.-J. Yao, D. Liu and G.-J. Jin, *Coord. Chem. Rev.*, 2015, **293-294**, 139; (b) B. Chen, M. C. Das, S. Xiang, Z. Zhang and B. Chen, *Angew. Chem. Int. Ed.*, 2011, **2**, 10510.
- [11] Selected examples: (a) I. Hod, W. Bury, D. M. Gardner, P. Deria, V. Roznyatovskiy, M. R. Wasielewski, O. K. Farha and J. T. Hupp, *J. Phys. Chem. Lett.*, 2015, **6**, 586; (b) Z.-M. Zhang, T. Zhang, C. Wang, Z. Lin, L.-S. Long and W. Lin, *J. Am. Chem. Soc.*, 2015, **137**, 3197; (d) A. J. Metherell and M. D. Ward, *Chem. Comm.*, 2014, **50**, 6330; (e) T. Matsumoto, M. Wakizaka, H. Yano, A. Kobayashi, H.-C. Chang and M. Kato, *Dalton Trans.*, 2012, **41**, 8303.
- [12] S.-S. Sun, C. L. Stern, S. T. Nguyen and J. T. Hupp, *J. Am. Chem. Soc.*, 2004, **126**, 6314.
- [13] A. W. Kleij, M. Kuil, D. M. Tooke, A. L. Spek and J. N. H. Reek, *Inorg. Chem.*, 2007, **46**, 5829.
- [14] S. Lipstman and I. Goldberg, *CrystEngComm*, 2010, **12**, 52.
- [15] (a) H. Krupitsky, Z. Stein, I. Goldberg and C. Strouse, *Journal Inclusion Phenomena Mol. Recogn. Chem.*, 1994, **18**, 177; (b) E. B. Fleischer and A. M. Shachter, *Inorg. Chem.*, 1991, **30**, 3763.
- [16] (a) G. Nandi and I. Goldberg, *Chem. Commun.*, 2014, **50**, 13612; (b) R. Koner and I. Goldberg, *Acta Crystallogr. C*, 2009, **65**, m139; (c) Y. Diskin-Posner, G. K. Patra and I. Goldberg, *J. Chem. Soc. Dalton Trans.*, 2001, **19**, 2775; (d) K.-J. Lin, *Angew. Chem., Int. Ed.*, 1999, **38**, 2730.

- [17] N. Fujita, K. Biradha, M. Fujita, S. Sakamoto and K. Yamagushi, *Angew. Chem. Int. Ed.*, 2001, **40**, 1718.
- [18] S.-H. Cho, B. Ma, S. T. Nguyen, J. T. Hupp and T. E. Albrecht-Schmitt, *Chem. Commun.*, 2006, 2563.
- [19] F. Song, C. Wang, J. M. Falkowski, L. Ma and W. Lin, *J. Am. Chem. Soc.*, 2010, **132**, 15390.
- [20] Selected examples: (a) A. Bhunia, S. Dey, J. M. Moreno, U. Diaz, P. Concepcion, K. Van Hecke, C. Janiak and P. Van Der Voort, *Chem. Commun.*, 2016, **52**, 1401; (b) J. Liu, L. Chen, H. Cui, J. Zhang, L. Zhang and C.-Y. Su, *Chem. Soc. Rev.*, 2014, **43**, 6011; (c) C. Zhu, G. Yuan, X. Chen, Z. Yang and Y. Cui, *J. Am. Chem. Soc.*, 2012, **134**, 8058.
- [21] (a) P. K  sgens, M. Rose, I. Senkovska, H. Fr  de, A. Henschel, S. Siegle and S. Kaskel, *Microporous Mesoporous Mater.*, 2009, **120**, 325; (b) G. F  rey, *Chem. Soc. Rev.*, 2008, **37**, 191.
- [22] J. H. Cavka, S. Jakobsen, U. Olsbye, N. Guillou, C. Lamberti, S. Bordiga and K. P. J. Lillerud, *J. Am. Chem. Soc.*, 2008, **130**, 13850.
- [23] Selected examples: (a) Y. Bai, Y. Dou, L.-H. Xie, W. Rutledge, J.-R. Li and H.-C. Zhou, *Chem. Soc. Rev.*, 2016, **45**, 2327; (b) M. Zhang, Y. P. Chen, M. Bosch, T. Gentle, K. Wang, D. Feng, Z. U. Wang and H. C. Zhou, *Angew. Chem. Int. Ed.*, 2014, **53**, 815; (c) H. Furukawa, F. Gandara, Y. B. Zhang, J. Jiang, W. L. Queen, M. R. Hudson and O. M. Yaghi, *J. Am. Chem. Soc.*, 2014, **136**, 4369; (d) Z. Wei, Z. Y. Gu, R. K. Arvapally, Y. P. Chen, R. N. McDougald, J. F. Ivy, A. A. Yakovenko, D. Feng, M. A. Omary and H. C. Zhou, *J. Am. Chem. Soc.*, 2014, **136**, 8269.
- [24] (a) B. Bueken, F. Vermoortele, M. J. Cliffe, M. T. Wharmby, D. Foucher, J. Wieme, L. Vanduyfhuys, C. Martineau, N. Stock, F. Taulelle, V. Van Speybroeck, A. L. Goodwin and D. De Vos, *Chem. - A Eur. J.*, 2016, **22**, 3264.
- [25] Selected examples: (a) K. Wang, X.-L. Lv, D. Feng, J. Li, S. Chen, J. Sun, L. Song, Y. Xie, J.-R. Li and H.-C. Zhou, *J. Am. Chem. Soc.*, 2016, **138**, 914; (b) H. Wu, T. Yildirim and W. J. Zhou, *J. Phys. Chem. Lett.*, 2013, **4**, 925; (c) M. Kandiah, M. H. Nilsen, S. Usseglio, S. Jakobsen, U. Olsbye, M. Tilset, C. Larabi, E. A. Quadrelli, F. Bonino and K. P. Lillerud, *Chem. Mater.*, 2010, **22**, 6632.
- [26] Selected examples: (a) Q. Lin, X. Bu, A. Kong, C. Mao, X. Zhao, F. Bu and P. Feng, *J. Am. Chem. Soc.*, 2015, **137**, 2235; (b) P. Li, R. C. Klet, S.-Y. Moon, T. C. Wang, P. Deria, A. W. Peters, B. M. Klahr, H.-J. Park, S. S. Al-Juaid, J. T. Hupp and O. K. Farha, *Chem. Commun.*, 2015, **51**, 10925; (c) J. Zheng, M. Wu, F. Jiang, W. Su and M. Hong, *Chem. Sci.*, 2015, **6**, 3466.
- [27] Selected examples: (a) D. Feng, W. C. Chung, Z. Wei, Z. Y. Gu, H. L. Jiang, Y. P. Chen, D. J. Darensbourg and H. C. Zhou, *J. Am. Chem. Soc.*, 2013, **135**, 17105; (b) D. Feng, Z. Y. Gu, J. R. Li, H. L. Jiang, Z. Wei and H. C. Zhou, *Angew. Chem. Int. Ed.*, 2012, **51**, 10307; (c) W. Morris, B. Voloskiy, S. Demir, F. Gandara, P. L. McGrier, H. Furukawa, D. Cascio, J. F. Stoddart and O. M. Yaghi, *Inorg. Chem.*, 2012, **51**, 6443.

- [28] W. J. Rieter, K. M. Pott, K. M. L. Taylor and W. Lin, *J. Am. Chem. Soc.*, 2008, **130**, 11584.
- [29] Selected examples : (a) D. Peer, J. M. Karp, S. Hong, O. C. Farokhzad, M. Rimona and R. Langer, *Nat. Nanotechnol.*, 2007, **2**, 751; (b) L. Kelland, *Nat. Rev. Cancer*, 2007, **7**, 573; (c) R. P. Feazell, N. Nakayama-Ratchford, H. Dai and S. Lippard, *J. Am. Chem. Soc.*, 2007, **129**, 8438.
- [30] L. Carlucci, G. Ciani, D. M. Proserpio and M. Visconti, *CrystEngComm*, 2011, **13**, 5891.
- [31] A. D. Burrows, C. G. Frost, M. F. Mahon, P. R. Raithby, C. L. Renouf, C. Richardson and A. J. Stevenson, *Chem. Commun.*, 2010, **46**, 5067.
- [32] (a) C. Wang, J.-L. Wang and W. Lin, *J. Am. Chem. Soc.*, 2012, **134**, 19895; (b) C. Wang, Z. Xie, K. E. deKrafft and W. Lin, *J. Am. Chem. Soc.*, 2011, **133**, 13445.
- [33] (a) D. Gust, T. A. Moore and A. L. Moore, *Acc. Chem. Res.*, 2009, **42**, 1890 ; (b) J. J. Concepcion, J. W. Jurss, M. K. Brennaman, P. G. Hoertz, A. O. v. T Patrocinio, N. Y. Murakami Iha, J. L. Templeton and T. J. Meyer, *Acc. Chem. Res.*, 2009, **42**, 1954.
- [34] A. J. Morris, G. J. Meyer and E. Fujita, *Acc. Chem. Res.*, 2009, **42**, 1983.
- [35] Selected examples: (a) Y. Zhang, B. Chen, F. R. Fronczek and A. W. Maverick, *Inorg. Chem.*, 2008, **47**, 4433; (b) B. Chen, F. R. Fronczek and A. W. Maverick, *Chem. Commun.*, 2003, 2166; (c) B. Moulton and M. J. Zaworotko, *Chem. Rev.*, 2001, **101**, 1629.
- [36] Selected examples: (a) T. M. McLean, J. L. Moody, M. R. Waterland and S. G. Telfer, *Inorg. Chem.*, 2012, **51**, 446; (b) V. S. Thoi, J. R. Stork, D. Magde and S. M. Cohen, *Inorg. Chem.*, 2006, **45**, 10688; (c) G. Ulrich, C. Goze, M. Guardigli, A. Roda and R. Ziessel, *Angew. Chem. Int. Ed.*, 2005, **44**, 3694; (d) W. Qin, M. Baruah, M. Van der Auweraer, F. C. DeSchryver and N. Boens, *J. Phys. Chem. A*, 2005, **109**, 7371.
- [37] Selected examples: (a) A. Béziau, S. A. Baudron, G. Rogez and M. W. Hosseini, *CrystEngComm*, 2013, **15**, 5980; (b) C. Bronner, M. Veiga, A. Guenet, L. De Cola, M. W. Hosseini, C. A. Strassert and S. A. Baudron, *Chem.-Eur. J.*, 2012, **18**, 4041.
- [38] Selected examples: (a) O. Kahn, Y. Pei, M. Verdaguer, J.-P. Renard and J. Sletten, *J. Am. Chem. Soc.*, 1988, **110**, 782; (b) H. Sigel and R. B. Martin, *Chem. Rev.*, 1982, **82**, 385; (c) K. Nag and A. Chakravorty, *Coord. Chem. Rev.*, 1980, **33**, 87.
- [39] Selected examples: (a) G. Kumar and R. Gupta, *Inorg. Chem. Commun.*, 2012, **23**, 103; (b) A. P. Singh, G. Kumar and R. Gupta, *Dalton Trans.*, 2011, **40**, 12454; (c) A. P. Singh, A. Ali and R. Gupta, *Dalton Trans.*, 2010, **39**, 8135.
- [40] Selected examples: (a) V. Cámara, N. Masciocchi, J. Gil-Rubio and J. Vicente, *Chem.-Eur. J.*, 2014, **20**, 1389; (b) J. Vicente, J. Gil-Rubio, N. Barquero, V. Camara and N. Masciocchi, *Chem. Commun.*, 2010, **46**, 1053; (c) V. Vajpayee, Y. H. Song, Y. J. Yang, S. C. Kang, T. R. Cook, D. W. Kim, M. S. Lah, I. S. Kim, M. Wang, P. J. Stang and K.-W. Chi, *Organometallics*, 2011, **30**, 6482.

- [41] Selected examples: (a) J.-J. Liu, Y.-J. Lin and G.-X. Jin, *Organometallics*, 2014, **33**, 1283; (b) J. Yang, J. K. Clegg, Q. Jiang, X. Lui, H. Yan, W. Zhong and J. W. Beves, *Dalton Trans.*, 2013, **42**, 15625.
- [42] D. H. Busch, *Rec. Chem. Progr.*, 1964, **25**, 107.
- [43] D. R. Boston and N. J. Rose, *J. Am. Chem. Soc.*, 1968, **90**, 6859.
- [44] Selected representative examples : (a) A. V. Dolganov, A. S. Belov, V. V. Novikov, A. V. Vologzhanina, G. V. Romanenko, Y. G. Budnikova, G. E. Zelinskii, M. I. Buzin and Y. Z. Voloshin, *Dalton Trans.*, 2015, **44**, 2476; (b) P. A. Petrov, A. V. Virovets, P. E. Plyusnin, E. Y. Filatov, I. V. El'tsov, Y. Z. Voloshin and S. N. Konchenko, *Russ. J. Inorg. Chem.*, 2014, **59**, 1162; (c) O. A. Varzatskii, S. V. Shul'ga, A. S. Belov, V. V. Novikov, A. V. Dolganov, A. V. Vologzhanina and Y. Z. Voloshin, *Dalton Trans.*, 2014, **43**, 17934; (d) Y. Z. Voloshin, O. A. Varzatskii, A. S. Belov, Z. A. Starikova, A. V. Dolganov, V. V. Novikov and Y. N. Bubnov, *Inorg. Chim. Acta*, 2011, **370**, 322; (e) S. E. Solovieva, A. A. Tyuftin, A. A. Muravev, M. Gruner, W. Habicher, S. V. Korobko, I. S. Antipin, A. I. Konovalov, Y. N. Bubnov and Y. Z. Voloshin, *Polyhedron*, 2013, **50**, 90 ; (f) Y. Z. Voloshin, V. E. Zavodnik, O. A. Varzatskii, V. K. Belsky, A. V. Palchik, N. G. Strizhakova, I. I. Vorontsov and M. Y. Antipin, *J. Chem. Soc. Dalton Trans.*, 2002, **6**, 1193 ; (g) Y. Z. Voloshin, O. A. Varzatskii, A. V. Palchik, A. I. Stash and V. K. Belsky, *New J. Chem.*, 1999, **23**, 355.
- [45] O. Pantani, S. Naskar, R. Guillot, P. Millet, E. Anxolabehere-Mallart and A. Aukauloo, *Angew. Chem. Int. Ed.*, 2008, **47**, 9948.
- [46] P. Zhang, M. Wang, J. Dong, X. Li, F. Wang, L. Wu and L. Sun, *J. Phys. Chem. C*, 2010, **114**, 15868.
- [47] Selected examples : (a) V. V. Novikov, I. V. Ananyev, A. A. Pavlov, M. V. Fedin, K. A. Lyssenko and Y. Z. Voloshin, *J. Phys. Chem. Lett.*, 2014, **5**, 496; (b) Y. Z. Voloshin and M. Y. Antipin, *Russ. Chem. Bull.*, 2004, **53**, 2097.
- [48] M. D. Wise, A. Ruggi, M. Pascu, R. Scopelliti and K. Severin, *Chem. Sci.*, 2013, **4**, 1658.
- [49] (a) J. Li, Y. Peng, H. Liang, Y. Yu, B. Xin, G. Li, Z. Shi and S. Feng, *Eur. J. Inorg. Chem.*, 2011, **17**, 2712; (b) D. N. Dybtsev, I. E. Sokolov, E. V. Peresyphkina and V. P. Fedin, *Russ. Chem. Bull.*, 2007, **56**, 225; (c) H. Chun, D. N. Dybtsev, H. Kim and K. Kim, *Chem.–Eur. J.*, 2005, **11**, 3521.
- [50] Y.-Y. Zhang, Y.-J. Lin and G.-X. Jin, *Chem. Commun.*, 2014, **50**, 2327.
- [51] Selected examples: (a) S. Mukherjee and P. S. Mukherjee, *Chem. Commun.*, 2014, **50**, 2239; (b) J. E. M. Lewis, A. B. S. Elliott, C. J. McAdam, K. C. Gordonab and J. D. Crowley, *Chem. Sci.*, 2014, **5**, 1833; (c) M. Han, R. Michel, B. He, Y.-S. Chen, D. Stalke, M. John and G. H. Clever, *Angew. Chem. Int. Ed.*, 2013, **52**, 1319.
- [52] M. D. Wise, J. J. Holstein, P. Pattison, C. Besnard, E. Solari, R. Scopelliti, G. Bricogne and K. Severin, *Chem. Sci.*, 2014, **6**, 1004.

- [53] S. M. Jansze, G. Cecot, M. D. Wise, K. O. Zhurov, T. K. Ronson, A. M. Castilla, A. Finelli, P. Pattison, E. Solari, R. Scopelliti, G. E. Zelinskii, A. V Vologzhanina, Y. Z. Voloshin, J. R. Nitschke and K. Severin, *J. Am. Chem. Soc.*, 2016, **138**, 2046.
- [54] D. K. Chand, K. Biradha, M. Kawano, S. Sakamoto, K. Yamaguchi and M. Fujita, *Chem. - Asian J.*, 2006, **1**, 82.
- [55] P. Chaudhuri, M. Winter, P. Fleischhauer, W. Haase, U. Flörke and H.-J. Haupt, *J. Chem. Soc., Chem. Commun.*, 1990, 1728.
- [56] (a) P. Chaudhuri, *Coord. Chem. Rev.*, 2003, **243**, 143. (b) F. Birkelbach, U. Flörke, H.-J. Haupt, C. Butzlaff, A. X. Trautwein, K. Wiegardt and P. Chaudhuri, *Inorg. Chem.*, 1998, **37**, 2000; (c) D. Burdinski, F. Birkelbach, M. Gerdan, A. X. Trautwein, K. Wiegardt and P. Chaudhuri, *J. Chem. Soc., Chem. Commun.*, 1995, **100**, 963.
- [57] C. Krebs, M. Winter, T. Weyhermüller, E. Bill, K. Wiegardt and P. Chaudhuri, *J. Chem. Soc., Chem. Commun.*, 1995, **28**, 1913.
- [58] S. Khanra, T. Weyhermüller, E. Bill and P. Chaudhuri, *Inorg. Chem.*, 2006, **45**, 5911.
- [59] For the importance of charge compensation in supramolecular assemblies, see: (a) J. B. Pollock, T. R. Cook, G. L. Schneider and P. J. Stang, *Chem. Asian J.*, 2013, **8**, 2423 ; (b) Y.-R. Zheng, Z.-G. Zhao, M. Wang, K. Ghosh, J. B. Pollock, T. R. Cook and P. J. Stang, *J. Am. Chem. Soc.*, 2010, **132**, 16873; (c) A. K. Bar, G. Mostafa and P. S. Makherjee, *Inorg. Chem.*, 2010, **49**, 7647.
- [60] M. Pascu, M. Marmier, C. Schouwey, R. Scopelliti, J. J. Holstein, G. Bricogne and K. Severin, *Chem.-Eur. J.*, 2014, **20**, 5592.
- [61] M. Marmier, G. Cecot, B. F. E. Curchod, P. Pattison, E. Solari, R. Scopelliti and K. Severin, *Dalton Trans.*, 2016, **45**, 8422.
- [62] Despite this inherent flexibility, it is possible to use linear ligands with terminal 3-pyridyl groups in supramolecular chemistry. For examples see: (a) A. K. Pal, B. Laramée-Milette and G. S. Hanan, *RSC Adv.*, 2014, **4**, 21262; (b) M.-E. Moon, H. J. Lee, B. S. Ko and K.-W. Chi, *Bull. Korean Chem. Soc.*, 2007, **28**, 311; (c) K.-W. Chi, C. Addicott, A. M. Arif, N. Das and P. J. Stang, *J. Org. Chem.*, 2003, **68**, 9798.
- [63] Selected examples: (a) O. A. Varzatskii, I. N. Denisenko, S. V. Volkov, A. S. Belov, A. V. Dolganov, A. V. Vologzhanina, V. V. Novikov, Y. N. Bubnov and Y. Z. Voloshin, *Eur. J. Inorg. Chem.*, 2013, **18**, 3178; (b) A. S. Belov, A. I. Prikhod'ko, V. V. Novikov, A. V. Vologzhanina, Y. N. Bubnov and Y. Z. Voloshin, *Eur. J. Inorg. Chem.*, 2012, **28**, 4507; (c) Y. Z. Voloshin, O. A. Varzatskii, S. V. Shul'ga, I. N. Denisenko, A. V. Vologzhanina and Y. N. Bubnov, *Inorg. Chem. Commun.*, 2012, **17**, 128; (d) O. A. Varzatskii, Y. Z. Voloshin, S. V. Korobko, S. V. Shulga, R. Krämer, A. S. Belov, A. V. Vologzhanina and Y. N. Bubnov, *Polyhedron*, 2009, **28**, 3431.

- [64] T. E. Barder, S. D. Walker, J. R. Martinelli and S. L. Buchwald, *J. Am. Chem. Soc.*, 2005, **127**, 4685.
- [65] G. Li, C. Zhu, X. Xi and Y. Cui, *Chem. Commun.*, 2009, 2118.
- [66] (a) P. Hohenberg and W. Kohn, *Phys. Rev. B*, 1964, **136**, B864; (b) W. Kohn and L. J. Sham, *Phys. Rev.*, 1965, **140**, 1133.
- [67] (a) J. P. Perdew, M. Ernzerhof and K. Burke, *J. Chem. Phys.*, 1996, **105**, 9982; (b) M. Ernzerhof and G. E. Scuseria, *J. Chem. Phys.*, 1999, **110**, 5029; (c) C. Adamo and V. Barone, *J. Chem. Phys.*, 1999, **110**, 6158.
- [68] (a) M. Dickmeis and H. Ritter, *Macromol. Chem. Phys.*, 2009, **210**, 776; (b) J. L. Neumeyer and J. G. Canon, *J. Org. Chem.*, 1961, **26**, 4681.
- [69] Selected examples: (a) C. J. Adams, M. C. Muoz, R. E. Waddington and J. A. Real, *Inorg. Chem.*, 2011, **50**, 10633; (b) S.-I. Noro, R. Kitaura, M. Kondo, S. Kitagawa, T. Ishii, H. Matsuzaka and M. Yamashita, *J. Am. Chem. Soc.*, 2002, **124**, 2568; (c) M.-L. Tong, S.-L. Zheng and X.-M. Chen, *Polyhedron*, 2000, **19**, 1809; (d) Y.-S. Zhang, G. D. Enright, S. R. Breeze and S. Wang, *New J. Chem.*, 1999, **23**, 625; (e) S. Subramanian and M. J. Zaworotko, *Angew. Chem. Int. Ed.*, 1995, **107**, 2295; *Angew. Chem. Int. Ed.*, 1995, **34**, 2127; (f) R. W. Gable, B. F. Hoskins and R. Robson, *J. Chem. Soc. Chem. Commun.*, 1990, 1677.
- [70] A. L. Spek, PLATON: A Multipurpose Crystallographic Tool, 2008, Utrecht University, Utrecht, The Netherlands.
- [71] M. Fujita, D. Oguro, M. Miyazawa, H. Oka, K. Yamaguchi and K. Ogura, *Nature*, 1995, **378**, 469.
- [72] (a) V. Crou  , S. Goeb, G. Szal  ki, M. Allain and M. Sall  , *Angew. Chem. Int. Ed.*, 2016, **55**, 1746; (b) S. Bivaud, S. Goeb, V. Crou  , M. Allain, F. Pop and M. Sall  , *Beilstein J. Org. Chem.*, 2015, **11**, 966; (c) S. Bivaud, S. Goeb, V. Crtou  , P. I. Dron, M. Allain and M. Sall  , *J. Am. Chem. Soc.*, 2013, **135**, 10018.
- [73] (a) J. Yang, M. Bhadbhade, W. A. Donald, H. Iranmanesh, E. G. Moore, H. Yan and J. E. Beves, *Chem. Commun.*, 2015, **51**, 4465; (b) S. Bivaud, S. Goeb, J.-Y. Balandier, M. Chas, M. Allain and M. Sall  , *Eur. J. Inorg. Chem.*, 2014, 2440; (c) S. Bivaud, J.-Y. Balandier, M. Chas, M. Allain, S. Goeb and M. Sall  , *J. Am. Chem. Soc.*, 2012, **134**, 11968; (d) A. K. Bar, S. Mohapatra, E. Zangrando and P. S. Mukherjee, *Chem. Eur. J.*, 2012, **18**, 9571; (e) D. C. Caskey, T. Yamamoto, C. Addicott, R. K. Shoemaker, J. Vacek, A. M. Hawkrige, D. C. Muddiman, G. S. Kottas, J. Michel and P. J. Stang, *J. Am. Chem. Soc.*, 2008, **130**, 7620; (f) Y. Yamanoi, Y. Sakamoto, T. Kusukawa, M. Fujita, S. Sakamoto and K. Yamaguchi, *J. Am. Chem. Soc.*, 2001, **123**, 980; (g) N. Fujita, K. Biradha, M. Fujita, S. Sakamoto and K. Yamaguchi, *Angew. Chem. Int. Ed.*, 2001, **40**, 1718.

- [74] (a) B. Roy, A. K. Ghosh, S. Srivastava, P. D'Silva and P. S. Mukherjee, *J. Am. Chem. Soc.*, 2015, **137**, 11916; (b) S. Goeb, S. Bivaud, V. Croué, V. Vajpayee, M. Allain and M. Sallé, *Materials*, 2014, **7**, 611.
- [75] A. K. Bar, R. Chakrabarty, G. Mostafa and P. S. Mukherjee, *Angew. Chem. Int. Ed.*, 2008, **47**, 8455.
- [76] Selected examples: (a) J. Li, G.-P. Yang, S.-L. Wei, R.-C. Gao, N.-N. Bai and Y.-Y. Wang, *Cryst. Growth Des.*, 2015, **15**, 5382; (b) M.-L. Ma, J.-H. Qin, C. Ji, H. Xu, R. Wang, B.-J. Li, S.-Q. Zang, H.-W. Hou and S. R. Batten, *J. Mater. Chem. C*, 2014, **2**, 1086; (c) L. Bai, H.-B. Wang, D.-S. Li, Y.-P. Wu, J. Zhao and L.-F. Ma, *Inorg. Chem. Commun.*, 2014, **44**, 188; (d) D. Wang, T. Zhao, Y. Cao, S. Yao, G. Li, Q. H and Y. Liu, *Chem. Commun.*, 2014, **50**, 8648; (e) X. Duan, R. Song, J. Yu, H. Wang, Y. Cui, Y. Yang, B. Chen and G. Qian, *RSC Adv.*, 2014, **4**, 36419; (f) J. Park, J.-R. Li, Y.-P. Chen, J. Yu, A. A. Yakovenko, Z. U. Wang, L.-B. Sun, P. B. Balbuena and H.-C. Zhou, *Chem. Commun.*, 2012, **48**, 9995; (g) P. Zhang, B. Li, Y. Zhao, X. Meng and T. Zhang, *Chem. Commun.*, 2011, **47**, 7722.
- [77] For examples of (3,4,5)-connected nets see: (a) Q.-Z. Sun, Y.-B. Yin, L.-Y. Chai, H. Liu, P.-F. Hao, X.-P. Yan and Y.-Q. Guo, *J. Mol. Struct.*, 2014, **1070**, 75; (b) J.-F. Liu, F.-P. Huang, H.-D. Bian and Q. Yu, *Z. Anorg. Allg. Chem.*, 2013, **639**, 2347; (c) M. Xue, G. Zhu, H. Ding, L. Wu, X. Zhao, Z. Jin and S. Qiu, *Cryst. Growth Des.*, 2009, **9**, 1481.
- [78] H. Li, M. Eddaoudi, M. O'Keeffe and O. M. Yaghi, *Nature*, 1999, **402**, 276.
- [79] S. S. Chui, S. M.-F. Lo, J. P. H. Charmant, A. G. Orpen and I. D. Williams, *Science*, 1999, **283**, 1148.
- [80] H.-C. Zhou and S. Kitagawa, *Chem. Soc. Rev.*, 2014, **43**, 5415.
- [81] Selected examples: (a) N. W. Ockwig, O. Delgado-Friedrichs, M. O'Keeffe and O. M. Yaghi, *Acc. Chem. Res.*, 2005, **38**, 176; (b) O. M. Yaghi, M. O'Keeffe, N. W. Ockwig, H. K. Chae, M. Eddaoudi and J. Kim, *Nature*, 2003, **423**, 705.
- [82] Selected examples: (a) H. Deng, C. J. Doonan, H. Furukawa, R. B. Ferreira, J. Towne, C. B. Knobler, B. Wang and O. M. Yaghi, *Science*, 2010, **327**, 846; (b) Q. Li, W. Zhang, O. Š. Miljanic, C.-H. Sue, Y.-L. Zhao, L. Liu, C. B. Knobler, J. F. Stoddart and O. M. Yaghi, *Science*, 2009, **325**, 855; (c) D. Britt, D. Tranchemontagne and O. M. Yaghi, *Proc. Natl. Acad. Sci. U. S. A.*, 2008, **105**, 11623; (d) A. G. Wong-Foy, A. Matzger and O. M. Yaghi, *J. Am. Chem. Soc.*, 2006, **128**, 3494; (e) M. Eddaoudi, J. Kim, N. Rosi, D. Vodak, J. Wachter, M. O'Keeffe, O. M. Yaghi, *Science*, 2002, **295**, 469.
- [83] Selected examples: (a) Y.-B. Dong, Y.-A. Li, C.-W. Zhao, N.-X. Zhu, Q.-K. Liu, G. Chen, J.-B. Liu, X.-D. Zhao, J.-P. Ma and S. Zhang, *Chem. Commun.*, 2015, **51**, 17672; (b) Y. Lee, S. Kim, J. K. Kang

- and S. M. Cohen, *Chem. Commun.*, 2015, **51**, 5735; (c) T. Zhang and W. Lin, *Chem. Soc. Rev.*, 2014, **43**, 5982.
- [84] Selected examples: (a) A. H. Chughtai, N. Ahmad, H. A. Younus, A. Laypkov and F. Verpoort, *Chem. Soc. Rev.*, 2015, **44**, 6804; (b) J. E. Mondloch, M. J. Katz, W. C. Isley, P. Ghosh, P. Liao, W. Bury, G. W. Wagner, M. G. Hall, J. B. DeCoste, G. W. Peterson, R. Q. Snurr, C. J. Cramer, J. T. Hupp and O. K. Farha, *Nat. Mater.*, 2015, **14**, 512; (c) M. H. Beyzavi, R. C. Klet, S. Tussupbayev, J. Borycz, N. A. Vermeulen, C. J. Cramer, J. F. Stoddart, J. T. Hupp and O. K. Farha, *J. Am. Chem. Soc.*, 2014, **136**, 15861; (d) A. Dhakshinamoorthy, M. Alvaro and H. Garcia, *Chem. Comm.*, 2012, **48**, 11275.
- [85] Selected examples: (a) H. Furukawa, U. Müller and O. M. Yaghi, *Angew. Chem. Int. Ed.*, 2015, **54**, 3417; (b) S. Henke, A. Schneemann and R. A. Fischer, *Adv. Funct. Mater.*, 2013, **23**, 5990; (c) J. Park, D. Yuan, K. T. Pham, J.-R. Li, A. Yakovenko and H.-C. Zhou, *J. Am. Chem. Soc.*, 2012, **134**, 99; (d) S. Henke, A. Schneemann, A. Wütscher and R. A. Fischer, *J. Am. Chem. Soc.*, 2012, **134**, 9464.
- [86] Selected examples: (a) P.-Z. Li, X.-J. Wang, S. Y. Tan, C. Y. Ang, H. Chen, J. Liu, R. Zou and Y. Zhao, *Angew. Chem. Int. Ed.*, 2015, **54**, 12748. (b) A. Schneemann, V. Bon, I. Schwedler, I. Senkovska, S. Kaskel and R. A. Fischer, *Chem. Soc. Rev.*, 2014, **43**, 6062; (c) J.-S. Qin, S.-R. Zhang, D.-Y. Du, P. Shen, S.-J. Bao, Y.-Q. Lan and Z.-M. Su, *Chem. A Eur. J.*, 2014, **20**, 5625.
- [87] Selected examples: (a) I. Senkovska and S. Kaskel, *Chem. Commun.*, 2014, **50**, 7089; (b) M. Zhang, M. Bosch, T. Gentle and H.-C. Zhou, *CrystEngComm*, 2014, **16**, 4069; (c) S. Chaemchuen, N. A. Kabir, K. Zhou and F. Verpoort, *Chem. Soc. Rev.*, 2013, **42**, 9304; (d) K. Sumida, D. L. Rogow, J. A. Mason, T. M. McDonald, E. D. Bloch, Z. R. Herm, T.-H. Bae and J. R. Long, *Chem. Rev.*, 2012, **112**, 724; (e) O. K. Farha, I. Eryazici, N. C. Jeong, B. G. Hauser, C. E. Wilmer, A. A. Sarjeant, R. Q. Snurr, S. T. Nguyen, A. Ö. Yazaydin and J. T. Hupp, *J. Am. Chem. Soc.*, 2012, **134**, 15016.
- [88] Selected examples: (a) V. Guillerm, D. Kim, J. F. Eubank, R. Luebke, X. Liu, K. Adil, M. S. Lah and M. Eddaoudi, *Chem. Soc. Rev.*, 2014, **43**, 6141; (b) M. Li, D. Li, M. O’Keeffe and O. M. Yaghi, *Chem. Rev.*, 2013, **114**, 1343; (c) M. O’Keeffe and O. M. Yaghi, *Chem. Rev.*, 2012, **112**, 675.
- [89] Selected examples: (a) H.-L. Jiang, T. A. Makal and H.-C. Zhou, *Coord. Chem. Rev.*, 2013, **257**, 2232; (b) D. Rankine, A. Avellaneda, M. R. Hill, C. J. Doonan and C. J. Sumby, *Chem. Comm.*, 2012, **48**, 10328; (c) K. L. Mulfort, O. K. Farha, C. D. Malliakas, M. G. Kanatzidis and J. T. Hupp, *Chem. Eur. J.* 2010, **16**, 276.
- [90] (a) H. Deng, S. Grunder, K. E. Cordova, C. Valente, H. Furukawa, M. Hmadeh, F. Gándara, C. C. Whalley, Z. Liu, S. Asahina, Kazumori, M. O’Keeffe, O. Terasaki, J. F. Stoddart and O. M. Yaghi,

- Science*, 2012, **336**, 1018; (b) S. Grunder, C. Valente, A. C. Whalley, S. Sampath, J. Portmann, Y. Y. Botros and J. F. Stoddart, *Chem. Eur. J.*, 2012, **18**, 15632.
- [91] D. W. Smithenry, S. R. Wilson and K. S. Suslick, *Inorg. Chem.*, 2003, **42**, 7719.
- [92] B. Kesanli, Y. Cui, M. R. Smith, E. W. Bittner, B. C. Bockrath and W. Lin, *Angew. Chem. Int. Ed.*, 2004, **44**, 72.
- [93] (a) M.-L. Ma, J.-H. Qin, C. Ji, H. Xu, R. Wang, B.-J. Li, S.-Q. Zang, H.-W. Hou and S. R. Batten, *J. Mater. Chem. C*, 2014, **2**, 1085; (b) J. K. Schnobrich, O. Lebel, K. A. Cychosz, A. Dailly, A. G. Wong-Foy and A. J. Matzger, *J. Am. Chem. Soc.*, 2010, **132**, 13941.
- [94] Selected examples (a) S. Han, Y. Wei, C. Valente, I. Lagzi, J. J. Gassensmith, A. Coskun, J. F. Stoddart and B. A. Grzybowski, *J. Am. Chem. Soc.*, 2010, **132**, 16358; (b) P. Horcajada, T. Chalati, C. Serre, B. Gillet, C. Sebrie, T. Baati, J. F. Eubank, D. Heurtaux, P. Clayette, C. Kreuz, J.-S. Chang, Y. K. Hwang, V. Marsaud, P.-N. Bories, L. Cynober, S. Gil, G. Férey, P. Couvreur and R. Gref, *Nat. Mater.*, 2010, **9**, 172; (c) J. Lee, O. K. Farha, J. Roberts, K. A. Scheidt, S. T. Nguyen and J. T. Hupp, *Chem. Soc. Rev.*, 2009, **38**, 1450.
- [95] G. Bricogne, E. Blanc, M. Brandl, C. Flensburg, P. Keller, P. Paciorek, P. Roversi, A. Sharff, O. Smart, C. Vonrhein and T. Womack, BUSTER version 2.13.0, 2011 Global Phasing Ltd., Cambridge, United Kingdom.
- [96] <http://grade.globalphasing.org>
- [97] G. M. Sheldrick, *Acta Cryst.*, 2008, **A64**, 112.
- [98] A. Thorn, B. Dittrich and G. M. Sheldrick, *Acta Cryst.*, 2012, **A68**, 448.
- [99] C. B. Hübschle, G. M. Sheldrick and B. Dittrich, *J. Appl. Cryst.*, 2011, **44**, 1281.
- [100] Selected examples (a) D. J. Tranchemontagne, J. R. Hunt and O. M. Yaghi, *Tetrahedron*, 2008, **64**, 8553; (b) J. L. C. Rowsell and O. M. Yaghi, *Microporous Mesoporous Mater.*, 2004, **73**, 3.
- [101] S.-Y. Zhang, Z. Zhang and M. J. Zaworotko, *Chem. Comm.*, 2013, **49**, 9700.
- [102] Selected examples: (a) C. K. Brozek, L. Bellarosa, T. Soejima, T. V. Clark, N. López and M. Dincă, *Chem. Eur. J.*, 2014, **20**, 6871; (b) C. K. Brozek and M. Dincă, *Chem. Soc. Rev.*, 2014, **43**, 5456; (c) C. K. Brozek and M. Dincă, *J. Am. Chem. Soc.*, 2013, **135**, 12886.
- [103] Q. Yue, Q. Sun, A.-L. Cheng and E.-Q. Gao, *Cryst. Growth Des.*, 2010, **10**, 44.
- [104] Selected examples: (a) A. Dutta, K. Koh, A. G. Wong-Foy and A. J. Matzger, *Angew. Chem. Int. Ed.*, 2015, **54**, 1; (b) L. Liu and S. G. Telfer, *J. Am. Chem. Soc.*, 2015, **137**, 3901; (c) H. K. Chae, D. Y. Siberio-Pérez, J. Kim, Y. Go, M. Eddaoudi, A. J. Matzger, M. O'Keeffe and O. M. Yaghi, *Nature*, 2004, **427**, 523.
- [105] Selected examples: (a) S. Wang, J. Wang, W. Cheng, X. Yang, Z. Zhang, Y. Xu, H. Liu, Y. Wu and M. Fang, *Dalton Trans.*, 2015, **44**, 8049; (b) H.-L. Jiang, D. Feng, K. Wang, Z.-Y. Gu, Z. Wei, Y.-P. Chen and H.-C. Zhou, *J. Am. Chem. Soc.*, 2013, **135**, 13934; (c) P. Deria, J. E. Mondloch, E.

- Tylianakis, P. Ghosh, W. Bury, R. Q. Snurr, J. T. Hupp and O. K. Farha, *J. Am. Chem. Soc.*, 2013, **135**, 16801.
- [106] Selected examples: (a) R. Wang, Z. Wang, Y. Xu, F. Dai, L. Zhang and D. Sun, *Inorg. Chem.*, 2014, **53**, 7086; (b) J. Jiang, F. Gándara, Y.-B. Zhang, K. Na, O. M. Yaghi and W. G. Klemperer, *J. Am. Chem. Soc.*, 2014, **136**, 12844; (c) D. Feng, K. Wang, J. Su, T.-F. Liu, J. Park, Z. Wei, M. Bosch, A. Yakovenko, X. Zou and H.-C. Zhou, *Angew. Chemie Int. Ed.*, 2014, **54**, 149.
- [107] Selected examples: (a) K. Wang, H. Huang, W. Xue, D. Liu, X. Zhao, Y. Xiao, Z. Li, Q. Yang, L. Wang and C. Zhong, *CrystEngComm.*, 2015, **17**, 3586; (b) J. B. DeCoste, G. W. Peterson, H. Jasuja, T. G. Glover, Y. Huang and K. S. Walton, *J. Mater. Chem. A*, 2013, **1**, 5642.
- [108] Selected examples: (a) M. Kim and S. M. Cohen, *CrystEngComm.*, 2012, **14**, 4096; (b) F. Vermoortele, R. Ameloot, A. Vimont, C. Sebrie and D. De Vos, *Chem. Commun.*, 2011, **47**, 1521.
- [109] (a) J. B. DeCoste, M. A. Browe, G. W. Wagner, J. A. Rossin and G. W. Peterson, *Chem. Commun.*, 2015, **51**, 12474; (b) E. López-Maya, C. Montoro, L. M. Rodríguez-Albelo, S. D. Aznar Cervantes, A. A. Lozano-Pérez, J. L. Cenís, E. Barea and J. A. R. Navarro, *Angew. Chemie Int. Ed.*, 2015, **54**, 6790; (c) S.-Y. Moon, Y. Liu, J. T. Hupp and O. K. Farha, *Angew. Chemie Int. Ed.*, 2015, **54**, 6795; (d) J. B. DeCoste, T. J. Demasky, M. J. Katz, O. K. Farha and T. J. Hupp, *New J. Chem.*, 2015, **39**, 2396; (e) J. B. Decoste and G. W. Peterson, *Chem. Rev.*, 2014, **114**, 5695.
- [110] Selected examples: (a) D.-X. Xue, Y. Belmabkhout, O. Shekhah, H. Jiang, K. Adil, A. J. Cairns and M. Eddaoudi, *J. Am. Chem. Soc.*, 2015, **137**, 5034; (b) J. Ren, H. W. Langmi, B. C. North, M. Mathe and D. Bessarabov, *Int. J. Hydrogen Energy*, 2014, **39**, 890; (c) H. Wu, Y. S. Chua, V. Krungleviciute, M. Tyagi, P. Chen, T. Yildirim and W. Zhou, *J. Am. Chem. Soc.*, 2013, **135**, 10525; (d) V. Bon, V. Senkovskyy, I. Senkovska and S. Kaskel, *Chem. Commun.*, 2012, **48**, 8407; (e) A. Schaate, P. Roy, A. Godt, J. Lippke, F. Waltz, M. Wiebcke and P. Behrens, *Chem. Eur. J.*, 2011, **17**, 6643; (f) S. Diring, S. Furukawa, Y. Takashima, T. Tsuruoka and S. Kitagawa, *Chem. Mater.*, 2010, **22**, 4531; (g) T. Tsuruoka, S. Furukawa, Y. Takashima, K. Yoshida, S. Isoda and S. Kitagawa, *Angew. Chem. Int. Ed.*, 2009, **48**, 4739; (h) T. Tsuruoka, S. Furukawa, Y. Takashima, K. Yoshida, S. Isoda and S. Kitagawa, *Angew. Chem Int. Ed.*, 2009, **121**, 4833.
- [111] Representative examples: (a) C. L. Luu, T. T. Van Nguyen, T. Nguyen and T. C. Hoang, *Adv. Nat. Sci. Nanosci. Nanotechnol.*, 2015, **6**, 025004; (b) B. Wang, H. Huang, X.-L. Lv, Y. Xie, M. Li and J.-R. Li, *Inorg. Chem.*, 2014, **53**, 9254. (c) Q. Yang, V. Guillermin, F. Ragon, A. D. Wiersum, P. L. Llewellyn, C. Zhong, T. Devic, C. Serre and G. Maurin, *Chem. Commun.*, 2012, **48**, 9831.
- [112] I. Beletskaya, V. S. Tyurin, A. Y. Tsivadze, R. Guilard and C. Stern. *Chem. Rev.*, 2009, **109**, 1659.
- [113] M. Marmier, G. Cecot, A. V. Vologzhanina, J. L. Bila, I. Zivkovic, H. M. Ronnow, B. Nafradi, E. Solari, P. Pattison, R. Scopelliti and K. Severin, *Dalton Trans.*, 2016, *accepted*.

- [114] (a) T. C. W. Mak and X.-L. Zhao, *Encyclopedia of Inorganic Chemistry*, 2006, John Wiley & Sons; (b) B. S. Fox, M. K. Beyer and V. E. Bondybey, *J. Am. Chem. Soc.*, 2002, **124**, 13613.
- [115] (a) C.-Y. Su, C.-L. Chen, J.-Y. Zhang and B.-S. Kang, in *Design and Construction of Coordination Polymers* (Eds: M.-C. Hong, L. Chen), 2009, John Wiley & Sons, pp. 111; (b) C.-L. Chen, B.-S. Kang and C.-Y. Su, *Austr. J. Chem.*, 2006, **59**, 3.
- [116] For examples see: (a) X.-M. Guo, L. Zhao, H.-Y. Zou, Y.-N. Yan, Y.-J. Qi and Q. Wang, *Inorg. Chem. Commun.*, 2015, **54**, 57; (b) S. P. Anthony, L. Wang, S. Varughese and S. M. Draper, *CrystEngComm*, 2013, **15**, 6602; (c) C. D. MacKinnon, S. L. M. Parent, R. C. Mawhinney, A. Assound and C. M. Robertson, *CrystEngComm*, 2009, **11**, 160; (d) Y.-B. Dong, H.-X. Xu, J.-P. Ma and R.-Q. Huang, *Inorg. Chem.*, 2006, **45**, 3325; (e) Y.-B. Dong, H.-Y. Wang, J.-P. Ma, D.-Z. Shen and R.-Q. Huang, *Inorg. Chem.*, 2005, **44**, 4679; (f) S. P. Anthony and T. P. Radhakrishnan, *Chem. Commun.*, 2004, 1058; (g) Y.-B. Dong, P. Wang and R.-Q. Huang, *Inorg. Chem.*, 2004, **43**, 4727; (h) J. Zhang, M. Nieuwenhuyzen, J. P. H. Charmant and S. L. James, *Chem. Commun.*, 2004, 2808; (i) Z. Xu, Y.-H. Kiang, S. Lee, E. B. Lobkovsky and N. Emmott, *J. Am. Chem. Soc.*, 2000, **122**, 8376; (j) K. A. Hirsch, S. R. Wilson and J. S. Moore, *Chem.-Eur. J.*, 1997, **3**, 765; (k) D. Venkataraman, S. Lee, J. S. Moore, P. Zhang, K. A. Hirsch, G. B. Gardner, A. C. Covey and C. L. Prentice, *Chem. Mater.*, 1996, **8**, 2030.
- [117] For examples see: (a) J. Ni, K.-J. Wei, Y. Liu, X.-C. Huang and D. Li, *Cryst. Growth Des.*, 2010, **10**, 3964; (b) Y.-Q. Sun, C. Yang, Z. Xu, M. Zeller and A. D. Hunter, *Cryst. Growth Des.*, 2009, **9**, 1663; (c) S. Banfi, L. Carlucci, E. Caruso, G. Ciani and D. M. Prosperpio, *Cryst. Growth Des.*, 2004, **4**, 29; (d) F. C. Pigge, M. D. Burgard and N. P. Rath, *Cryst. Growth Des.*, 2003, **3**, 331; (e) Y.-H. Kiang, G. B. Gardner, S. Lee, Z. Xu and E. B. Lobkovsky *J. Am. Chem. Soc.*, 1999, **121**, 8204; (f) W. Choe, Y.-H. Kiang, Z. Xu and S. Lee, *Chem. Mater.*, 1999, **11**, 1776; (g) G. B. Gardner, Y.-H. Kiang, S. Lee, A. Asgaonkar and D. Venkataraman, *J. Am. Chem. Soc.*, 1996, **118**, 6946; (h) D. Venkataraman, G. B. Gardner, S. Lee and J. S. Moore, *J. Am. Chem. Soc.*, 1995, **117**, 11600; (i) G. B. Gardner, D. Venkataraman, J. S. Moore and S. Lee, *Nature*, 1994, **374**, 792.
- [118] For examples see: (a) Z. Zhang, H. Zhao, M. M. Matsushita, K. Awaga and K. R. Dunbar, *J. Mater. Chem. C*, 2014, **2**, 399; (b) B. Blankschein, A. Schulz, A. Villinger and R. Wustrack, *ChemPlusChem*, 2014, **79**, 973; (c) C. S. Hawes, S. R. Batten and D. R. Turner, *CrystEngComm*, 2014, **16**, 3737; (d) A. V. Mossine, P. Thavornnyutikarn and J. Atwood, *CrystEngComm*, 2013, **15**, 1673; (e) K. Akimoto, Y. Kondo, K. Endo, M. Yamada, Y. Aoyama and F. Hamada, *Tetrahedron Lett.*, 2008, **49**, 7361; (f) Y.-B. Dong, Y.-Y. Jiang, J.-P. Ma, F.-L. Liu, B. Tang, R.-Q. Huang and S. R. Batten, *J. Am. Chem. Soc.*, 2007, **129**, 4520; (g) K. S. Min and M. P. Suh, *J. Am. Chem. Soc.*, 2000, **122**, 6834; (h) C. Kleina, E. Graf, M. W. Hosseini, A. De Cian and J. Fischer, *Chem. Commun.*, 2000, 239–240; (i) I. Ino, J. Chu, M. Munakata, T. Kuroda-Sowa, M. Maekawa, Y.

- Suenaga and Y. Kitamori, *Inorg. Chem.*, 2000, **39**, 4273; (j) G. Mislin, E. Graf, M. W. Hosseini, A. De Cian, N. Kyritsakas and J. Fischer, *Chem. Commun.*, 1998, 2545; (k) F.-Q. Liu and T. D. Tilley, *Inorg. Chem.*, 1997, **36**, 5090.
- [119] For examples see: (a) C. A. Hollis, S. R. Batten and C. J. Sumby, *Cryst. Growth Des.*, 2013, **13**, 2350; (b) C. A. Hollis, L. R. Hanton, J. C. Morris and C. J. Sumby, *Cryst. Growth Des.*, 2009, **9**, 2911.
- [120] (a) A. Wang, C. Merckens and U. Englert, *CrystEngComm*, 2015, **17**, 4293; (b) Q. Guo, C. Merckens, R. Si and U. Englert, *CrystEngComm*, 2015, **17**, 4383; (c) C. Merckens, N. Becker, K. Lamberts and U. Englert, *Dalton Trans.*, 2012, **41**, 8594; (d) C. Merckens and U. Englert, *Dalton Trans.*, 2012, **41**, 4664; (e) B. Kilduff, D. Pogozhev, S. A. Baudron and M. W. Hosseini, *Inorg. Chem.*, 2010, **49**, 11231; (f) D. Pogozhev, S. A. Baudron and M. W. Hosseini, *Inorg. Chem.*, 2010, **49**, 331; (g) M. Kondracka and U. Englert, *Inorg. Chem.*, 2008, **47**, 10246; (h) A. D. Burrows, K. Cassar, M. F. Mahon and J. E. Warren, *Dalton Trans.*, 2007, 2499–2509.
- [121] L. Carlucci, G. Ciani, S. Maggini, D. M. Proserpio and M. Visconti, *Chem.-Eur. J.*, 2010, **16**, 12328.
- [122] M. Karsch, H. Lund, A. Schulz, A. Villinger and K. Voss, *Eur. J. Inorg. Chem.*, 2012, 5542–5553.
- [123] H. J. Sakiyama, *Chem. Software*, 2001, **7**, 171.
- [124] L. J. Daumann, P. Comba, J. A. Larrabee, G. Schenk, R. Stranger, G. Cavigliasso and L. R. Gahan, *Inorg. Chem.*, 2013, **52**, 2029.
- [125] (a) M. O’Keeffe, M. A. Peskov, S. J. Ramsden and O. M. Yaghi, *Acc. Chem. Res.*, 2008, **41**, 1782; (b) <http://rcsr.anu.edu.au/>
- [126] T. G. Mitina and V. A. Blatov, *Cryst. Growth Des.*, 2013, **13**, 1655.
- [127] E. V. Alexandrov, V. A. Blatov, A. V. Kochetkov and D. M. Proserpio *CrystEngComm.*, 2011, **13**, 3947.
- [128] V. A. Blatov, A. P. Shevchenko and D. M. Proserpio, *Cryst. Growth Des.*, 2014, **14**, 3576.
- [129] For a self-penetrated net based on a rigid metalloligand see: L. Carlucci, G. Ciani, D. M. Proserpio and F. Porta, *Angew. Chem. Int. Ed.*, 2003, **115**, 331.
- [130] H. Ma, D. Sun, L. Zhang, R. Wang, V. A. Blatov, J. Guo and S. Dun, *Inorg. Chem.*, 2013, **52**, 10732.
- [131] C. F. Macrae, I. J. Bruno, J. A. Chisholm, P. R. Edgington, P. McCabe, E. Pidcock, L. Rodriguez-Monge, R. Taylor, J. van de Streek and P. A. Wood, *J. Appl. Cryst.*, 2008, **41**, 466.
- [132] For examples see: (a) B. Nohra, R. Réau and C. Lescop, *Eur. J. Inorg. Chem.*, 2014, 1788; (b) A. I. A. Perez, T. Biet, S. Graule, T. Agou, C. Lescop, N. R. Branda, J. Crassous and R. Réau, *Chem.-Eur. J.*, 2011, **17**, 1337; (c) Y. Yao, W. Shen, B. Nohra, C. Lescop and R. Réau, *Chem.-Eur. J.*, 2010, **16**, 7143; (d) B. Nohra, S. Graule, C. Lescop and R. Réau, *J. Am. Chem. Soc.*, 2006, **128**,

- 3520; (e) F. Fochi, P. Jacopozzi, E. Wegelius, K. Rissanen, P. Cozzini, E. Marastoni, E. Fisicaro, P. Manini, R. Fokkens and E. Dalcanale, *J. Am. Chem. Soc.*, 2001, **123**, 7539; (f) P. Jacopozzi, E. Dalcanale, *Angew. Chem. Int. Ed.*, 1997, **36**, 613.
- [133] H. Schiff, *Justus Liebigs Ann. Chem.*, 1864, **131**, 118.
- [134] Selected examples : (a) S.-L. Huang, G.-X. Jin, H.-K. Luo and T. S. A. Hor, *Chem.-Asian J.*, 2015, **10**, 24; (b) G. Zhang and M. Mastalerz, *Chem. Soc. Rev.*, 2014, **43**, 1934; (c) K. D. Okochi, Y. Jin and W. Zhang, *Chem. Commun.*, 2013, **49**, 4418; (d) Y. Jin, C. Yu, R. J. Denman and W. Zhang, *Chem Soc Rev*, 2013, **42**, 6634.
- [135] J. Clayden, N. Greeves and S. Warren, *Organic Chemistry*, Oxford University Press, 2nd edition edn., 2012.
- [136] Selected examples: (a) M. Matache, E. Bogdan and N. D. Hădade, *Chem.-Eur. J.*, 2014, **20**, 2106; (b) K. D. Okochi, Y. Jin and W. Zhang, *Chem. Commun.*, 2013, **49**, 4418;
- [137] Selected examples: (a) M. Mastalerz, *Chem. A Eur. J.*, 2012, **18**, 10082; (b) R. McCaffrey, H. Long, Y. Jin, A. Sanders, W. Park and W. Zhang, *J. Am. Chem. Soc.*, 2014, **136**, 1782; (c) K. Acharyya, S. Mukherjee and P. S. Mukherjee, *J. Am. Chem. Soc.*, 2013, **135**, 554.
- [138] Selected examples: (a) G. Lin, H. Ding, D. Yuan, B. Wang and C. Wang, *J. Am. Chem. Soc.*, 2016, **138**, 3302; (b) L. Ascherl, T. Sick, J. T. Margraf, S. H. Lapidus, M. Calik, C. Hettstedt, K. Karaghiosoff, M. Döblinger, T. Clark, K. W. Chapman, F. Auras and T. Bein, *Nat. Chem.*, 2016, **8**, 310; (c) X. Feng, X. Ding and D. Jiang, *Chem. Soc. Rev.*, 2012, **41**, 6010.
- [139] (a) C. Schouwey, R. Scopelliti and K. Severin, *Chem.-Eur. J.*, 2013, **19**, 6274; (b) A. Granzhan, C. Schouwey, T. Riis-Johannessen, R. Scopelliti and K. Severin, *J. Am. Chem. Soc.*, 2011, **133**, 7106.
- [140] Selected examples: (a) Y. Zeng, R. Zou, Z. Luo, H. Zhang, X. Yao, X. Ma, R. Zou and Y. Zhao, *J. Am. Chem. Soc.*, 2015, **137**, 1020; (b) K.-D. Zhang and S. Matile, *Angew. Chemie Int. Ed.*, 2015, **54**, 8980.
- [141] Selected examples: (a) S. Lascano, K.-D. Zhang, R. Wehlauch, K. Gademann, N. Sakai and S. Matile, *Chem. Sci.*, 2016, **7**, 4720; (b) A. Wilson, G. Gasparini and S. Matile, *Chem. Soc. Rev.*, 2014, **43**, 1948.
- [142] (a) D. A. Roberts, A. M. Castilla, T. K. Ronson and J. R. Nitschke, *J. Am. Chem. Soc.*, 2014, **136**, 8201; (b) M. Hutin, G. Bernardinelli and J. R. Nitschke, *Proc. Natl. Acad. Sci.*, 2006, **103**, 17655.
- [143] Selected examples: (a) W. J. Ramsay, F. T. Szczypiński, H. Weissman, T. K. Ronson, M. M. J. Smulders, B. Rybtchinski and J. R. Nitschke, *Angew. Chemie Int. Ed.*, 2015, **54**, 5636; (b) I. A. Riddell, T. K. Ronson, J. K. Clegg, C. S. Wood, R. A. Bilbeisi and J. R. Nitschke, *J. Am. Chem. Soc.*, 2014, **136**, 9491; (c) R. A. Bilbeisi, T. K. Ronson and J. R. Nitschke, *Angew. Chem. Int. Ed.*, 2013, **52**, 9027; (d) W. Meng, B. Breiner, K. Rissanen, J. D. Thoburn, J. K. Clegg and J. R. Nitschke, *Angew. Chemie Int. Ed.*, 2011, **50**, 3479.

- [144] Selected examples: (a) J. Park, D. Feng and H.-C. Zhou, *J. Am. Chem. Soc.*, 2015, **137**, 1663; (b) P. Deria, W. Bury, J. T. Hupp and O. K. Farha, *Chem. Commun.*, 2014, **50**, 1965; (c) H.-L. Jiang, D. Feng, T.-F. Liu, J.-R. Li and H.-C. Zhou, *J. Am. Chem. Soc.*, 2012, **134**, 14690.
- [145] A. P. Hammersley, *ESRF Internal Report*, ESRF97HA02T, "FIT2D: An Introduction and Overview", 1997.
- [146] CrysAlisPRO, Oxford Diffraction /Agilent Technologies UK Ltd, Yarnton, England.
- [147] G. M. Sheldrick, *Acta Crystallogr. Sect. C Struct. Chem.*, 2015, **71**, 3.
- [148] L. Palatinus and G. Chapuis, *J. Appl. Crystallogr.*, 2007, **40**, 786.
- [149] D. Kratzert, J. J. Holstein and I. Krossing, *J. Appl. Crystallogr.*, 2015, **48**, 933.
- [150] P. van der Sluis and A. L. Spek, *Acta Cryst. A*, 1990, **46**, 194.
- [151] A. L. Spek, *Acta Crystallogr., Sect. D.: Biol. Crystallogr.*, 2009, **65**, 148.
- [152] L. F. Lindoy, G. V. Meehan and N. Svenstrup, *Synthesis*, 1998, **7**, 1029.

Curriculum Vitae

Mathieu Marmier

Avenue Nestlé 9, 1800 Vevey
Switzerland

☎ +41 79 398 00 62

✉ mathieu.marmier@a3.epfl.ch

🔑 Researcher ID N-5700-2015

27 years old, Swiss citizen

Education

- Ph.D in Supramolecular Chemistry**, Laboratory of Supramolecular Chemistry, EPFL, Lausanne, Switzerland
Director: Prof. Kay Severin. **Oct. 2012 – present**
- M.Sc in Molecular and Biological Chemistry**, EPFL, Lausanne, Switzerland
Master thesis: “Synthesis and Evaluation of Sunitinib Derivatives for Early Cancer Diagnosis”, Laboratory of Synthesis of Natural Products. **Sep. 2010 – Feb. 2012**
- B.Sc in Chemistry and Chemical Engineering**, EPFL, Lausanne, Switzerland **Sep. 2007 – Jul. 2010**

Research Experience

- Ph.D Student – Prof. K. Severin, EPFL, Switzerland** **Oct. 2012 – present**
Currently working as a Ph.D student under the guidance of Prof. Kay Severin, developing new strategies for the incorporation of anionic dinuclear clathrochelate complexes in supramolecular assemblies.
- Internship – Prof. S. Gerber & Dr. HDR C. Roussel, EPFL** **Feb. 2012 – Jul. 2012**
Worked for six months studying the dipolar cycloaddition of nitrones with α -methylene- γ -butyrolactone.
- M.Sc Thesis – Prof. S. Gerber, EPFL** **Sep. 2011 – Feb. 2012**
Final year project synthesizing analogues of potent anti-cancer drugs coupled to multivalent organic linkers for the early stage detection of tumors.
- M.Sc Semester Project – Prof. P. Dyson, EPFL** **Feb. 2011 – Jul. 2011**
Worked during one semester under the supervision of Prof. Paul Dyson, developing new phosphine ligands for the catalytic reduction of CO₂.

Leadership/Teaching Experience

- Safety Delegate of Laboratory – EPFL** **Oct. 2012 – present**
Worked as safety delegate for Prof. Kay Severin. Conducted all new collaborators’ safety introduction, assessed security issues in laboratories and set up laboratories in a safe environment.
- Supervisor – EPFL** **Jul. 2013 – present**
Responsible for a first year Ph.D student, elaborated and designed a project related to my own research (since Oct. 2015). Co-responsible of a third-year

laboratory technician (since Feb. 2015). Supervisor of a graduate student performing a three months internship (Jul. – Sep. 2013).

Teaching Assistant – EPFL

Responsible for 1st to 3rd year undergraduates' practicals in organic and inorganic chemistry (groups of 8 to 15 students). Teaching assistant to lecturer of several undergraduate courses, supervision of exercise sessions.

**Sep. 2011 –
present**

Supervisor – EPFL/University of Lausanne

Responsible of a Master project research, criminal science and forensics institute, group of two M.Sc students.

**Feb. 2012 –
Jul. 2012**

High-School Assistant Teacher – La Tour-de-Peilz, Switzerland

Substitute teacher in secondary school, teaching physics, mathematics, chemistry and biology to young students (classes of 15-25).

2010-2012

Publications

1. M. Marmier, A. Blyth, S. Gerber-Lemaire and C. Roussel, *[3+2] Cycloadditions of C,N-Diphenylnitrone and C-Benzoyl-N-Phenylnitrone with Tulipalin A: A stereochemical study*, manuscript in preparation.

2. M. Marmier, G. Cecot, A. V. Vologzhanina, J. L. Bila, I. Zivkovic, H. M. Ronnow, B. Nafradi, E. Solari, P. Pattison, R. Scopelliti and K. Severin, *Dalton Trans.*, 2016, accepted.

3. M. Marmier, G. Cecot, B. F. E. Curchod, P. Pattison, E. Solari, R. Scopelliti and K. Severin, *Dalton Trans.*, 2016, **45**, 8422.

4. M. Marmier, M. D. Wise, J. J. Holstein, P. Pattison, K. Schenk, E. Solari, R. Scopelliti and K. Severin, *Inorg. Chem.*, 2016, **55**, 4006.

5. M. Pascu, M. Marmier, C. Schouwey, R. Scopelliti, J. J. Holstein, G. Bricogne and K. Severin, *Chem. Eur. J.*, 2014, **20**, 5592. Invited as the cover picture of the journal issue: *Chem. Eur. J.*, 2014, **20**, 5517.

Scientific Contributions

Oral talk, "Polytopic Clathrochelates Ligands: Versatile Toolbox for Applications in Supramolecular Chemistry", *Swiss Young Chemists' Association Snow Symposium*, Saas Fee, Switzerland

Jan. 2016

Poster presentation at the *Swiss Young Chemists' Association Snow Symposium*, Saas Fee, Switzerland

Jan. 2016

Poster presentation at the *Swiss Chemical Society Fall Meeting*, Lausanne, Switzerland

Sep. 2015

Poster presentation at the *10th International Symposium on Macrocyclic and Supramolecular Chemistry (ISMCS)*, Strasbourg, France

**Jun. – Jul.
2015**

Poster presentation at the <i>Swiss Young Chemists' Association Snow Symposium</i> , Saas Fee, Switzerland	Jan. 2015
Poster presentation at the <i>Swiss Chemical Society Fall Meeting</i> , Zürich, Switzerland	Sep. 2014
Poster presentation at the <i>Swiss Young Chemists' Association Snow Symposium</i> , Saas Fee, Switzerland	Jan. 2014

Awards

DSM poster award for the best poster presentation in Inorganic Chemistry, Swiss Chemical Society Fall Meeting, Zürich.	2014
SCGC Master Project Poster Prize for the third best poster of M.Sc Chemistry, EPFL.	2012
Syngenta Monthey (Chimie) Prize for the best average grade (M.Sc), EPFL.	2012
Nestlé Prize for excellence in mathematics and chemistry, Swiss Maturity, Burier, Switzerland	2007

Skills

Chemical syntheses: organic and inorganic syntheses, rational design of self-assembled supramolecular architectures, crystallization techniques.

Analytical techniques: multinuclear NMR, UV-VIS, fluorescence, IR, SCXRD, TGA, gas sorption (CO₂, N₂, H₂, CH₄), ESI-MS.

Softwares: ChemDraw, MestReNova, Mercury, Diamond, Igor Pro, Reaxys, SciFinder, Solidworks.

Languages: French (native), English (C1 level).

References

Prof. Kay Severin

Ecole Polytechnique Fédérale de Lausanne
 Institut des sciences et ingénierie chimiques
 EPFL SB ISIC LCS
 CH-1015 Lausanne
 Switzerland
Phone : +41 21 693 93 01
E-mail : kay.severin@epfl.ch

Prof. Sandrine Gerber-Lemaire

Ecole Polytechnique Fédérale de Lausanne
 Institut des sciences et ingénierie chimiques
 EPFL SB ISIC GFB
 CH-1015 Lausanne
 Switzerland
Phone : +41 21 693 93 72
E-mail : sandrine.gerber@epfl.ch